CHAPTER - 1

INTRODUCTION

1.1 Solar Energy

Now a days, world's total energy consumption is continually increasing year by year due to the rapid industrial development and growth of global population and high living standards. However, the use of conventional sources to supply this energy demand should be extremely limited due to the growing awareness towards the dual threats of depleted storage of fossil fuel resources resulting with global inflation in fuel prices **(Gullison et al., 2007; Asnaghi and Ladjevardi, 2012**) and a deep concern of environmental impact like global temperature rise **(IPCC, 2007)** and air pollution due to burning of fossil fuel. Therefore, all these concerns urgently need to find sustainable, safe and renewable energy sources and use them to replace conventional fuel or at least mitigate their excessive consumption and consequent impact on the environment.

The most common renewable energy technologies currently being used are solar, wind, biomass, and geothermal. Among these technologies, utilization of solar energy is the largest exploitable resource due to wide availability across the world and providing a clean, safe and free of charge source of energy. It emits electromagnetic radiation with an average irradiance of 1353 W/m^2 near the earth's surface. The solar radiation incident on the earth's surface is comprised of two types of radiations – beam and diffuse, ranging in the wavelengths from the ultraviolet to the infrared (300 to 2000 nm). It is reported that the amount of solar energy delivered to the earth every year is up to 1×10^{18} kWh, which is

almost ten thousand times that of the energy humanity uses annually **(Jefferson 1998).** As illustrated in Fig. 1.1, solar energy can be converted into three forms of energy, i.e. power generation, photochemical, and thermal energy. In the first type of system solar energy is directly converted into electric energy by exciting electrons called photovoltaic devices. Secondly, it can produce chemical fuel by natural photosynthesis in green plants or artificial photosynthesis in human-engineered systems. At last, the solar thermal thermodynamic systems are used to collect and convert solar energy into thermal energy for fluid heating purposes directly at lower temperature (T<300°C) according to requirement of different end users or creating steam for further electricity generation at high temperatures **(Lewis and Crabtree 2005).**

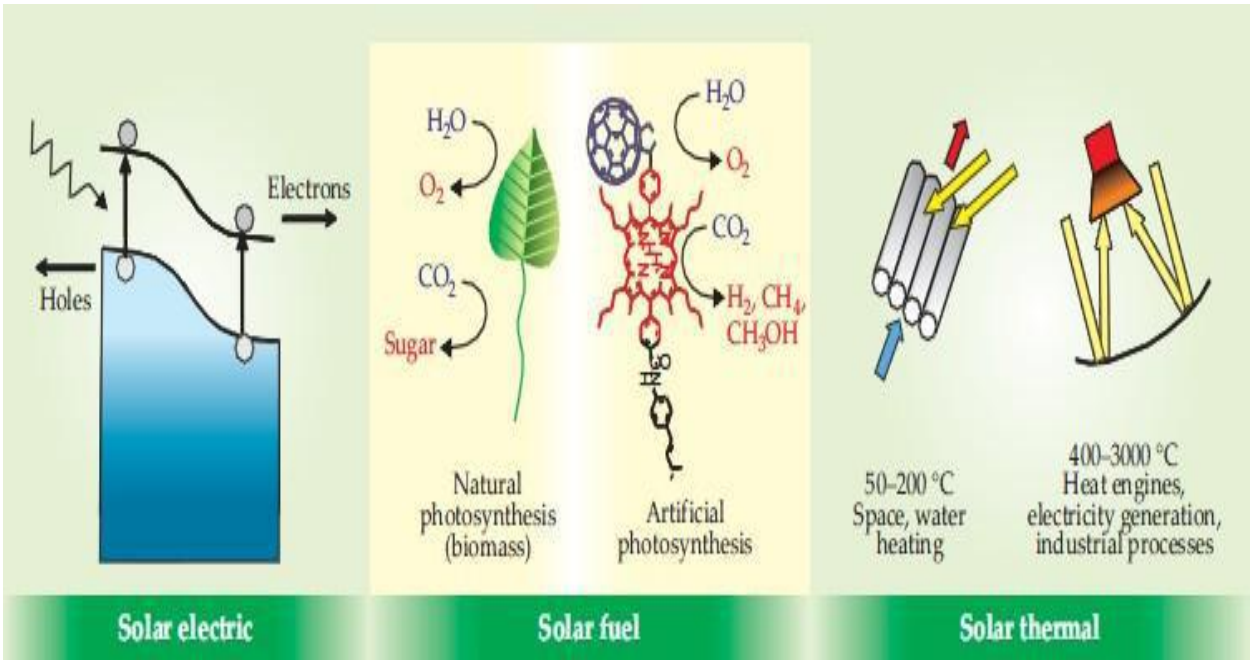

Fig. 1.1: Three forms of solar energy conversion (Lewis and Crabtree 2005)

Solar thermal energy utilization is the convenient, efficient and the most popular application and has been widely applied for water heating, space heating, space cooling and process heat generation.

1.1.1 Solar thermal conversion

The basic principle of solar thermal collection is that when solar radiation is incident on a surface (such as that of a black-body), part of this radiation is absorbed, thus increasing the temperature of the surface. As the temperature of the body increases, the surface loses heat at an increasing rate to the surroundings. Steady-state is reached when the rate of the solar heat gain is balanced by the rate of heat loss to the ambient surroundings.

In order to collect and convert incident solar energy into thermal energy for some useful mean, diverse types of solar collectors are available for a wide range of applications (Kalogirou, 2004).

1.2 Solar thermal collectors

Conventionally solar thermal collectors are represented by two types of systems:

i) Concentrating or focusing type

ii) Non-concentrating or flat plate type

1.2.1 Concentrating collector

Concentrating collectors utilize a parabolic trough or dish system to concentrate the incident solar flux. These systems also utilize optical devices to increase the solar energy

incident on the medium to be heated and result in high temperatures in the collector. Concentrating solar collectors are generally used for high temperature water heating or electricity production.

1.2.2 Non-concentrating collector

When no optical concentration is done, the device in which the collection achieved is called a non-concentrating type solar collector. A variety of non-concentrating type collectors are available on the market today and in general are described thoroughly in **Duffi and Backmen (2006).** Depending on the type of collector used, and the level of solar radiation available, fluid working temperatures can be achieved ranging from 50^0C for simple, unglazed "swimming-pool" collectors, to 85^0C for glazed flat-plate collectors, and up to 120^0C for evacuated-tube collectors. The glazed flat plate collector is most commonly used and most important type of solar collector because it is simple in design, has no moving parts and requires less maintenance. Flat plate collectors use the insolation as it is. The absorber and collector area in flat plate solar collectors is numerically the same. The flat plate collector or arrays of flat plate collector is generally used for a variety of applications of water heating according to requirements. Flat plate collectors collect both beam and diffused solar radiations; they are also effective on cloudy days where there is no direct radiation.

Flat plate collectors are one of the most successful solar thermal devices which replace or at least lower the conventional fuel energy consumption needed to run conventional water heaters for residential, commercial and industrial purposes **(Kalogirou, 2009).** The other advantages for the popularity of flat plate solar collector water heaters are relatively easy to build and install, short payback period and long life.

In spite of a lot of hindrance that come in the way of utilizing these solar thermal energy systems, it has drawn a lot of interests in research for raising efficiency of these solar thermal collectors and decreasing the cost of energy production to make them more attractive economically and environmentally.

1.2.3 Flat plate solar collector

The most commonly used solar thermal device i.e. flat plate solar collector, absorbs the incident solar radiation on black absorber plate housed in an insulated box with one or more transparent glazing and transforms solar radiation into heat which is transferred to a fluid flowing in the tubes that are attached (or integral) to the absorber plate. Heated fluid can be used for various residential and industrial purposes. Water or glycols are generally used as heat conducting fluid. These flat plate collectors have a fixed area for collecting the incoming radiation and are typically stationary throughout the day **(Kalogirou, 2004).** Figure 1.2 (a) and 1.2 (b) shows the typical components of a conventional flat plate collector. The conventional flat plate collector assembly typically consists of an absorber plate, fluid tubes, a transparent cover, a housing or frame and insulation.

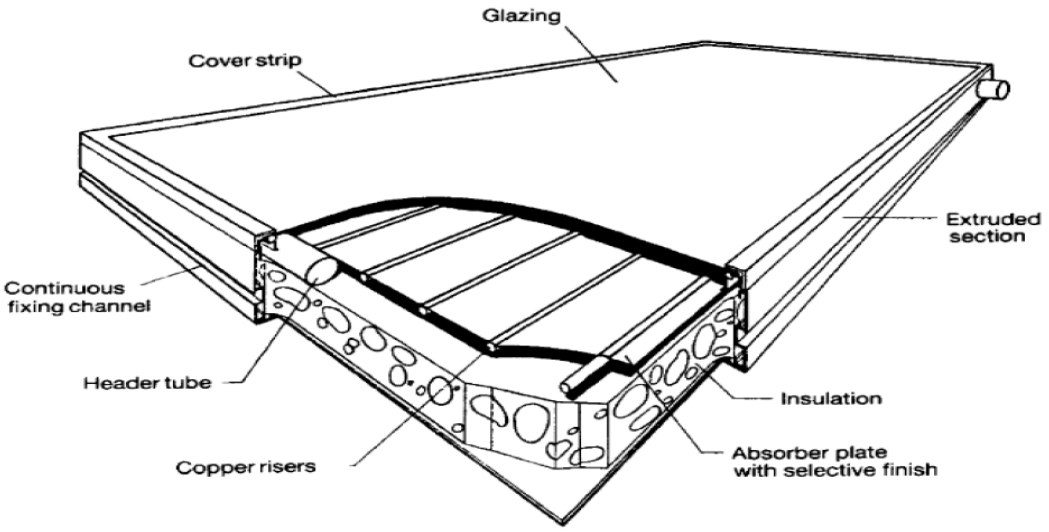

Figure 1.2 (a): Pictorial view of conventional flat plate solar collector

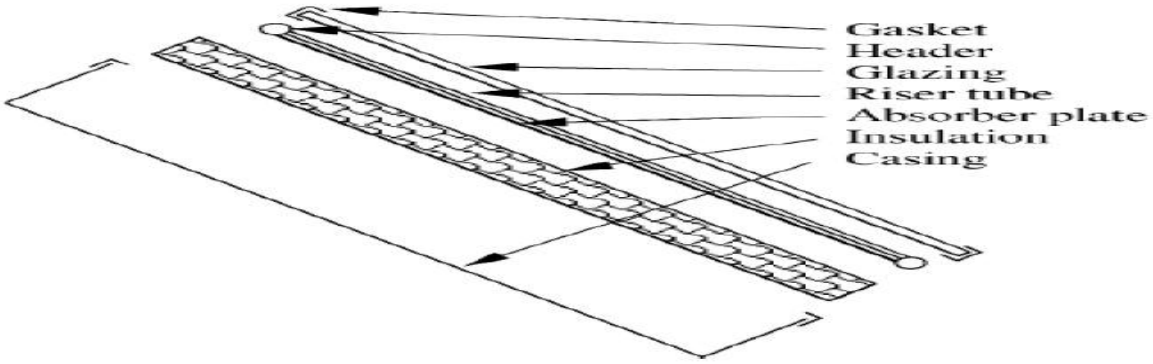

Figure 1.2 (b) Exploded view of a conventional flat-plate solar collector

The absorber plate is the heart of a solar collector, which is made by several copper or aluminum strips painted with matt black paint to absorb the maximum amount of incoming solar radiation. It then transfers that solar energy to the heat carrying fluid flowing in the tubes attached or integral to the plate. The fluid tubes act as a heat remover from the absorber plate. The clear glass is generally used as a highly transparent cover for the incoming short wave length (0.3-2.5μm) radiation as well as to trap outgoing long wave length (2.5-20μm) radiation from the absorber plate. The transparent cover also minimizes convection losses

and protects the absorber plate from adverse weather condition together with the housing. The insulation on the back of the absorber plate and on the side walls reduces the conduction heat losses.

The efficiency of solar collector is the fraction of received solar thermal energy on the absorber surface which is transferred to the working fluid as usable thermal energy. Improving this energy transfer, by maximizing solar absorption and minimizing outgoing heat losses, will result in improved collector efficiency.

A layer of selective materials are also employed on its plates and tubes to increase efficiency of solar collector (**Otanicar and golden 2009, Mu et al 2010**). Despite several improvements, the working mode of these conventional solar thermal collectors still exhibit several shortcomings, such as relatively high thermal radiation losses due to maximum temperature on the absorption surface limit incident flux density (**Tyagi et al 2009**), and conduction and convection losses due to indirect heat transfer to working fluid from absorber plate results lesser collector efficiency.

In order to overcome these drawbacks of conventional surface based collector, the idea has been proposed to enhance the efficiency of the collectors by directly absorbing the incident solar energy within the fluid volume flowing over the absorber plate (i.e. base plate) named as Direct Absorption Solar Collector (DASC), or alternatively also termed as Volumetric Absorption Collector (VAC).

1.3 Direct absorption solar collector

The direct absorption solar collector (DASC) works on the principle of directly absorbing the incident solar radiations by the thin fluid film flowing over the back plate and thin film volumetrically absorbs the insolation.

The basic difference between the working principle for capturing the solar energy in conventional (indirect) and direct absorption solar collectors can be easily understood from Fig. 1.3. In the direct absorption collector system, the entire volume of the fluid directly participates in the conversion of solar energy, in contrast to just the absorber surface of a conventional solar thermal collector. In addition to this, in the case of conventional collector the solar irradiance is first absorbed by the absorber surface, which transfers the collected heat to the working fluid via conduction and convection. In such systems an inherent thermal barrier of conduction and convection resistances comes in the way of solar irradiance (Fig. 1.3a). This results in relatively inefficient heat transfer to the working fluid. In the case of direct absorption collectors the solar radiant energy directly interacts with the working fluid volume reducing conduction and convection resistances (Fig. 1.3b).

From design point of view DASC closely resembles a conventional flat plate solar collector design (Fig. 1.4) except that in the case of the DASC, there is no absorber tube and instead there is a flow of fluid volume as a thin film over the base plate. Fig. 1.4 (b) shows the conceptual schematic of the proposed DASC system. The sun's rays directly strike the flowing fluid film volume. This is then employed for raising the temperature of pure water via a heat exchanger.

Fig. 1.3 a: Conventional collector b: Direct absorption solar collector

(a)

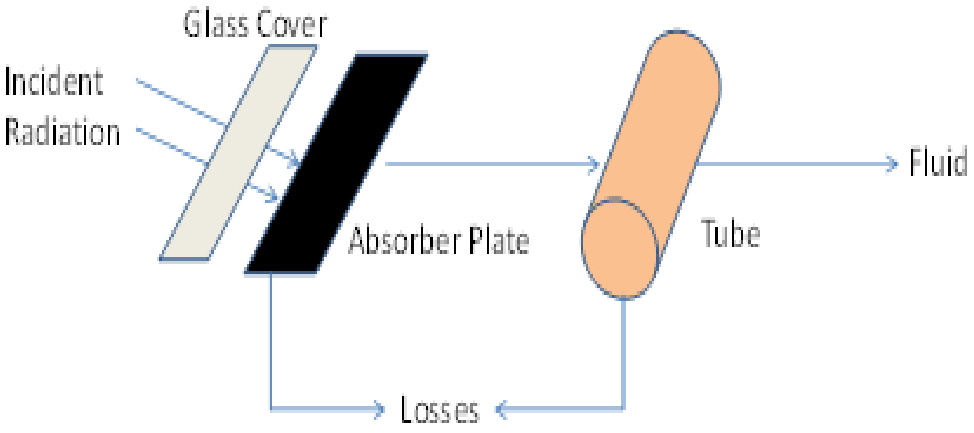

(b)

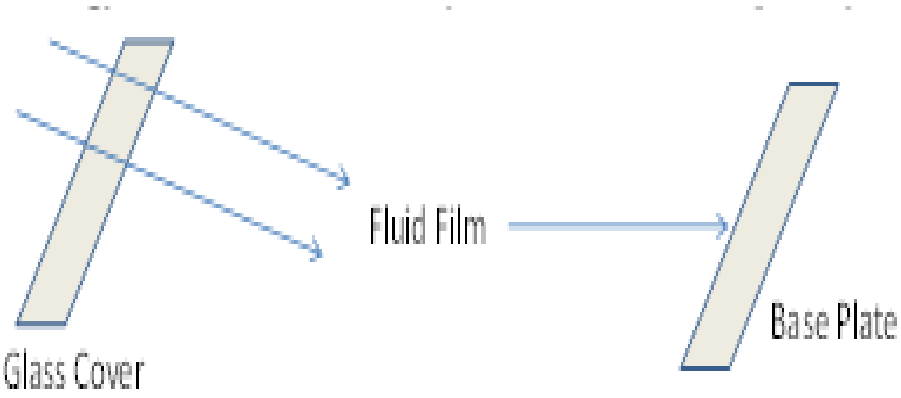

Fig. 1.4 a: Conventional collector b: Direct absorption solar collector

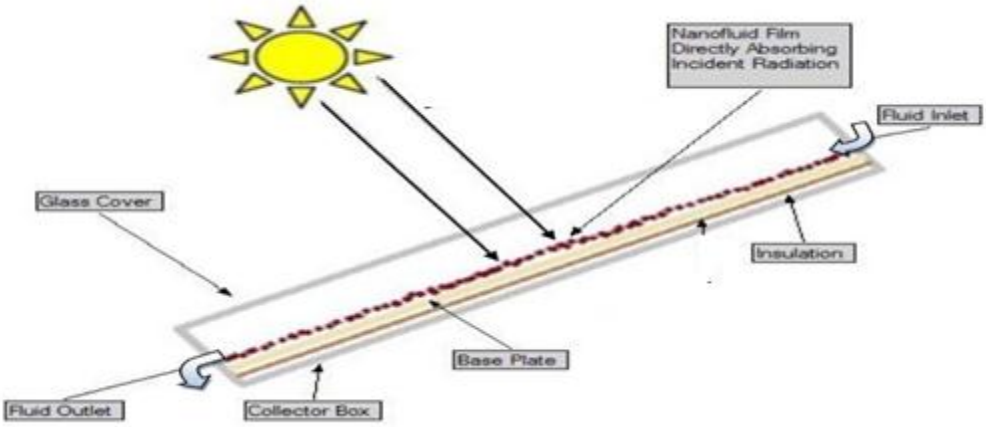

Fig.1.5 The schematic of direct absorption solar collector

Fig. 1.5 shows the schematic working of direct absorption solar collector. The highest temperature occurs within the fluid in the direct absorption solar collector; whereas for indirect absorption the highest temperature occurs at the absorber plate, leading to higher emission losses in the latter. Moreover, the glass cover acts as a barrier for the transmittance of low energy radiations from the fluid to the surroundings. Thus, DASC leads to the use of a higher amount of solar energy, resulting in higher efficiencies and fluid outlet temperatures as compared to conventional flat plate collectors. All this leads to a large number of potential applications of such systems.

The performance of a collector not only depends on how effective the absorber is but also on how effective is the heat transfer and thermo-physical properties (e.g. Thermal Conductivity, Heat capacity) of the working fluid. The absorption properties of the fluids generally used in solar collectors are very poor which in turn limits the efficiency of the solar

collector. Since, in DASC all of the heat is to be absorbed by the working fluid so the light absorption properties of the working fluid should be high enough to absorb incident solar radiation. So, there is a need to use energy efficient heat transfer fluids to get high heat transfer performance and efficiency. In order to meet all these requirements nanofluids is used in direct absorption solar collectors **(Saidur et al; 2011)**.

1.4 Surface absorption v/s volumetric absorption

In conventional tube-in-plate type solar collector, solar energy is absorbed through black solid surface resulting in surface absorption phenomenon whereas in case of direct absorption solar collector, absorption of solar energy through fluid volume, making it case of volumetric absorption. The main differences in these two absorption methods are given in the following Table 1.1.

Table 1.1 Surface absorption v/s volumetric absorption

S.No.	Surface absorption	Volumetric absorption
1	Tube carries fluid i.e. water	No tubes, only nanofluid film flows over the plate
2	Black coated absorber plate	Adiabatic and transparent plate
3	Absorber plate absorbs incoming solar radiation. Then thermal energy is transferred from the absorber plate to water passing through the tubes	Fluid film directly absorbs the incoming solar radiations.

4	Indirect heat transfer through the solid absorber plate and tube to the fluid (Surface absorption)	Direct heat transfer to the fluid film (Volumetric absorption)
5	High absorber plate temperature causes greater surface and convection heat losses Higher bottom losses	No absorber plate, only fluid film is flowing, hence, minimized surface and convection heat losses Lesser bottom losses
6	Relatively lower outlet fluid temperature, useful heat and efficiency.	Relatively greater outlet fluid temperature, useful heat and efficiency.

1.4.1 Advantage of DASC system

The potential advantages of the DASC concept compared to conventional surface absorption solar collector are summarized below:

- In a DASC, incident radiation is directly absorbed by the working fluid volume. The top cover/surface is semi-transparent (glass) to solar radiation. The entire volume of the working fluid of a DASC participates in conversion of solar energy to thermal energy via absorption of radiation, as opposed to only the surface of a conventional receiver as discussed previously. The former has potential to deliver higher collector efficiencies **(Javadi et al., 2013).**
- Heating within the fluid volume, transfers heat to a small area of fluid and allowing the peak temperature to be located away from surfaces losing heat to the environment.

- Walls of the channel enclosing the working fluid of a DASC do not participate appreciably in the absorption process, and hence do not attain soaring temperatures resulting in reduced heat loss from the surface.
- There are no limitations on the magnitude and uniformity of flux imposed by conventional designs.

Direct absorption solar collectors have been proposed for a variety of applications such as water heating **(Mahian et al; 2013)**; however the efficiency of these collectors is limited by the thermo physical and absorption properties of the working fluid, which are very poor for typical fluids to be used alone in direct absorption solar collectors.

1.5 Nanofluids

Nanofluid is the term coined by C**hoi (1995)** to describe this new class of nanotechnology-based heat transfer fluids prepared by suspension of nanoparticles into conventional heat transfer fluids such as water, ethylene glycol etc. These special types of fluids exhibit absorption and thermal properties superior to those of their host fluids **Choi (1999)**. The goal of nano-fluids is to achieve the highest possible heat transfer properties at the smallest possible concentrations by uniform dispersion and stable suspension of nanoparticles in base fluids. Nano-fluids are having different properties as compared to the base fluid because in the nanoscale range, the fundamental properties of nano-fluids depend strongly on particle size, shape and the surface area. Earlier the heat transfer of fluids is increased by conventional methods of suspending micrometer or millimeter sized particles in the base fluid. The major problem with these fluids is the rapid settling of micrometer or millimeter sized particles and also these particles cannot be used in micro channels because they can

clog micro channels. **Choi (1995)** presented the remarkable possibility of doubling the convection heat transfer coefficients using nano-fluids. Besides, thermal conductivity of nanofluids has been reported to be substantially higher than that of the base fluid by **Murshed et al. (2008)**. **Chen et al. (2009)** suggested that significant enhancement in solar energy absorption capability, thermal conductivity and at the same time excellent stability makes nanofluid an ideal choice for solar thermal applications. Having such characteristics, nanofluids can be used as working fluids in solar collectors for effectively capturing and transporting thermal energy.

Increase in opacity is experienced when fine particles are suspended in a transparent liquid (e.g. pure water). This phenomenon occurs because a fine particle suspension absorbs more radiation than a pure liquid, especially within the visible wavelength range. Thus, applying this physical phenomenon to solar energy collection processes, the radiation and absorption characteristics of FPSS (Fine-particle Semitransparent Liquid Suspension) may be controlled as one desires and thus one may expect remarkable increases in the rate and efficiency of heat collection.

The impact of particles on the absorption of radiative energy has been of interest for many years for a variety of applications. More recently researchers have become interested in the radiative properties of nanoparticles in liquid suspensions especially for medical and other applications due to the tunability of the absorption spectrum and the large potential modifications to the effective optical properties of the system. One of the unique benefits offered by the nanofluids is that when metallic nanoparticles are used, which are smaller than the mean free path of the material, the absorption spectrum is typically broadened while

maintaining a distinct absorption peak leading to a further enhancement in the absorption efficiency through the solar spectrum. This broadening allows the nanofluid to absorb a larger portion of the spectrum, but maintaining a peak can allow the user to tailor the wavelength at which the absorption is to be maximized. Besides the benefits to the optical and radiative properties, nanofluids provide other benefits such as increased thermal conductivity and particle stability over micron-sized suspensions, which provide potential improvements to the operating efficiency of a DASC.

A study is carried out to investigate the performance of flat plate direct absorption solar collector using nanofluids. Nanofluids can replace conventional heat transfer fluids in solar collectors.

1.5.1 Potential benefits of nanofluids

Well-dispersed and stable nanofluids are formed after properly dispersing nanoparticles into base fluids and the resulting nanofluids are expected to exhibit several beneficial features:

i. Suspended nanoparticles increase the surface area and the heat capacity of the fluid due to the very small particle size. A thin film of about 150 μm of 30 nm diameter particles at about 1% volume fraction have 300 times more surface area than the bottom of the surface itself .
ii. The suspended nanoparticles enhance the effective (or apparent) thermal conductivity of fluid which results improvement in efficiency of collector.
iii. Smaller pressure drop and reduction in pump power

iv. Elimination of clogging and reduction of erosion of components, such as pipelines, pumps and heat exchangers.

v. Volumetric absorption using nanoparticles minimizes the temperature difference between the absorber and the carrier fluid due to the large surface to volume ratio of the particles and promises to be a more efficient heat transfer mechanism.

vi. Because of the extremely small size, nanoparticles can pass through pumps and plumbing with modest adverse effects.

vii. Adding nanoparticles will enhance scattering and absorption of incident radiation when passing through the fluid. Besides, by employing nanofluids in solar receivers, more uniform receiver temperatures can be achieved inside the collector. This will reduce material constraints.

1.6 Motivation for the present research

The need for working fluids with improved performance has increased the scientific interest in nanofluid. A lot of research has undergone for the last ten years in the use of nanofluid for various engineering applications especially in heat exchange systems. Several researchers have so far determined the enhanced heat transfer potential of nanofluid in automobile radiators for engine cooling systems, evaporators and condensers for HVAC systems, oil coolers, intercoolers etc (Pantzali et al; 2009, Leong et al; 2010, Peyghambarzadeh et al; 2011). Relatively very less work has been carried out on nanofluid based solar systems in particular on direct absorption flat plate collector from enhanced solar radiation absorption point of view by the nanofluids. In one study on direct absorption flat plate solar collector using nano fluid only miniature collector in indoor condition has been considered.

A few experimental and theoretical studies suggested that significant enhancement in solar energy absorption capability and at the same time excellent stability is experienced with the use of nanofluids. Having such characteristics, nanofluids can be used as working fluids in solar collectors for effectively capturing and transporting thermal energy.

These studies show nanofluid an ideal choice for solar thermal applications but none of them have made an attempt of using nanofluid in full scale or prototype direct absorption solar flat plate collector experimentally in actual outdoor condition. In this context the use of variety of nanofluids for performance study on direct absorption solar flat plate collector is relevant, important and need of the hour from the point of view of performance enhancement as well as energy saving.

1.7 Research objectives

Research gaps revealed that only one indoor experimental study on miniature direct absorption solar collector using nanofluid is reported in published literature. This experimental study encouraged to perform outdoor experimental study on prototype direct absorption flat plate collector using nanofluid. In the present study, a real size direct absorption flat plate solar collector system was developed in order to carry out performance analysis using nanofluid as heat transfer fluid in outdoor condition. Following were the objectives in the present research work:

- To develop a nanofluid based Direct Absorption type Flat Plate Solar Collector of full scale
- To carry out performance study and parametric analysis on developed system with

different nanofluids

- To develop design guidelines for nanofluid based Direct Absorption type Flat Plate Solar Collector

1.8 Outline of the thesis

Present thesis has been organized into six chapters. First chapter of the thesis introduces about conventional solar collector, direct absorption solar collector, nanofluid and illustrates the benefit of using nanofluid in solar collector. This chapter also describes the motivation towards present research along with research objectives. Chapter 2 covers the exhaustive literature review currently available regarding use of different working fluid such as water, glycols, alcohols and refrigerants in solar collector of various configurations for heat transfer enhancement. Results of experimental and theoretical studies performed using nanofluid in concentrating and tube-in-plate type solar collector are also included in chapter 2. Chapter 3 is related to nanoparticles and nanofluids used for carrying out the research. It includes the determination of requirement of different nanoparticle for different concentration and techniques of nanofluid preparation. Design and development of direct absorption flat plate solar collector has been discussed in Chapter 4. This chapter covers the complete experimental setup describing the different components and measuring instruments used in the study. It also includes the detailed standards for conducting the tests on solar collector. Chapter 5 covers the results and discussion part. The last chapter 6 is related to conclusions drawn from the study and future scope for the research work. At the last, appendices, references, list of publications and profile of the author are presented.

CHAPTER - 2

LITERATURE REVIEW

Solar collector of a water heating system traps solar energy in the form of heat and heated water is stored in storage tank. Researchers have analyzed different working fluids with various configurations for improving performance of Solar Water Heating Systems (SWHS). A detail literature review of such studies using different working fluids with different types of solar collectors is presented in this chapter along with studies on use of nanofluid for similar applications.

2.1 Heat transfer fluids for solar thermal collector

Working fluid plays a key role in the heat transfer performance of solar water heating systems. In conventional water heating system, working fluid (i.e. water) flowing through tubes or channels, absorbs incident solar energy indirectly through absorber plate and tube, transfers heat to the water in the storage tank. Heat transfer performance of a SWHS depends on the physical and chemical properties of the working fluid along with the geometrical parameters of solar collector. Main requirements for the selection of working fluid to be used in SWHS should be as follows:

I. Working fluid should have high latent heat of evaporation, high specific heat, low boiling point, low freezing temperature and low viscosity.

II. Thermal conductivity should be high for better heat transfer.

III. Working fluid should be chemically stable, non toxic and non explosive.

IV. Working fluid should be environmental friendly, non-corrosive for most of the fabrication materials, and easily available in the market with wide useful range and low cost.

Air and water have been commonly used as working fluids in solar water heating systems. Air has certain advantages compared to water, i.e. non-corrosive in nature and has no issue of boiling/ freezing. However, it has very low heat capacity enforces limitation to low temperature applications and is not used for domestic water heating purposes.

Different working fluids commonly being used in solar thermal applications are air, water, glycol–water mixture, acetone, methanol, ethanol, and different refrigerants. These are discussed in the following sections:

2.1.1 Water

Water has been widely accepted as the most suitable working fluid for SWHS for transferring the captured heat to a storage tank through 'water-to-water' heat exchanger. Water is heated with solar energy in risers of a solar collector and this heat is transferred directly or indirectly in a storage tank depending on the application. The basic unit in conventional SWHS is tube-in-plate type flat-plate solar collector to capture solar energy at the maximum possible efficiency with minimum cost. They are relatively having low cost and require maintenance. Water is preferred due to high specific heat, low viscosity, non toxic, easy availability and low cost.

Different types of SWHS with water as working fluid have been designed, developed and investigated analytically and experimentally in detail by several researchers.

Close (1962) developed a mathematical model to predict heat gain in a thermosyphon driven SWHS with no draw-off during the hours of operation and the model was validated with experimental data.

DeSa (1964) numerically evaluated the performance of a solar collector integrated to a SWH system which was subjected to the load removal and introduced a simplified lumped parameter model to predict the water temperature at the collector outlet.

Gupta and Garg (1968) analyzed thermal performance of domestic SWHS for the natural circulation mode of operation. Solar collector's efficiency factor in terms of the shape of the absorber surface and the material's thermal specifications were incorporated in their model. Radiation intensity as well as ambient temperature was also taken into account.

Ong (1974) in his initial study on solar water heater predicted the average water temperature and the water flow rate using a finite-difference method (FDM). However, the measured experimental data were not in line to the theoretical predictions. Hence, the model was modified by taking into account of the experimental conditions and used FDM to predict the gain in the temperature at a given time step.

Ong (1976) further revised his model by taking into account of the fin efficiency, collector plate efficiency, and heat loss coefficient of the collector plate. The simulated values agreed well with the measured data confirming the validation of the model.

Sodha and Tiwari (1981) used explicit expressions to analyze the performance of a thermosyphon type solar water heating system with natural circulation between the storage tank and the collector. The results showed that it was possible to predict the performance of solar water heating system accurately using simple explicit equations.

Kudish et al. (1985) measured the thermosyphon flow as a function of thermosyphon head and water inlet temperature in their laboratory. A standard efficiency test curve was drawn based on thermosyphon flow data and confirmed that their method can be used to test solar collectors which operates in thermosyphon circulation mode. Instantaneous solar collector efficiency as a function of time was also predicted and analyzed.

Morrison and Braun (1985) used a horizontal tank instead of the conventional vertical storage tank for solar water heating, and studied the numerical operational characteristics and compared with the conventional ones. Their results showed that an optimum result could be achieved when the daily collector flow volume approximately equalled the daily hot water consumption volume. However, their results showed that horizontally placed tank did not perform well compared to the vertically positioned tank.

Uhlemann and Bansal (1985) carried out a performance comparative study between a pressurized SWHS and a non pressurized type under the identical meteorological conditions and found that the efficiency of the pressurized type, and non pressurized type of SWH was 41% and 47%, respectively.

Hobson and Norton (1989) identified thermal characteristics, and operating conditions of thermosyphon SWHS, and determined a characteristic thermal performance curve for a directly heated individual system based on a 30 day test data. A perfect fit between the predicted annual solar fraction (SF) and the characteristic curve was obtained. Analysis was further extended to identify precise design parameters of a direct thermosyphon SWHS.

Shariah and Shalabi (1997) designed a SWHS for Amman (mild climate) and Aqaba (hot climate) in Jordan and by using TRNSYS (Transient System Simulation Tool), software package optimized the design parameters which in turn could enhance the solar fraction of

the system by about 7% to 25%. The study also revealed that the variation in design parameters in performance of SWHS is highly sensitive to mild climate (Amman) than hot climate (Aqaba) of Jordan.

Zerrouki et al. (2002) studied a separated storage-collector system in Algeria. This system had a copper plate absorber with steel connector pipes and storage tank, and a header-riser flat collector. This system also relied upon natural circulation to store the hot water in a tank located up gradient from the collector. The maximum temperature was observed to be 57ºC starting from an initial temperature of 17ºC at 7:00 am.

Nahar (2002) found that the price of SWH system with a galvanized steel-aluminum collector ($160) was considerably less that that with a copper copper collector ($205) while both had comparable performance.

Nahar (2003) studied a separated storage-collector system and found that this system could produce 60.6ºC water at 4:00 pm and 51.6ºC water the next morning. The overall efficiency of this system was determined to be 57%.

Reddy and Kaushika (1999) did experimental work under outdoor conditions on the transparent insulation materials for evacuated tube and integrated collector storage, and concluded that it was possible to attain the storage efficiencies around 20–40%.

Canbazoglu et al. (2005) compared phase change material (PCM) charged SWHS with that of the conventional SWHS with no PCM. PCM-filled polyethylene bottles were set in their storage system in three rows. Various hydrated salt-PCMs, such as zinc nitrate hexahydrate ($Zn\ (NO_3)_2.6H_2O$), disodium hydrogen phosphate dodecahydrate ($Na_2HPHO4.12H_2O$), calcium chloride hexahydrate ($CaCl_2.\ 6H_2O$), and sodium sulfate decahydrate (Glauber's salt–$Na_2SO_4.10H_2O$) were tested. The variations in water temperatures at the midpoint of the

water storage system with respect to the collector outlet temperatures were investigated. Without drawing-off the hot water during night, the system could attain about 46^{o}C. Results were compared with the conventional SWH system and found that the hot water production and the accumulated heat in the SWHS were roughly 2.6–3.5 times higher in case of with the PCM-charged system.

Redpath et al. (2009) carried out an experimental study on a heat-pipe evacuated tube solar water heating system. A two dimensional Particle Imaging Velocimetry (PIV) was used to visualize the thermosyphon fluid regime. It was concluded from the study that the overall cost of the heat-pipe evacuated tube solar water heating system could be reduced by using thermosyphonic flow instead of forced circulation.

Budihardjo and Morrison (2009) carried out thorough simulation studies on the evacuated tube collector having water-in-glass tube design to analyze the optical and heat loss characteristics of a single-ended tube. The study concluded that the system's performance was less dependent on tank size compared to the commonly used flat plate collector system; however, the system had a limitation as it could be used only in low ambient conditions due to its limited tolerance for high pressure.

Huang et al. (2010) investigated a flat-plate collector integrated with a mantle heat exchanger to show its applicability for inherent freeze protection. It was observed that the mean daily efficiency of the solar water heating system using a mantle heat exchanger was up to 50%. While this was lower than the efficiency of a thermosyphon flat-plate system without a heat exchanger, it was higher than the all-glass evacuated tube solar water heating system.

Arab et al. (2012) constructed Pulsating Heat Pipes (PHP) based thermosyphon solar water heating having many U-turns with the capillary dimensions in order to investigate the performance with various filling ratios of distilled water as working fluid. The configuration having 70% filling ratio performed satisfactorily with heat collection efficiency of about 54% while the only thermosyphon mode without the PHP could reach a maximum efficiency of 31–36%.

Walker et al. (2004) designed and installed a direct circulation SWHS at the Social Security Administration's Mid- Atlantic Center in Philadelphia. Evacuated-tube heat-pipe solar collector of $36m^2$ net absorber area was employed to energize the storage tank. The simplicity in design and low erection cost made the system attractive to be implemented in commercial buildings. In this system, the incoming water was preheated in the recirculation loop.

Li et al. (2010) developed the heat transfer model for evaluating the performance of vacuum tube collectors. This simplified model took into account of natural circulation in single glass tube as well as forced flow circulation in the manifold header. The flow equations were obtained by analyzing the friction losses and buoyancy forces inside the tube. A positive agreement was observed between the predicted and computed collector outlet temperatures, and the deviation was within 5%.

Important experimental and theoretical studies on different type of solar water heating systems using water as heat transfer fluid are summarized in Table 2.1.

Table 2.1: A summary of studies on solar water heating system with water as working fluid

S.No.	Investigator(s)	Type of study	Type of collector	Type of flow	Results
1	Close(1962)	Experimental	Tube-in-plate type FPC	Thermosyphon	$\acute{\eta}_{SWH}$ = 38%; $\acute{\eta}_c$ = 38%
2	DeSa (1964)	Experimental and Theoretical	Tube-in-plate type FPC	Thermosyphon	$\acute{\eta}_c$ = 75%
3	Gupta and Garg (1968)	Experimental and Theoretical	Tube-in-plate type FPC	Thermosyphon	Water temperature varies 55^oC–65^oC
4	Ong (1974)	Experimental and Theoretical	Tube-in-plate type FPC	Thermosyphon	$\acute{\eta}_{SWH}$ = 52% (Max)
5	Sodha and Tiwari (1981)	Experimental	Tube-in-plate type FPC	Thermosyphon	$\acute{\eta}_{SWH}$ = 55% (Max)
6	Kudish et al. (1985)	Experimental	Tube-in-plate type	Thermosyph	$\acute{\eta}_{SWH}$ = 46-54% (Max)

			FPC	on	
7	Morrison and Braun (1985)	Experimental and Theoretical	Tube-in-plate type FPC	Thermosyphon	Water temperature 63^{o}C and SF = 0.65
8	Uhlemann and Bansal (1985)	Experimental	Tube-in-plate type FPC	Thermosyphon and forced	Pressurized system: $\acute{\eta}_{th}$ = 41-45%; $\acute{\eta}_{c}$ = 48% Non pressurized system: $\acute{\eta}_{th}$ = 47-57%; $\acute{\eta}_{c}$ = 58%
9	Hobson and Norton (1989)	Experimental	Tube-in-plate type FPC	Thermosyphon	Design a nomogram for thermosyphon SWHS
10	Shariah and Shalabi (1997)	Experimental	Tube-in-plate type FPC	Thermosyphon	Max Solar fraction achieved: Aqaba: SF=0.92 Amman: SF=0.85
11	Arab et al. (2012)	Experimental	FPC with PHP	Thermosyphon	$\acute{\eta}_{c}$ = 54%
12	Ng et al. (2000)	Experimental	Evacuated tube	Thermosyphon	$\acute{\eta}_{c}$ = 59 to 66%

			heat pipe		
13	Chinnappa and Gnanalingam (1973)	Experimental and Theoretical	Built-in-storage	Forced	Total energy collection for the year was 1250 kW h
14	Mohamad (1997)	Experimental and Theoretical	FPC storage	Thermosyphon	$\acute{\eta}_c$ = 50%
15	Schmidt and Goetzberger (1990)	Theoretical	Single tube ICS	Forced	Annual $\acute{\eta}$ = 32%; SF = 0.65
16	Smyth et al. (1999)	Experimental and Theoretical	Built-in-storage	Forced	Overall heat loss reduction up to 20% and thermal energy retention up to 30%
17	Garg and Rani (1982)	Experimental	Built-in-storage	Forced	Using insulating cover performance improved 70%
18	Kaptan and Killic (1996)	Experimental and	Built-in-storage	Thermosyphon	$\acute{\eta}_c$ = 50-55%

		Theoretical			
19	Chauhan and Kadambi (1976)	Experimental	Built-in-storage	Thermosyphon	Collection efficiency 72% for mass flow rate of 75.9 kg/h
20	Sokolov and Vaxman (1983)	Experimental and Theoretical	Built-in-storage	Thermosyphon	Daily efficiency = 53%
21	Ecevit et al. (1989)	Experimental	Built-in-storage	Thermosyphon	For 0.9 m^2 collector area bulk efficiency 57% and 1.9 m^2 collector area bulk efficiency 53%
22	Reddy (2007)	Experimental	Built-in-storage	Thermosyphon	Water delivery temp. can be achieved over 50^oC with a drop of 1.5–2^oC during night-time
23	Canbazoglu et al. (2005)	Experimental	Built-in-storage	Forced	Heat storage capacity with PCM was 2.59 –3.45 times higher than conventional SWH system
24	Goetzberger and	Experimental	Built-in-storage	Thermosyph	Annual ή = 26–35% ; annual SF = 0.41–

	Rommel (1987)			on	0.56; for 4 m^2 collector area
25	Reddy and Kaushika (1999)	Experimental and Theoretical	Built-in-storage	Thermosyph on	Collection efficiency 20 – 40% at collection temperature of 40 – 50^oC.
26	Li et al. (2010)	Experimental and Theoretical	Evacuated tube	Direct circulation	Established a heat transfer model of all-glass vacuum tube collector used in SWHS
27	Walker et al. (2004)	Theoretical	Evacuated tube heat pipe	Forced	System efficiency 34% for commercial building

2.1.2 Glycols

The climatic conditions and municipal hard water with questionable water quality restrict the use of conventional thermosyphon systems in several regions **(Xinjian et al., 2007; Solar Center Information, 2002; Arizona Solar Center, 2011).** The hard water, with high concentrations of mineral particles like calcium oxide tends to block the small water pipelines (for example, the risers) used in flat plate solar collectors. Other water characteristics, as the high level of PH and minerals lead to corrosive nature (especially at high temperatures), scaling or fouling issues and decrease the lifetime of the system. To avoid these problems, an indirect thermosyphon or indirect forced system is employed. The indirect system prevents mixing of household water with distilled water as working fluid**.**

The another problem with these types of direct and indirect SWHS using water or distilled water as heat transfer fluid suffer from freezing in winter season due to extreme cold climate, approaching freezing of water near zero or below temperature may break the riser tubes of collector due to expansion of water. To overcome relatively high freezing point of water, glycol additives are generally used along with water to act as antifreeze.

Since glycols have lower freezing point with respect to water, the glycols or mixtures of glycol (50/50 glycol to water ratio) are used as working fluids in the solar collector.

Lee and Sharma (2007) investigated the feasibility of ethylene glycol as heat transfer fluid for active and passive indirect solar water heating systems and also the thermal performance of these solar water heating systems based on annual operation. They suggested active solar water heating system for use in the cold climate. For the active and passive solar water heating system the highest collector efficiency was found to be 47% and 49% respectively.

The anti-freezing devices may also be installed to protect the collectors but increase the initial cost of t he system. Moreover, these anti-freezing valves have mechanical parts, and can fail after a few years of use.

Closed-loop systems with glycols are popular in areas with low temperatures because they offer good antifreeze protection. However, glycol antifreeze systems are more expensive to purchase and install and the glycol must be checked every year and replaced after every few years. The high boiling point of glycols increases the operating temperature of solar collectors so higher emission losses.

To overcome the limitation posed by high boiling points of glycols, several researches have been conducted to study the effectiveness in operating the solar water heating system involving two-phase heat transfer process using various refrigerants/phase change liquids compared to the conventional single phase flow using water.

2.1.3 Phase change liquids/Refrigerants

A fluid's lower boiling point presents some advantages in flat plate solar collector water heating systems. First, the collector operates at lower fluid saturation temperatures, preventing higher heat losses. Second, the evaporation condensation recirculation cycle starts earlier and hence the heat transfer to the water in the storage tank increases. Third, the latent heat of vaporization is greater at lower temperature and pressure of saturation, so more energy is transferred to the water.

Based on this concept, alternative working fluids such as acetone, methanol or ethanol have been considered for substituting water or glycols in the flat plate collector in view of the fact

that the fluids have low boiling point coupled with high latent heat of evaporation.

These working fluids are also in liquid state near the atmospheric pressure and ambient temperature, therefore it is possible to extract air from the closed circuit and reach a partial vacuum just after each fluid charge and reduce the boiling point of the fluid.

Table 2.2: Thermodynamic properties of the working fluids used (NIST, 2007)

Working Fluid → / Property↓	Acetone	Methanol	R134a	R410A
$T_{freezing}$ at P_{atm} (^{0}C)	-94.7	-97.7	-101	-136
$T_{boiling}$ at P_{atm} (^{o}C)	56.5	64.4	-26.1	-52.7
h_{fg} at 0^0C (kJ/kg)	558.8	1205.1	198.6	221.3
h_{fg} at 50^0C (kJ/kg)	508.1	1127.9	151.8	135.1
P_{sat} at 50^0C (bar)	0.8	0.55	13.2	30.7

For instance, as shown in Table 2.2, the latent heat of vaporization of acetone at 0^0C is 558.8 kJ/kg and it is reduced to 508.1 kJ/kg at 50^0C. Methanol is an attractive working fluid due to its high latent heat of vaporisation, in comparison to other working fluids. Although methanol has a high boiling point at P_{atm} (64.4^0C), the boiling point of methanol is reduced to 43.1^0C at Pi = 0.46 bar (absolute).

Soin et al. (1979, 1987) stated that the problems like corrosion, fouling and freezing

presented in the single phase systems are eliminated in two-phase systems. They investigated the thermal performance of a thermosyphon solar collector charged with acetone and petroleum ether as working fluids in an experimental set up consisted of a collector, a vapour liquid separator and a condenser. They examined the effect of insolation and the liquid level on the collector performance and reported that the efficiency of two-phase collector was only 6–11% which was lower than a direct thermosyphon SWH system.

Kaushika et al. (1982) found increased collector efficiency with the increase in liquid length until a point is reached, when the region of super heating causes the vapor to disappear. They also found that the efficiency was high when a heat removal fluid of high latent heat of vaporization was used in the collector. An increase in the saturation temperature of the working fluid in the collector reduced its efficiency.

Esen and Yuksel (2000) manufactured a two-phase thermosyphon solar collector with heat pipes, and studied experimentally various phase-change fluids (acetone, methanol, and ethanol) to evaluate the effect of insolation and mass of fluid on the collector performance. It was observed that such a collector could be successfully used, especially during cold, cloudy and windy days.

Mathioulakis and Belessiotis (2002) presented the results of a theoretical and an experimental investigation of the energy behaviour of a new type of solar system employing a heat-pipe filled with ethanol. The energy behaviour of the system was characterised by high instantaneous efficiencies up to 60%.

Islam et al. (2005) reported two singular tests in a two phase solar collector with acetone and methanol as a working fluid for a whole day in each case. They calculated the instantaneous

hourly efficiency and heat removal factor and found the maximum instantaneous efficiencies of 63% and 55% for methanol and acetone systems respectively. They concluded methanol to yield the best performance due to lowest top loss coefficient and the highest instantaneous efficiency.

Ordaz-Flores et al. (2011) used acetone and methanol as two different working fluids with two initial pressure condition (atmospheric pressure and partial vacuum) in the closed circuit using coil lengths of 6 m and 10 m with different filled fraction to obtain a good performance of the investigated two phase solar collector, and reduce the high pressures reached with the refrigerants fluids. They found that with methanol, the highest experimental efficiency obtained was 43.7%, in the 10 m coil at a filled fraction of 0.53 while for acetone 49.7% working in the 6 m coil at a filled fraction of 0.55 for two phase solar collector.

Among these working fluids, acetone has a lower boiling point of 57°C at atmospheric pressure and hence this may be chosen as the working medium. Since acetone is inflammable, irritating and easily evaporating fluid, care should be taken while filling the fluid.

Use of refrigerant as working fluid in solar collectors is one of the important development in SWHS. Low freezing points, low boiling point, high heat capacities and use of latent heat to transfer energy from one place to another of the refrigerants find special interest in solar applications and prove them more effective than other fluids especially during cloudy conditions.

In indirect (closed-loop) SWHS, chlorofluorocarbon (CFC) refrigerants are more commonly used as heat transfer fluids due to their stability, non-flammable, and noncorrosive properties,

low toxicity and low freezing point. Specific examples of refrigerants include: R-11, R-12, R-13, R-113, R-114, and R-115. Several research studies have been conducted in order to study the effectiveness in operating the SWHS involving two-phase heat transfer process using refrigerants as working fluid.

Schreyer (1981) experimentally investigated the effectiveness of fluorocarbon refrigerant (R-11) in a thermosyphon solar collector and found that, the energy collection improved at low collector temperature and peak instantaneous efficiency increased by 6% for two phase refrigerant charged solar collector.

Farrington et al. (1981) carried out a similar work on R-11 charged domestic SWHS for a single-family residence. The SWHS when operated on forced circulation mode could realize an efficiency of 35%.

Bottum (1981) analyzed the observations of more than four years on both hydronic and phase change domestic water heating systems and concluded that with proper installation and maintenance, hydronic system could also yield higher output. However, refrigerant charged systems were more efficient, usually required less maintenance, and the possibility of freezing for collector's working fluids was eliminated.

Kamal (1984) reported that the low efficiency of refrigerant charged SWHS might be increased by charging the collector to the fullest; i.e., the fluid levels in the inlet of the tubes to be nearly the same as the outlet.

Fanney and Terlizzi (1985) conducted indoor experiments on R-11 driven SWHS to determine the effect of irradiance level on the thermal performance, and concluded that it was negligible for the irradiance levels considered. To further analyze the R-11 driven SWH

system, they developed ‘‘Fanny-Terlizzi correlation’’ to predict the heat transfer by R-11 and were validated with experimental data.

Yilmaz and Ogulata (1990) used a two-phase solar collector in a water heating system with refrigerant as working fluid. They reported the feasibility of refrigerants in flat plate solar collector without the risk of freezing, corrosion and fouling. They also suggested greater tank height than half of collector height for satisfactory performance of two phase collectors.

Radhwan et al. (1990) investigated experimentally the thermal performances of two R-11 charged integrated solar water heaters for forced and natural circulation water flows. The results showed that the inclination of the condenser integrated within the collector frame had a remarkable effect for natural circulation water flow, while it had no significant effect for forced circulation flow.

Radhwan and Zaki (1993) depicted the thermal non equilibrium vapor generation process with fully refrigerant-filled collector tubes and showed the dependency of the thermophysical properties (temperature, pressure, and heat flux) of the refrigerant on the circulation flow rate while in phase change.

Pluta and Pomierny (1995) investigated the two phase thermosyphon domestic SWHS and emphasized on choosing the proper heat transfer medium, because it played an important role in operating conditions of a thermosyphon system.

Ghaddar and Nasir (1998) fabricated and tested an R-11 charged solar collector with an integrated condenser for secondary-cooling water flow. Forced circulation flow demonstrated instantaneous system efficiency values varying from 60% to 20%, which was in range of conventional water solar collectors.

Joudi and Al-Tabbakh (1999) conducted a theoretical analysis by computer simulation of a two phase thermosyphon solar domestic hot water system using R-11. The computer program and calculation procedure were first validated by comparing the results with established results of single phase systems. Then, calculations were performed for the two-phase thermosyphon system. The collector efficiency of the two-phase system was approximately 20% higher than a single phase collector. The system could attain instantaneous efficiency as high as 60%, which was in the range of conventional solar water collectors. Also; the response of the two-phase system was faster than a single phase system.

Payakaruk et al. (2000) studied the inclined thermosyphons employed with R-22, R-123, R-134a, ethanol, and water. The selected filling ratios were 50%, 80%, and 100% and reported its influence on the thermal efficiency of the system. It was found from the experiments that the filling ratio had no effect on the ratio of heat transfer characteristics at any angle to that of the vertical position, but the latent heat of vaporization of the working fluid affected the mentioned ratio of heat transfer rate. Lower the latent heat of vaporization, higher will be the heat transfer rate.

Esen and Esen (2005) also investigated the thermal performance of a two-phase thermosyphon flat plate solar collector with heat pipes, using different refrigerants under sky clear conditions. They constructed three small-scale solar water heating systems for their experiments, and compared the performance of systems, simultaneously under same operating conditions using R134a, R407C and R410A as working fluids. They found that the R410A offered the highest solar thermal energy collection performance among the working fluids used.

Chen et al. (2009) analyzed the influence of various heat transfer mechanisms, such as natural convection, geyser boiling, nucleate boiling, and film condensation in the two phase thermosyphon SWH process. It was reported that by maintaining two-phase flow, it was possible to minimize heat losses and the system could attain about 18% in its characteristic efficiency.

Chien et al. (2011) developed a theoretical model to find the optimal filling ratio for the maximum solar intensity values, and the model was validated with the experimented data. They reported a charge efficiency of 82% in their test result which was higher compared to the conventional SWH systems.

The refrigerants working fluids like R134a or R410A have low boiling points at atmospheric pressure (below 0^{o}C) (NIST, 2007), and low latent heat of vaporization below 250 kJ/ kg at 0^{o}C. Both acetone and methanol have higher latent heat of vaporization than R134a and R410A.

R134a and R410A work at very high pressures, as observed from Table 2. The high operating pressures of R134a (13.2 bar at 50^{o}C) and R410A (30.7 bar at 50^{o}C) might compromise the technical feasibility and integrity of this system.

Then, working with acetone and methanol converge on the safety of the equipment. Furthermore, the thickness of the tubes could be reduced and the construction could be easier; this, because the need to construct the systems to bear high pressure would become redundant, and ordinary welded joints could be used instead of special and more expensive ones. According to the Copper Development Association 2011a, b both acetone and methanol can be used with copper without corrosion problems. Although boiling points of

acetone and methanol at atmospheric pressure are higher than those of R134a and R410A, they can be compensated by their higher latent heat of vaporization (558.8 kJ /kg at 0^oC for acetone, and 1205.1 kJ /kg at 0^oC for methanol).

Most of the refrigerants that are commonly being used are either chloro-fluorocarbon (CFC) or hydro-chloro-fluorocarbon (HCFC) which is known to have a detrimental impact on the environment. On the basis of global warming potentiality (GWP), the European Union (2006) has passed legislation approving the phase-out process of refrigerants having GWP more than 150. Research on natural refrigerants, such as ammonia (NH_3), carbon dioxide (CO_2), air has gained momentum. The study reported that it was possible to effect natural convective flow, when CO_2 fluid is heated to supercritical state, because its density was strongly dependent on temperature and pressure. This was sufficient to affect the water heating process. Salient features of different types of SWH systems using phase change fluids are summarized in Table 2.3.

Table 2.3: Summary of studies on indirect SWH systems using phase change liquids as working fluid

S.No.	Investigator(s)	Type of study	Type of collector	Working fluid	Results
1	Soin et al. (1979, 1987)	Experimental	FPC	Acetone Petroleum ether	Efficiency of the two-phase collector was 6–11% than similar thermosyphon SWHS
2	Farrington et al. (1981)	Experimental	FPC	R-11	$\acute{\eta}_{SWH}$ = 35%
3	Radhwan and Zaki (1993)	Experimental	FPC	R-11	$\acute{\eta}_{SWH}$ = 60-80%
4	Essen and Essen (2005)	Experimental	FPC with heat pipe	R-134a, R-407C, R-410A	Detailed temp. distribution and cumulative collector efficiencies were determined
5	Chien et al. (2011)	Experimental and Theoretical	FPC with heat pipe	Alcohol	$\acute{\eta}_{SWH}$ = 82%
6	Chen et al. (2009)	Experimental and Theoretical	FPC with heat pipe	Alcohol	$\acute{\eta}_{SWH}$ = 63%

7	Chaturvedi et al.(1998)	Experimental and Theoretical	FPT	R-12	COP = 2.5–4.0 (30–70 Hz frequency range)
8	Hawlader et al.(2003)	Experimental and Theoretical	Air collector		COP (system) = 6.0; ή(air-collector) = 0.77;
9	Chyng et al.(2003)	Experimental and Theoretical	Tube-in-sheet type	R-134a	COP = 1.7–2.5 (year round); T_{water} = 57.2^{0}C;
10	Kuang et al.(2003)	Experimental and Theoretical	FPC	R-22	COP (monthly avg.) = 4–6; ή(collector) = 0.4–0.6;
11	Li et al.(20 07)	Theoretical	Aluminum plate	R-22	COP (seasonal) = 5.25; ή(collector) = 1.08; T_{water} = 50.5^{o}C
12	Huang et al.(2005)	Theoretical	Tube-in-sheet type	R-134a	COP (HP-mode) = 2.58; COP (hybrid-mode) = 3.32
13	Guoying et al.(2006)	Experimental and Theoretical	Cu–Al spiral-finned tubes	R-22	COP (monthly avg.) = 3.98 – 4.32; T_{water} = 55^{o}C

2.2 Particle-laden fluids

Common heat transfer fluids such as water, ethylene glycol, and refrigerants have relatively low thermal conductivity and thus cannot reach high heat exchange rates in solar collectors. A way to overcome this barrier is using ultra fine solid particles (millimeter, micron and nano sized) suspended in common fluids to improve their thermal conductivity and to enhance heat transfer rates in SWHS.

Otanicar et al (2009) investigated solar-weighted absorption coefficient for fluid's baseline capacity for absorbing solar energy and found that water was the best absorber among the four tested liquids namely water, ethylene glycol, propylene glycol and Therminol VP- 1. However, water was still a weak absorber, only absorbing 13% of the energy over the solar spectrum, demonstrating the necessity of seeding the fluid with some sort of particle to enhance the absorption properties of the base fluid.

The advantage of using a particle-laden-fluid is that due to the presence of the small particles, scattering of incident radiation takes place, which can increase radiative absorption, and hence an enhancement in collector efficiency by using direct solar absorption concept through particle laden fluids.

The idea of volumetric absorption using fluid suspended with small particles has been proposed long before **(Minardi and Chuang, 1975; Copeland et al., 1982)** the ability to controllably synthesize nanoparticles. Researchers have suggested various alternative configurations for solar absorption by using particle laden fluids instead of conventional fluid including the concept of direct solar absorption. Both experimental and numerical models were presented by different researchers to assess the feasibility of particle laden direct absorption solar collectors.

2.2.1 Millimeter and micron sized particles based fluids

Minardi and Chuang (1975) one of the first instances, tested low flux solar collector using black liquids containing millimeter to micrometer sized particle, from a water soluble dye, to directly absorb incident solar radiation and showed improvements to efficiency**.** This water soluble dye solution produced a "black" fluid with black particles agglomerated in the micron size and having excellent photo thermal properties.

Hunt (1978) and Abdelrahman (1979) conducted their studies on solar central receivers and originally proposed gas-particle suspension based volumetric absorption for solar central receivers. They showed that this volumetric absorption could be greatly enhanced by suspending small particles within the working fluid.

To model the coupled radiative and convective heat transfer inside the particle based receivers, researchers have developed numerical models capable of predicting the response of these systems at high temperatures. Several studies on development of mathematical framework for modeling of solar radiation absorption in thin films have been reported. Initial models of fluid-based volumetric receivers focused on non-scattering semi-transparent fluids flowing over opaque surfaces.

Copeland et al. (1982) proposed the concept of direct absorption for enhancing the efficiency of cavity-type collectors in power towers. In this type of receivers, a thin film of molten salt flew over an inclined surface due to gravity, and was exposed to highly concentrated solar radiation.

Houf et al. (1984) developed a three-dimensional laminar flow model to predict effects of liquid velocities, radiative properties of liquid and substrate, intensity of solar irradiation and influence of buoyancy forces on hydrodynamic and thermal conditions.

Webb and Viskanta (1985) numerically investigated the heat transfer characteristics of gravity-driven semitransparent molten salts flowing over an opaque substrate subjected to solar irradiation. The effects of model parameters such as substrate emissivity, fluid layer opacity, spectral nature of incident radiative flux, flow model, and fluid layer physical thickness on collector efficiency was investigated.

Yuncu et al. (1987) presented a new solar collector employing black liquids as working fluid within a transparent tube and showed exceeded thermal performance levels of conventional collectors in the low and medium temperature range.

Kumar and Tien (1990) investigated a flowing molten salt receiver seeded with small particle. They proposed a detailed mathematical model for absorption of solar radiation in particulate-laden falling liquid film. The model accounted for radiative and convective transport, absorption, emission, scattering, and spectral and angular variations of radiation and radiative properties. Effects of particle loading, particle diameter, and film thickness and variable thermo-physical properties on temperature distribution within the fluid layer were analyzed.

Miller and Koenigsdorff (2000) found that in addition to the benefit of absorbing within the volume, the surface area of 1 gram of 0.5 μm particles is nearly 6 m^2 resulting in large areas for absorption at relatively low particle loadings. The temperature difference between the absorbing particles and the fluid had been shown to be negligible owing to the particles large surface to volume ratio. They also numerically modeled solar absorption inside a high-flux gas particle rectangular receiver and the oxidation of carbon particles in a three-dimensional model.

Bertocchi et al. (2004) experimentally presented to assess the feasibility and advantage of suspending micron-sized particle in a high-velocity gas stream for high flux collectors. They demonstrated carbon particles in gases as both solar radiation absorbers and heat transfer medium to be very efficient in the high temperature range.

These studies all focus on concentrated flux sources incident upon gas-particle suspensions, but **Arai et al. (1984)** performed numerical studies of the transient response of a solar collector using a "fine particle semitransparent liquid suspension". The particles in the study by Arai were limited to the 5 micron range (5000 nm) and tests were performed under indoor infrared heat lamps.

2.2.2 Disadvantages of using millimeter and micron sized particles

Usually, black liquids are ink-based fluids which contain various organic compounds and inorganic particles. Organic inks, however, show serious drawbacks because they suffer light-induced degradation, thermal degradation at the high operating temperatures, instability of solutions with the passage of time and fouling of inks on the internal side of exposed surfaces.

The application of these micron-sized particles for direct absorption solar collector (DASC) suffer from particles settling out of solution, clogging of pumps and valves from coarse particles, fouling of transparent tubing and absorption spectrums dominated by the bulk material properties **(Minardi and Chuang, 1975).**

For these reasons, with the advancement in nanotechnology for producing nano size particles, a recent development in solar thermal collectors is the use of nanofluids as heat transfer fluid to directly absorb solar radiation. Nanofluids, compared to suspensions with particles of

millimeter-or-micrometer size, show better stability, rheological properties, and considerably higher thermal conductivities.

2.3 Nano sized particles based fluids (nanofluids)

The term ‘nanofluids’ applies to colloidal suspensions of nano sized particles (1-100 nm), in a conventional base fluid, which have been the subject of much recent study for their potentially enhanced thermal transport characteristics **(Wang and Majumdar, 2007; Trisaksri and Wongwises, 2007; Angayarkanni and Philip, 2015).**

Nanofluid is a new class of heat transfer fluids containing stably suspended nano-sized particles, fibers, or tubes in the conventional heat transfer fluids such as water, ethylene glycol, engine oil, etc. **(Choi, 1995)**. Several researchers have reported that nanofluids could effectively improve the solar energy utilization **(Mao et al., 2008)**.

Nanofluids consisting of such particles suspended in liquids (typically conventional heat transfer liquids) have been shown to enhance the thermal conductivity and convective heat transfer performance of the base liquids (**Natarajan and Sathish; 2009).**

Initially, some studies conducted on thermal conductivity and optical properties of nanofluids are briefly reviewed, because these parameters can determine the potential of nanofluids to enhance the performance of solar collector systems. Then, the application of nanofluids in solar collectors and water heaters are investigated from the performance aspects **(Moghadam et al., 2014; Zamzamian et al., 2014**).

Sani et al. (2010, 2011) reported the optical characterization of a new fluid consisting of single-wall carbon nanohorns (SWCNH) and ethylene glycol for solar energy applications. They concluded that carbon nanohorns could enhance remarkably the sunlight absorption with respect to pure base-fluid. The results obtained were compared with those obtained for

fluids suspending more conventional carbon forms, i.e., carbon-black particles. They found that spectral features of nanohorns were considerably more favourable than those of amorphous carbon for a specific application. This result shows that using carbon nanohorns-based nanofluids in thermal solar devices leads to the enhancement of efficiency and compactness of the system.

Mercatelli et al. (2011 and 2012) investigated the potential of single-wall carbon nanohorns nanoparticles with two different base fluids including water and glycol. Their measurements showed that these nanofluids are very suitable for direct absorption solar devices because only about 5% of the total extinction is scattered by SWCNH particles. They also applied a simple spectrophotometric to estimate the spectral scattering albedo of SWCNHs/water nanofluid.

Said et al. (2013, 2014) investigated the effects of the size, shape, and structure of nanoparticles on the optical properties of the nanofluids and perceived that the shape and size of the nanoparticle have great effect on the optical properties of a nanofluid.

Sajid et al (2014) reviewed the optical properties of aluminum nanoparticles and studied the shape and size dependence of radiative, and photo thermal properties of nanocrystals.

Long et al (2014) investigated the optical properties of ethanol based nanofluids containing multiwalled carbon nanotubes (MWCNTs), carbon and aluminum nanoparticles. They concluded that MWCNTs led to more absorption than aluminum and carbon nanoparticles.

Saidur et al. (2012) investigated the potential of Aluminum/water nanofluid to use in direct absorption solar collectors. They concluded that Aluminum/water nanofluid with 1% volume

fraction improved considerably the solar absorption so that it was a fine solution for a direct solar collector. They also found that the extinction coefficient varied linearly with volume fraction.

Kameya and Hanamura (2011) found experimentally that the solar radiation absorption for the nanofluid of Ni/alkyl naphthalene with 0.1% volume fraction was much higher than the base fluid.

Colangelo et al. (2012) measured the thermal conductivities of CuO, Al_2O_3, ZnO and Cu with different shapes and volume fraction up to 3%, where water and diathermic oil were the base fluids, to evaluate their potential to use for high temperature applications such as in solar collectors. They found that the thermal conductivity enhancement of the nanofluids with diathermic oil was higher than that with water, with the same nanoparticles and at the same conditions. They observed thermal conductivity reduction with increasing the size of particles.

The application of nanofluids as a working medium for solar collectors is a relatively new concept. Due to their small size and physical properties a comprehensive analysis of radiative heat transfer of nanofluids is inherently complex. In some recent studies, same aspects of this complex behaviour have been addressed **(Prasher et al, 2005)**.

Addition of nanoparticles to a base fluid, offers potential of improving the radiative properties of liquids because of enhanced scattering and absorption leading to an increase in the efficiency of DASCs. Additionally, the mixing of nanoparticles in a liquid has been shown to enhance other liquid thermo physical properties such as thermal conductivity and particle stability over micron-sized suspensions, which provide potential improvements to the

operating efficiency of a DASC. Besides larger solar absorption area and actual installation surface area ratio due to the contribution of nanoparticle surface area, the impact of particles on the absorption of radiative energy has been of interest for a solar collector application (**Ladjevardi et al; 2013, Karami et al; 2014, Seung et al; 2015**).

Lenert and Wang (2012) and **Lenert et al (2010)** presented a combined theoretical and experimental work to optimize the efficiency of liquid-based solar receivers seeded with carbon-coated absorbing nanoparticles. They concluded that the efficiency of nanofluid volumetric receivers increased with increasing solar concentration and nanofluid height.

Tyagi et al. (2009) numerically investigated the feasibility of a non-concentrating direct absorption solar collector using nanoparticle suspension in water and compared its performance with a typical low flux flat plate solar collector. They simplified past models to specifically model a nanofluid collector and reported the effects of different parameters on the efficiency of a nanofluid based DASC. Aluminum-water nanofluids were used and it was observed that the presence of small particles causes scattering of the incident radiation leading to nine times higher levels of radiative absorption over that of pure water. The modelling results showed that the absolute efficiencies of the Al-water nanofluid-based direct absorption solar collectors were about 10% higher than that of the conventional flat-plate type collector using pure water under similar operating conditions. The results showed that by adding nanoparticles to the working fluid, the efficiency increased remarkably for low volume fraction of nanoparticles (0.1% to 2%). They attributed the increase of collector efficiency to the increase in attenuation of sunlight passing through the collector due to the addition of nanoparticles. However, for a volume fraction higher than 2%, the efficiency

remained nearly constant, so adding more nanoparticles was not beneficial. The study also investigated the effects of nanoparticles size on the collector efficiency for volume fraction of 0.8% and result showed slight efficiency increase with nanoparticle size.

Otanicar et al. (2010) built their model by including multiple and dependent scattering, and size-dependent optical properties for nanofluid systems. They conducted numerical and experimental analyses on a micro scale direct absorption solar collector of size 3 cm x 5 cm with a channel depth of 150 μm and investigated the experimental results for variety of nanoparticles such as Graphite, Carbon Nano Tubes, and Silver using water as base fluid. The flow rate was controlled via a syringe pump and was set to 42 ml/h. These fluids were tested by varying volume fraction of the nanoparticles in the base fluid and varying particle size. They demonstrated that adding small quantities of nanoparticles leads to the enhancement of the efficiency up to maximum of 5% until a volume fraction of approximately 0.5%. After a volume fraction of 0.5%, the efficiency began to level off and even decreased slightly with increasing volume fraction. The authors attributed this reduction to the high increase of the fluid absorption at high particle loadings. When silver nanoparticle size reduced from 40 to 20 nm, a 6% efficiency increase was observed.

Li et al. (2011) studied the effects of three different nanofluids, Al_2O_3-water, ZnO-water, and MgO-water, on the performance of a tubular solar collector. The results showed that ZnO–H_2O nanofluid with 0.2% volume concentration was the best selection for the collector.

Taylor et al. (2011a) investigated the performance of a newly designed laboratory scale nanofluid-based concentrating solar thermal receiver and compared with a conventional one. The authors claimed that nanofluids had excellent potential for solar thermal power plants and 10% improvement in efficiency might be possible by substituting the working medium,

water, with 0.125% volume fraction of graphite nanofluid. They also described the economic implications for the application of nanofluid in high flux solar collector and concluded that nanofluids were not found to be suitable for dish or trough solar power system due to the high cost and economic factors.

Taylor et al. (2011b) investigated the optical property characterization of graphite, silver, copper, gold, and aluminum nanoparticles with water and VP1 as the base fluids to determine their potential to be used in direct absorption solar collectors. Study revealed that over 95% of incoming sunlight can be absorbed (in a nanofluid thickness ≥10 cm) with very low nanoparticle volume fractions (less than 1×10^{-5}, or 10 ppm).

Andrej (2010) investigated nanofluid-based receivers for high-temperature, high-flux direct solar collectors where using volumetric receivers were more efficient at higher levels of concentration and could lead to ideal power generation efficiencies exceeding 55% in these regimes.

Lenert and Wang (2012) concluded that volumetric nanofluid receivers when integrated with a power cycle can cause the efficiency to go higher than 35%. They also outlined that optical thickness and solar concentration play substantial role in the performance.

Lu et al. (2011) stated that mass concentration of nano particles can remarkably affect the performance and heat transfer in a solar collector (evaporating heat transfer coefficient was augmented up to 30%).

He et al. (2013) studied the light heat alteration features of water-carbon nanotube (CNT) and water–TiO_2 nanofluids in a vacuum tube solar collector. The experiment was performed under both sunny and cloudy weather conditions. The investigation outcomes showed excellent light heat conversion characteristic for nanoparticles weight concentration of 0.5%

CNT–H_2O nanofluid. Because of the better light-heat conversion characteristics of the CNT–H_2O nanofluid compared to the TiO_2–H_2O nanofluid, the temperature of the CNT–H_2O nanofluid was higher than that of the TiO_2–H_2O one. This means that CNT–H_2O nanofluid is more suitable than the TiO_2–H_2O for utilized in a vacuum tube solar collector.

Yousefi et al. (2012a) examined the experimental results on a tube-in-plate type conventional solar collector (size 2 m^2) using Al_2O_3-H_2O nanofluid as a working fluid for various mass flow rates with two different weight fractions of the nanofluid, 0.2 % and 0.4 % , with and without Triton X-100 surfactant and showed that using 0.2 wt% Al_2O_3 nanofluid increased the efficiency of solar collector by 28.3% in comparison with water and by using the surfactant, the maximum enhanced efficiency was 15.63%. The solar collector was tested for mass flow rates of 1, 2, and 3 liter/min. Study concluded that for higher mass flow rate the efficiency of the collector was high and as the mass flow rate was reduced the collector efficiency also decreased. The experimental data were fitted with linear equations to provide the characteristic parameters of the flat-plate solar collector in order to compare the effect of various mass flow rates.

Yousefi et al. (2012b) used the experimental setup and examined the effects of multi wall carbon nanotubes (MWCNT)-water nanofluid on the efficiency of the flat plate solar collector. They observed that:

(i) Efficiency of the collector using MWCNT-water nanofluid without surfactant was remarkably increased up to 35% for 0.4 wt% nanofluid, whereas with 0.2 wt % the efficiency reduced compared to water as the working fluid.

(ii) For 0.2 wt% nanofluid, using surfactant increased the efficiency of the collector compared to water.

Yousefi et al. (2012c) investigated the effects of pH variation of the MWCNT–water nanofluid on the efficiency of the flat plate collector. They used 0.2 wt% MWCNT with three pH values of 3.5, 6.5, and 9.5 and Triton X-100 as an additive. Study concluded that an increase on the difference between the pH of nanofluid and that of the isoelectric point causes higher efficiency. The isoelectric point is the point at which the molecules carry no electrical charge. For MWCNT, the pH of the isoelectric point is 7.4.

Khullar et al. (2010) theoretically examined a concentrating parabolic solar collector with nanofluid as the heat transfer fluid. The collector was modelled as a two dimensional steady system, and the finite difference method was employed to numerically solve the equations. They computed all the parameters quantitatively and compared the results obtained with the experimental results of conventional parabolic solar collectors under similar conditions. Aluminum nanoparticles with 0.05 vol% were suspended in Therminol VP-1 as base fluid for the analysis. Analysis revealed that the thermal efficiency of nanofluid based collector compared to a conventional parabolic solar collector was about 5-10% higher under similar weather conditions.

Khullar et al. (2013) studied solar energy harvesting using nanofluids-based concentrating solar collector. The theoretical study indicated that the nanofluid-based concentrating parabolic solar collectors had the potential to harness solar radiant energy more efficiently than a conventional parabolic trough.

Phelan et al. (2012) analyzed and compared the theoretical and experimental results of a nanofluid-based concentrating parabolic solar collector (NCPSC) with conventional concentrating parabolic solar collectors under similar conditions. They injected 0.05 vol% aluminum nanoparticles suspended in Therminol VP-1 as the base fluid. They realized that

5–10% improvement in thermal efficiency of NCPSC could be conceivable when comparing it to a conventional parabolic solar collector.

Tiwari et al. (2013) theoretically investigated the effect of Al_2O_3 nanofluid as an absorbing medium in a flat-plate solar collector and also studied the effect of mass flow rate and particle volume fraction on the efficiency of the collector. Their results showed that use of the optimum particle volume fraction of 1.5% Al_2O_3 nanofluid increased the thermal efficiency of solar collector in comparison with water as working fluid by 31.64%.

Chaji et al. (2013) tested a small flat plate solar collector for studying the effects of different nano particle concentration at various flow rates using TiO_2-Water nanofluid as a working fluid. European standard EN 12975-2 test method was selected for experimentation. The authors observed 6.7% and 15.7% enhancement in the maximum collector efficiency for 72 and 108 liter/m^2hr mass flow rate in comparison with 36 liter/m^2hr.

Liu et al. (2013) designed a novel evacuated tubular solar air collector to deliver air with high and moderate temperature. They integrated it with simplified compound parabolic concentrator and special open thermosyphon employing water based CuO nanofluid as the working fluid. Experimental outcomes revealed that the air outlet temperature and system collecting efficiency of the solar air collector using nanofluid as the open thermosyphon's working fluid were higher than water.

Polvongsri and Kiatsiriroat (2014) investigated the thermal enhancement of a flat plate solar collector with silver nanofluid. In this study, 20 nm silver particles mixed with water at the concentrations of 1,000 and 10,000 ppm were undertaken in 3 small identical closed-loop flat-plate solar collectors, each with an area of 0.15 m × 1.0 m. The mass flux of the working fluid varied between 0.8 and 1.2 l/min-m^2 and the inlet temperatures were controlled in the

range of 35–65^{o}C. The tests were performed outdoor under steady-state condition. The experimental results showed that at 10,000 ppm concentration, the heat transfer coefficient was about 2 times that of water. They also concluded that use of this nanofluid could improve thermal performance of flat plate collector compared with water especially at high inlet temperature.

Table 2.4 summarizes the important outcomes from different types of solar collectors for water heating using nanofluid as heat carrier fluid from the previous research work.

Table 2.4 Summary of research works on solar collectors using nanofluids.

S. No.	Reference	Type of study	Collector type	Nanofluid type and nanoparticle size	Results
1	Tyagi et al. (2009)	Theoretical	Direct absorption flat plate	Al-water (0-20 nm)	Efficiency increases for volume fraction less than 2% and remains nearly constant for volume fraction higher than 2%
2	Otanicar et al. (2010)	Theoretical and experimental	Micro-scale, Direct absorption flat plate	Graphite/ water (30 nm) silver/ water (20 and 40 nm) carbon nano tube/ water (6–20 nm dia, 1000–5000 nm length)	Efficiency increases for volume fractions less than 0.5% and for volume fractions higher than 0.5% may even decrease
3	Taylor et al. (2011)	Theoretical and	Concentrating Direct absorption	Graphite/therminolVP1, Al/ Therminol VP-1,	Efficiency increases up to 10% by using a nanofluid in the receiver

		experimental	For dish/power towers	Silver/Therminol VP-1 Copper/Therminol VP-1 (10–100 nm)	Using graphite/therminol VP-1 nanofluid with volume fractions less than 0.001% is beneficial for 10–100 MW power plants
4	He et al. (2011)	Experimental	Vacuum tube	TiO_2/water (5–10 nm) CNT/water (10– 50 nm diameter, 100–1000 nm length)	CNT/water nanofluid is more suitable than the TiO_2/water to be used in a vacuum tube solar collector
5	Li et al. (2011)	Experimental	Tube type	Al_2O_3/water ZnO/water MgO/ Water (size < 20 nm)	ZnO/water nanofluid with 0.2% volume concentration is the best selection for the collector
6	Taylor et al. (2011)	Theoretical and experimental	Direct absorption (Lab Testing of optical properties)	Graphite/water and graphite/VP1 Al/water and Al/VP1 cu/water and cu/VP1, silver/water and	Over 95% of incoming sunlight can be absorbed for nanofluid thickness ≥10 and nanoparticle

				silver/VP1gold/water and silver/VP1	volume fractions less than $1x10^{-5}$.
7	Lenert et al. (2011)	Theoretical and experimental	Direct solar absorption column, Lab-testing	Graphite shell and cobalt core particle with VP-1 oil base fluid	Up to 10% efficiency improvement
8	Lenert et al. (2012)	Theoretical and experimental	Concentrating collectors	Graphite shell and cobalt core particle with VP-1 oil base fluid	Up to 10% efficiency improvement
9	Veeraragavan et al.	Theoretical	Concentrating collectors	Graphite with VP-1 oil base fluid	Significant efficiency enhancement
10	Khullar et al. (2010)	Theoretical	Concentrating Parabolic	Aluminum/therminol VP-1 (5 nm)	Thermal efficiency of nanofluid concentrating parabolic collectors compared to a conventional

					parabolic solar collector is about 5– 10% higher
11	Yousefi et al. (2012)	Experimental	Tube in plate type	Al_2O_3/water (15 nm) Triton X-100 is used as a surfactant	Efficiency of the solar collector with 0.2% weight fraction (wt) nanofluid is higher than that with water by 28.3%
12	Yousefi et al. (2012)	Experimental	Tube in plate type	Water-MWCNT (10–30 nm), Triton X-100 is used as a surfactant	Efficiency of the collector increases remarkably for 0.4 wt.% by 35%
13	Yousefi et al. (2012)	Experimental	Tube in plate type	Water-MWCNT with various pH values: 3.5, 6.5, and 9.5 Triton X-100 is used as a surfactant	A bigger difference between the pH of nanofluid and pH of isoelectric point leads to higher efficiency

2.4 Potential Challenges of Nanofluids as working fluid

The use of nanofluids seems attractive in a broad range of applications due to their improved heat transfer and energy efficiency in a variety of thermal systems. But the development in the area of nanofluid application is hindered by many factors in which long term stability of nanofluid in suspension is a major reason. So, the following section focuses the possible challenges in the application of nanofluids that should be resolved in the near future.

(i) Instability and agglomerating

Long term physical and chemical stability of nanofluids is an important practical issue because of aggregation of nanoparticles due to very strong Vander walls interactions. So the suspension is not homogeneous. It should be also noted that for high temperature gradients the agglomeration of nanoparticles seems to be more serious. Physical or chemical methods have been applied to get stable nanofluids such as (i) an addition of surfactant; (ii) surface modification of the suspended particles; (iii) applying strong force on the clusters of the suspended particles. Researchers found that Al_2O_3 nanofluids kept after 3 days exhibit some settlement compared to fresh nanofluids. Particles settling must be examined carefully since it may lead to clogging of coolant passages.

(ii) Increased pressure drop and pumping power

Pressure drop and required pumping power during the flow of fluid determines the efficiency of nanofluid application. Using a nanofluid, density and viscosity of the fluid increases as compared to base fluid giving rise to higher pressure drop and consequently higher required pumping power. In some studies, up to 40% increase of pumping power has been estimated.

(iii) Lower specific heat

An ideal heat transfer fluid should possess higher value of specific heat so that the fluid can contain more heat. As nanofluids exhibit lower specific heat than base fluid, it limits the use of nanofluid application.

(iv) High cost of nanofluids

Nanofluids are prepared by either one step or two step methods. Both methods require advanced and sophisticated equipments. This leads to higher production cost of nanofluids. Therefore high cost of nanofluids is drawback of nanofluid applications.

(v) Erosion and corrosion of components

The presence of nanoparticles in nanofluid may lead to corrosion and erosion of thermal devices over a long period. **Celata et al. (2011)** recently investigated the effects of nanofluid flow effects on erosion and corrosion of metal surfaces. They conducted their experiments for TiO_2, Al_2O_3, SiC, and ZrO_2 nanoparticles with water as the base fluid where the nanofluids flow in pipes of three different materials, i.e., aluminium, copper and stainless. Study concluded that the nanofluids have no effect on the erosion of the stainless pipe, while the aluminium pipe has highest erosion. It was also observed that ZrO_2 and TiO_2 nanoparticles led to highest erosion while SiC nanoparticles resulted in lowest erosion.

2.5 Research Gap Identified/Learning's from literature review

The need for working fluids with improved performance has increased the scientific interest in nanofluid. A lot of research has undergone for the last decade for use of nanofluid in various engineering applications, especially in heat exchange systems. Several researchers have so far determined the enhanced heat transfer potential of nanofluid in automobile radiators for engine cooling systems, evaporators and condensers for HVAC systems, oil coolers, intercoolers etc. Relatively very less work has been

carried out on nanofluid based solar systems in particular on flat plate collector and studies are theoretical. In the theoretical studies on flat plate solar collector using nano fluid only miniature collector has been considered. None of them have made an attempt of using nanofluid in full scale or prototype solar flat plate collector experimentally.

A few international theoretical studies on solar collector show improved performance with the use of nano fluids in place of conventional fluid i.e. water. These studies show the importance of use of nano materials for thermal applications but no full scale study on solar flat plate collector has been performed using nanofluids. In this context the use of variety of nano materials for performance enhancement on direct solar flat plate collector is relevant, important and need of the hour from the point of view of performance enhancement.

With increasing worldwide awareness about the serious environmental problems due to fossil fuel consumption, efforts are being made to develop energy-efficient and environmentally friendly systems by utilization of non-polluting renewable energy sources. It is envisaged that through the use of nanofluid, economics and efficiency of solar flat plate collector system can be significantly improved. These systems would also be useful in saving energy in semi-urban/urban areas, as well as would find application in rural areas where power outage hours are long.

This research would therefore attempt to develop guidelines for determining the feasibility of nanofluid based solar flat plate collector indirect water heating system through experimental investigations.

CHAPTER 3

PREPARATION OF NANOFLUIDS

Nanofluids are prepared by dispersing nano size particles into the base fluid. Water, ethylene glycol and different types of oils are commonly used base fluids and Al_2O_3, TiO_2, CuO, copper, carbon nanotubes, gold and silver are nanoparticles that have been used mostly for this purpose. It is important to know the constituents of nanofluid for understanding the exact mechanism of various property change and heat transfer enhancement. Thus, preparation of nanofluids is an important stage for carrying out experimental studies that should be performed in a systematic and careful manner for uniform dispersion of nanoparticles into the base fluids. Basically nanofluids are not simply liquid-solid mixtures. While preparing nanofluid, it is necessary to fulfill the following conditions.

(i) There should be no chemical reactions between nano particles and the base fluid

(ii) There should be no agglomeration of the nanoparticles

(iii) Suspension should be even and stable

In general, nanofluids are prepared by two methods that are commonly known as one step and two step method. In the one-step method, the synthesis and dispersion of nanoparticles occur simultaneously. In two-step method, nanoparticles are added into a base fluid and then made into a stable suspension using mechanical methods. Both these

methods have their specified applications and advantages. In either case, the synthesis of nanoparticles is essential for preparation of nanofluid.

3.1 Synthesis of nanoparticles

Advances in nanotechnology provide great opportunities to produce materials at nanometer scales. Nanostructured materials are made of nanometer-sized particles engineered on the atomic or molecular scale to produce either new or enhanced physical properties that are usually not exhibited by conventional bulk solids.

A large variety of nanoparticles have been made using various materials, such as oxide ceramics (Al_2O_3, CuO), nitride ceramics (AlN, SiN), carbide ceramics (SiC, TiC), metals (Cu, Ag, Au), semiconductors (TiO_2, SiC), carbon nanotubes, and composite materials such as alloyed nanoparticles $Al_{70}Cu_{30}$ or nanoparticle core–polymer shell composites.

Methods for preparing nanoparticles are typically classified as physical and chemical methods. A number of different techniques are used by different researchers for synthesis of ultrapure nano size particles such as physical and chemical vapor deposition [Wu and Liu (2002)], co precipitation [Bacri et al. (1990), Gnanaprakash et al. (2006, 2007a, 2007b, 2007c)], sono chemical technique [Kumar et al. (2000), Okitsu et al. (2000), Carotenuto (2001)], sol–gel [Gurin et al. (2006)], hydrothermal [Li et al. (2004), Eftekhari et al. (2006)], solution phase method [Pastoriza and Liz (2002), Yin et al. (2002), Lin et al. (2003), Raveendran et al. (2003)], electrochemical synthesis [Zhu et al. (2000), Penner (2002), Yin et al. (2003), Qiu et al. (2003)] and laser ablation [Bjerneld et al. (2003), Fouchet et al. (2004)].

In the physical method, mechanical alloying was mostly used for preparation of nano size particles. In this method, high energy ball induces high energy impact on the charged powder by collision between balls and powder causing severe plastic deformation,

repeated fracturing and cold welding of charged powder leading to the formation of nanoparticles [Gleiter (1989, 2000), Suryanarayana (1995)].

Bönnemann et al. (1999a) developed a method for the production of very small (< 2 nm) and stable nanoparticles via chemical reduction pathways, which might be suitable for application in nanofluid synthesis. Organoaluminum compounds were used for the "reductive stabilization" of mono- and bi-metallic nanoparticles. Triorganoaluminum compounds were employed as both the reducing agent and colloid stabilizer, which led to the formation of an organo-metallic colloidal protecting shell around the particles [Bönnemann et al. (2002, 2003)]. This "modification" of the Al-organic protecting shell leaves the particle size untouched and allows tailoring of the dispersion characteristics of the original organosols at will. A vast spectrum of this solubility of the colloidal methods in hydrophobic and hydrophilic media including water has been achieved this way [Bönnemann et al. (1999b)].

The disadvantages of the electrolysis and sol-gel methods are their high cost and low yield of the product. In addition micro emulsion method leads to difficulties in controlling the size and reaction when preparing nanoparticles because it is a complicated process. The chemical reduction method is often preferred because it allows the mass production of nanoparticles through a relatively easy process.

3.2 Methods for nanofluid preparation

Preparation of nanofluids is the first key step to investigate the heat transfer performance of nanofluids. A nanofluid does not mean a simple mixture of liquid and solid nanoparticles. Techniques for proper dispersions of nanoparticles in liquids or directly producing stable nanofluids are crucial. Nanofluids are produced by dispersing nanometer-sized solid particles into liquids such as water, ethylene glycol, or oils. As

discussed earlier, single step method and two step method are the two techniques used for preparation of nanofluids. The earliest investigations of nanofluids used a two-step method in which nanoparticles are first produced as a dry powder and then dispersed into a fluid in a second processing step. The single step and two step methods are discussed in more detail in the following sections.

3.2.1 Single step method

The single step method consists of simultaneous preparation and dispersion of nanoparticles in the conventional heat transfer fluid. There are few methods available for the production of nanofluids by this technique which have been developed by different researchers.

Akoh et al. (1978) developed direct evaporation approach called Vacuum Evaporation onto a Running Oil Substrate (VEROS) technique to produce nanofluid. But, difficulty was faced in separating the particles from the fluids.

Wagener et al. (1997) proposed a modified VEROS method which employed a high pressure magnetron sputtering for the preparation of suspensions with metal nanoparticles.

Eastman et al. (1997) developed a modified VEROS technique in which Cu vapor was directly condensed into nanoparticles by contacting with a flowing vapor-pressure liquid mainly ethylene glycol.

Choi et al. (2001) developed a direct evaporation technique for the preparation of nanofluids in single step. Their setup consists of a rotating cylinder in which fluid was filled. In the middle of the cylinder, a source material was vaporized under vacuum conditions. As the vapor was condensed, it comes in contact with cooled liquid and nanofluids were prepared. The major advantage of this method is minimized

agglomeration of nanoparticles. The disadvantages are that the liquid have a very low vapor pressure and production of very limited quantity of nanofluids.

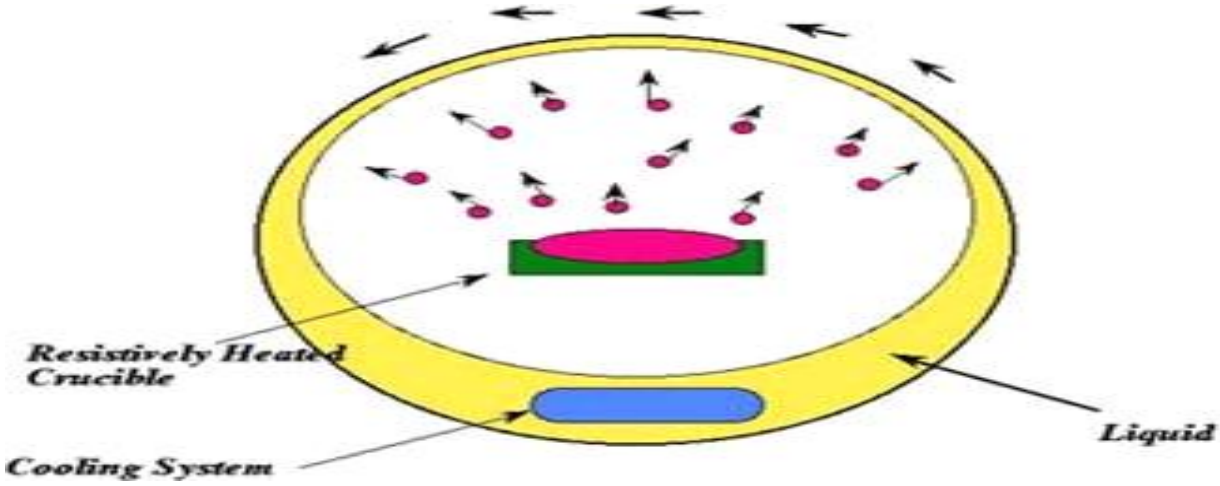

Fig 3.1 Diagram of direct evaporation single step nanofluid production system

Various single-step chemical synthesis techniques can also be employed to produce nanofluids.

Brust et al. (1994) developed a technique for producing metallic nanoparticles in various solvents by the reduction of metal salts to produce colloidal suspensions for a wide range of applications, including studies of thermal transport. Excellent control of size and very narrow size distribution was obtained by using such methods **(Keblinski et al., 2002**).

Zhu et al. (2004) presented a one step chemical method for the preparation of Cu nanofluids by reducing $CuSO_4 \cdot 5H_2O$ with $NaH_2PO_2 \cdot H_2O$ in ethylene glycol under microwave irradiation. Study observed that reaction rate and the properties of Cu nanofluids were greatly affected by microwave irradiation and with the addition of $NaH_2PO_2 \cdot H_2O$.

Lo et al. (2005) developed a Vacuum Submerged Arc Nanoparticle Synthesis System (SANSS) method to prepare CuO nanofluid by dispersing CuO nanoparticles uniformly

in a dielectric liquid (deionized water) with 30%, 50%, and 70% volume solution of ethylene glycol. This method successfully produced a stable nanofluid. In principle, a pure copper rod is submerged in a dielectric liquid in a vacuum chamber. A suitable electric power source is used to produce an arc between 6000 -12000°C which melts and vaporizes the metal rod in the region where the arc is generated. At the same time, the deionized water is also vaporized by the arc. The vaporized metal undergoes nucleation, growth and condensation resulting in nanoparticle dispersion in deionized water. Various copper based nanofluids such as Cu, CuO, Cu_2O can be prepared by this method. The major disadvantage of this technique is only low vapor pressure fluids can get along with this method.

The major advantage of single step method is no need of processes for drying, storage, and transportation, so the possibility for agglomeration of nanoparticles is minimized, and the stability of prepared fluids is increased. This method can prepare evenly dispersed nanoparticles, and the same can be stably suspended in the base fluid.

The main disadvantage with single step physical method is that it cannot prepare nanofluids in large scale, and the cost is also high, so the one-step chemical method developed rapidly. However, there are some disadvantages for this method also. The most important one is that the residual reactants are left in the nanofluids due to incomplete reaction or stabilization. It is difficult to elucidate the nanoparticle effect without eliminating this impurity effect.

3.2.2 Two step method

The preparation of nanofluids in two step method begins with formation of nanoparticles and subsequent dispersion of the nanoparticles in the base fluid. In the first step of this method, nanomaterials are synthesized and obtained as dry powders by chemical or

physical methods. Then, the nanosized powder is dispersed into the base fluid in second step with the help of any one of the following methods:

- Intensive magnetic force agitation
- Ultrasonic agitation
- High shear mixing
- Homogenizing
- Ball milling

In order to achieve stable and even suspension of nanofluids and suppress agglomeration, some researchers apply techniques during the preparation which include addition of surface activators and dispersants, control of the pH value of the suspension and use of ultrasonic vibration. The technique applied is usually such that properties of the constituents of the nanofluid are not significantly affected. This is because addition of surface active agents can affect the heat transfer performance of the nanofluid. Surface activators and dispersants that have been used by researchers include oleic acid, thiols, laurate salts and sodium dodecylsulfate. Fig. 3.2 shows the procedure for preparation of nanofluid.

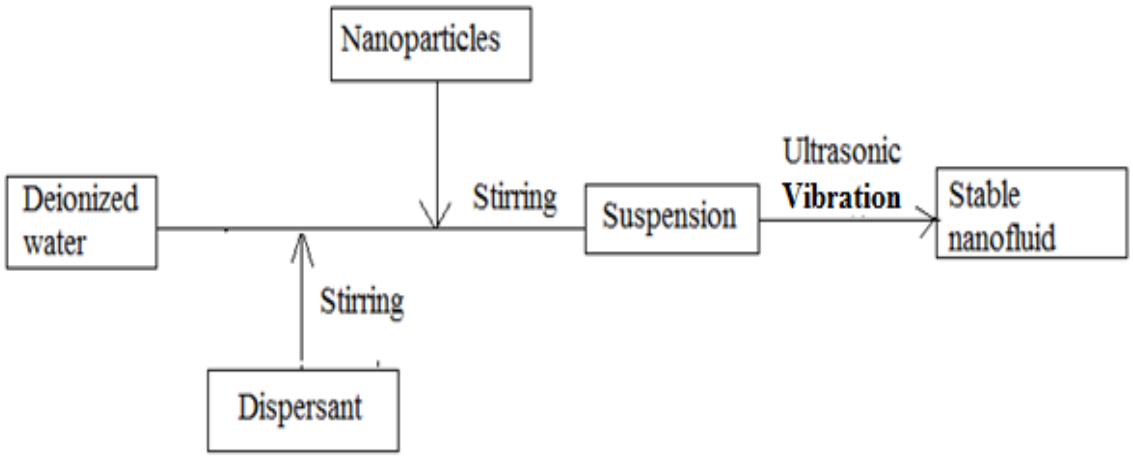

Fig 3.2: Procedure of preparation of Nanofluid

Three different methods available for preparation of stable and even suspension of nanofluids are outlined below (Edlestein and Cammarata, 2001).

(a) Addition of surfactants to the base fluid

In this method a small amount of suitable surfactant, generally one tenth of the mass of nanoparticles, is added to the base fluid and stirred continuously for few hours. Nanofluids prepared using surfactants will give a stable suspension with uniform particle dispersion in the host liquid. The nanoparticles remain in suspension state for a long time without settling down at the bottom of the container.

(b) Acid treatment of base fluid

The pH value of the base fluid can be lowered by adding a suitable acid to it. A stable nanofluid with uniform particle dispersion can be prepared by mixing nanoparticles in an acid treated base fluid. But acid treated nanofluids may cause corrosion on the pipe wall material with prolonged usage of nanofluids. Hence acid treated base fluids are not preferred for preparation of nanofluids even though formation of stable nanofluids is possible with such base fluids.

(c) Ultrasonic mixing

In this method, the nanoparticles are directly mixed in the base liquid and thoroughly stirred. Nanofluids prepared in this method give poor suspension stability, because the nanoparticles settle down due to gravity, after some time of nanofluid preparation. The time of particle settlement depends on the type of nanoparticles used, density and viscosity of the host fluid and duration of mixing.

Eastman et al. (1997), Wang et al. (1999) and Lee et al. (1999) have used ultrasonic method to prepare Al_2O_3 nanofluids. Similarly **Murshed et al. (2005)** employed the same method to prepare TiO_2 nanofluids. It was observed that this technique holds good for the

preparation of nanofluids having oxides nanoparticles. While for metallic nanoparticles this method is being less preferred.

Xuan et al. (2000) have used commercially available Cu nanoparticles to prepare nanofluids in both water and transformer oil by sonication in the presence of stabilizers.

Kim et al. (2005) prepared nanofluids consisting of commercially obtained CuO nanoparticles in ethylene glycol by sonication without stabilizers. The optimum duration of sonication was found to be 9 hours and the average nanoparticle size was 60 nm.

At present, most researchers use the two-step process to produce nanofluids by dispersing commercial or self-produced nanoparticles in a liquid. Some believe that the two-step process is more efficient only for preparing nanofluids containing oxide nanoparticles dispersed in de-ionized water as opposed to those containing heavier metallic nanoparticles (**Eastman et al., 2001**). Since nano powders can be obtained commercially in large quantities, some economic advantage exists in using two-step preparation methods that rely on the use of such powders. So, two step method can be economically used to produce nanofluids in large quantity. Due to difficulty in preparing stable nanofluids by two step method, several advanced techniques are developed to produce nanofluids, including one-step method.

The one-step method is a better method for preparing metallic nanofluids and it has the advantage of reduced agglomeration in the nanofluid. The one step process prepares uniformly dispersed nanoparticles and the particles can be stably suspended in the base fluid. One-step physical method cannot synthesize nanofluids on large scale and the cost is also high.

It has recently been shown that a two stage approach of synthesizing nanometric powders by mechanical alloying and subsequently dispersing the same in a given fluid could be a

more flexible method of producing nanofluid with greater scope of scaling up the process of synthesis.

3.3 Selection of base fluid and nanoparticles for the study

The use of nanofluid in solar collector is a new concept as it is in developing stage, and nanofluid based solar collectors are not available commercially. First of all base fluid to be used for the preparation of nanofluids is selected. Commonly used base fluids are water, ethylene glycol, oil etc. The choice between these fluids is based on the operating temperature of the solar collector. Since in the present study flat plate solar collector is being used this operates between 0^oC and 100^oC and treated as a low temperature solar collector. So, it is decided to use distilled water as base fluid, because:

(i) Water is easily available, cost effective and commonly used in solar collector for low temperature application.

(ii) Water is visibly transparent i.e. the incident solar photons will have relatively large mean free paths inside the medium.

(iii) Water have maximum solar absorption coefficient of 13% as compared to other base fluids.

Different type of nano-particles are available commercially in the form of nano powders, and its use in a particular application depends upon the factors like; comparative improvement of properties, easy availability and cost. In the present study alumina (Al_2O_3) nanoparticles are used for nanofluid preparation, because:

(i) Alumina nanoparticle exhibit relatively better heat transfer characteristics, stability and uniformity thus opening many possibilities with respect to technological applications. Alumina is one of the most frequently studied nanomaterials.

(ii) Alumina is one of the good thermal conductive metals and its use in heat transfer applications would be beneficial.

(iii) Alumina has a predictable broadband absorption in the visible and near infra red range of solar spectrum.

(iv) The nanoparticles suspended in the base fluid are free of any noticeable chemical change of the base fluid i.e. water.

(v) The physical properties of alumina nanofluid can be determined by using analytical methods.

3.4 Requirement of Nanoparticles

The amount of nanoparticles required in preparation of nanofluids is calculated using the law of mixture formula. A mass balance (make-citizen, model-CTG 602 and resolution-0.1mg) is used to weigh the nanoparticles. Weight of the nanoparticles required for preparation of Al_2O_3 and TiO_2 based nanofluid of a particular volume concentration, using distilled water as base fluid is calculated as follows.

The volume fraction and the density of the nanoparticles in suspension are defined as follows:

$$VF_{np} = V_{np} / V_t \tag{3.1}$$

$$V_{np} = m_{np} / \rho_{np} \tag{3.2}$$

By using equation (3.1) & (3.2), the required mass of nanoparticles for suspension in given total fluid volume is determined as follows:

$$m_{np} = V_t \,.\, VF_{np} . \rho_{np} \qquad (3.3)$$

where VF_{np} is the volume fraction of nanoparticles, V_{np} is the volume of nanoparticles, V_t is the total volume of nanofluid (m^3), m_{np} is the mass of nanoparticles (kg), and ρ_{np} is the density of nanoparticles (kg/m^3).

Sample calculation

Nanoparticles used are Al_2O_3

Concentration of the nanofluid to be prepared (Φ) = 0.001 vol. %

Density of nanoparticles used (ρ_{np}) = 3700 kg/m^3

Volume of fluid used (V) = 30 liter

Density of base fluid, water (ρ_f) = 1000 kg/m^3

Mass of nanoparticle used:

$\mathbf{m_{np}} = V_t \,.\, VF_{np} . \rho_{np}$

$= (30x10^{-3} * 0.001 * 3700) /100$

$= 0.00111$ kg

$\mathbf{m_{np}}$ = 1.11 gm

Similar calculations were carried out for Al_2O_3 and TiO_2 water based nanofluids for different volumetric concentrations. By mixing the estimated amount of nanoparticles and distilled water in the ultrasonic vibrating mixer (UVM) for the required time the nanofluid was prepared.

The amount of Al_2O_3 and TiO_2 nanoparticles required to prepare nanofluids of different volume concentration in 30 litres of distilled water base fluid is presented in the Table 3.1.

Table 3.1: Estimated weight of Al_2O_3 and TiO_2 nanoparticle for different concentrations

Volume concentration, (%)	0.001	0.003	0.005	0.007	0.01
W_{Al2O3}, (g)	1.11	3.33	5.55	7.77	11.1
W_{TiO2}, (g)	1.365	4.095	6.825	9.555	13.65

3.5 Nanofluid preparation

In the present study, suspension of Al_2O_3 and TiO_2 nanoparticles in distilled water is used to prepare nanofluids of different volumetric concentrations by two step method. The commercially available Al_2O_3 and TiO_2 nano particles of 20 nm average size and 99.99% purity is procured from a USA based company (Nanoshel-Intelligent Materials Private Ltd) and used as received for experimental investigations in the present study. Properties of the nanoparticles used are shown in Table 3.2.

The particle size was measured by Scanning Electron Micro-scope. Fig. 3.3 and Fig. 3.4 report an example of a SEM image of the Al_2O_3 – water and TiO_2 – water nanofluid respectively, dried for SEM analyses. The particles are nearly spherical and the average diameter is about 30 nm (Al_2O_3) and 20 nm (TiO_2). There are a few larger particles, which are likely aggregates of the smaller ones, but the whole distribution of the particles is relatively well dispersed. The transmission electron micrograph (TEM) of Al_2O_3 – water and TiO_2 – water nanofluid is shown in Fig. 3.5 and Fig. 3.6.

The received dry nanoparticles are in the form of agglomerates and in order to break down the large agglomerates and improve dispersion behaviour, ultrasonic vibration mixer is used, which is an approved sonication technique for dispersing the aggregated nanoparticles **(Li et al., 2007**).

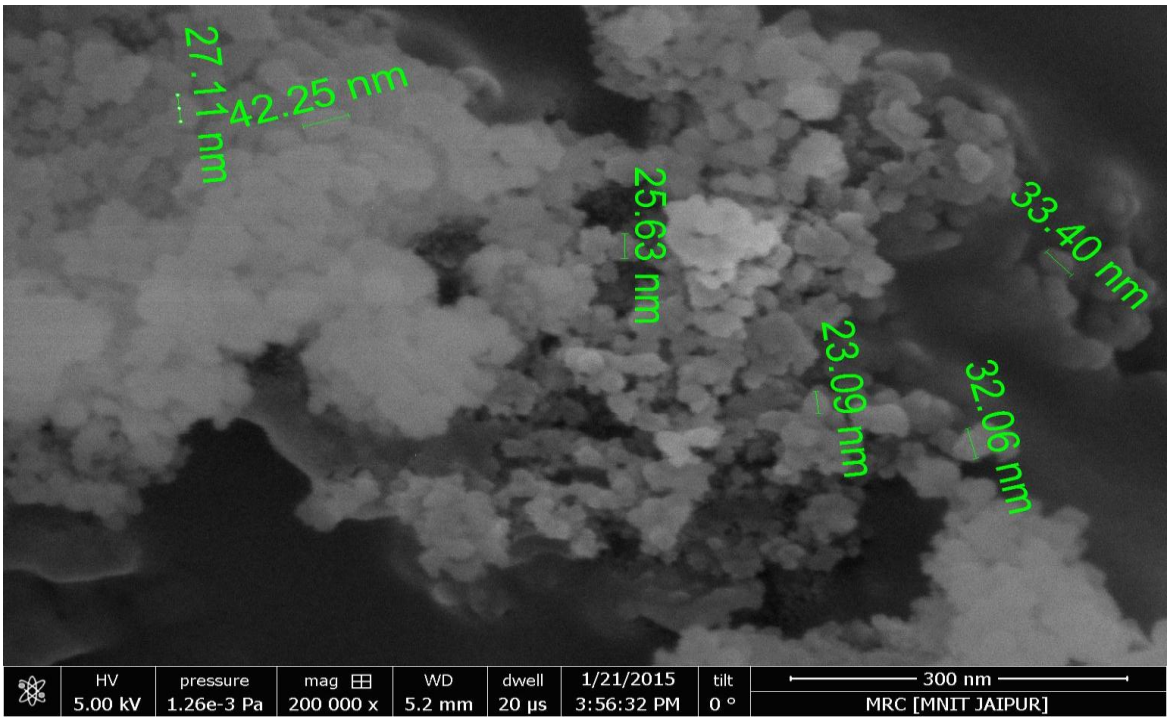

Fig. 3.3 SEM photograph of Al_2O_3 nanoparticles

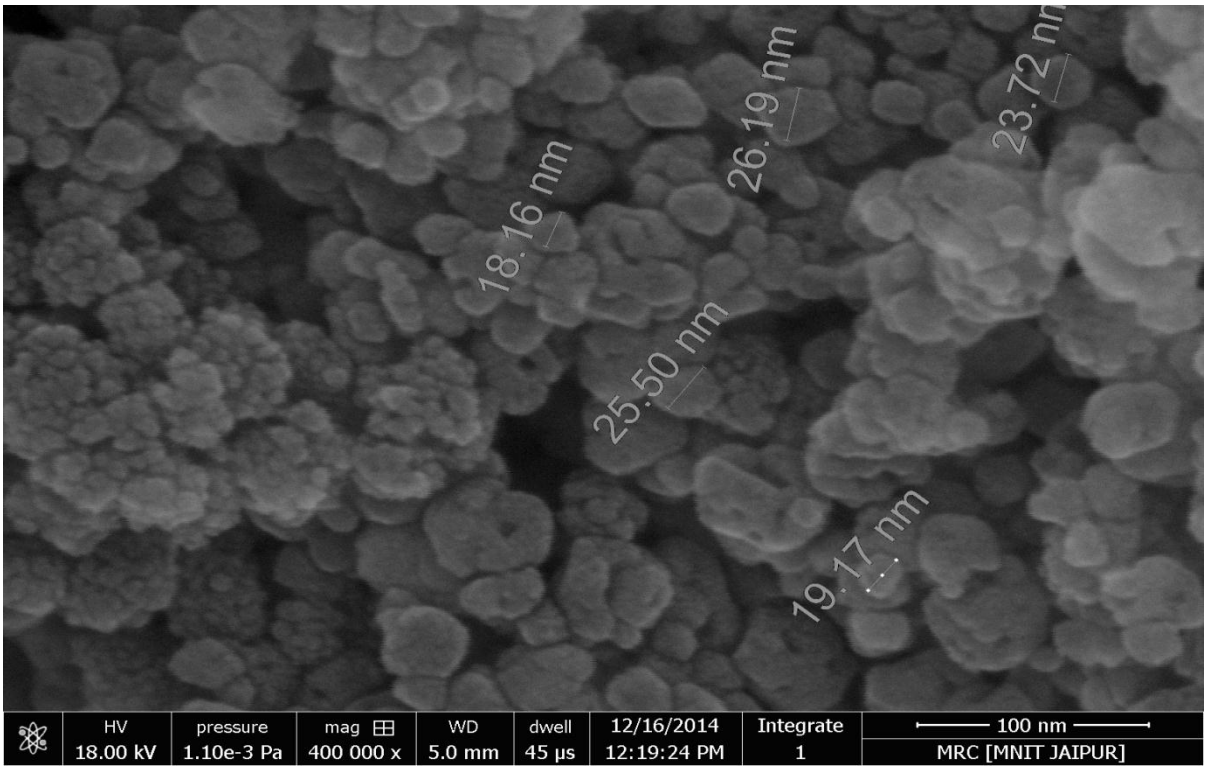

Fig. 3.4 SEM photograph of TiO_2 nanoparticles

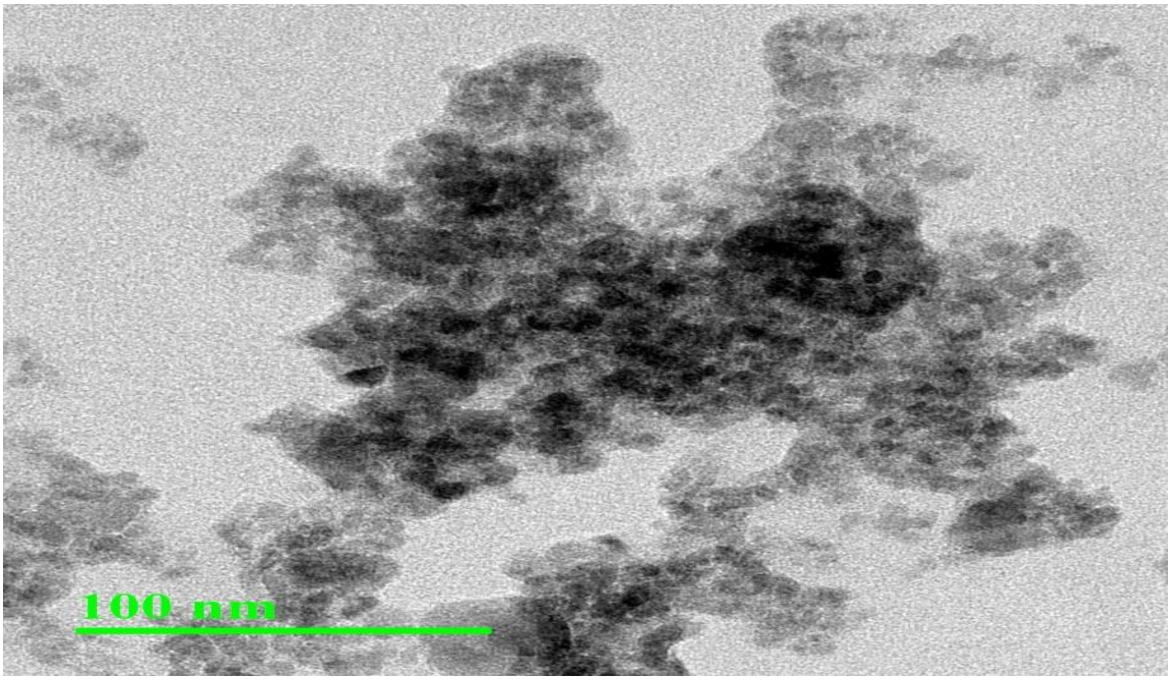

Fig. 3.5 TEM photograph of Al_2O_3 nanoparticles

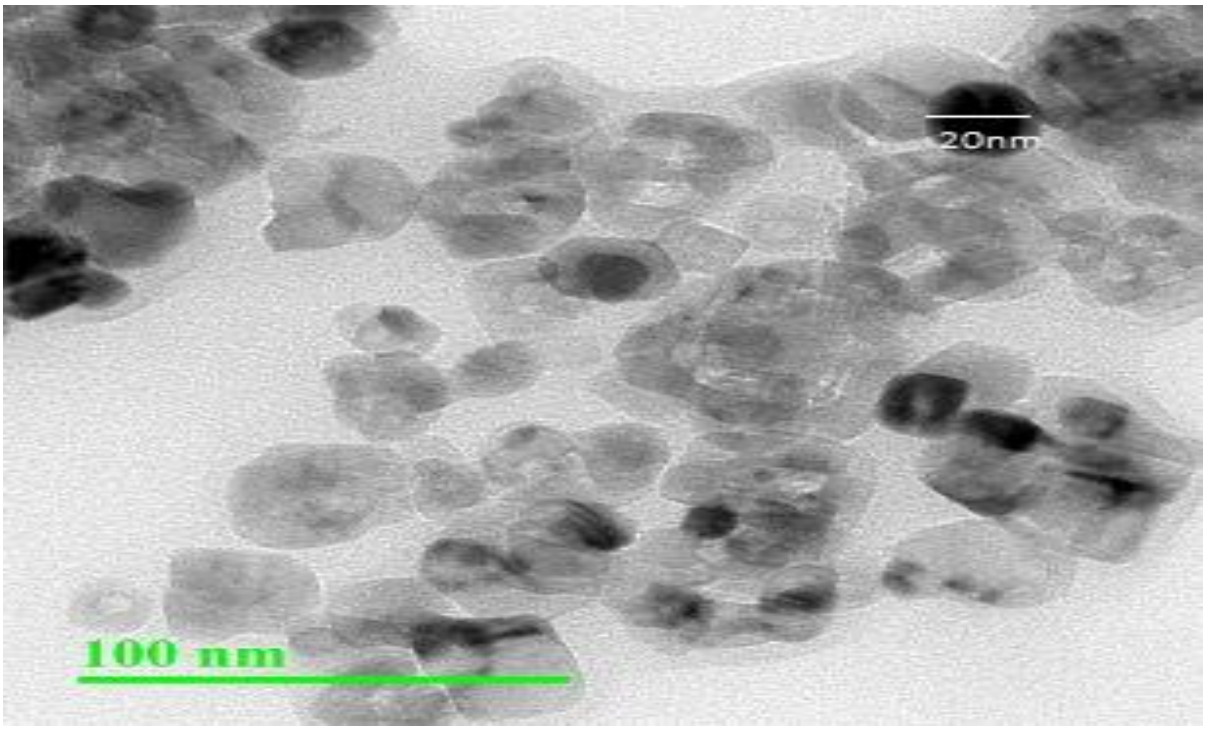

Fig. 3.6 TEM photograph of TiO_2 nanoparticles

Table 3.2 Physical characteristics of Al_2O_3 and TiO_2 nanoparticles

S.No.	**Parameter**	Al_2O_3 nanoparticle	TiO_2 nanoparticle
1	Size of particles	25-30 nm	20-25 nm
2	Shape of particles	Spherical	Spherical
3	Density	3700 kg/m^3	3900 kg/m^3
4	Surface area per unit weight	15-20 m^2/g	15-20 m^2/g
5	Crystal Form	Gamma	Gamma
6	Purity	99.99%	99.99%

In the absence of any kind of agitation and sonication, the Al_2O_3 particles start to settle down at the bottom of the container after 24 hrs. as observed in the experimental study. While the stability of the nanofluid could potentially be improved with the addition of a surfactant, however commonly used surfactants (SDBS, Triton X-100, sodium dodecyl-sulfate etc.) are not stable at higher temperature. In addition, the effect of surfactants on the thermophysical and radiative properties of nanoparticles in suspension could be complicated, and even unpredictable. In the present experimental study it was decided not to introduce any surfactant in the suspension.

Estimated amount of nanoparticles are mixed in the distilled water for preparation of nanofluid of given volume concentration using Eq. (3.1), using ultrasonic vibration mixer (with UP-600S ultrasonic model, the power available in the ultrasonic bath is 600 W and the ultrasonic frequency is 27 ± 3 kHz). In UVM machine, the ultrasonic energy is produced by converting electrical energy into mechanical vibrations using generator and

piezo-electric transducers. However, the dry nanoparticles are present in the form of large agglomerates and in order to breakdown the agglomerates and to obtain a homogenously dispersed solution, ultrasonication was done for 6–8 hours to produce desired nanoparticle concentration. The photographic view of Ultrasonic Cleaner for sonication process is shown in the Fig.3.7.

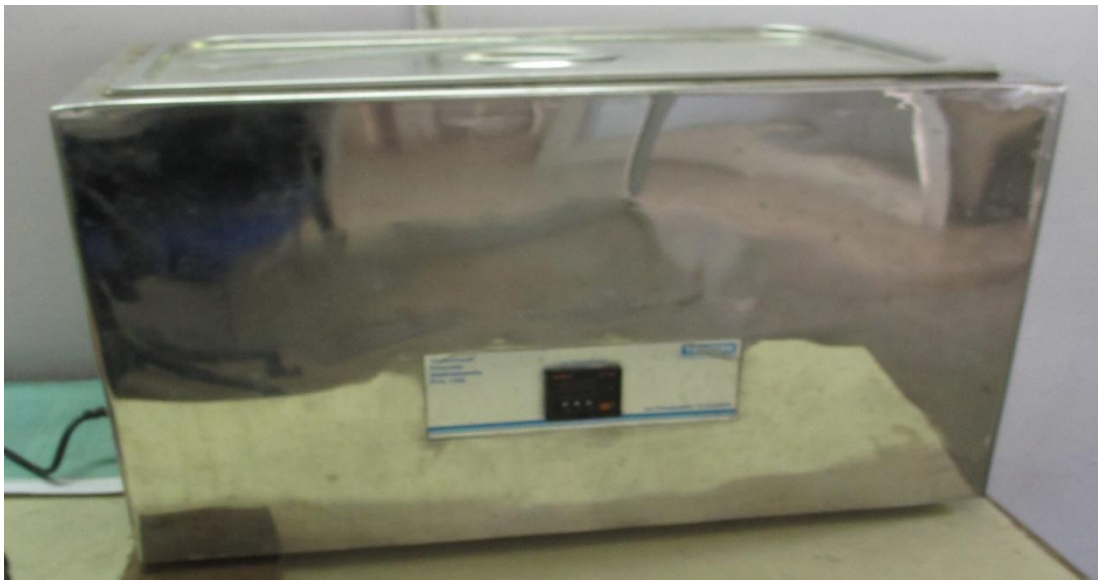

Fig. 3.7 Ultrasonic Cleaner apparatus for sonication

The Al_2O_3 and TiO_2 nanofluid samples thus prepared are kept for observation and no particle settlement was observed at the bottom of the flask even after twenty four hours. The photographic view of Al_2O_3 nanofluid suspension prepared using sonication process is as shown in Fig. 3.8.

Fig. 3.8 Al_2O_3-water sample nanofluid

Aluminum oxide and Titanium oxide nanofluids of four different volume concentrations 0.001, 0.003, 0.005 and 0.007 are prepared for the experimentation study. During the experimentation with Al_2O_3 and TiO_2 nanofluids, the time taken to complete the experiment is lesser than the time required for first sedimentation to take place hence surfactants are not mixed in the nanofluids.

3.6 Properties of nanofluid

Properties of nanofluids (**Khanafer and Vafai; 2011)** are calculated by the method explained below:

1. **Density**

   The density of nanofluid is based on the physical principle of the mixture rule. As such it can be represented as:

$$\rho_{eff} = \left(\frac{m}{V}\right)_{eff} = \frac{m_f + m_p}{V_f + V_p} = \frac{\rho_f V_f + \rho_p V_p}{V_f + V_p} = (1 - \emptyset_p)\rho_f + \emptyset_p \rho_p \quad (3.4)$$

Where,

ρ_{eff}= effective density of nanofluid

ρ_f = density of fluid

ρ_p = density of particle

m_f = mass of fluid

m_p = mass of particle

V_f = volume of fluid

V_p = volume of particle

Φ_p= volume fraction of particle

2. Heat capacity

The specific heat of nanofluid can be determined by assuming thermal equilibrium between the nanoparticles and the base fluid and given as follows:

$$C_{eff} = \frac{\{(1-\emptyset_p)\rho_f c_f + \emptyset_p \rho_p c_p\}}{\rho_{eff}} \quad (3.5)$$

Where,

C_{eff} = heat capacity of nanofluid

C_f = heat capacity of fluid

C_p = heat capacity of particle

3. Thermal expansion coefficient

Thermal expansion coefficient of nanofluids can be estimated utilizing the volume fraction of the nanoparticles on the weight basis as follows:

$$\beta_{eff} = (1 - \emptyset_p)\beta_f + \emptyset_p\beta_p \quad (3.6)$$

Where,

β_{eff} = thermal expansion coefficient of nanofluid

β_f = thermal expansion coefficient of fluid

β_p = thermal expansion coefficient of nanoparticle

4. Thermal conductivity

Thermal conductivity of nanofluid is given by the following formula:

$$k_{eff} = k_f + \left[\frac{3\emptyset_p(k_p - k_f)}{k_p + 2k_f - \emptyset_p(k_p - k_f)}\right] \quad (3.7)$$

Where,

k_{eff} = thermal conductivity of nanofluid

k_f = thermal conductivity of fluid

k_p =thermal conductivity of nanoparticle

5. Effective viscosity

Effective viscosity of nanofluid is given by following relation:

$$\mu_{eff} = (1 + 5.45\emptyset_p + 108.2\emptyset_p^2)\mu_f \quad (3.8)$$

Where,

μ_{eff} = viscosity of nanofluid

μ_f = viscosity of fluid

Table 3.3 Properties of different nanoparticles

Type of nanomaterial	Nanomaterial	Thermal conductivity (W/m-K)	Density (kg/m^3)	Specific heat (kJ/kg-K)
Metallic	Silver	429	10490	0.23
	Copper	401	8940	0.39
	Gold	316	19312	0.13
	Aluminum	237	2712	0.91
	Zinc	116	7135	0.39
	Titanium	21.9	4500	0.54
Non metallic	Alumina (Al_2O_3)	40	3700	0.765
	CuO	20	6500	0.535
	ZnO	21	5610	0.635
	Titania (TiO_2)	8.4	3900	0.692

Table 3.4 Properties of different base fluids

S. No.	Base fluid	Thermal conductivity (W/m-K)	Density (Kg/m^3)	Specific heat (kJ/kgK)
1	Water	0.609	1000	4.182
2	Ethylene glycol	0.258	1097	2.36
3	Acetone	0.18	784.6	2.15

Table 3.5 Properties of Al_2O_3-Water nanofluid at different volume fraction

Nanoparticle	Volume fraction of NP (%)	Effective density of nanofluid (kg/m^3)	Heat capacity (kJ/kg-K)	Thermal conductivity (W/m-K)
Al_2O_3	0.001	1002.97	4.18196	0.61187
	0.002	1005.94	4.18194	0.614745
	0.003	1008.91	4.181897	0.617626
	0.004	1011.88	4.18186	0.620512
	0.005	1014.85	4.18183	0.623404
	0.006	1017.82	4.181795	0.626301
	0.007	1020.79	4.181761	0.629204
	0.008	1023.76	4.181726	0.632113
	0.009	1026.73	4.181692	0.635027
	0.01	1029.7	4.181658	0.637947

Table 3.6 Properties of TiO_2-Water nanofluid at different volume fraction

Nanoparticle	Volume fraction of NP (%)	Effective density of nanofluid (kg/m3)	Heat capacity (kJ/kg-K)	Thermal conductivity (W/m-K)
TiO_2	0.001	1002.9	4.16544	0.611432
	0.002	1005.8	4.151958	0.613868
	0.003	1008.7	4.138554	0.616308

	0.004	1011.6	4.125227	0.618752
	0.005	1014.5	4.111975	0.6212
	0.006	1017.4	4.0988	0.623652
	0.007	1020.3	4.085699	0.626108
	0.008	1023.2	4.072672	0.628568
	0.009	1026.1	4.05972	0.631032
	0.01	1029	4.04684	0.6335

3.7 Stability study of nanofluid

The biggest problem associated with nanofluid is its stability. There are various methods for nanofluid preparation but still it is a challenge to prepare a homogeneous mixture and stable suspension of nanoparticles into the base fluid with negligible agglomeration, and without affecting the thermo physical properties.

It is very important to know the settlement time of nanoparticles in the base fluid for the exact study of thermal performance of direct absorption solar collector. For this small amount of nanofluid prepared was collected in a transparent container and the settlement of the nanofluid was seen visually. As the experiment was carried out for 5-6 hours in a day. So the nanoparticles remain suspended in the base fluid for at least 10-12 hours.

The Al_2O_3 nanofluid thus prepared was kept for visual observation. Fig. 3.9 indicates the Al_2O_3 nanofluid stability over time span. It was found that nanofluids kept for 24 hours exhibit settlement at the bottom of the flask compared to initial fresh nanofluid. During the experimentation, the time taken to complete the experiment is less than the time required for first sedimentation to take place and hence surfactants are not mixed in the nanofluids. Four different volume concentrations of 0.001, 0.003, 0.005 and 0.007 % were used in the study.

(a) Just after preparation (b) After 6 hrs of preparation (c) After 24 hrs of preparation

Fig. 3.9 Stability observation of Al_2O_3-Water nanofluid of 0.005% concentration

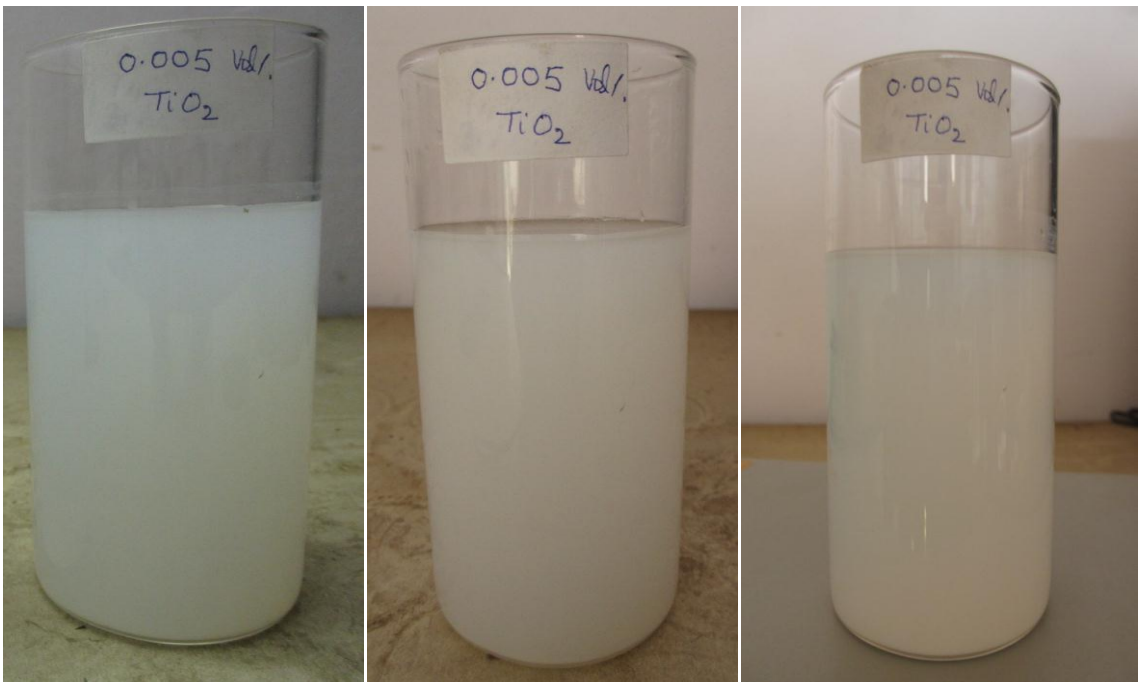

(a) Just after preparation (b) After 6 hrs of preparation (c) After 24 hrs of preparation

Fig. 3.10 Stability observation of TiO_2-Water nanofluid of 0.005% concentration

It was observed from Fig. 3.9 & 3.10 that there was not much difference between the fresh nanofluid and the nanofluid after 6 hours, so it had been considered stable for 5-6 hours experimental study on direct absorption solar collector. It was also observed that after 24 hours considerable amount of nanoparticles settled down at the bottom. So we had to prepare fresh nanofluid every day for exact experimentation.

3.8 Summary

This chapter provides theoretical insight for the synthesis of nanoparticles studied by different researchers through the two methods of preparing nanofluids i.e. one step process and two step process. In the present study water and alumina nanoparticles are chosen as base fluid and nanoparticle respectively, for preparing nanofluid by two step method. This nanofluid has been used as working fluid for experimentation with direct absorption type flat plate solar collector.

CHAPTER - 4

DEVELOPMENT OF EXPERIMENTAL SET UP

This chapter describes about the design and development of a new type of direct absorption solar collector (DASC) for fluid heating purposes. The concept of a DASC is that incident solar radiations will be absorbed directly by the working fluid thin film flowing over the base plate, thus not allowing any solar radiation to pass through it and avoiding conduction and convection losses that occur in conventional tube-in-plate type flat plate collector due to indirect heating of working fluid via absorber plate and tube. Development of a DASC comprises step by step fabrication and installation of set up followed by instrumentation details for experimental data collection and recording in outdoor conditions. In this chapter, standards for testing solar collectors are also discussed.

4.1 Specifications of Direct Absorption Solar Collector

The dimensions of the developed collector were chosen for establishing a uniform thin fluid film over the entire base plate and the minimum requirement of the nanofluids for study. The effective area of the absorber plate is 1440 x 800 mm and the total area of the collector including wooden box is 1540 x 910 mm. In order to minimize the losses glass wool insulation was provided at the side walls and at the bottom. Outer casing of the collector was made of wood. The glazing was used as low reflectance glass with transmittance percentage of about 90%. The absorber plate was toughened glass and uncoated aluminum plate and the size of collector is kept small in order to reduce the use of nanofluids.

The fluid is contained within the enclosed space of the DASC. The fluid through the collector is water based Al_2O_3 nanofluid. The bottom wall is considered to be adiabatic, i.e., no heat flux is allowed to pass through it, except for transmitted radiation. The fluid is enclosed at the top by a glass surface, which allows most of the incident solar flux to pass through. This top surface is assumed to be exposed to the ambient atmosphere and thus loses heat by convection.

The setup consists of a collector box with base plate, perforated pipe, inlet and outlet piping, cover glass, storage and overhead tank and a frame or stand. Wood is used as collector box material as wood is a good insulator of heat. The specifications of the DASC are as follows:

Table 4.1 DASC Setup Specifications

Specification	Details	Remarks
Area (l*b)	1.54 * 0.91	1.40 m^2
Effective Area (l*b)	1.44 * 0.80	1.15 m^2
Insulation	Glass wool (50 mm)	Below base plate
	Glass wool (25 mm)	Inside part of the side walls
Base plate	Toughened Glass (6 mm)	Base plate and Cover Plate
	Plain Glass (6 mm)	Side Walls
	Aluminum (16 gauge)	In metal set up
Frame or Stand	Iron angles	Height (20 inches)
Fluid Pump	Make : Alpha	50 W / Head 25 Feet
Tanks	Material : Steel	Capacity 30 liters each diameter = 30 cm
Perforated Pipe	Aluminum	Holes of Diameter 2 mm with

		7.5 mm pitch
Pipe Fittings	¾” CPVC pipe	For inlet and outlet from collector
	½” flexible rubber pipe	In between storage and overhead tanks
Valve	Ball type valve	Control the flow rate
	Non-return valve	To stop reverse flow in storage tank

The 6 mm toughened glass plate was used as a base plate. The glass was used as a base plate because of the straightness of glass, fluid film flow will be more uniform and also the toughened glass can sustain high temperatures. In another set up aluminum sheet (16 gauge) was used as base plate due to high thermal conductivity and opaque surface. The overhead tank was placed at a height of around eight feet above the ground level. A 50 W motor was used to lift the fluid from the storage tank to the overhead tank. The collector glazing is low reflectance glass which acts as transparent to the incoming short wavelength solar radiations but becomes opaque for high wavelength radiations emitted by the absorber plate. In this collector we are using direct absorption system in which the solar radiations are directly allowed to strike the working fluid. So, the conduction and convection losses are eliminated in this collector.

4.2 Development of Direct Absorption Solar Collector

Development of DASC comprises a series of steps having fabrication of each component separately and then assembly of each part to develop a complete experimental set up of DASC. The detailed specifications and photographic view of step by step fabrication are shown below:

4.2.1 Fabrication of collector Box

Collector housing was fabricated with wood (Fig. 4.1). The box base contains 6 mm thick water proof plywood and the, bottom and the side walls are of 30 mm thickness. The height of the side walls is 100 mm. Wood is used as collector box material as it is a good insulator of heat and easy to do fabrication work with wood.

Fig. 4.1 Wooden Collector Box

4.2.2 Insulation

Glass wool is used as an insulating material to reduce the heat losses from bottom and side walls. Thermal conductivity of glass wool is very low i.e.0.04 W/m-K. 50 mm thick glass wool sheet is used on the bottom surface and 25 mm thick on the side walls of the collector box (Fig. 4.2).

Fig. 4.2 Insulated Collector Box

4.2.3 Base plate

Aluminum flat plate was used as base plate so that, if any fraction of solar radiation transmitted by the fluid film reaches at the aluminum base plate will be reflected back to the fluid flowing over the base plate. Fig. 4.3 shows the aluminum flat plate and assembly of plate to the insulated collector box. Fig. 4.3 also shows the two thermocouples attached to the bottom of plate to measure the temperatures at two different points of plate during the fluid flow. Dimensions of base plate are 144 cm length and 80 cm width. Aluminum plate thickness is 16 gauges (1.65 mm).

(a)

(b)

Fig. 4.3 Aluminum base plate

4.2.4 Fluid distribution system over base plate

Formation of uniform fluid film and even distribution throughout the base plate surface is very important towards the efficient direct absorption of solar energy by the flowing fluid film and performance enhancement of DASC.

Two possible methods have been identified for film formation:

(i) Using slotted pipe

(ii) Using perforated pipe

(i) Using slotted pipe

This technique is very similar to gating system of dams for release water. In this case a glass slit of nearly the same length and height is used just near the inlet to restrict the flow of water and a very minute opening is given throughout the slit for the formation of fluid film.

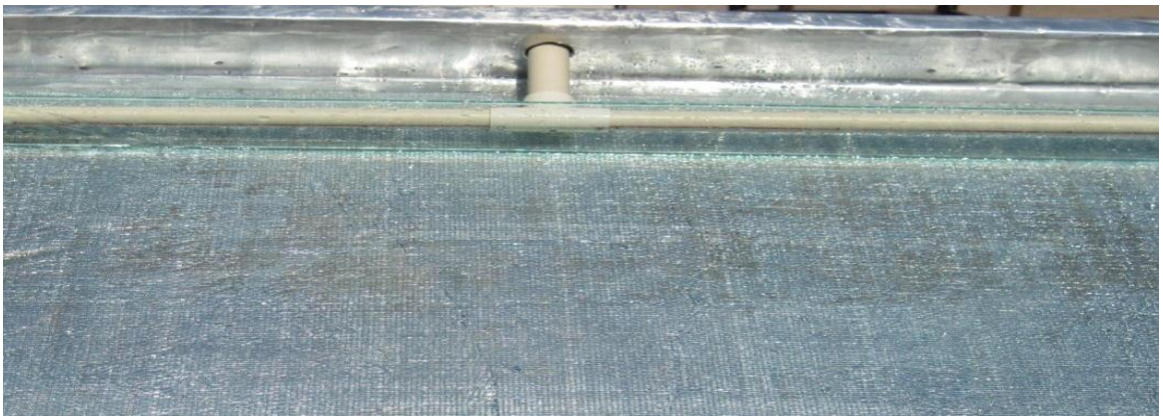

Fig. 4.4 Slotted pipe for Film Formation

During the experiment, this technique was found very difficult for uniform film formation due to non uniform opening from the glass slit throughout the collector width.

(ii) Using Perforated Pipe

By using the perforated pipe, the film formation on the base plate was almost uniform. For making the uniform film over the base plate, appropriate size of holes and pitch between the holes was to be optimized. During the experimental study different

combinations of number of holes (of 2mm dia.) and pitch were tried for getting the uniform film of the fluid over the base plate as shown in Table 4.2

Table 0.2 Optimizing number of holes in header pipe

S.No	No of Holes	Result
1.	8 Holes with a pitch of100 mm	Film not Formed
2.	14 Holes with a pitch of 58 mm	Film not Formed
3.	26 Holes with a pitch of 30 mm	Film not Formed
4.	53 Holes with a pitch of 15 mm	Film not Formed
5.	106 Holes with a pitch of 7.5 mm	Uniform film over the base plate

So after fifth step, a uniform film of fluid over the glass plate was formed with optimum number of holes of 106 with a pitch of 7.5 mm.

Fig. 4.5 Perforated pipe method for film formation

In the present study, for uniform film formation a ¾" perforated aluminum pipe having optimum number of holes by hit and trial method was used. The diameter of the holes

was approximately 2 mm and the pitch of holes was 7.5 mm. CPVC and copper pipe may also be used but in CPVC pipe, bending takes place due to high temperature after some time. Copper is costly material and also difficult to make small holes in comparison to aluminum.

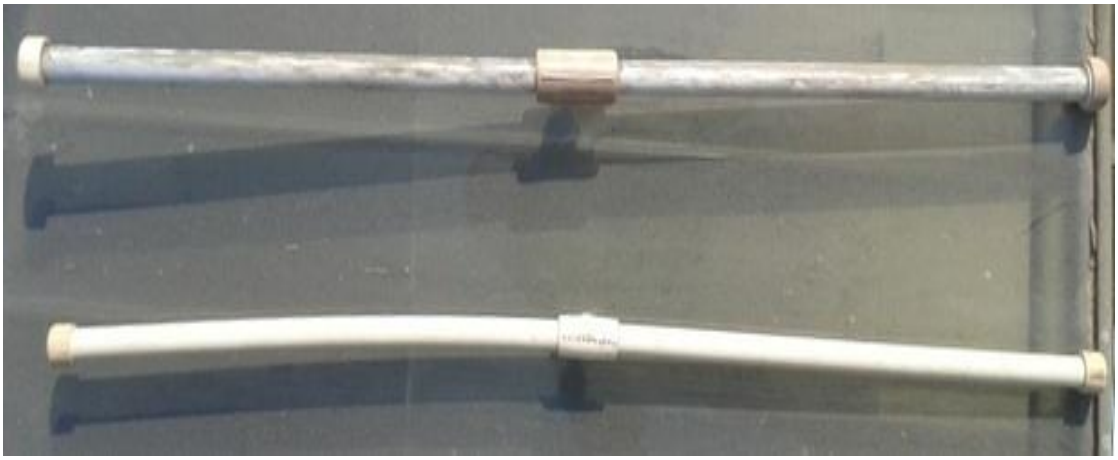

Fig. 4.6 Effect of Temperature on Aluminum Pipe and CPVC Pipe

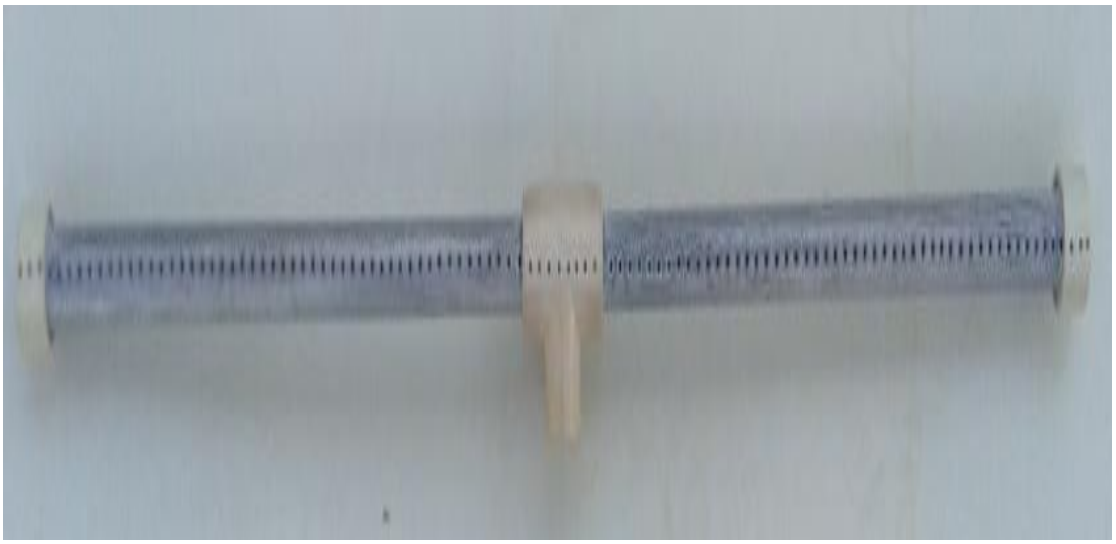

Fig. 4.7 Aluminium Perforated Pipe

Fig. 4.8 Film formations using perforated pipe

4.2.5 Collection and Overhead storage Tank

Two steel tanks of capacity 30 litres and diameter of 30 cm were used as storage and overhead tanks. Glass wool insulation covered with Al foil was done on the tanks to reduce the heat losses from the tank.

Fig. 4.9 Storage and overhead tanks

4.2.6 Pump

Centrifugal type pump was used for circulating the fluid for making the closed system. Pump circulates working fluid from the bottom storage tank to overhead tank for entering into the collector. The pump used in this study is shown in Fig. 4.10.

Fig. 4.10 Pump

4.2.7 Transparent cover

Single glass cover of thickness 5mm was used for glazing or top cover of collector. For the cover material, reflection and absorption should be as low as possible and transmittance should be high enough. In addition to this, while selecting cover material, consideration factors include material durability, non degradability to UV light exposure and low cost. Generally, glass and plastics can be used as covers for solar collectors, but glass is the most common material due to having high transmittance of as much as 90% of the incoming short wave radiation and negligible transmittance of outward long wave radiation. The toughened glass used in solar collectors resists breaking and scratching. When sunlight passes through glass, it is directly absorbed by the fluid film flowing over the base plate and fluid is heated. Although glass allows sunlight to pass through, it also traps the heat produced inside the collector.

4.2.8 Flow control valve

Flow control valve consists of a changeable aperture that opens or closes to increase or decrease flow rates respectively. Flow control valve regulates the flow of circulating fluid in the collector inlet.

Fig. 4.11 Ball Type Control Valve

Ball valves are among the simplest control valves, as they consist merely of an inner ball attached to a handle. As the handle is turned a quarter turn, a hole through the center of the ball is aligned with or turned perpendicular to the valve openings, thereby permitting or shutting off flow. So the ball type of control valve is commonly used because of smooth operation and easy functioning also it is not very expensive.

4.2.9 Assembly

Silicon paste was used for sealing the collector with glazing to avoid any leakage.

Iron Angles were used for making stand frame for solar collector.

4.3 Complete Experimental Set up

Complete experimental setup of DASC with all the components listed and placed at their respective positions with piping to have closed DASC fluid heating system has been shown below:

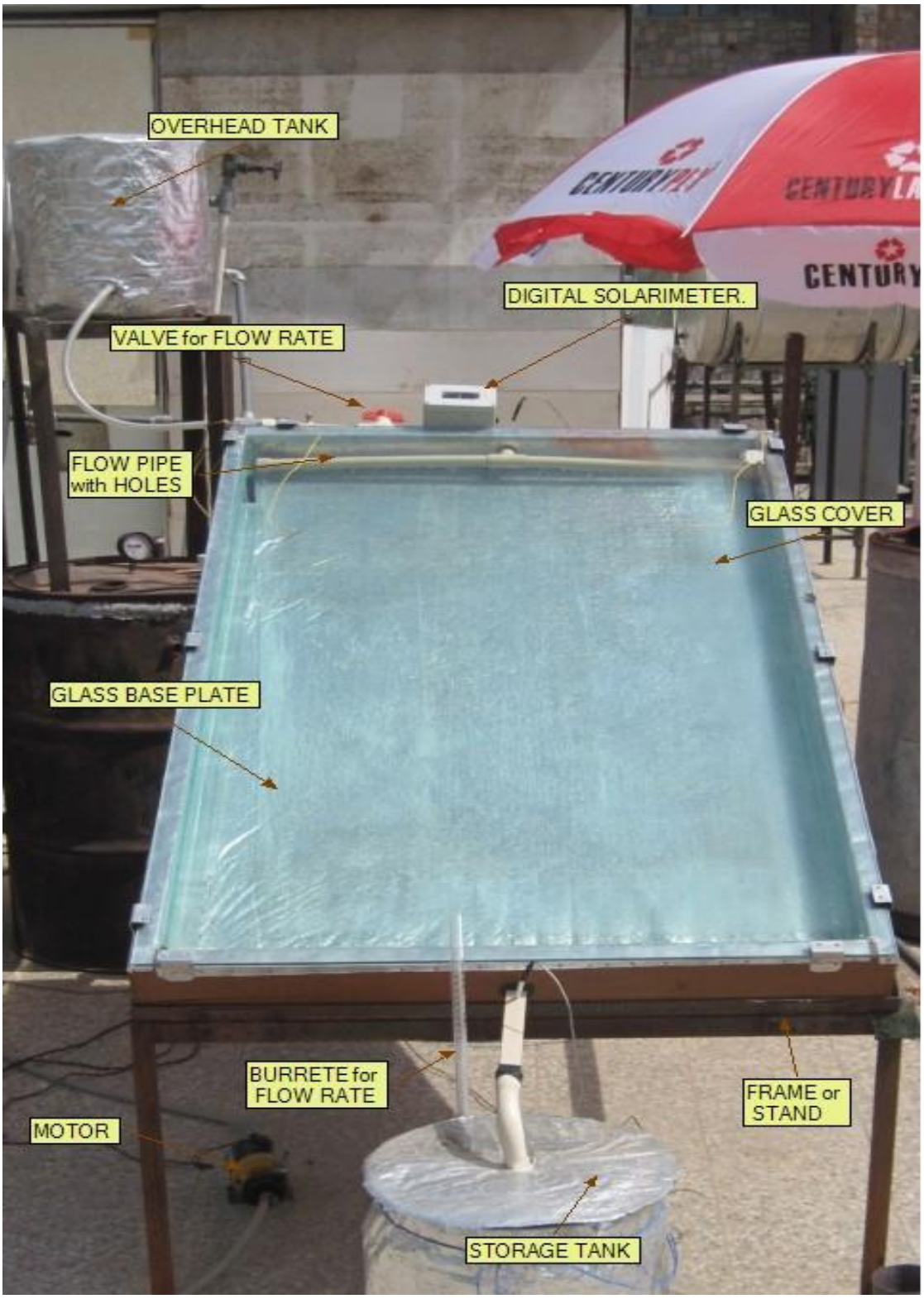

Fig. 4.12 Experimental Setup-I of DASC with glass base plate

Fig. 4.13 Experimental Setup-II of DASC with aluminum base plate

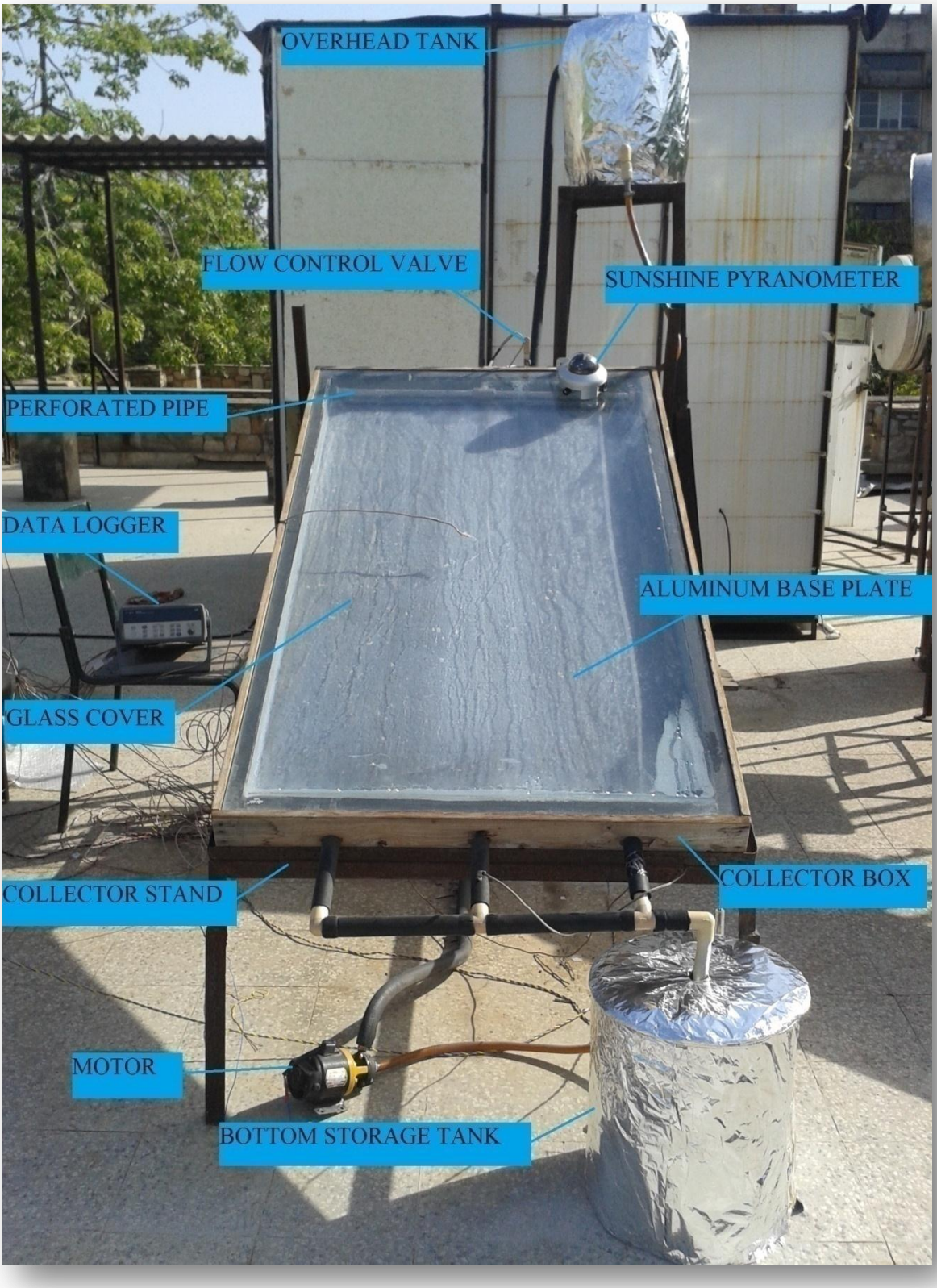

Fig. 4.14 Experimental Setup-III of DASC with aluminum base plate

4.4 Instrumentations

Accuracy in the investigation of heat transfer performance of a DASC system depends on the quality, accuracy and precision of instruments used. Properly calibrated instruments were used in measuring the different experimental parameters such as various temperatures, intensity of solar radiation, fluid flow rate and wind velocity etc. Description along with the specifications and photographic view of the instruments, used in the process of measurement, is given below.

4.4.1 Weather station

Automatic weather station was installed on the roof of MNIT Director's office, which was in close vicinity of experimental set up of DASC system. Weather station measured ambient air temperature, relative humidity, intensity of solar radiation and wind speed along with its direction. For the measurement of dry bulb temperature and relative humidity of ambient air, weather station is fitted with capacitive transducer which is mounted in a shielding device. Pyranometer is also fitted on main frame of weather station to measure intensity of solar radiation. Wind speed and wind direction are measured with the help of a 3-cup anemometer.

Data logging system is also a part of weather station which automatically saves all the parameters at an interval of 15 minutes. All sensors are powered directly from data logger and there is no need of external power source. This time interval can further be changed by programming of the same. Data logging system is self powered and gets its power from a battery, which is charged during sunshine hours, by solar photovoltaic panel, also mounted on weather station. Fig. 4.15 shows the photographic view of weather station used for the measurement and recording of data. Weather station was supplied and installed by Moinee systems (India). Specifications and other technical details of each sensor are given in Table 4.3.

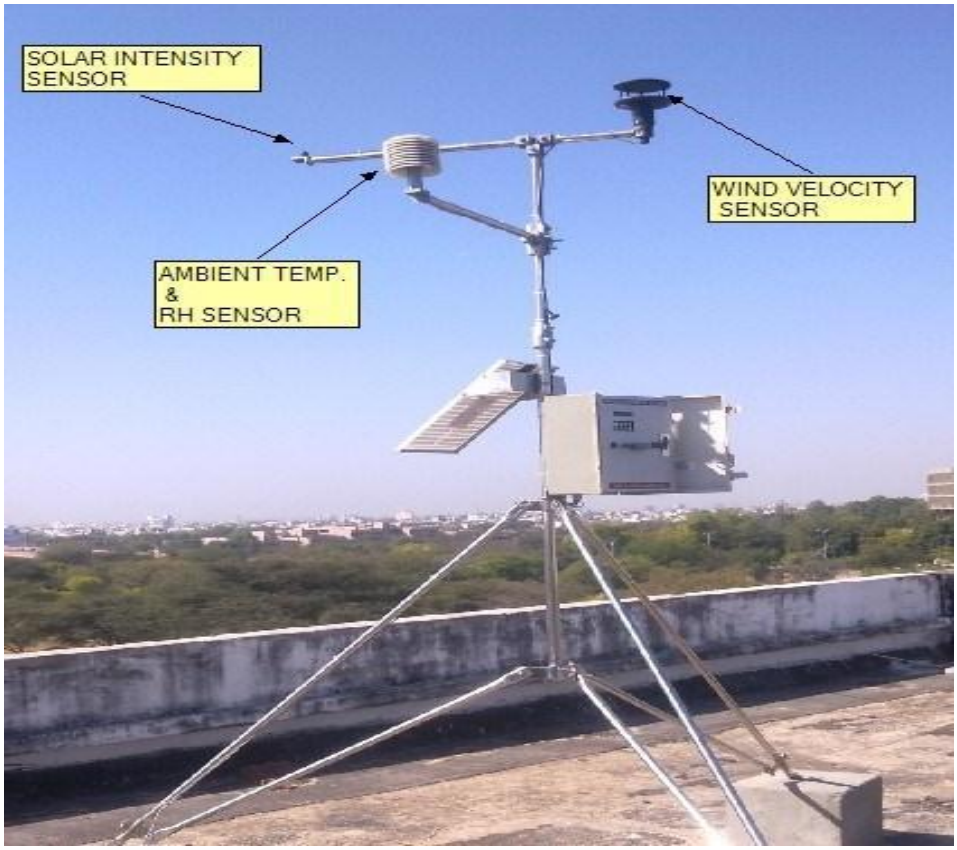

Fig. 4.15 Weather Station

Table 4.3: Specification of sensors mounted on weather station

1	**Air Temperature & Relative Humidity Sensor**	
	Temperature Range	- 40 to 100^{0}C
	Accuracy	± 0.5^{0}C
	Resolution	0.01^0 C
	RH Range	0 to 100%
	Resolution	0.1 %
	Accuracy	± 2%
2	**Wind Speed Sensor**	
	Sensor	3 Cup Anemometer
	Range	0 to 50 m/s
	Resolution	0.1 m/s
3	**Solar Radiation Sensor (Pyranometer)**	
	Spectral Range	305-2800 nm

	Sensitivity (Nominal)	15 μ V / Wm-2
	Temperature Range	- 40^0 C to +80^0 C
	Range	0 to 2000 Wm-2

4.3.2 Thermocouples

Various types of thermocouples are available in market like J, K, T, E, R, S, B etc. In the present study, J (Iron-constantan) type thermocouples (Make-Omega, Model-JMQSS-IM050U-300, 1 mm wire diameter) ungrounded covered with stainless steel sheath were used for collector inlet, outlet fluid temperatures, ambient temperature, two base plate and glass cover temperature measurement. The temperature range and sensitivity of J type thermocouples are -210 to 1200℃, and 51 μV/℃ respectively.

Fig. 4.16 J type thermocouple

Fig. 4.17 Thermo-Hygrometer

4.3.3 Thermo hygrometer

Thermo-hygrometers are instruments used for measuring relative humidity and temperature simultaneously. In our experimentation, Fluke-971 thermo hygrometer was used to measure the relative humidity of air inside the test room and at the outlet of EATHE pipe. The Fluke 971 meter is built for field use with an impact resistant housing, rugged holster, convenient belt clip, and bright backlit display includes °F/°C selection, Min/Max reading, hold feature, averaging function, and 99 record data logging capacity. A large LCD simultaneously displays relative humidity and temperature readings, along with calculating dew point and wet bulb temperatures. Fig. 4.17 shows picture of Fluke-971 Thermo Hygrometer and technical specifications of the device are presented in Table 4.4.

Table 4.4: Specifications of Thermo hygrometer

Relative Humidity Range	5 to 95%
Relative Humidity	± 2.5%

Temperature Range	- 4 to 140°F (- 20 to 60°C)
Relative Humidity Resolution	0.10%
Temperature Accuracy	±1.0°F @ 32 to 113°F, ±2.0°F for remaining range
Temperature Resolution	0.2 °F (0.1°C)

4.3.4 Pyranometer

The sunshine pyranometer SPN1 was used for measurement of solar irradiation which gives both diffuse and total irradiations. The sunshine pyranometer uses an array of seven, miniature thermopile sensors and a computer-generated shading pattern to measure the direct and diffuse components of incident solar radiation. The shading pattern and thermopiles are arranged so that at least one thermopile is always fully exposed to the solar beam, and at least one is fully shaded from it, regardless of the position of the sun in the sky. All seven thermopiles receive an equal amount of diffuse light. From the individual thermopile readings, a microprocessor calculates the global and diffuse horizontal irradiance and from these values an estimate of sunshine state is made.

Fig. 4.18 Sunshine pyranometer (SPN1 type) and computer generated shadow mask

The sunshine pyranometer provides two analogue voltage outputs for global and diffuse radiation, and a digital output for sunshine duration, which can be connected to data loggers, such as the DL2e and GP1. Readings can also be obtained directly from the RS-232 port. In present study GP1 data logger was used and solar irradiation was stored for every minute. An internal heater keeps the dome clear of dew, ice and snow down to -20℃ (in still air conditions), ensuring reliable readings in difficult climatic conditions.

A pyranometer is a type of action meter used to measure broadband solar irradiance and diffuse radiation separately on a planar surface. The operating principle is generally based on the measurement of the difference in temperature between a clear surface and a dark one. There are mainly three components of Pyranometer as given below:

- **Thermopile** – A sensor consisting of thermocouples connected in series and provided with a black coating for absorbing all solar radiation.
- **Glass Dome** – This dome restricts the spectral response from 300 to 2800 nm from a field of view of 180 degrees. This hemispherical glass dome also shields the thermopile from wind, rain and convection.
- **Osculating Disc** – It is used for measuring the diffuse radiation and blocking beam radiation from the surface.

The black coating on the thermopile sensor absorbs the solar radiation, while the clear surface reflects it, and hence less heat is absorbed. The thermopile is used to measure this temperature difference. The potential difference created in the thermopile owing to the temperature gradient between the two surfaces is used for measuring the amount of solar radiation. The voltage produced by the thermopile can be measured using a potentiometer. Technical specifications of the SPN 1 pyranometer are presented in Table 4.5.

Table 4.5: Specifications of pyranometer

Overall accuracy: Total (Global) and Diffuse radiation	±5% Daily integrals ±5% ±10 $W.m^{-2}$ Hourly averages ±8% ±10 $W.m^{-2}$ Individual readings
Resolution	0.6 $W.m^{-2}$ = 0.6 mV
Range	0 to >2000 $W.m^{-2}$
Analogue output sensitivity	1 mV = 1 $W.m^{-2}$
Analogue output range	0 – 2500 mV
Sunshine status threshold	120 $W.m^{-2}$ in the direct beam
Temperature coefficient	±0.02% per °C typical
Temperature range	-20 to + 70°C
Stability	Recalibration recommended every 2 years
Response time	< 200 ms
Spectral response	400 - 2700 nm
Spectral sensitivity variation	10% typical
Power requirement	2 mA (excluding heater power), 5V – 15V DC
Heater power	12 V - 15 V DC, up to 1.5 A

Size & Weight	126 mm dia. x 94 mm high, 786g

4.3.5 Anemometer

The anemometer used in experimentation is Lutron AM-4201 which is a Vane Probe type as shown in Fig. 4.19. This is a portable anemometer which provides fast and accurate readings with digital readability and the convenience of a remote sensor separately. It also comes with multi-functions for air flow measurement: m/s, km/h, ft/min, knots. It consists of a sensitive balanced vane wheel that rotates freely in housing case in response to air flow. This device is fitted with low-friction ball-bearing design resulting in accuracy at both high and low velocities and this special feature eliminates all sources of unreliability. Specifications of the device are given in Table 4.6.

Table 4.6: Specifications of Vane Probe Anemometer

Velocity range	0.4-30.0 m/s
Resolution	0.1 m/s
Accuracy	± (2 % + 1 d)
Operating temperature	0°C to 50°C
Operating humidity	Less than 80 % RH

Fig. 4.19 Vane Probe Type Anemometer

4.3.6 Full Bore Electromagnetic flow Meter

Electronet series ELMAG-200 is micro-controller based full bore type electromagnetic flow meter. These flow meters accurately measure the flow rate of conductive liquid & slurries in closed pipes. Due to simple & rigid design, the flow meter is an obstruction less & maintenance free instrument in place of conventional mechanical flow measuring device. The use of Pulsed DC technology offers highest ability & better measuring accuracy in the form of electrical signal 4-20 mA DC linearly proportional to volumetric flow. The instrument is based on Faraday's law of electro-magnetic induction. A magnetic field is generated by the instrument in the flow tube. The fluid flowing through this magnetic field generates a voltage that is proportional to the flow velocity Corresponding electrical output is provided with respect to measuring flow range. The specifications of ELMAG-200 electromagnetic flow meter are tabulated below:

Table 4.7: Technical specifications of electromagnetic flow meter

Media	Liquids (Conductive)
Calibration range	0-5 LPM
Conductivity	> 5 µs/cm
Viscosity	200 cp max
Line Size	15 NB (1/2 “)
Type of Output	4 to 20 mA DC, Isolated
Display	16 x 2 LCD - 4 digit for Flow Rate & 8 digit
Accuracy	+/- 0.5% of F. S. (for 20 to 100% flow)
Linearity	+/- 0.5% of F. S.
Repeatability	+/- 0.2% of F. S.
Process Temperature	120°C for PTFE Lining
Process Pressure	10 kg/cm² max
Working temperature of fluid	0 to 120°C
Material of construction	Lining - PTFE (Teflon) (3mm +/-1mm thick)
Flange	MS
Electrode	SS 316L
Coil Housing	MS
Power Supply	90 - 260 V AC, 50 Hz
Power Consumption	< 10 VA
Response Time	< 100m Sec
Mounting	In-Line Horizontal
Operating Conditions	Temperature 0 to 55°C / Humidity 5 to 95%

Fig. 4.20 Electromagnetic type flow meter

4.3.7 Data Logger

Data logger was used to collect and store the temperature reading sensed by the thermocouples. In present study Agilent 34972A data acquisition / data logger switch unit was used as shown in Fig 4.21. It displays the temperature reading of a channel at a time and by moving the knob, all channel readings can be displayed. It is a 16 channel data logger, while recording readings for every minute. The unit is consists of a 3-slot mainframe with a built-in 6 ½ digit DMM and 8 different switch & control modules. LAN and USB interfaces are also in built in the data logger for connecting to a PC or laptop without needing additional converter interfaces. Simply connecting the USB interface exports the reading in the form of excel sheet. The complete specifications of data logger with module are presented below:

Fig. 4.21 Data logger

Table 4.8 Specifications of data logger

3-slot LXI data acquisition unit with 6 ½-digit DMM (22-bit) and 8 plug-in modules to choose from
Measures 11 different input signals including temperature with thermocouples, RTDs and thermistors; DC/AC volts or current; 2- or 4-wire resistance; frequency and period
Accepts all 34970A switch and control plug-in modules, and is backward compatible with the 34970A SCPI command set
1Gbit LAN and USB 2.0 for easy connectivity to the PC
USB memory port for data storage or transfer
Graphical Web interface for easy set up and contro
Free BenchLink data logger software to create tests without programming

4.5 Standards for Testing of Solar Collectors

Solar water heating systems have been adopted throughout the world and also being exploited commercially in several countries. A large number of manufacturing companies have emerged on the global as well as Indian scene. In view of this, a need was felt to adopt a testing procedure for solar collector which could provide a basis for designing and selection of the equipment. Testing of solar collectors also provide collector parameters that are needed to predict the long term performance of solar thermal systems. Collector tests using standard such as BIS, ASHRAE are also required for certification and for rebates.

4.5.1 BIS 12933 (Part 5): 1992 Test Procedure

This Indian standard specifies the test methods for flat plate solar collectors. According to this standard, while testing for thermal performance, the collector is tested over its operating temperature range from 10^{o}C to 60^{o}C above ambient temperature under clear sky conditions in order to determine its efficiency characteristics.

The following measurements are obtained during collector testing:

(i) The gross area and the aperture area.

(ii) The global solar irradiance.

(iii) The surrounding air speed.

(iv) The surrounding air temperature.

(v) The temperature of the fluid at the collector inlet & outlet.

(vi) The flow rate of the fluid.

The test conditions required by the IS 12933 in performing the steady state thermal efficiency test are presented in Table 4.9. A collector may be considered to have been

operating in steady state conditions over a given test period if none of the experimental parameters deviate from their mean values by more than the limits given in Table 4.10.

Table 4.9 Required BIS test conditions

Variable	Absolute limits
Total solar radiation normal to sun	≥ 600 (W/m^2)
Fluid flow rate	Approx 0.02 $kg/s/m^2$ of collector gross area
Wind speed	$3 \leq u \leq 6$ (m/s)

Table 4.10 Permitted deviation of measured parameters during a steady state period

Parameter	Deviation from the mean value
Total solar radiation normal to sun	$\pm$ 50 (W/m^2)
Ambient temperature	$\pm 1^oC$
Mass flow rate	$\pm$ 1%
Fluid inlet temperature	$\pm 0.1^oC$
Collector inlet and outlet temperature difference	$\pm 0.1^oC$

4.5.1.1 Transmittance of glass covers

According to BIS codes 12933(Part 2):1992 transmittance test is to measure the solar radiation with pyranometer directly (without Glass) and then with glass in between the

direct radiation and the pyranometer. The ratio of the two readings shall be minimum 0.8. The transmittance test was performed on June 7, 2014.

Solar intensity without glass was 763.2 W/m^2

Solar intensity with glass at a distance 5cm above pyranometer was 635.7 W/m^2

Transmittance (τ) = 635.7/763.2 = 0.8329 or 83.29%

4.5.2 ASHRAE standard 93-1986

The ASHRAE 93 standard requires an experimental determination of the steady state collector efficiency under prescribed suitable environmental conditions for a range of collector fluid temperatures.

The specific environmental conditions required by the ASHRAE 93 in performing the thermal efficiency test are presented in Table 4.11. While testing it is also required that steady state conditions be maintained during the testing period. Table 4.12 shows the allowed maximum variation of key variables that define a steady state condition in accordance to ASHRAE 93.

Table 4.11 Required environmental conditions

Variable	Absolute limits
Total solar radiation normal to sun	≥ 790 (W/m^2)
Diffuse fraction	≤ 20 %
Wind speed	$2.2 \leq u \leq 4.5$ (m/s)

Table 4.12 Maximum variations of key variables

Variable	Maximum variations
Total solar radiation normal to surface	± 32 (W/m^2)
Surrounding air temperature	± 1.5 K
Inlet temperature	The greater of ± 2 % or 1 K
Mass flow rate	The greater of ± 2 % or 0.02 lpm

All the methods are essentially based on the Hottel-Whillier-Bliss equations and differ only either in the recommendations or in the parameters to be monitored. Out of these, the ASHRAE method has been chosen in this study for carrying out the testing of solar collector.

4.6 Experimental Procedure

The experimental procedure includes following steps:

(i) Following the ASHRAE standards for fabrication of the collector.

(ii) Selection of materials for different components.

(iii) Identifying the best options available i.e. for nanoparticle and base fluid selection, formation of fluid film, insulation etc.

(iv) Record of experimental results.

(v) Calculations and Graphs

(vi) Comparisons

However the ASHRAE and BIS codes must be applied for the fabrication of any solar collector but as these codes are developed for tube-in-plate type flat plate collector based on the concept of surface absorption and DASC is a different concept which is based on volumetric absorption which applies formation of a thin fluid film over the base plate. Formation of thin fluid film is challenging therefore length and width should be optimally select. The size of the collectors is kept about 1.4 m^2 in which the effective area is 1.15 m^2.The material selected for the collector box is wood because wood is a good insulator and also can be cut easily into whatever required shape and size. The thermal conductivity of wood is nearly about 0.04 W/m K.

Method

Initial steps into the experiment:

The experiment consists in a series of processes that are listed as follows:

(i) Turn on the pump to circulate the water / nanofluid.

(ii) Record the inlet and outlet temperatures

(iii) Take records every 15 minutes

(iv) Keep taking readings until the temperature stop to increase.

(v) Plot the records in a graph.

CHAPTER 5

PERFORMANCE ANALYSIS

Performance analysis of direct absorption solar collector is discussed in this chapter which includes the collector efficiency variation under different test conditions i.e. at different fluid flow rates, at different solar irradiance, at different nanoparticles volume fraction.

The experimental study of direct absorption solar collector is performed first with distill water and then with two types of nanofluids (Al_2O_3-water and TiO_2-water) of different concentrations (0.001%, 0.003%, 0.005% and 0.007%) at three different flow rates (1.5 lpm, 2.0 lpm and 2.5 lpm) and these experimental data are used to carry out collector performance analysis to get the optimum values of operating parameters. Results of the analysis are plotted in the form of collector performance curves.

The following measurements were taken during the experimental study:

- Fluid inlet temperature (T_i)
- Fluid outlet temperature (T_o)
- Base plate temperature (T_{bp})
- Glass cover temperature (T_g)
- Ambient air temperature (T_a)
- Global solar radiation (I_T)
- Fluid flow rate ($\dot{m}$)

5.1 Collector Efficiency Calculations

The experiments were conducted at different fluid inlet temperatures according to ASHRAE Standard 93-86. Useful heat gain by the fluid can be calculated using equation 5.1.

$$Q_u = \dot{m}\, C_p\,(T_o\text{-}T_i) = A_c F_R[I_T(\tau\alpha)\text{-}U_L(T_i\text{-}T_a)] \quad (5.1)$$

where Q_u is the useful heat gain (W), $\dot{m}$ is the fluid mass flow rate (kg/min), C_p is the heat capacity of water or nanofluid (J/kg K), A_c is the aperture area of solar collector (m^2), F_R is the heat removal factor, (τα) is absorptance–transmittance product, I_T is the global solar radiation (W/m^2), U_L is the overall heat loss coefficient of solar collector (W/m^2 K), and T_a is the ambient temperature (K).

The heat capacity of nanofluid ($C_{p,nf}$) is calculated using equation 5.2 [Khanafer and Vafai (2011)].

$$C_{p,nf} = C_{p,np}(\phi) + C_{p,bf}(1\text{-}\phi) \quad (5.2)$$

where ϕ indicates the volume fraction of nanoparticles, and $C_{p,np}$ and $C_{p,bf}$ are heat capacities of nanoparticles and base fluid respectively. Instantaneous collector efficiency relates the useful heat gain to the incident solar energy by equation 5.3 and 5.4.

$$\eta_i = \frac{Q_u}{A_c\, I_T} = \frac{\dot{m}\, C_p\,(T_o - T_i)}{A_c I_T} \quad (5.3)$$

$$\eta_i = F_R(\tau\alpha) - F_R U_L \frac{(T_i - T_a)}{I_T} \quad (5.4)$$

If the thermal efficiency test is performed at the normal incidence conditions then $F_R(\tau\alpha)$, and $F_R U_L$ is constant for the normal temperature range of the collector. When the efficiency values obtained from averaged data are plotted against $\frac{(T_i - T_a)}{I_T}$ a straight line will result according to equation 5.4. Intersection of the line with vertical axis equals to absorbed energy parameter, $F_R(\tau\alpha)$ as shown in Fig. 5.1.

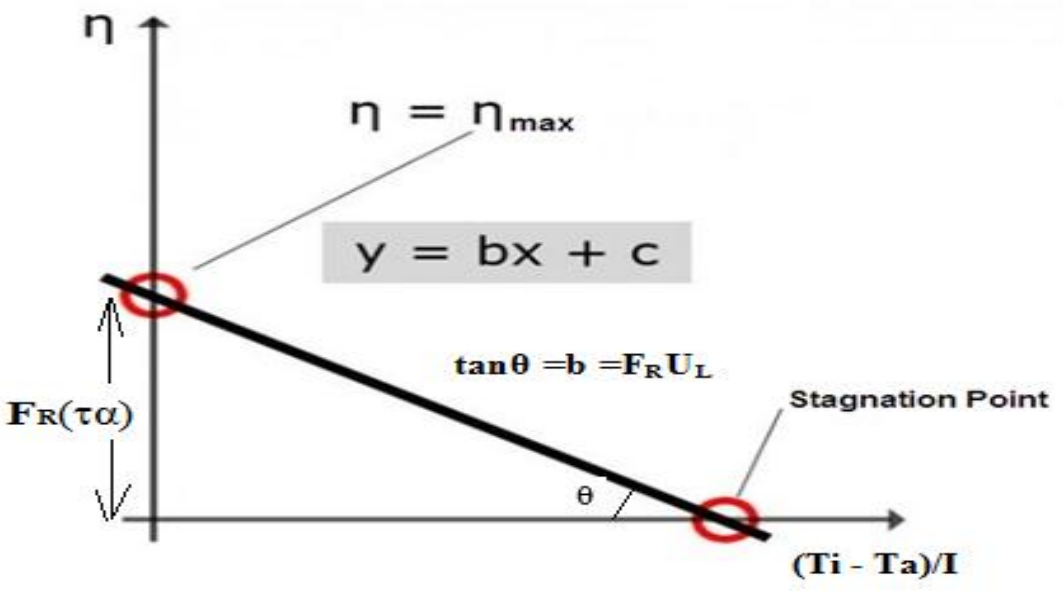

Fig. 5.1 Performance characteristics curve for solar collectors

At the intersection point collector efficiency is the maximum and temperature of the fluid entering the collector equals the ambient temperature. Slope of the line indicates energy loss from the collector that is nominated as energy loss parameter $F_R U_L$. At the intersection of the line with the horizontal axis collector efficiency is zero and designated as stagnation point, with no fluid temperature gain due to equality of input solar energy and loss energy.

5.2 Experimental Observations with Glass base plate using distilled water

Experiments were performed initially using distilled water as the collector fluid on direct absorption solar collector from 10 AM to the time at which stagnation point is reached for three different flow rates of 1.5, 2 and 2.5 lpm in the month of October, 2013. The experiment was performed several times and the data satisfying conditions of ASHRAE standard 93-86 have been considered. Fig. 5.2 shows the variation of collector efficiency

versus the reduced temperature parameter, $(T_i - T_a)/I_T$, for each flow rate. The experimental data are best fitted with linear equations to provide the collector performance characteristic parameters for different flow rates. Experimental and calculated data at each flow rate are presented in the Table 5.1 to 5.3 and performance parameters (i.e. F_RU_L and $F_R(\tau\alpha)$) in Table 5.4.

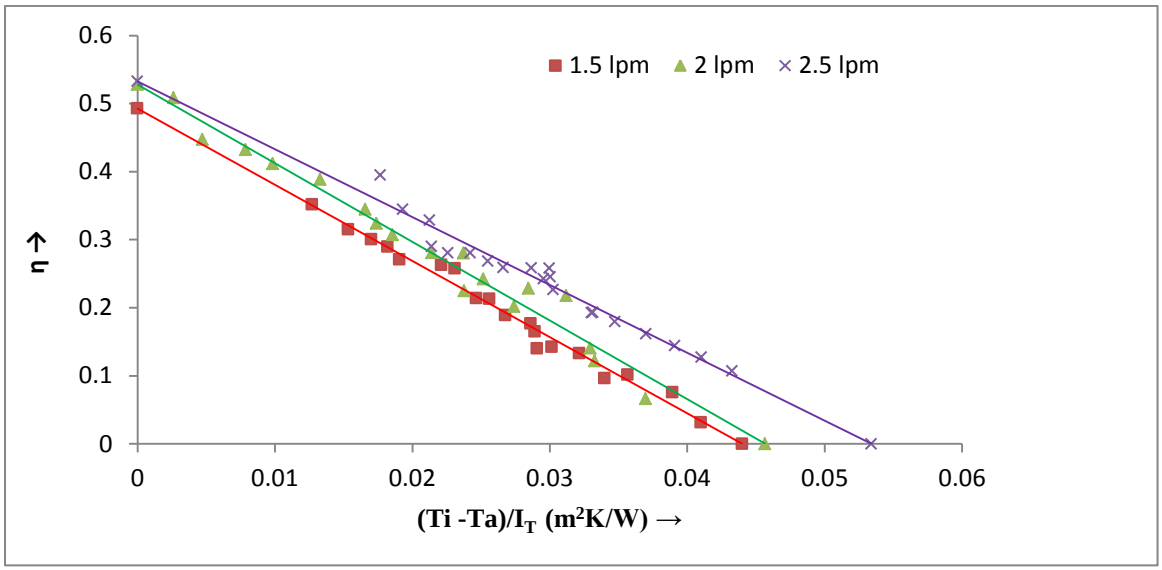

Fig. 5.2 Efficiency versus $(T_i - T_a)/I_T$ curve at three flow rates for distilled water

Table 5.1 Experimental and calculated data for distilled water at 1.5 lpm

Time	Temperature (°C)						I_T (W/m²)	(Ti-Ta)/I_T (m²K/W)	η
	T_i	T_o	T_g	T_{bp}	T_a	$(T_o - T_i)$			
10:00	30.8	33.3	33.8	36	29.2	2.1	566	0.012	0.35
10:15	32.7	35	35.1	38.1	29.7	2.1	606	0.015	0.31
10:30	35.9	38.3	36.9	40.5	30.5	2.1	635	0.017	0.30
10:45	37.4	39.7	38.1	42.6	30.6	2.1	668	0.018	0.29
11:00	40.5	42.7	39.6	44.1	31.2	2	691	0.019	0.27
11:15	43.4	45.4	40.8	46.1	31.5	2	690	0.022	0.26
11:30	44.4	46.3	41.9	47.4	31.8	2	722	0.023	0.25
11:45	46.6	48.5	43.9	50.6	32.4	1.7	748	0.024	0.22
12:00	47.6	49.2	44.5	52.1	32.5	1.7	750	0.025	0.21

12:15	48.6	50.1	45.7	53.4	32.9	1.5	751	0.026	0.19
12:30	50.2	51.5	46.2	54.2	33.2	1.4	738	0.027	0.18
12:45	51.4	52.8	47.1	55.7	33.4	1.3	729	0.028	0.16
13:00	52.7	53.8	47.8	56.4	34.2	1.1	724	0.029	0.14
13:15	53.1	54.3	48.5	57.8	34.6	1.1	694	0.030	0.14
13:30	53.6	54.7	49.2	58.5	34.1	1	696	0.032	0.13
13:45	54.4	55.1	49.4	59.2	34.1	0.7	665	0.034	0.09
14:00	54.4	55	49.3	59.5	34.1	0.7	646	0.036	0.10
14:15	54.5	54.8	49.6	59.4	33.8	0.5	619	0.039	0.07
14:30	54.5	54.7	49	59.7	33.9	0.2	585	0.041	0.03

Table 5.2 Experimental and calculated data for distilled water at 2 lpm

Time	Temperature (°C)						I_T (W/m^2)	$(Ti-Ta)/I_T$ (m^2K/W)	η
	Ti	To	Tg	Tbp	Ta	$(T_o - T_i)$			
10:00	30.8	33.3	40	37.2	29.2	2.5	608	0.002	0.51
10:15	32.7	35	41.2	39	29.7	2.3	636	0.005	0.45
10:30	35.9	38.3	43.1	42.7	30.5	2.4	687	0.008	0.43
10:45	37.4	39.7	44	44.2	30.6	2.3	691	0.009	0.41
11:00	40.5	42.7	45.1	47.1	31.2	2.2	700	0.013	0.39
11:15	43.4	45.4	45.7	50	31.5	2	718	0.016	0.34
11:30	44.4	46.3	46.1	50.9	31.8	1.9	725	0.017	0.32
11:45	46.6	48.5	48.1	53.2	32.4	1.9	765	0.018	0.31
12:00	47.6	49.2	48.3	54	32.5	1.6	705	0.021	0.29
12:15	48.6	50.1	48.4	54.7	32.9	1.5	662	0.023	0.28
12:30	50.2	51.5	49.4	56.5	33.2	1.3	715	0.024	0.23
12:45	51.4	52.8	50.6	57.6	33.4	1.4	715	0.025	0.24
13:00	52.7	53.8	50.3	58.8	34.2	1.1	675	0.027	0.20
13:15	53.1	54.3	50.7	59	34.6	1.2	650	0.028	0.21

13:30	53.6	54.7	50.4	59	34.1	1.1	625	0.031	0.21
13:45	54.4	55.1	50.1	59.1	34.1	0.7	616	0.033	0.14
14:00	54.4	55	50.4	59.2	34.1	0.6	610	0.034	0.12
14:15	54.5	54.8	49.4	59	33.8	0.3	560	0.037	0.07

Table 5.3 Experimental and calculated data for distilled water at 2.5 lpm

Time	Temperature (°C)						I_T (W/m^2)	$(Ti-Ta)/I_T$ (m^2K/W)	η
	T_i	T_o	T_g	T_{bp}	T_a	$(T_o - T_i)$			
10:00	34	35.5	36.2	39.7	24	1.5	566	0.018	0.39
10:15	36.5	37.9	38	42.2	24.8	1.4	606	0.019	0.34
10:30	38.6	40	39.6	44.3	25.1	1.4	635	0.021	0.32
10:45	40.3	41.6	40.7	46.6	26	1.3	668	0.022	0.29
11:00	42.2	43.5	42.4	48.5	26.6	1.3	691	0.023	0.28
11:15	43.3	44.6	42.8	49.8	26.6	1.3	690	0.024	0.28
11:30	45.8	47.1	44.2	52.4	27.4	1.3	722	0.025	0.27
11:45	47.3	48.6	45.1	53.9	27.4	1.3	748	0.027	0.26
12:00	49.6	50.9	46.9	56.1	28.1	1.3	750	0.028	0.26
12:15	50.2	51.5	47.2	56.6	27.7	1.3	751	0.029	0.26
12:30	51.4	52.6	47.3	57.5	29.6	1.2	738	0.029	0.24
12:45	52.1	53.3	48	58.3	30.2	1.2	729	0.030	0.24
13:00	52.5	53.6	48.5	58.6	30.6	1.1	724	0.030	0.23
13:15	53.7	54.6	48.7	59.3	30.7	0.9	694	0.033	0.20
13:30	53.8	54.7	49.2	59.9	30.8	0.9	696	0.033	0.19
13:45	54	54.8	49.1	59.9	30.9	0.8	665	0.035	0.18
14:00	54.2	54.9	48.8	59.9	30.3	0.7	646	0.037	0.16
14:15	54.5	55.1	48.8	59.9	30.3	0.6	619	0.039	0.14
14:30	54.5	55	48.2	59.3	30.5	0.5	585	0.041	0.13
14:45	54.2	54.6	47.9	59.2	30.1	0.4	557	0.043	0.11

Table 5.4 Collector efficiency parameters at three flow rates with water

S.No.	Flow rate (lpm)	F_RU_L	$F_R(\tau\alpha)$	R^2
1	1.5	11.197	0.4926	0.9817
2	2	11.56	0.528	0.968
3	2.5	9.973	0.5326	0.9557

It is observed from Table 5.4 that absorbed energy parameter, $F_R(\tau\alpha)$ at 2.5 lpm is the maximum and energy loss parameter F_RU_L is the minimum and so the instantaneous efficiency of the collector is the highest at this flow rate. Since emission of radiation from the fluid increases with the fourth power of temperature, the fluid suffers higher emissive losses at lower flow rates (1.5 lpm), which results in lower collector efficiencies.

At higher flow rates, the smaller fluid temperature rise is observed (Fig. 5.3) resulting in progressively weaker emissive losses, this result into greater collector efficiencies at high flow rates. At low flow rates, fluid residence time in collector is higher i.e. more solar heat absorption by the fluid and getting greater fluid temperature.

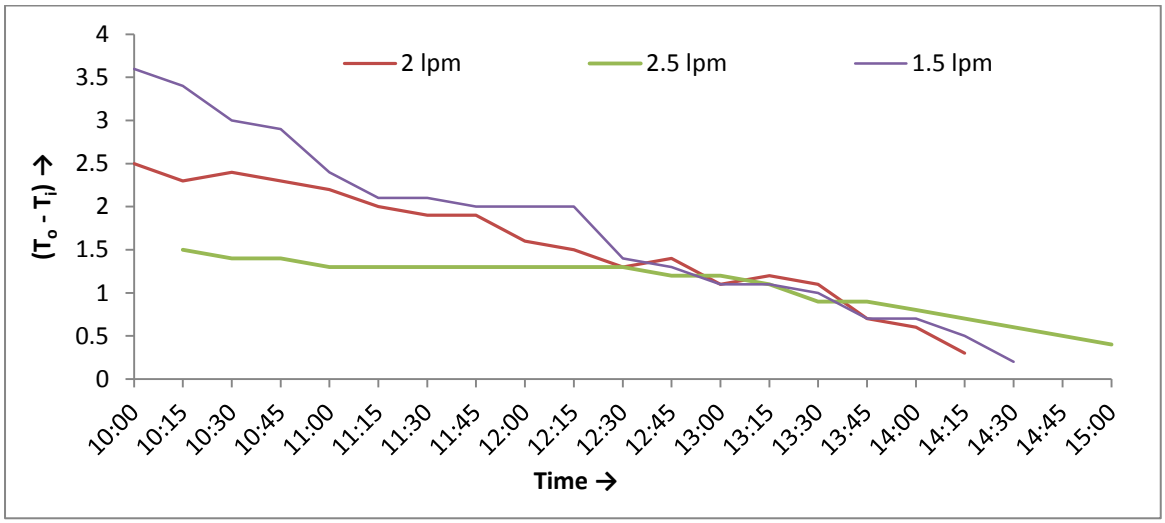

Fig. 5.3 Single pass temperature rise for three flow rates with time

5.3 Glass base plate using Al_2O_3-water nanofluid

5.3.1 Effect of volume fraction

Al_2O_3-water nanofluid of four different concentrations 0.001 vol%, 0.005 vol%, 0.01 vol% and 0.05 vol% were prepared and studied at different inlet fluid temperature in quasi steady state conditions from 10.00 AM to the time when stagnation temperature is reached. Nanofluid coming out of the collector is stored temporarily in the bottom collection tank and then pumped to overhead storage tank.

Experimental study was carried out with distilled water and Al_2O_3-water nanofluid of four different concentrations at constant flow rate of 2 lpm and the planned experimental schedule was as follows:

Day 1: 27 October 2013, distilled water

Day 2: 28 October 2013, Al_2O_3 nanofluid (0.001% v.f)

Day 3: 29 October 2013, Al_2O_3 nanofluid (0.005% v.f)

Day 4: 30 October 2013, Al_2O_3 nanofluid (0.01% v.f)

Day 5: 31 October 2013, Al_2O_3 nanofluid (0.05% v.f)

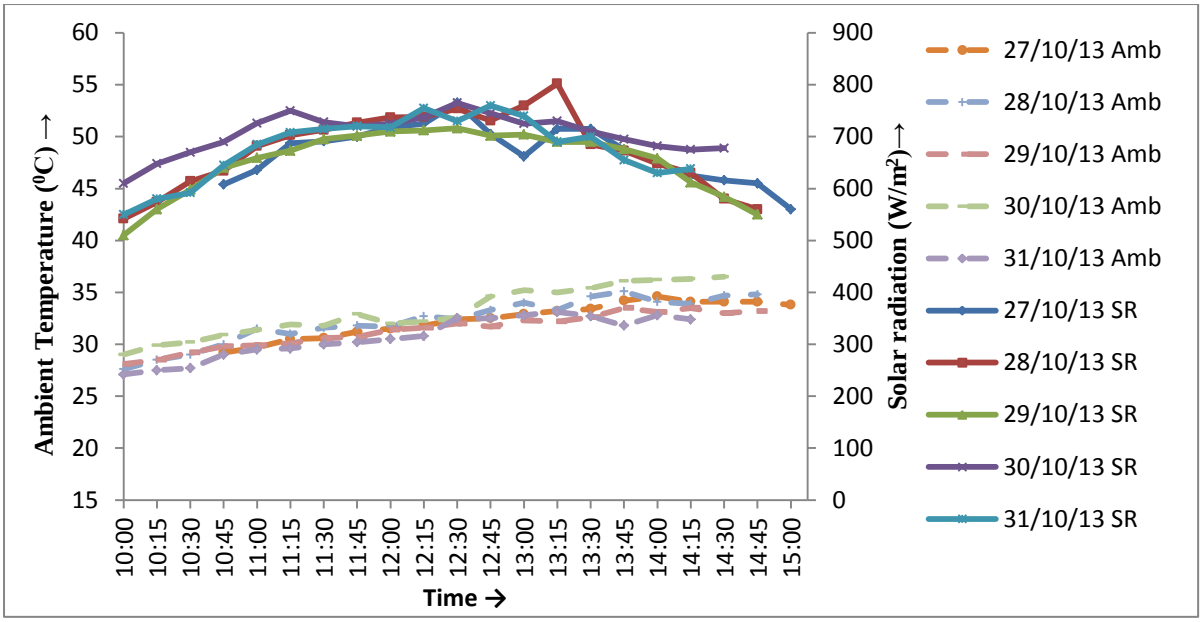

Fig. 5.4 Ambient and solar radiation data during the test period

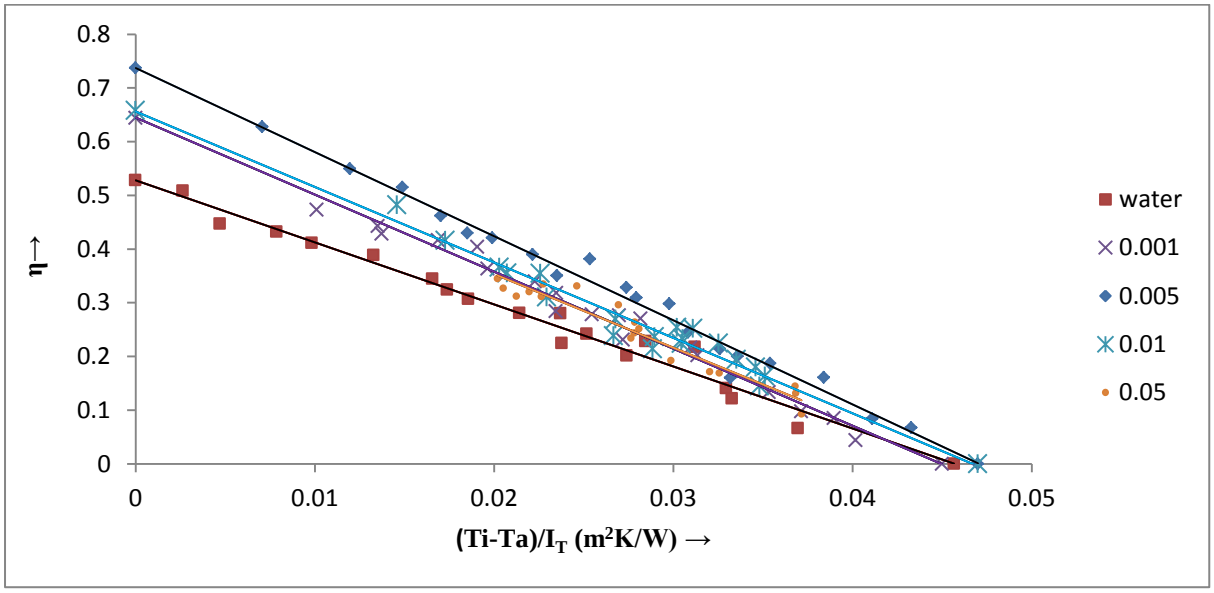

Fig. 5.5 Efficiency plots for water and nanofluid

Fig. 5.4 shows typical recorded data for ambient temperature and total incident solar radiation during the test period. The experimental results for distill water and for four different concentrations of nanofluids are plotted in the form of efficiency curves as shown in Fig. 5.5. Experimental and calculated data at each concentration are presented in Table 5.5 to 5.8 and collector performance parameters (i.e. F_RU_L and $F_R(\tau\alpha)$) in Table 5.9.

It is observed from Fig.5.5 that collector efficiency with nanofluid is higher than water due to greater values of absorbed energy parameter $F_R(\tau\alpha)$ for nanofluids as compared to water which is also clear from Table 5.9. For 0.001 vol % concentration of nanofluid the absorbed energy parameter ($F_R(\tau\alpha)$) and maximum collector efficiency is 22.1% higher than distill water in low temperature range because absorbed energy parameter dominates over heat loss parameter. However, in high temperature range heat loss parameter dominates and reduces collector efficiency. It is also noticed that collector efficiency for all the fluids become nearly equal in higher temperature range.

Table 5.5 Experimental and calculated data for 0.001 vol% nanofluid at 2 lpm

Time	Temperature (°C)						I_T (W/m^2)	(Ti-Ta)/I_T (m^2K/W)	η
	T_i	T_o	T_g	T_{bp}	T_a	$T_o - T_i$			
10:00	32.4	34.9	38.6	38.3	27.6	2.5	542	0.008	0.57
10:15	34.3	36.5	39.6	40.4	28.5	2.2	574	0.010	0.47
10:30	37.3	39.5	42	43.8	29	2.2	614	0.013	0.44
10:45	38.7	40.9	42.8	45.3	30	2.2	634	0.014	0.43
11:00	43	45.3	46.4	50.2	31.5	2.3	682	0.017	0.42
11:15	44.4	46.7	47.2	51.6	31	2.3	703	0.019	0.40
11:30	45.6	47.7	47	52.9	31.6	2.1	713	0.020	0.36
11:45	48	50	49.2	55	31.8	2	727	0.022	0.34
12:00	49	50.9	49.4	56.2	31.7	1.9	737	0.023	0.32
12:15	50	51.7	49.6	56.9	32.7	1.7	738	0.024	0.29
12:30	51.6	53.3	50.9	59	32.4	1.7	754	0.026	0.28
12:45	53.9	55.5	53.1	60.8	33.3	1.6	731	0.028	0.27

13:00	54.5	56.2	53	61.1	34	1.7	760	0.027	0.27
13:15	55.1	56.6	52.8	61.7	33.3	1.5	802	0.027	0.23
13:30	55.8	57	53.4	62.2	34.6	1.2	685	0.030	0.22
13:45	56.2	57.3	53.6	62.4	35.1	1.1	673	0.031	0.20
14:00	57	57.7	53.6	62.6	34.1	0.7	648	0.035	0.13
14:15	57.3	57.8	53.4	62.4	33.9	0.5	630	0.037	0.10
14:30	57.3	57.7	40.7	61.9	34.7	0.4	580	0.039	0.08
14:45	57.3	57.5	38.9	61.7	34.8	0.2	560	0.040	0.04

Table 5.6 Experimental and calculated data for 0.005 vol% nanofluid at 2 lpm

Time	Temperature (°C)						I_T (W/m^2)	(Ti-Ta)/I_T (m^{2}K/W)	η
	T_i	T_o	T_g	T_{bp}	T_a	$T_o - T_i$			
10:00	31.7	34.3	38.6	37.7	28.1	2.6	510	0.007	0.63
10:15	35.2	37.7	39.9	41	28.5	2.5	560	0.012	0.55
10:30	38.1	40.6	42.4	44	29.2	2.5	598	0.015	0.52
10:45	40.7	43.1	44.9	47	29.8	2.4	640	0.017	0.46
11:00	42.1	44.4	46.1	48.4	29.9	2.3	659	0.019	0.43
11:15	43.5	45.8	47.1	49.8	30.1	2.3	673	0.020	0.42
11:30	46	48.2	48	52.6	30.6	2.2	695	0.022	0.39
11:45	47.2	49.2	48.1	53.8	30.7	2	702	0.024	0.35
12:00	49.4	51.6	49.4	56.1	31.4	2.2	710	0.025	0.38
12:15	51.1	53	51.1	58	31.6	1.9	712	0.027	0.33
12:30	52	53.8	52	58.4	32	1.8	716	0.028	0.31
12:45	52.6	54.3	52	59.2	31.7	1.7	702	0.030	0.30
13:00	54	55.4	52.7	60.6	32.3	1.4	704	0.031	0.25
13:15	54.7	55.9	53.6	61.2	32.2	1.2	690	0.032	0.22

13:30	55.5	56.4	53.8	61.5	32.6	0.9	690	0.033	0.16
13:45	56.2	57.3	53.8	62	33.5	1.1	676	0.034	0.20
14:00	56.4	57.4	54.1	62.1	33.1	1	658	0.035	0.18
14:15	57	57.8	53.5	62	33.5	0.8	612	0.038	0.16
14:30	57	57.4	53.1	61.6	33	0.4	584	0.041	0.08
14:45	57	57.3	53	61.4	33.2	0.3	550	0.043	0.07

Table 5.7 Experimental and calculated data for 0.01 vol% nanofluid at 2 lpm

Time	Temperature (°C)						I_T (W/m^2)	$(Ti-Ta)/I_T$ (m^2K/W)	η
	T_i	T_o	T_g	T_{bp}	T_a	$T_o - T_i$			
10:00	37.9	40.3	41.2	45	29	2.4	610	0.014	0.48
10:15	41.1	43.3	42.9	47.4	29.9	2.2	648	0.017	0.42
10:30	43.8	45.8	45.1	50.2	30.2	2	670	0.020	0.37
10:45	45.2	47.2	46.4	51.5	30.9	2	690	0.021	0.36
11:00	47.8	49.9	48.5	54.9	31.4	2	726	0.022	0.35
11:15	49.1	51	49.3	56.1	31.9	1.9	750	0.023	0.31
11:30	51.3	52.9	49.6	58.1	31.8	1.6	728	0.026	0.27
11:45	52.1	53.5	50.6	59.1	32.9	1.4	720	0.027	0.24
12:00	53	54.4	50.3	60	32	1.4	725	0.029	0.24
12:15	54.7	56.1	52.3	61.2	32.2	1.4	737	0.030	0.23
12:30	55.9	57.3	54	62.1	32.6	1.4	765	0.030	0.22
12:45	56.1	57.4	53.4	63.5	34.6	1.3	745	0.029	0.21
13:00	57.1	58.6	53.5	64.4	35.2	1.5	725	0.030	0.25
13:15	57.7	59.2	53.9	65	35	1.5	730	0.031	0.25
13:30	58.5	59.8	53.3	65.1	35.4	1.3	710	0.032	0.22
13:45	59.4	60.5	54.8	66.1	36.1	1.1	695	0.033	0.19
14:00	59.8	60.8	55.2	65.8	36.2	1	682	0.034	0.18

14:15	60	60.9	55.5	65.8	36.3	0.9	675	0.035	0.16
14:30	60.1	60.9	54.4	65.4	36.5	0.8	678	0.035	0.14

Table 5.8 Experimental and calculated data for 0.05 vol% nanofluid at 2 lpm

Time	Temperature (°C)						I_T (W/m^2)	(Ti-Ta)/I_T (m^{2}K/W)	η
	T_i	T_o	T_g	T_{bp}	T_a	$T_o - T_i$			
10:00	38.2	39.8	36	44	27.1	1.6	580	0.020	0.35
10:15	39.4	41	38.7	45.4	27.5	1.6	585	0.021	0.33
10:30	40.7	42.3	39	46.6	27.7	1.6	592	0.022	0.32
10:45	42.7	44.4	41.4	49.6	29	1.7	645	0.021	0.31
11:00	45	46.8	41.5	52	29.5	1.8	685	0.022	0.31
11:15	45.7	47.7	43.1	53	29.6	2	708	0.023	0.34
11:30	47.6	49.6	44.5	54.9	30	2	715	0.025	0.33
11:45	49.6	51.4	46.5	56.7	30.2	1.8	720	0.027	0.30
12:00	50.5	52.1	47.3	57.3	30.5	1.6	718	0.028	0.26
12:15	52	53.6	48.2	59.1	30.8	1.6	755	0.029	0.25
12:30	52.8	54.3	46.6	59.8	32.5	1.5	730	0.028	0.24
12:45	53.5	55	49.2	61.1	32.5	1.5	760	0.028	0.23
13:00	54.9	56.1	49.2	61.6	32.8	1.2	740	0.030	0.19
13:15	55.2	56.2	49.5	62	33.1	1	690	0.032	0.17
13:30	55.5	56.5	50	62.1	32.7	1	700	0.033	0.17
13:45	55.9	56.7	49.6	61.7	31.8	0.8	655	0.036	0.14
14:00	56	56.7	47.6	62.3	32.8	0.7	630	0.037	0.13
14:15	56.1	56.6	49.7	62.2	32.4	0.5	638	0.037	0.09

Table 5.9 Collector efficiency parameters for nanofluid and water at 2 lpm flow rate

S.No.	Working fluid	Volume fraction (%)	F_RU_L	$F_R(\tau\alpha)$	R^2
1	Water	0	11.56	0.528	0.968

2	Al_2O_3 nanofluid	0.001	14.346	0.6447	0.9789
3		0.005	15.663	0.7372	0.982
4		0.01	14.132	0.6579	0.9426
5		0.05	13.693	0.6271	0.9315

The maximum collector efficiency increased by 14.35% with the increase in nanoparticle concentration from 0.001 to 0.005 vol% due to enhancement in absorbed energy parameter. Heat loss parameter also increased but by lesser amount of 9.2 % as observed from Table 5.9. Nanoparticle concentration increase beyond 0.005 vol% resulted in collector efficiency loss.

Collector efficiency is maximum for certain volume fraction (ϕ) of nano fluid and it decreases for lower and higher values of nanofluid volume fractions. At lower nano fluid volume fraction, some fraction of the incident solar radiations are absorbed by the nanofluid film and remaining portion by the bottom base plate. This raised the nanofluid temperature near the bottom plate causing extra emissive losses hence lower collector efficiency. At certain nanofluid volume fraction where peak collector efficiency is reached uniform temperature distribution within nanofluid volume is expected. For higher nanofluid volume fraction, top layers of nanofluid absorb most of the incident radiation and allowing little or no radiation to penetrate the lower fluid layer and reach the bottom plate. This results in uneven temperature distribution within nanofluid film and higher top layer temperature causes excessive emissive losses and drop in collector efficiency.

Tyagi et al. (2009) also explained that increasing the nano particle volume fraction leads to a corresponding increase in attenuation of sunlight passing through the collector, and this, in turn, increases the collector efficiency. Since the attenuation varies exponentially with the extinction coefficient (and hence also with volume fraction), the efficiency initially increases very rapidly at low volume fraction and quickly reaches an asymptotic

value at higher volume fractions. The results of present study also indicate that addition of nanoparticles will be advantageous only up to a certain limit, beyond which the increase in efficiency would be miniscule and thus the experimental results are in tune with the Tyagi's finding.

The net extinction caused by the nanofluid is obtained by adding the individual contributions from the nanoparticles as well as the base fluid water. The intensity distribution within the solar collector is obtained using

$$\frac{\partial I_\lambda}{\partial y} = -k_{e\lambda,nanofluid}\, I_\lambda = -\left(K_{a\lambda,water} + K_{e\lambda,nanoparticles}\right) I_\lambda \qquad (5.5)$$

In general, the extinction coefficient can be given as

$$K_{e\,\lambda} = \frac{3\, f_v\ Q_{e\,\lambda}(\alpha,m)}{2D} \qquad (5.6)$$

Where f_v is the particle volume fraction and $Q_{e\lambda}$ is the extinction efficiency, D is the diameter of the particles and m is defined as the normalized refractive index of the particles to the fluid, α is defined as the size parameter.

Fig. 5.6 shows nanofluid temperature rise at different concentrations for constant flow rate of 2 lpm and maximum collector efficiency is observed at 0.005 vol%. Fluid temperature rise increased with increase in nanoparticle concentration from 0.001 to 0.005 vol% due to increase in absorbed energy parameter and further increase in nanoparticle concentration beyond 0.005 vol% resulted decrease in fluid temperature rise as observed from Fig. 5.6.

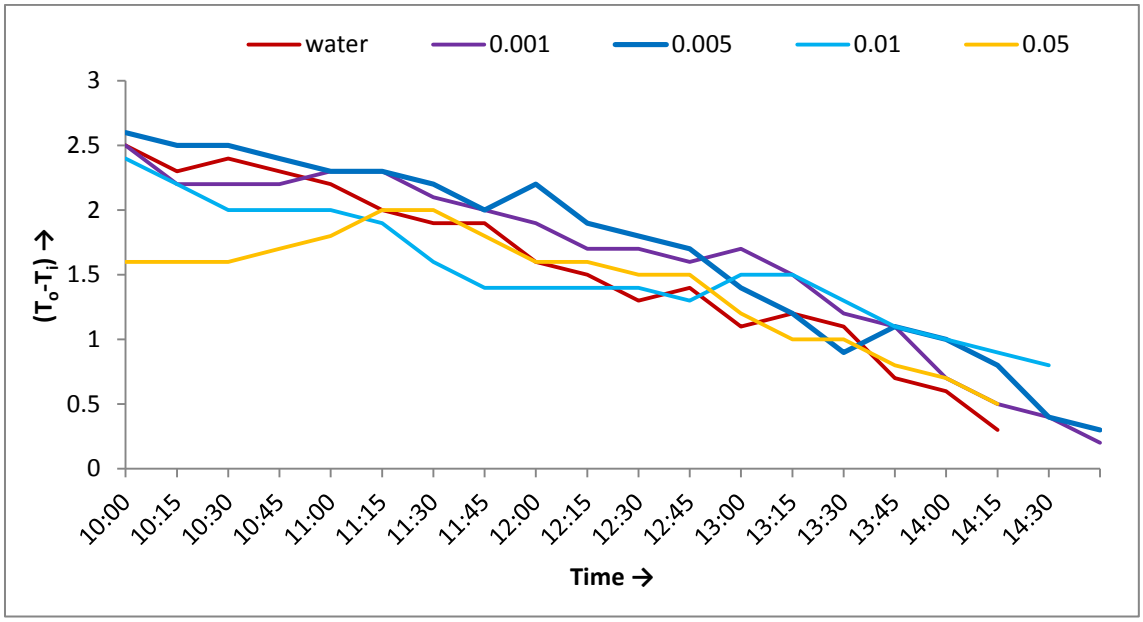

Fig. 5.6 Nanofluid temperature rise at four different concentrations for 2 lpm

5.3.2 Effect of fluid flow rate

Al_2O_3-water nanofluid of 0.005% volume fraction concentration is used to investigate the effect of three different flow rates of 1.5, 2 and 2.5 lpm. At each flow rate experiments for several test periods at different inlet fluid temperature in quasi steady state conditions were conducted from 10.00 AM to the time when stagnation temperature is reached on each day and the experimental results are plotted as shown in Fig. 5.7 and Fig. 5.8. The collector efficiency parameters $F_R(\tau\alpha)$ and F_RU_L for three flow rates of Al_2O_3 nanofluid are presented in Table 5.10.

It is observed from Fig.5.7 and Fig.5.8 that the collector efficiency lines for 2 and 2.5 lpm intersect each other. For low temperature range, the collector efficiency is greater at 2 lpm due to higher value of absorbed energy parameter. However for high temperature range, the collector efficiency is greater at 2.5 lpm due to reduced heat losses. As collector is

operated most of the time in the low temperature range hence, 2 lpm is the optimum flow rate for maximum efficiency of the collector.

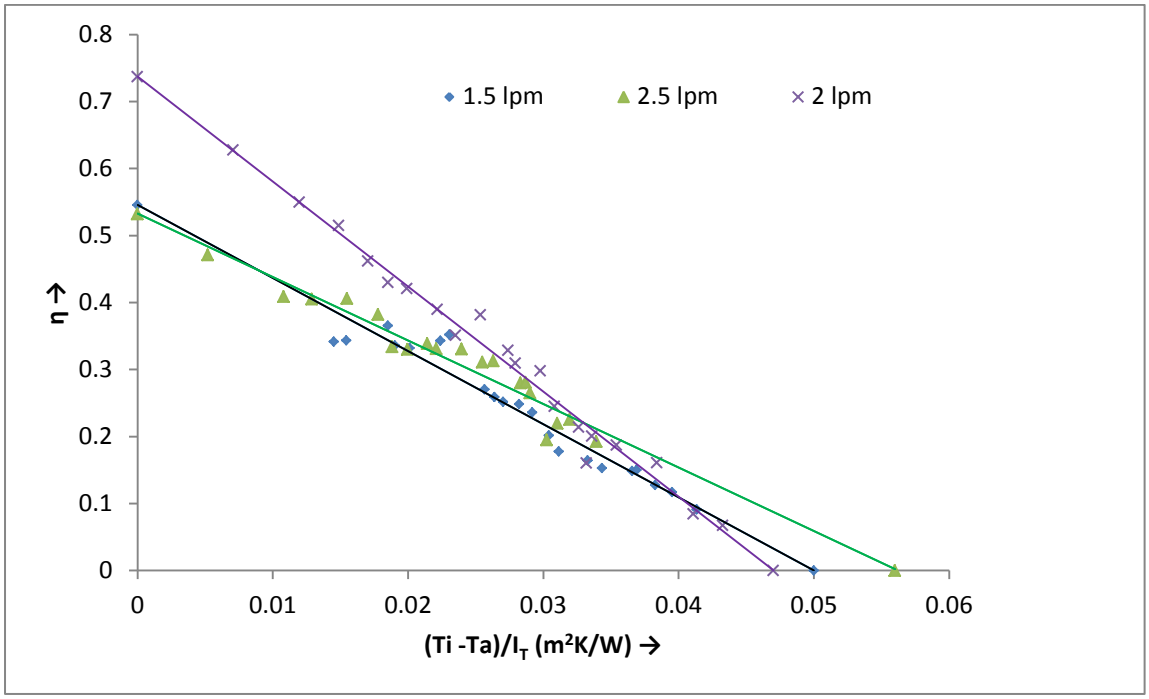

Fig. 5.7 Efficiency versus $(T_i - T_a)/I_T$ curve at three flow rates for 0.005 vol% nanofluid

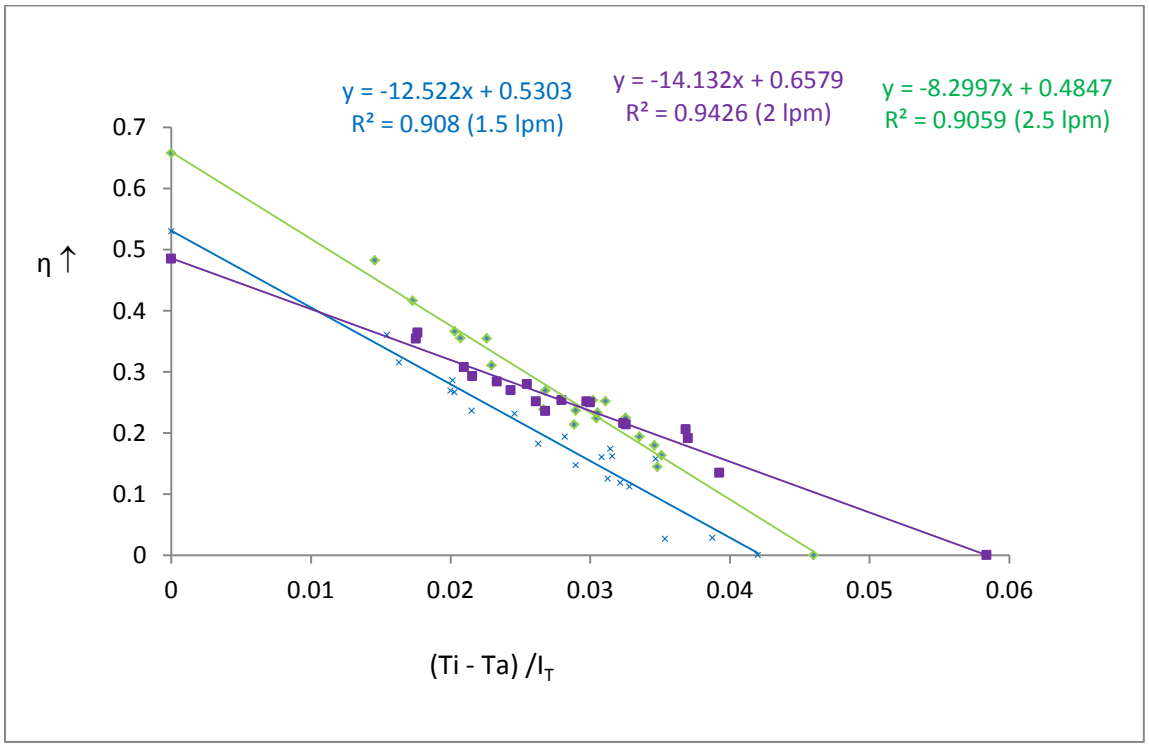

Fig. 5.8 Efficiency versus $(T_i - T_a)/I_T$ curve at three flow rates for 0.01 vol% nanofluid

Table 5.10 Collector efficiency parameters for Al_2O_3-water nanofluid of 0.007%

S.No.	Flow rate (lpm)	F_RU_L	$F_R(\tau\alpha)$	R^2
1	1.5	10.903	0.5455	0.9349
2	2	15.663	0.7372	0.982
3	2.5	9.4418	0.5322	0.925

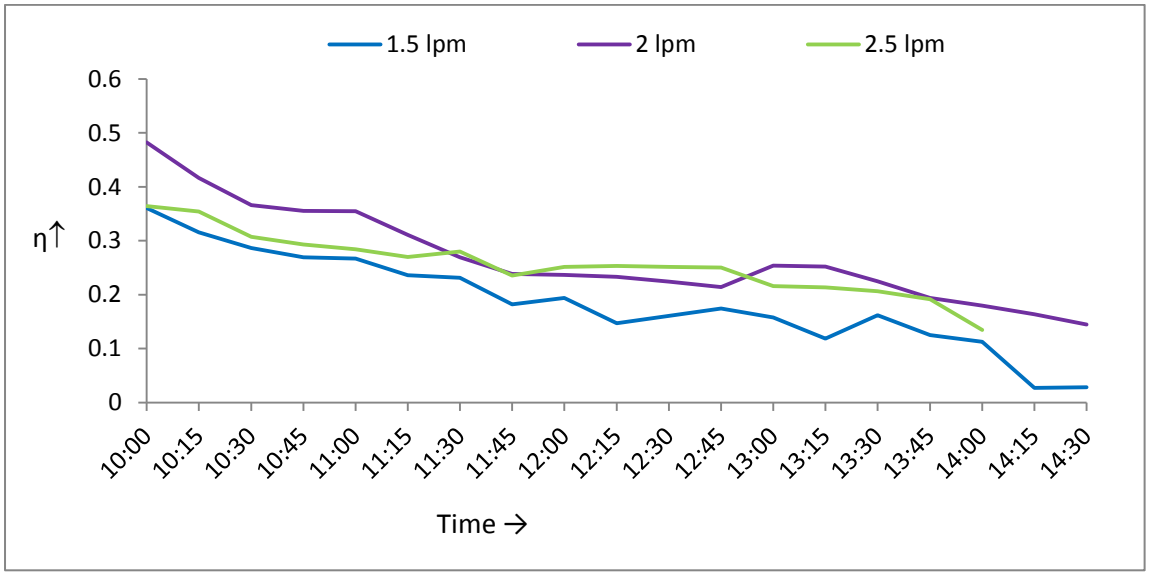

Fig. 5.9 Efficiency variation with time at three flow rates for 0.01 vol% nanofluid

Fig. 5.9 shows the collector efficiency variation with time of the experimental day at three different flow rates for 0.01 vol% Al_2O_3-water nanofluid. Efficiency decreases with passage of time and maximum efficiency is obtained at 2 lpm for most of time in a day.

5.4 Aluminum base plate using water

Efficiency of direct absorption solar collector for three flow rates of water, versus the reduced temperature parameter $(T_i - T_a)/I_T$ is plotted as shown in Fig. 5.10. The experimental data are fitted with best linear equations to provide the collector performance characteristic parameters.

It is observed from Fig. 5.10 that for pure water the value of loss parameter F_RU_L is almost constant with different flow rates. However, the absorbed energy parameter $F_R(\tau\alpha)$ increases up to 2 lpm and after that it becomes nearly constant resulting highest instantaneous efficiency at 2 lpm.

It is noticed from Fig. 5.11 that highest temperature rise is obtained at 2 lpm for fixed inlet water temperature and least temperature rise is obtained at 1.5 lpm. With increase in water inlet temperature, lower increment in fluid temperature is observed due to higher radiation losses.

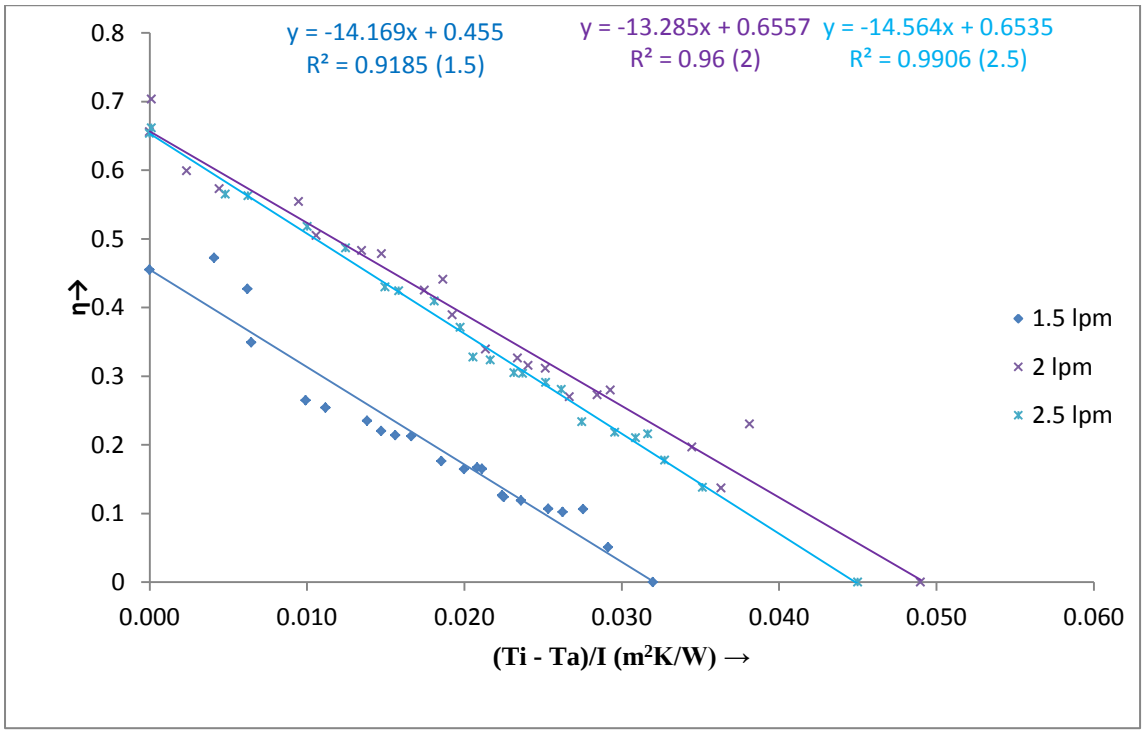

Fig. 5.10 Efficiency versus $(T_i - T_a)/I_T$ curve at three flow rates for water

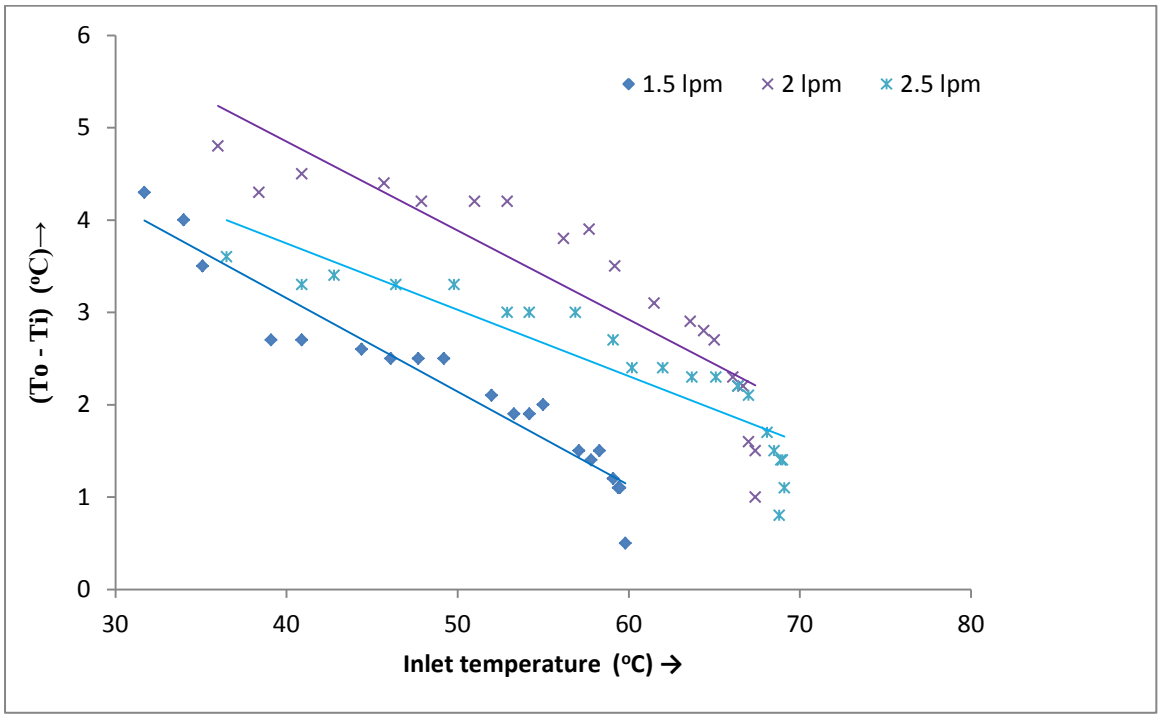

Fig. 5.11 Temperature rise of water for three flow rates with inlet temperature

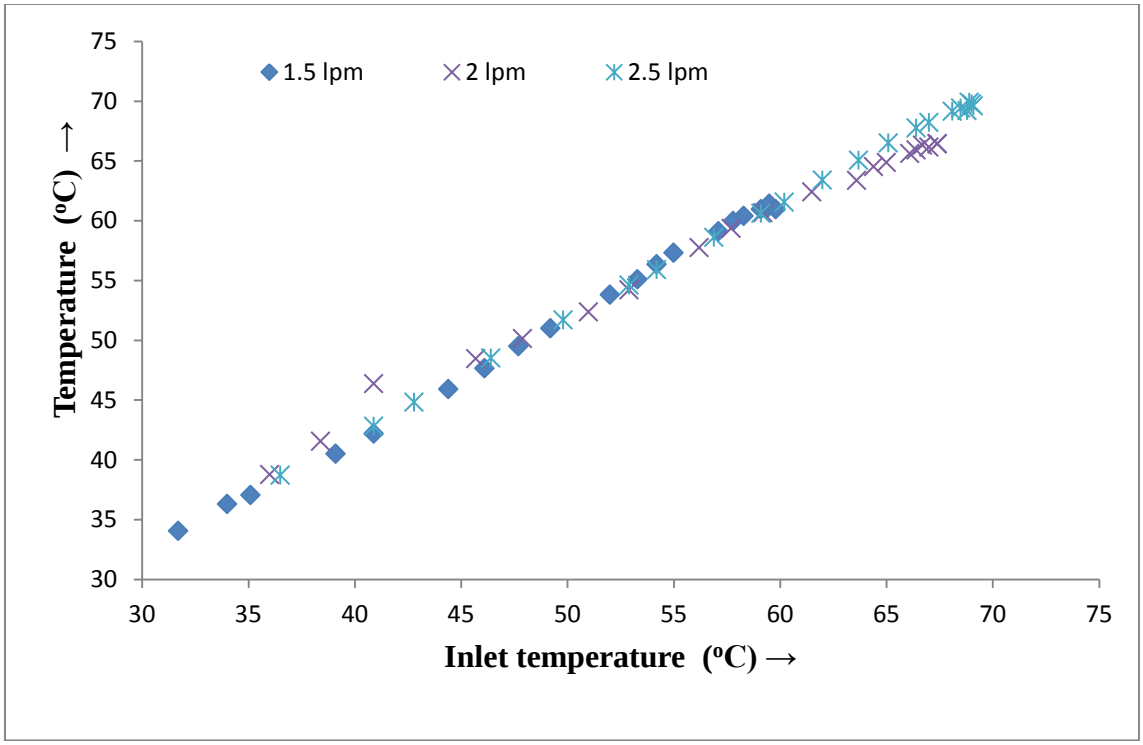

Fig. 5.12 Absorber plate temperature with inlet temperature for three flow rates

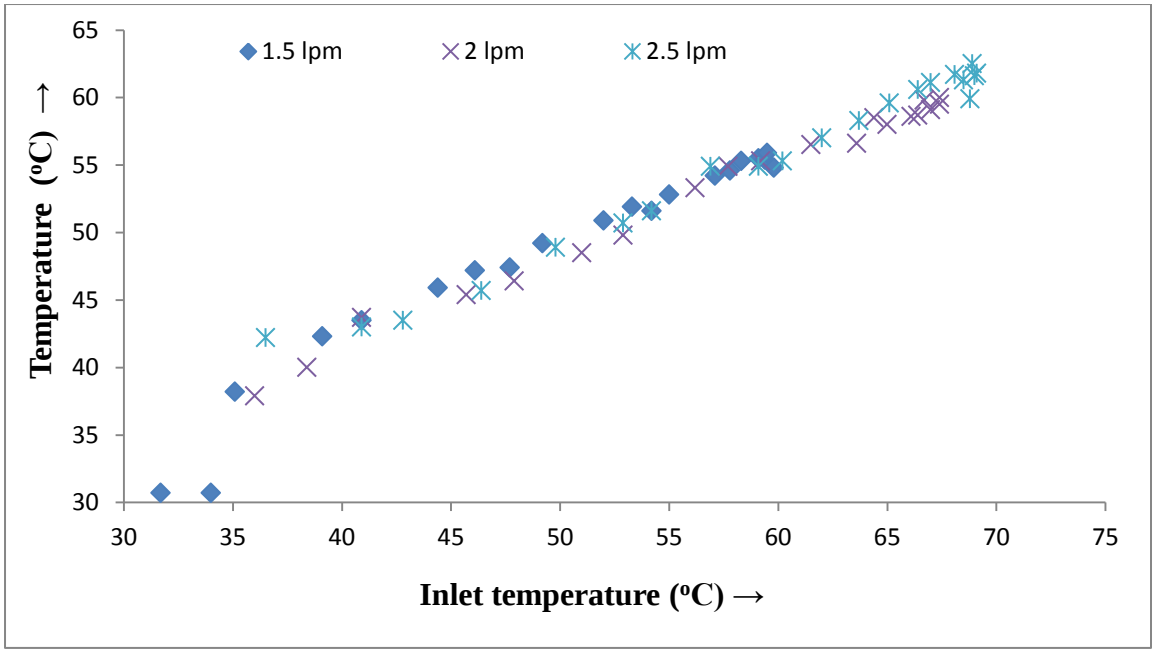

Fig. 5.13 Glass cover temperature with water inlet temperature for three flow rates

Fig. 5.12 and 5.13 shows base plate and glass cover temperature increase with increase in water inlet temperature for all three flow rates. At higher water inlet temperature, higher radiation losses takes place resulting in greater glass temperature, and lower temperature rise and lower efficiency are noticed with increase in water inlet temperature. These temperatures are not much affected with flow rates considered because water is transparent for incident solar radiation and mostly absorbed by the base plate having opaque surface.

5.5 Aluminum base plate using Alumina–Water nanofluid

5.5.1 Effect of flow rate

Al_2O_3 nanoparticles are mixed in base fluid distilled water to get nanofluid of 0.001% volume fraction and investigations are performed to determine the effect of different flow rates i.e.1.5, 2 and 2.5 lpm. Fig. 5.14 shows the effect of nanofluid flow rate on collector efficiency for 0.001 vol% Al_2O_3 nanofluid. Maximum efficiency increases with flow rate

up to 2 lpm and then it becomes constant. The increase in absorbed energy parameter is greater than loss parameter. Thus, collector efficiency increases with the use of nanofluid for smaller flow rates and after that efficiency becomes constant.

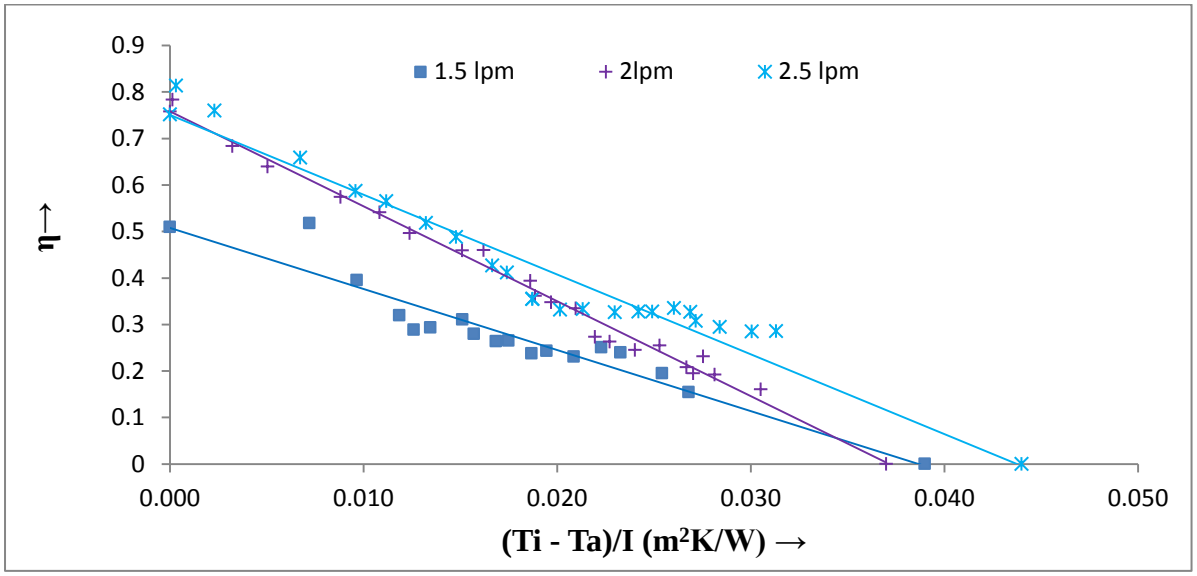

Fig. 5.14 Efficiency versus $(T_i - T_a)/I_T$ curve at three flow rates for 0.001% nanofluid

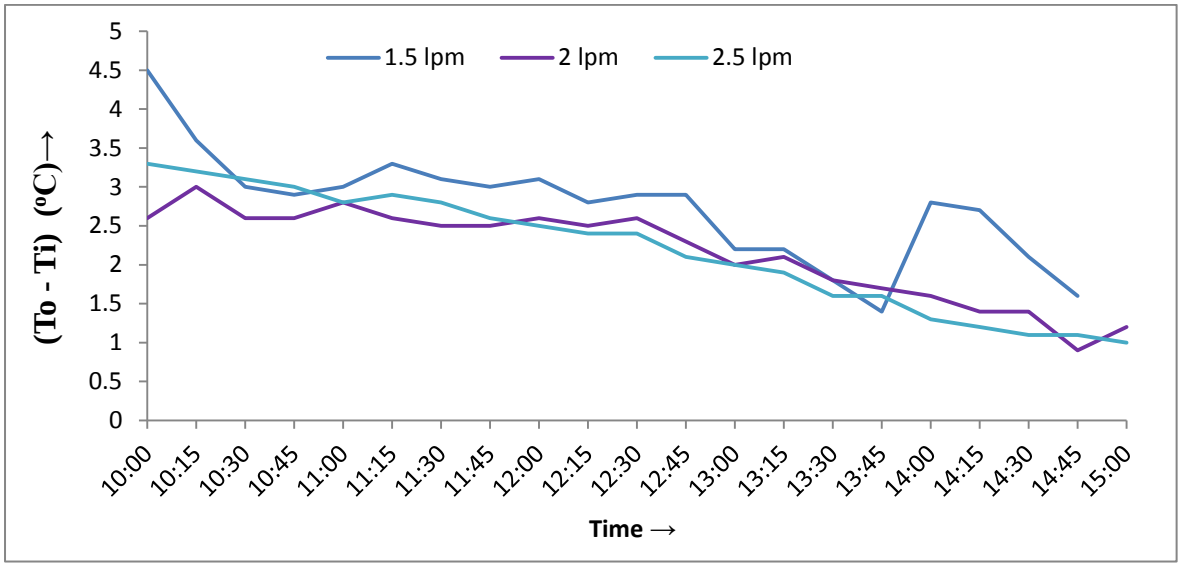

Fig. 5.15 Single pass temp rise with time at three flow rates

Fig. 5.15 and 5.16 shows the single pass temperature rise of nanofluid through collector. Temperature rise is higher at lower flow rates i.e. at 1.5 lpm due to greater stay period in

the collector. It is also found that with increase in inlet fluid temperature the temperature rise decreases at same flow rate.

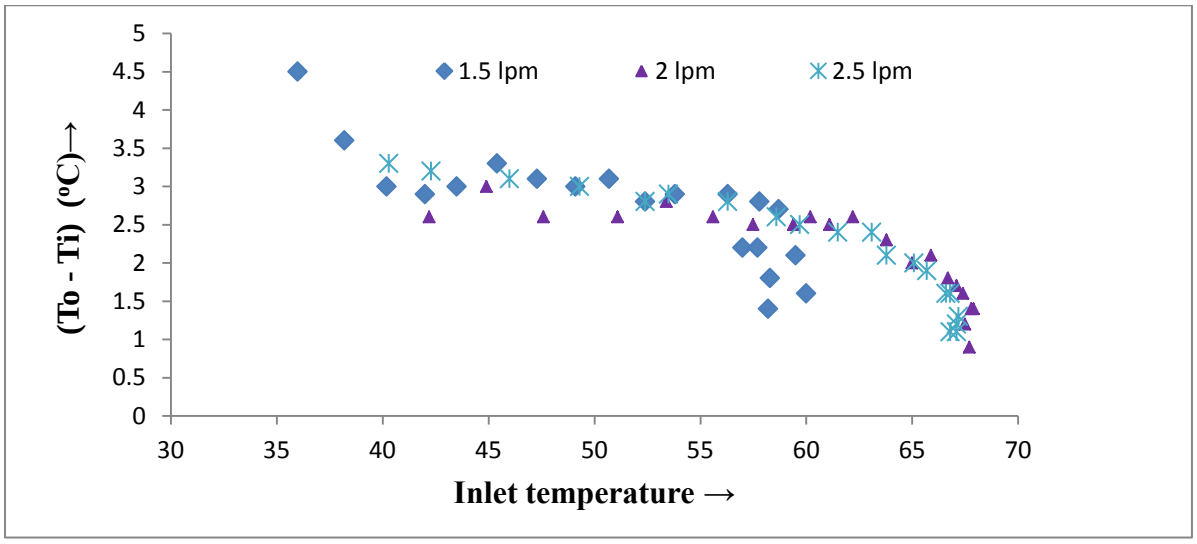

Fig. 5.16 Single pass temperature rise with inlet temperature for various flow rates

Fig. 5.17 and 5.18 shows the variation in base plate temperature at different flow rates and inlet fluid temperature. The base plate temperature is the highest at 1.5 lpm flow rate and lowest at 2 lpm flow rate. With increase in the inlet fluid temperature, base plate temperature also increased reaching to a maximum temperature of 68^0C.

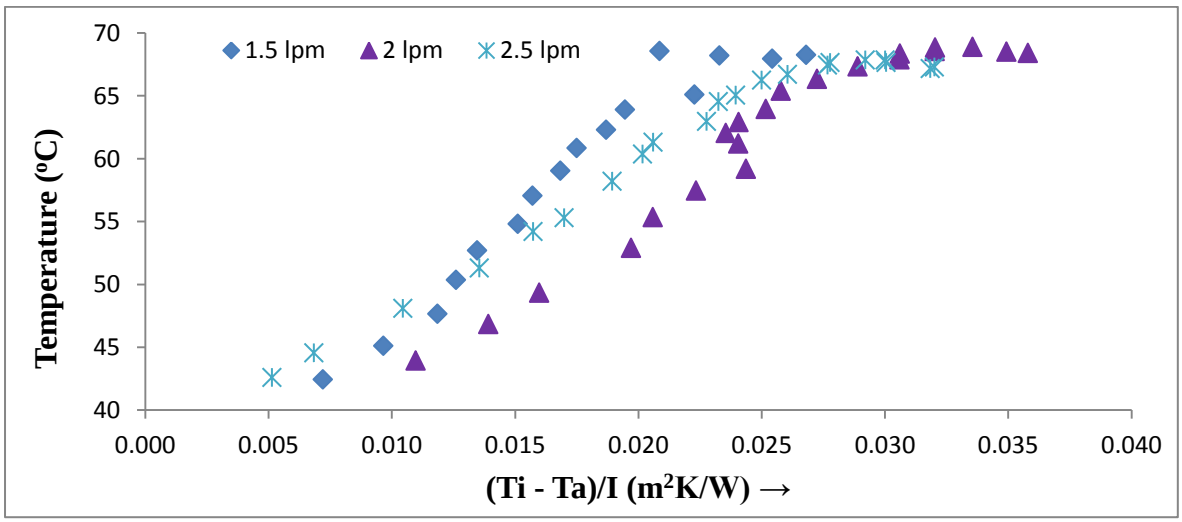

Fig. 5.17 Base plate temperature for various flow rates

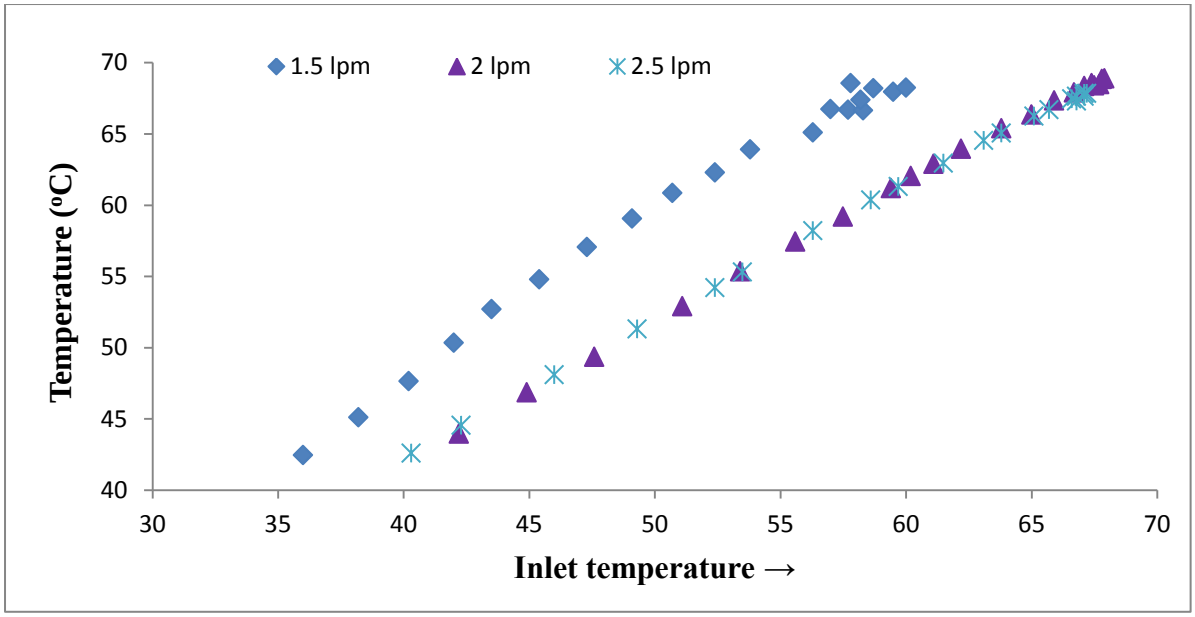

Fig. 5.18 Base plate temperature with inlet temperature for various flow rates

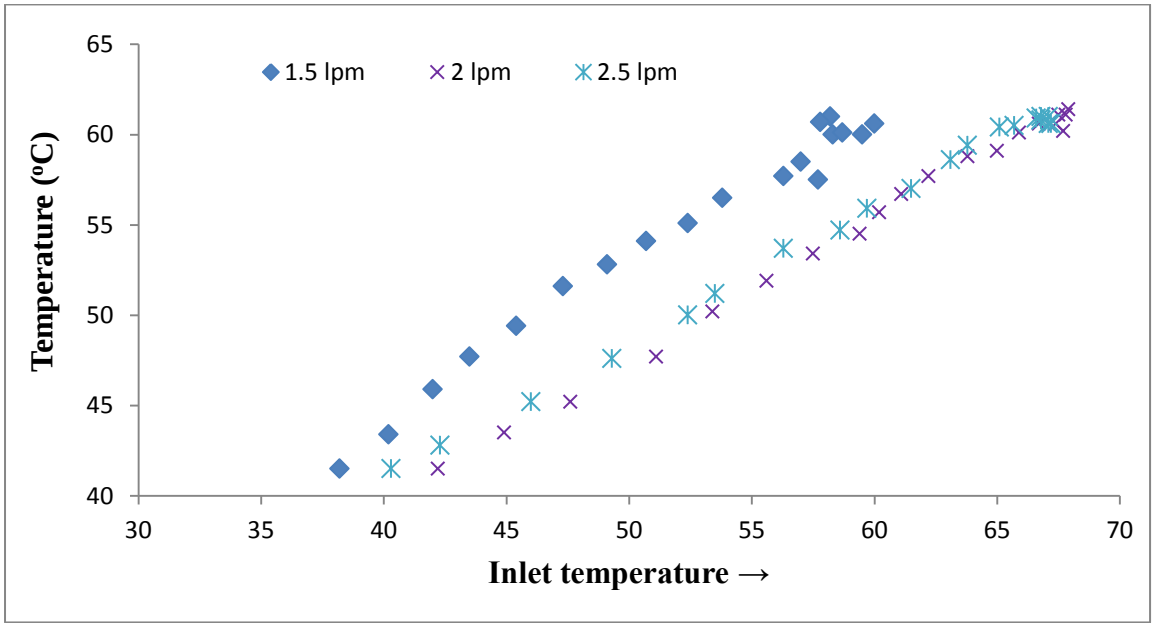

Fig. 5.19 Glass plate temperature with inlet temperature for various flow rates

Fig. 5.19 shows the variation in glass plate temperature with inlet fluid temperature at different flow rates. The glass plate temperature observed is higher at 1.5 lpm flow rate and almost same for 2 lpm and 2.5 lpm flow rate. As the inlet fluid temperature increases, glass plate temperature also increases reaching to maximum temperature of 62^0C.

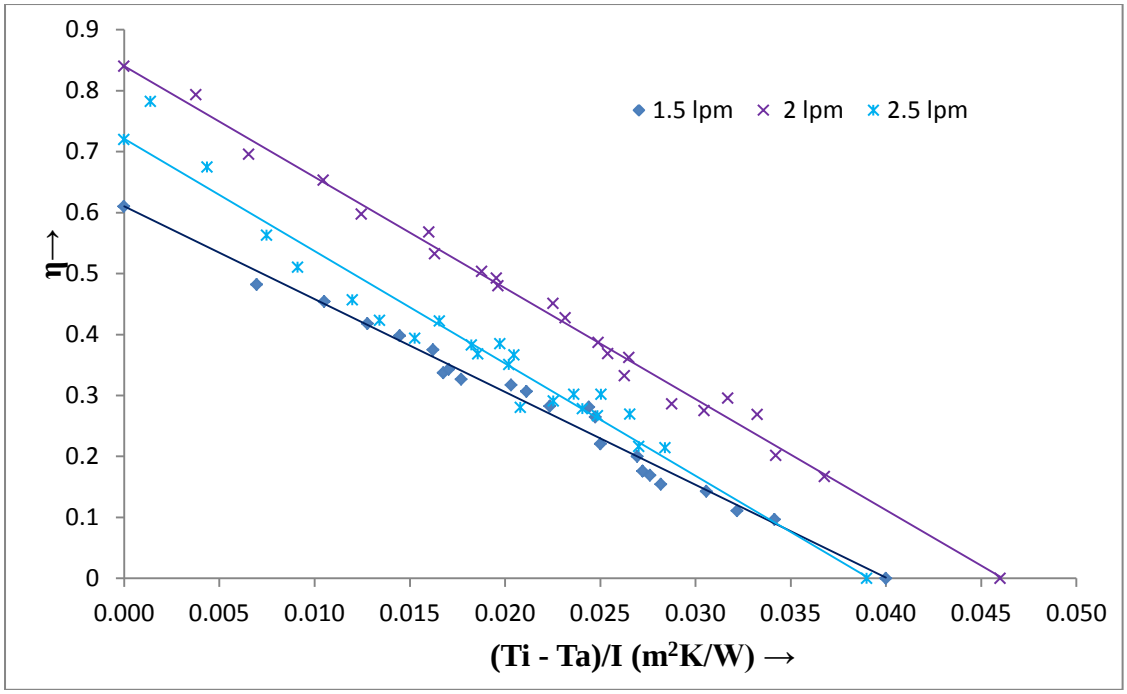

Fig.5.20 (a) Efficiency curve at three flow rates for 0.003% Al_2O_3 -water nanofluid

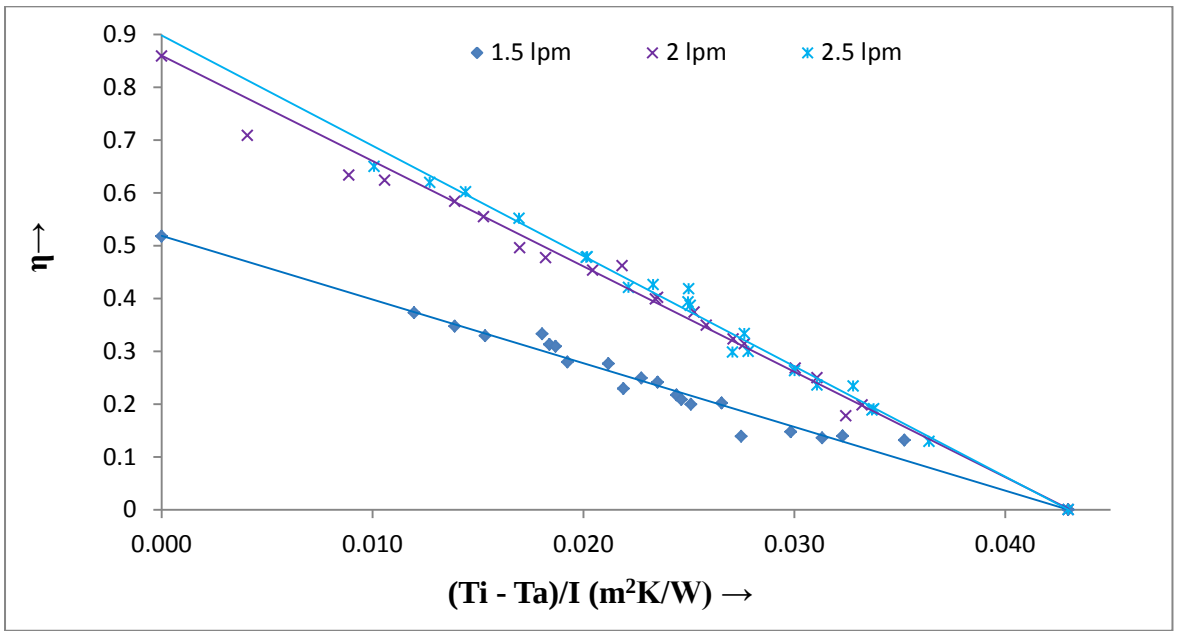

Fig.5.20 (b) Efficiency curve at three flow rates for 0.005% Al_2O_3 -water nanofluid

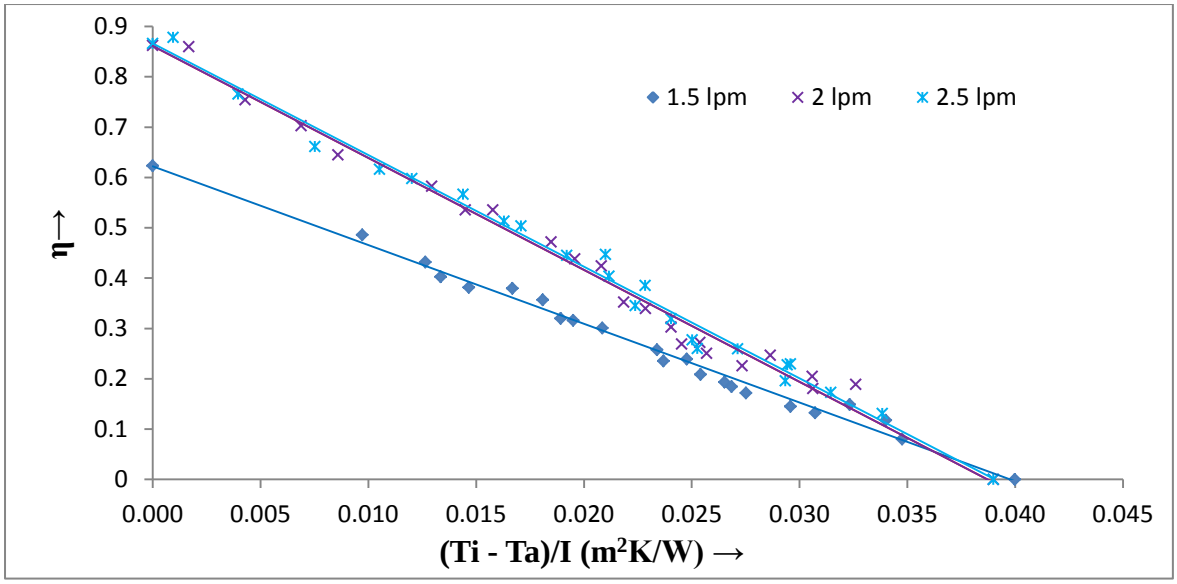

Fig.5.20 (c) Efficiency curve at three flow rates for 0.007% Al_2O_3 -water nanofluid

Fig. 5.20 (a) to (c) shows the effect of three flow rates on efficiency for three different concentrations of nanofluid i.e. 0.003%, 0.005% and 0.007% respectively. For 0.003% and 0.007% nanofluid, both efficiency parameters increased up to 2 lpm and then energy absorbed parameter reduced but energy loss parameter became nearly constant. Therefore, maximum efficiency increased up to 2 lpm and then decreased with increase in flow rate. At 0.005% concentration, both efficiency parameters increased with flow rates and observed increase in absorbed energy parameter is higher than loss parameter. Thus, maximum efficiency is achieved at 2.5 lpm for 0.005% concentration.

Table 5.11 Collector efficiency parameters for Al_2O_3-water nanofluid

S.No.	Nanofluid volume fraction	F_RU_L			$F_R(\tau\alpha)$			R^2		
		Flow rate (lpm)								
		1.5	2	2.5	1.5	2	2.5	1.5	2	2.5
1	0% (pure water)	14.17	14.09	14.59	45.50	66.67	65.35	0.9185	0.96	0.99
2	0.001%	13.24	19.99	17.86	50.94	83.33	73.86	0.794	0.945	0.992
3	0.003%	15.10	18.17	18.4	60.58	83.96	72.0	0.974	0.983	0.938

4	0.005%	12.07	19.93	21.43	71.7	85.9	89.4	0.957	0.962	0.989
5	0.007%	15.69	22.31	22.17	62.3	86.2	86.6	0.982	0.982	0.986

5.5.2 Effect of volume fraction

Four different concentrations of Al_2O_3-water nanofluid i.e. 0.001 vol%, 0.003 vol%, 0.005 vol% and 0.007 vol% were prepared and used for the study at three flow rates of 1.5, 2 and 2.5 lpm. The experimental results for pure water and different concentrations of Alumina nanofluids are presented in the form of efficiency curves in Fig. 5.21 (a) to (c).

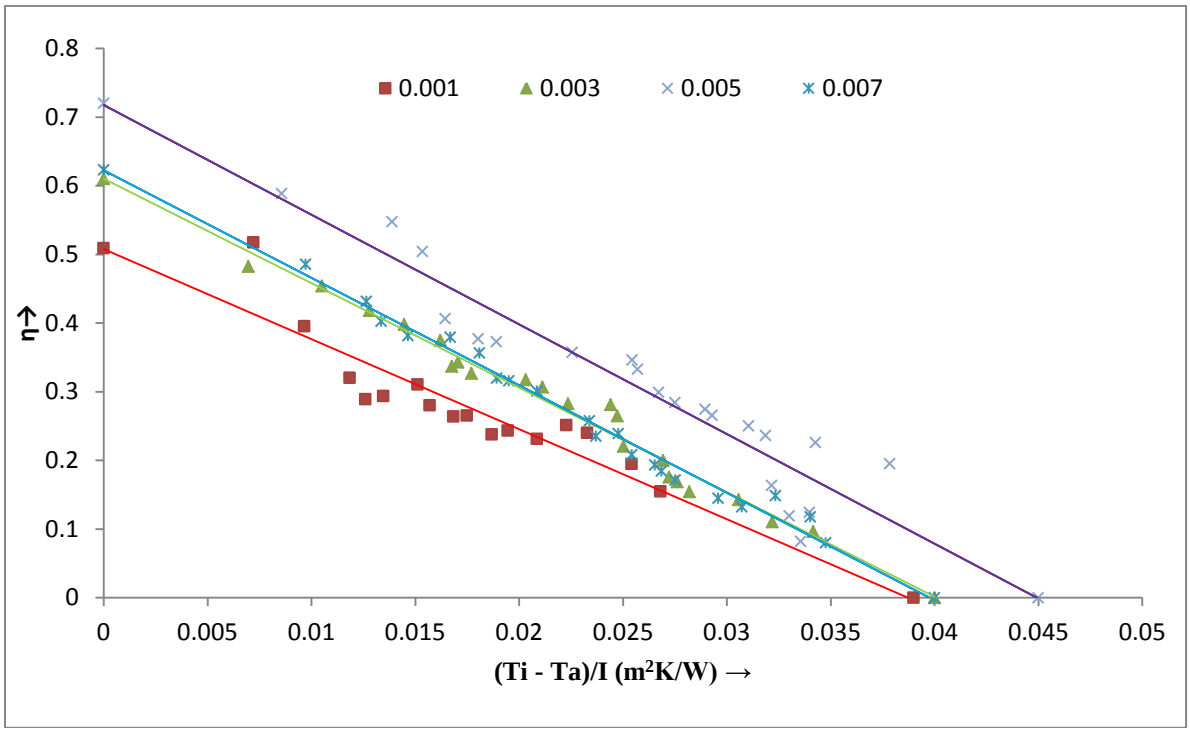

Fig.5.21 (a) Efficiency plots for different Al_2O_3 nanoparticle concentrations at 1.5 lpm flow rate

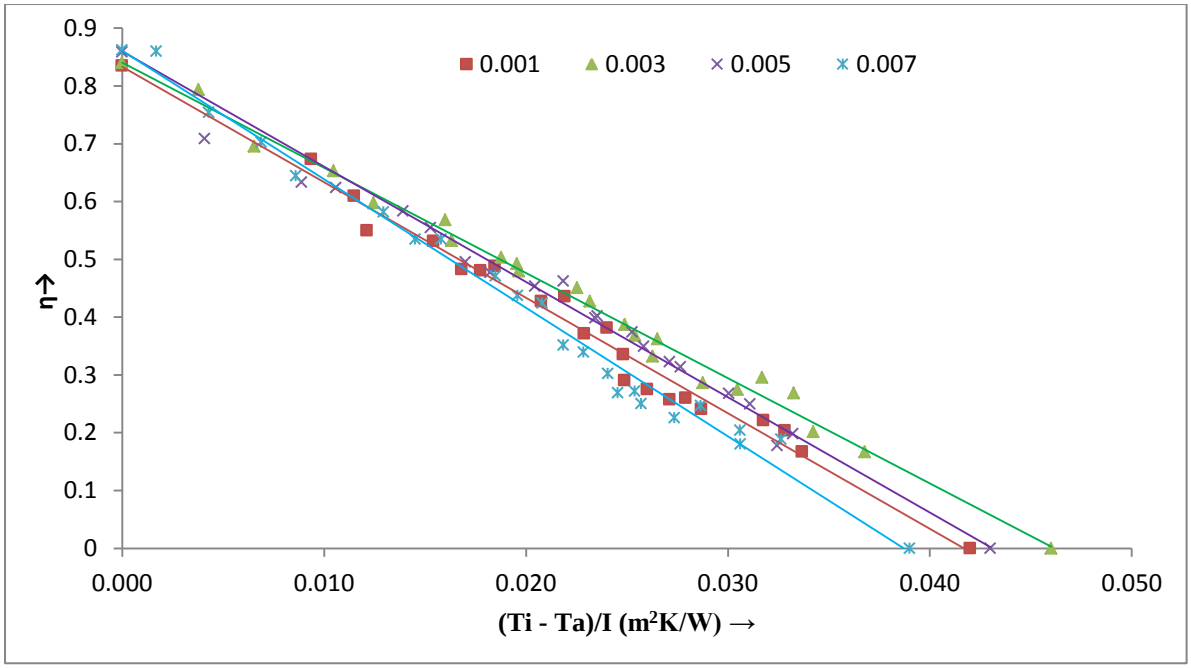

Fig.5.21 (b) Efficiency plots for different Al_2O_3 nanoparticle concentrations at 2 lpm flow rate

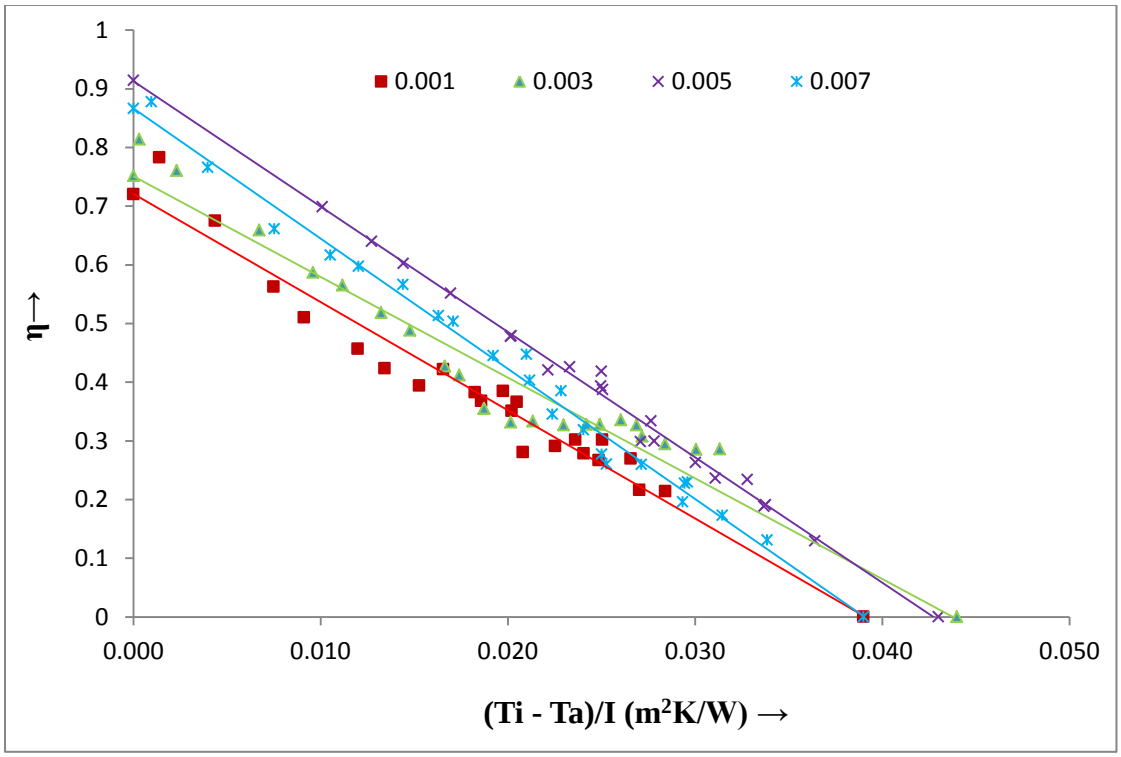

Fig.5.21 (c) Efficiency plots for different Al_2O_3 nanoparticle concentrations at 2.5 lpm flow rate

It is observed from Fig. 5.21 (a) to (c) that, at all three flow rates, increase in nanoparticle concentration from 0.001 to 0.005%, increased the absorbed energy

parameter $F_R(\tau\alpha)$ and loss parameter F_RU_L of collector and for 0.007% volume fraction these parameters reduced. Maximum collector efficiency increased with nanofluid concentration from 0.001% to 0.005% and noticed that increase in parameter $F_R(\tau\alpha)$ is greater than parameter F_RU_L. The highest increase in absorbed energy parameter is 75.5% as compared to 51.6% in energy loss parameter for 0.005% concentration at 2.5 lpm flow rate.

The amount of incident solar radiation absorbed by a flowing nanofluid film is proportional to the nanoparticles volume fraction (ϕ) for a fixed collector depth and flow rate. For direct absorption solar collector, which operated in actual outdoor conditions, the maximum efficiency is obtained at 0.005 vol% and for lower and higher nanoparticle concentrations than 0.005% the maximum collector efficiency decreased. At lower nano particle concentration (< 0.005%), some fraction of the incident solar radiations are absorbed by the flowing nanofluid film by absorption and scattering of nano size particles and the remaining fraction by the bottom base plate. This raised the nanofluid temperature near the bottom base plate causing extra emissive losses resulting in lower collector efficiency. At optimum nanoparticle concentration (i.e. at 0.005 vol %) uniform temperature distribution is achieved throughout nanofluid film volume resulting in maximum collector efficiency. For higher nanoparticle concentration (> 0.005 vol%), upper layers of nanofluid absorbed most of the incident radiations, allowing little or no radiation to penetrate through the nanofluid layer and reach the bottom plate. This results in uneven temperature distribution in nanofluid film with higher temperature region near the upper surface, consequently higher emissive losses and lower collector efficiency. The trade-off between two effects at lower and higher nanoparticle volume fractions described in Fig. 5.21 (a) to (c).

Tyagi et al. (2009) explained that increasing the nanoparticle volume fraction leads to a corresponding increase in attenuation of sunlight passing through the collector, and this, in turn, increases the collector efficiency. Since the attenuation varies exponentially with the extinction coefficient (and hence also with volume fraction), the efficiency initially increases very rapidly at lower volume fraction and quickly reaches an asymptotic value at higher volume fractions. The results of present study also indicate that addition of nanoparticles will be advantageous only up to a certain limit, beyond which the increase in efficiency would be miniscule and thus the experimental results are in tune with the Tyagi's finding.

Sajid et al. (2014) measured experimentally and calculated theoretically the increase in optical properties like extinction coefficient and absorption coefficient of alumina-water nanofluid at lower volume fraction and suggested improvement in efficiency of direct absorption solar collector. The present experimental results for efficiency improvement are in line and well justified.

Some other factors may also be responsible for lower collector efficiency at increased nanoparticle volume fraction beyond optimum value of 0.005 vol%. Particle agglomeration and deposition on the surface, would reduce the intensity of the sunlight into the fluid, and this effect increases with particle concentration. Increased radiation heat loss as the particle volume fraction exceeds a certain value could be another possible effect.

5.5.3 Effect of volume fraction on single pass temperature rise

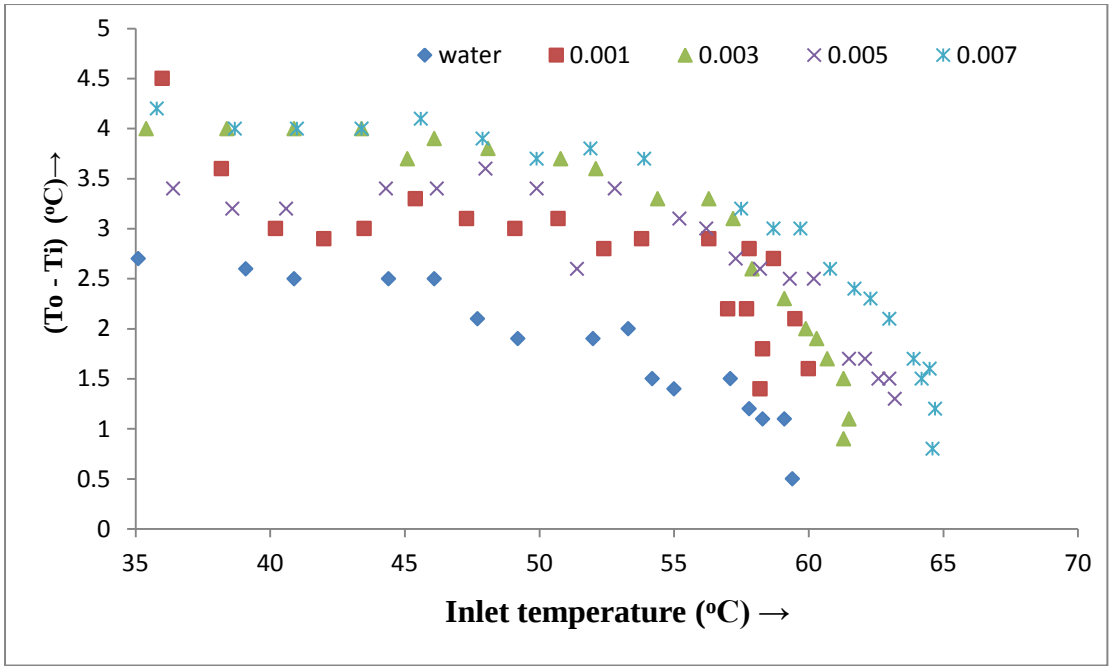

Fig. 5.22 (a) Temperature rise for different nanoparticle concentrations at 1.5 lpm flow rate

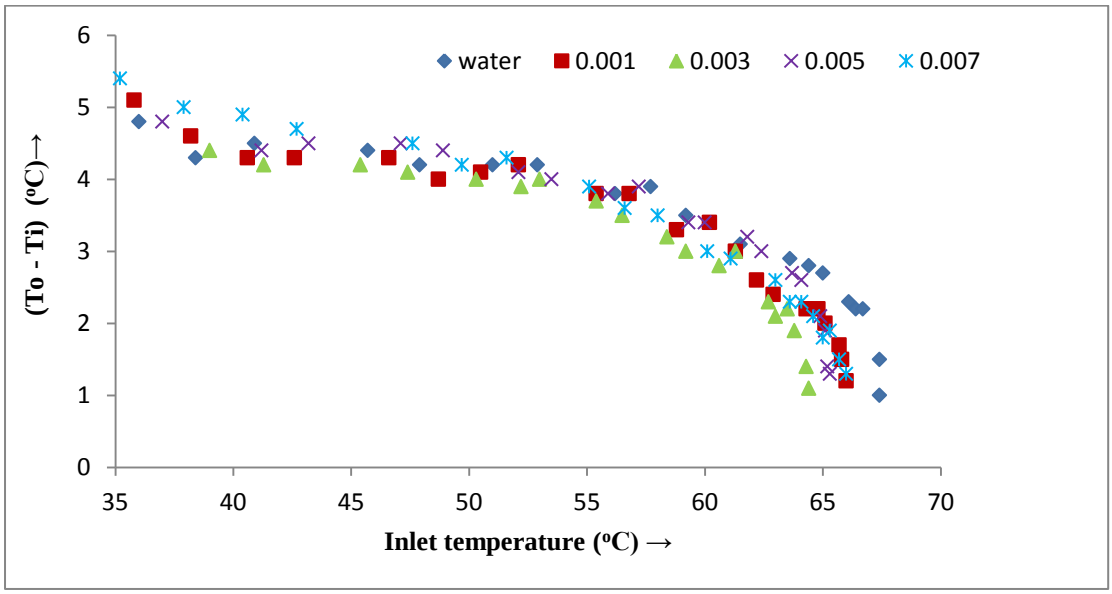

Fig. 5.22 (b) Temperature rise for different nanoparticle concentrations at 2 lpm flow rate

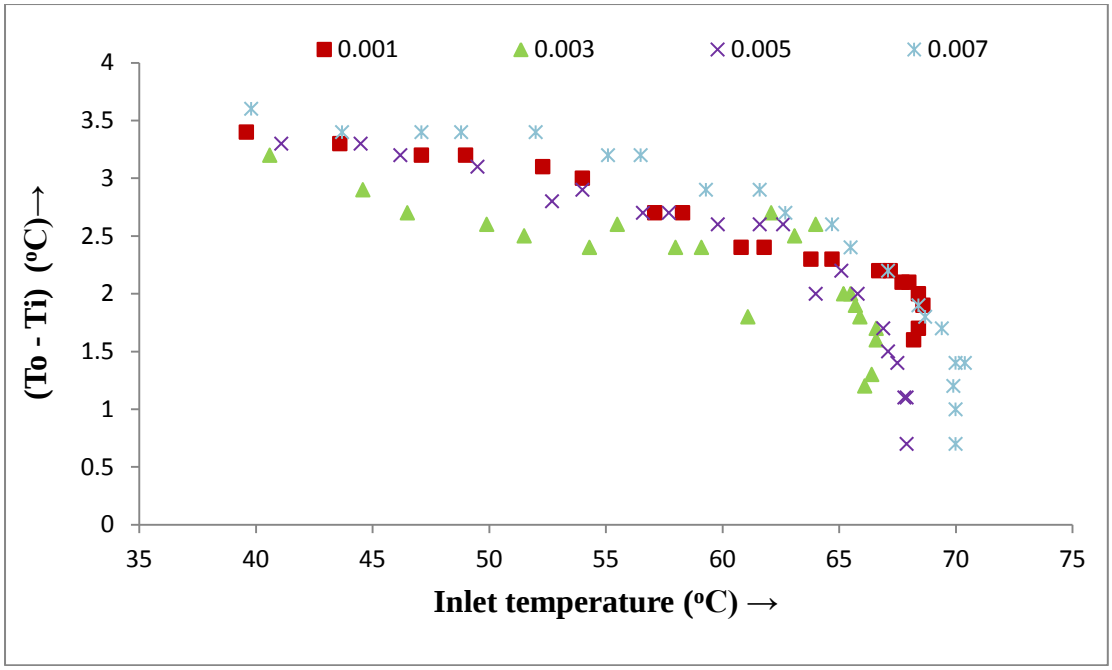

Fig. 5.22 (c) Temperature rise for different nanoparticle concentrations at 2.5 lpm flow rate

Fig. 5.22 (a) to (c) shows the effect of nano particle volume fraction on single pass fluid temperature rise at three different flow rates. The use of nanofluid in the present study gives better fluid temperature rise as compared to water at all three flow rates which justify the use of nanofluids for solar collector. For all the flow rates it is observed that fluid temperature rise increased with volume fraction at fixed inlet fluid temperature. But, at fixed nanoparticle volume fraction, the increase in inlet fluid temperature decreased fluid temperature rise due to higher radiation losses at high temperature.

5.5.4 Effect of volume fraction on base plate temperature

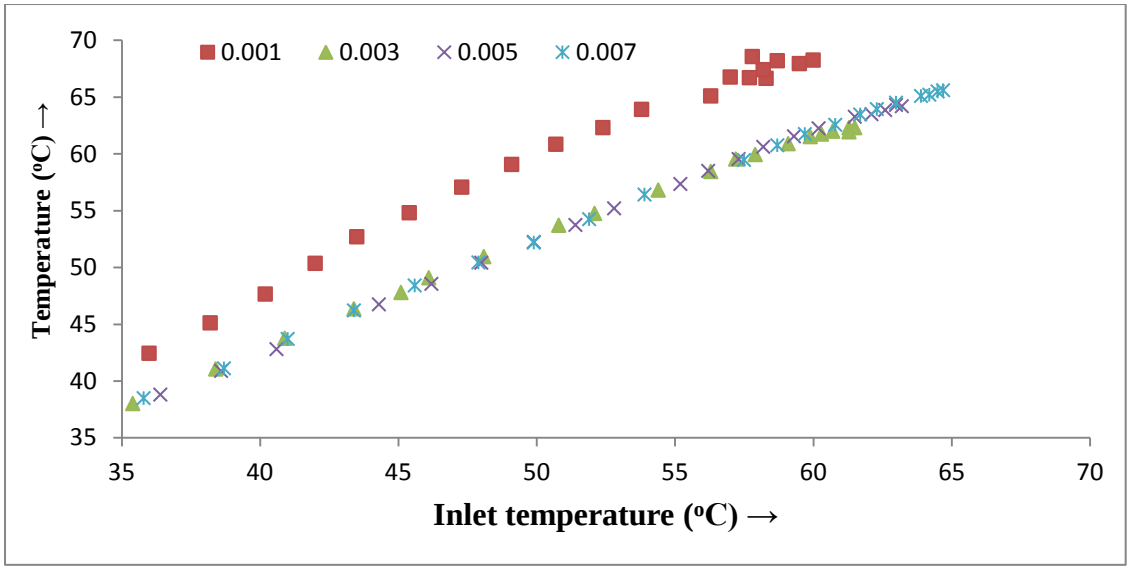

Fig. 5.23 (a) Effect of nanoparticle volume fraction on base plate temperature at 1.5 lpm

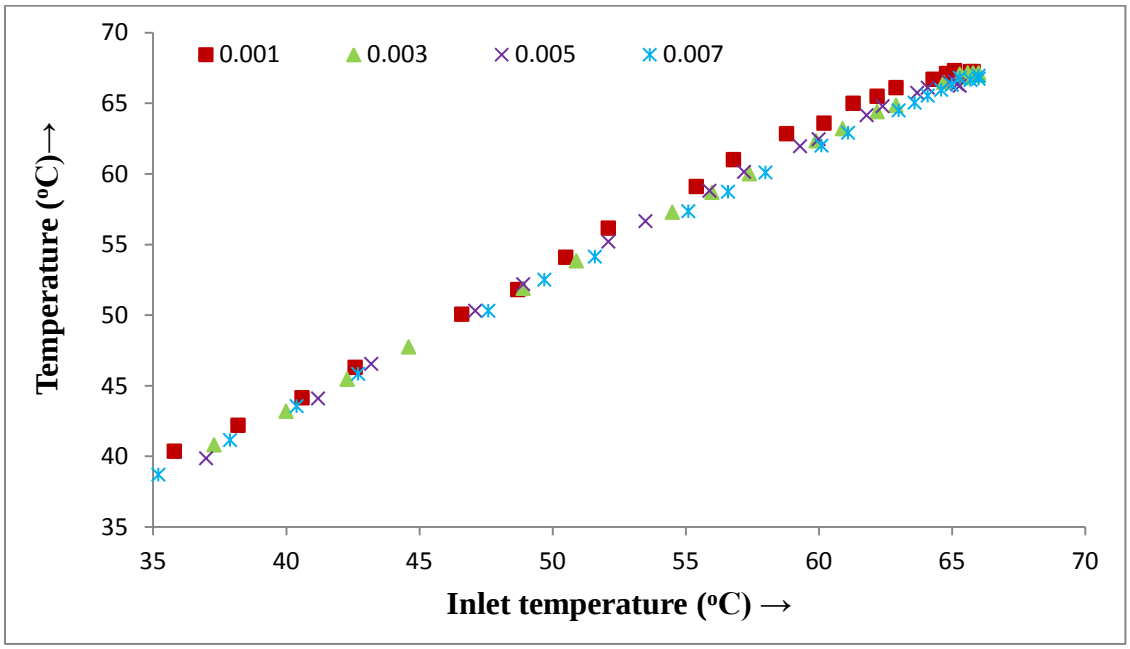

Fig. 5.23 (b) Effect of nanoparticle volume fraction on base plate temperature at 2 lpm

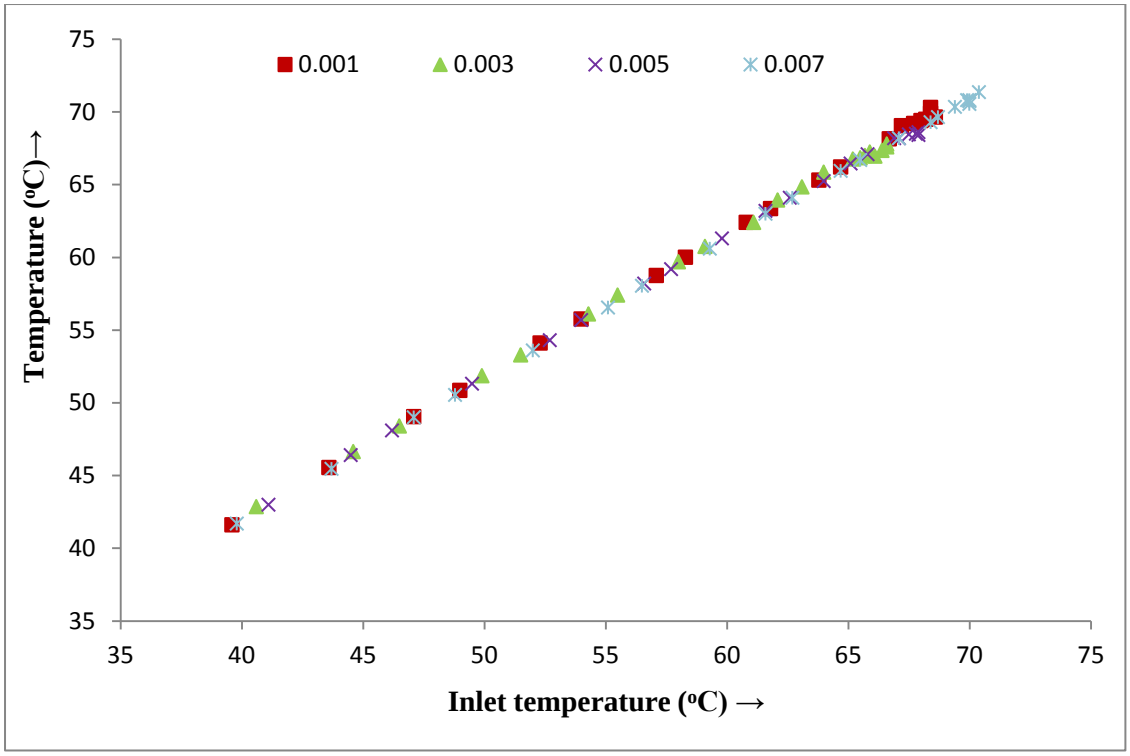

Fig. 5.23 (c) Effect of nanoparticle volume fraction on base plate temperature at 2.5 lpm

Fig. 5.23 (a) to (c) shows the effect of nanoparticle volume fraction on base plate temperature at different flow rates. For all three flow rates, it is observed that minimum base plate temperature is obtained at 0.005 vol% nanoparticle concentration indicating uniform temperature distribution within nanofluid film and for lower and higher volume fraction of nanofluid than 0.005%, base plate temperature is slightly higher. These results show optimum nanoparticle volume fraction to be 0.005 vol%. Results also show that at fixed nanoparticle volume fraction, the increase in inlet fluid temperature increased base plate temperature. The base plate temperature is almost same for different nanoparticle volume fraction at 2 lpm which is the optimum flow rate as shown in Fig. 5.23 (b).

5.5.5 Effect of volume fraction on glass cover temperature

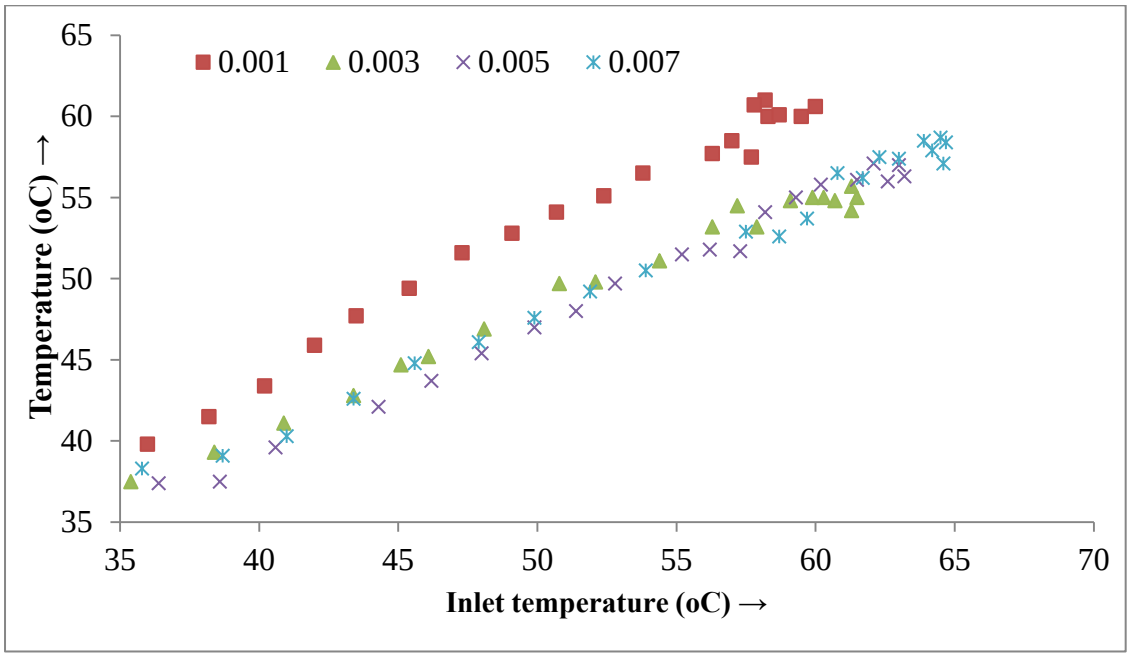

Fig. 5.24 (a) Effect of volume fraction on glass plate temperature at 1.5 lpm flow rate

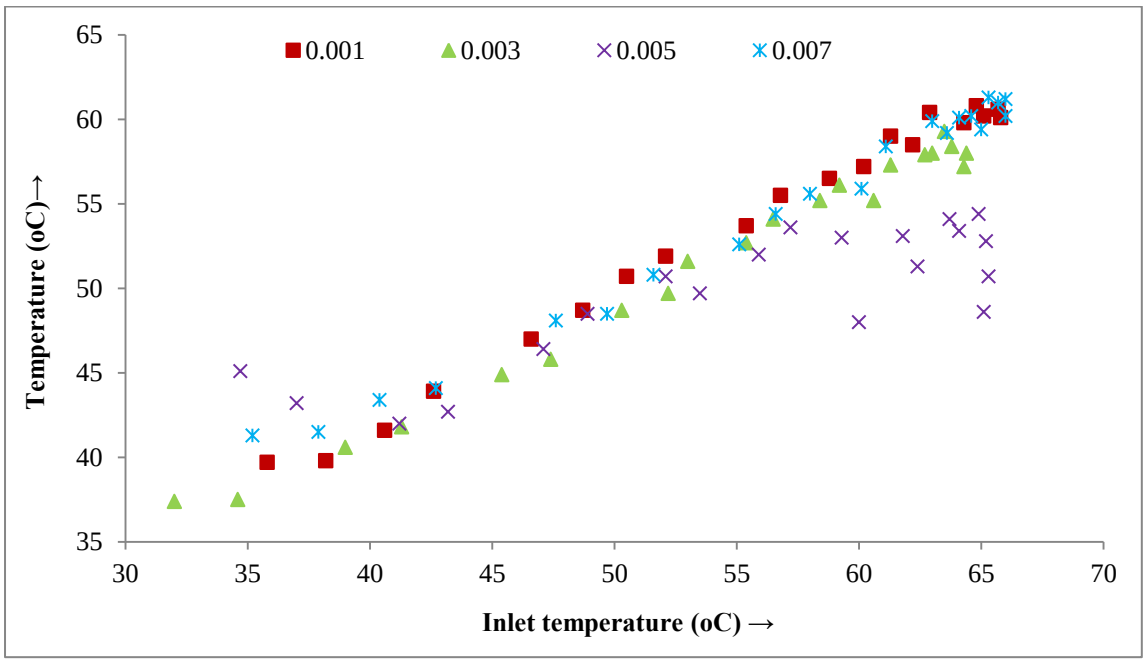

Fig. 5.24 (b) Effect of volume fraction on glass plate temperature at 2 lpm flow rate

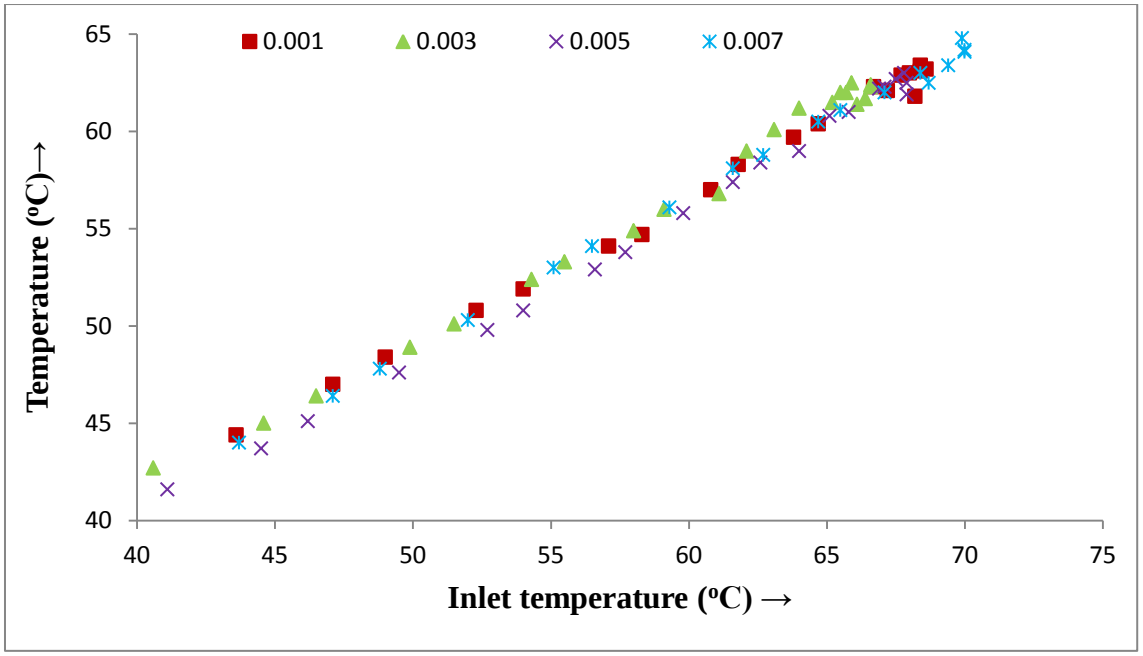

Fig. 5.24 (c) Effect of volume fraction on glass plate temperature at 2.5 lpm flow rate

Fig. 5.24 (a) to (c) shows the effect of volume fraction on glass plate temperature at different flow rates with inlet fluid temperature. For all three flow rates, it is found that glass plate temperature decreased with nanoparticle volume fraction increase and minimum glass plate temperature is obtained at 0.005 vol% again indicating uniform temperature distribution within nanofluid film at this volume fraction causing minimum heat losses. For lower and higher volume fraction than 0.005%, glass plate temperature is slightly higher. But, at fixed nanoparticle volume fraction, the increase in inlet fluid temperature increased glass plate temperature due to higher radiation losses at high temperature.

5.5.6 Effect of volume concentration on outlet temperature

(a) At different flow rate

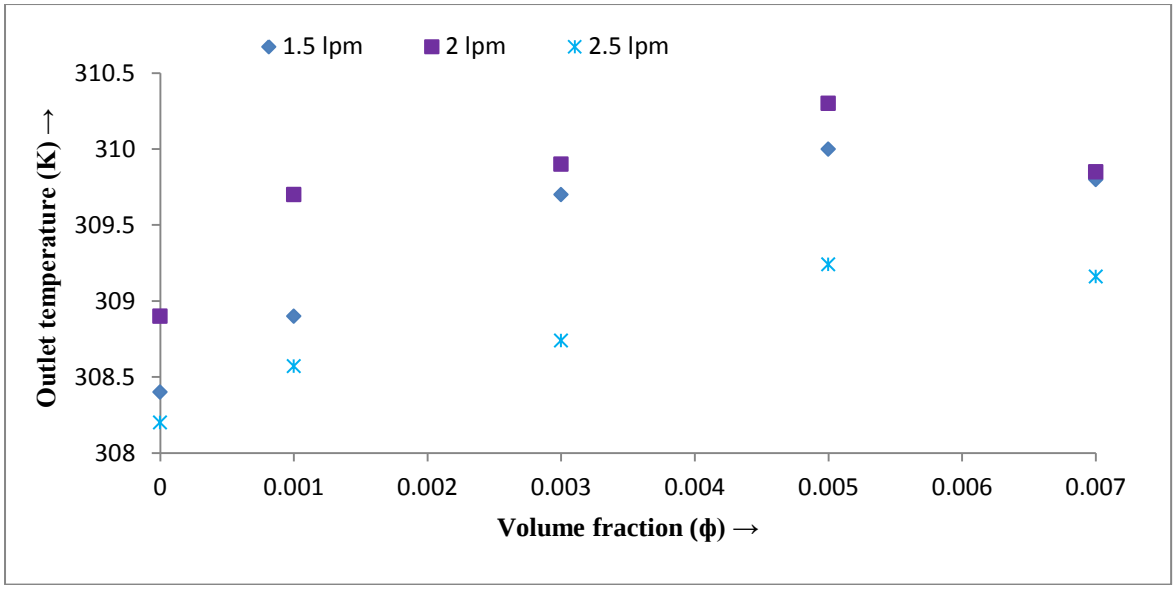

Fig. 5.25 Effect of volume concentration on outlet temperature at three flow rate

(b) At different inlet temperature

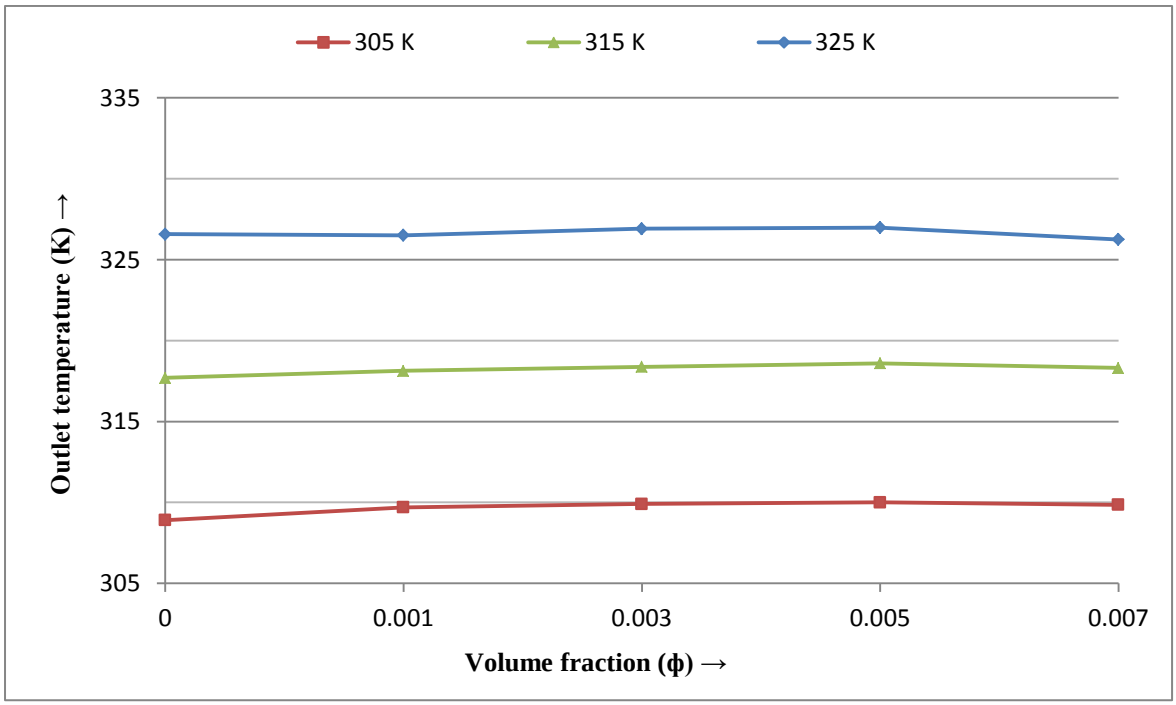

Fig. 5.26 Effect of volume concentration on outlet temperature at different inlet temperature

Fig. 5.25 shows the effect of different nanoparticle volume concentration on outlet fluid temperature for three flow rates. For all the nanoparticle volume fraction, the maximum outlet fluid temperature is obtained at 2 lpm indicating the optimum flow rate at 2 lpm.

Fig. 5.26 shows the effect of different nanoparticle volume concentration on outlet fluid temperature with different inlet fluid temperature. For all the inlet fluid temperature, the maximum outlet temperature is obtained at 0.005% nanoparticle volume fraction, indicating the optimum volume fraction at 0.005 vol%.

5.6 Aluminum base plate using Titania –Water nanofluid

5.6.1 Effect of fluid flow rate

TiO_2 nanoparticles of average size 20-25 nm are mixed in base fluid distilled water and sonicated for two hours to get nanofluid of different nanoparticle volume fraction and performance investigations are performed to determine the effect of three different flow rates i.e. 1.5, 2 and 2.5 lpm.

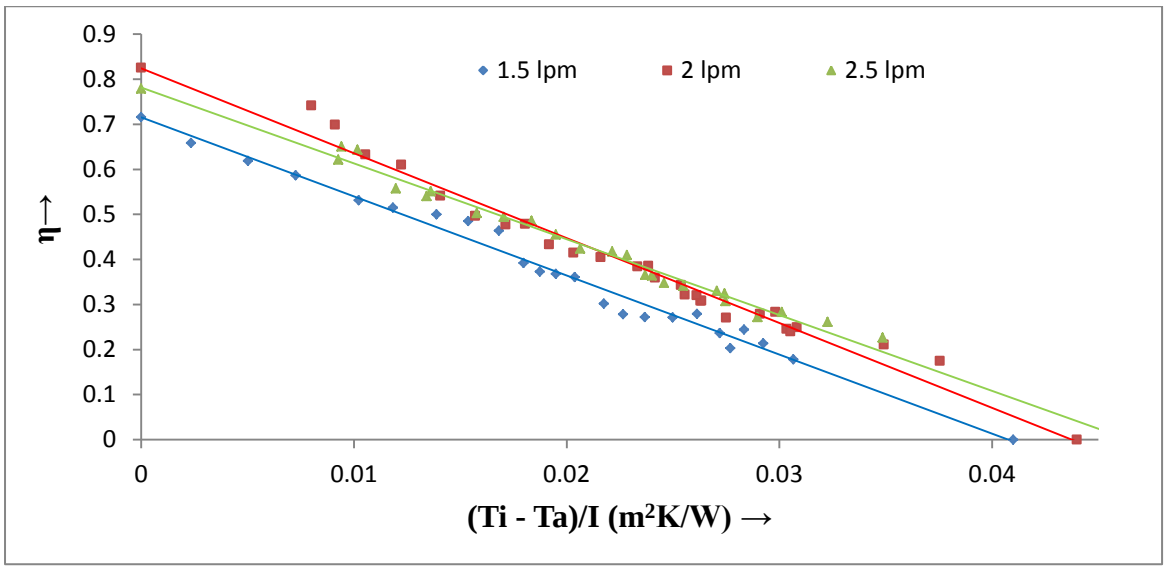

Fig. 5.27(a) Efficiency versus $(T_i - T_a)/I_T$ curve at three flow rates for 0.001% nanofluid

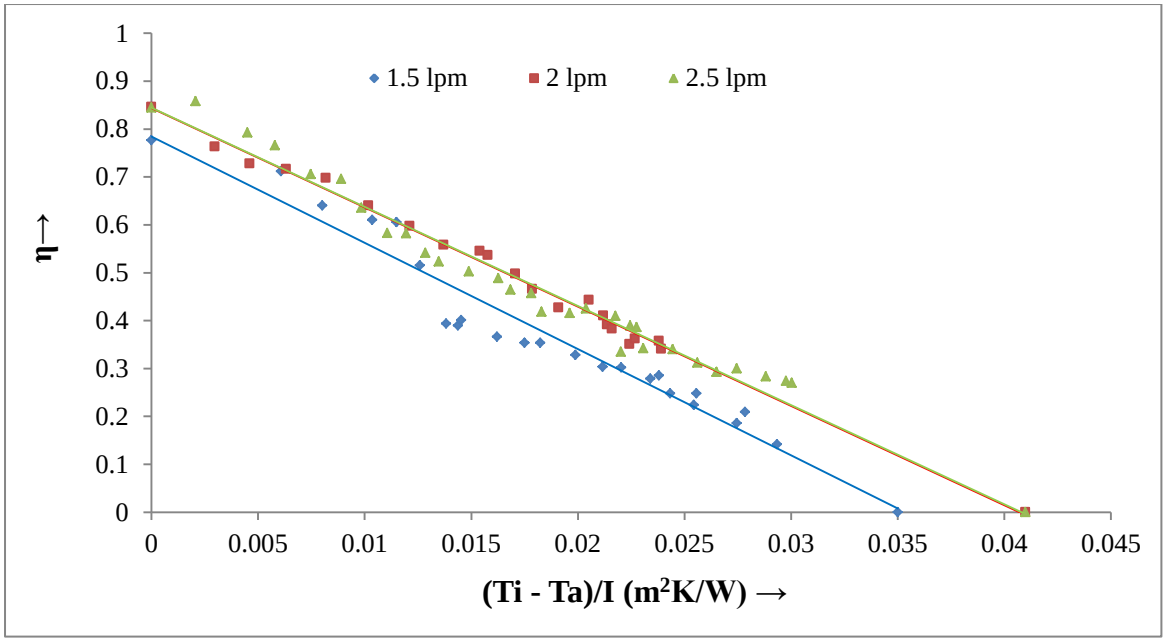

Fig. 5.27(b) Efficiency versus $(T_i - T_a)/I_T$ curve at three flow rates for 0.003% nanofluid

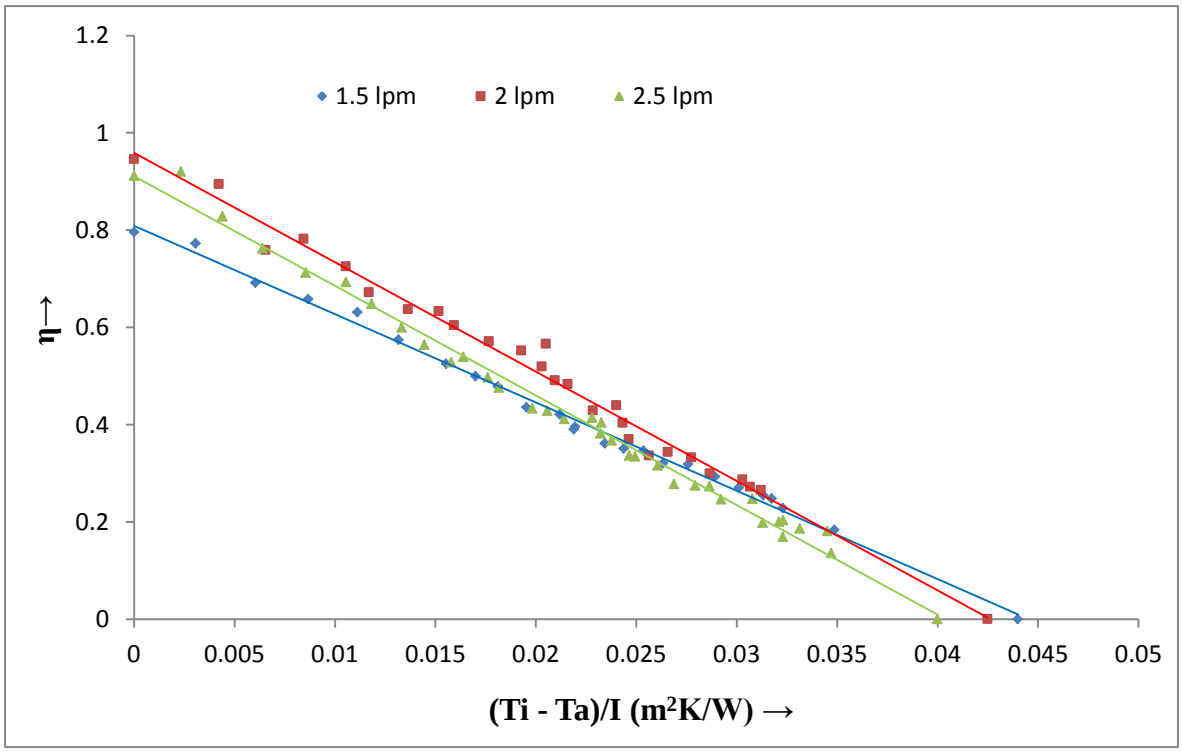

Fig. 5.27(c) Efficiency versus $(T_i - T_a)/I_T$ curve at three flow rates for 0.005% nanofluid

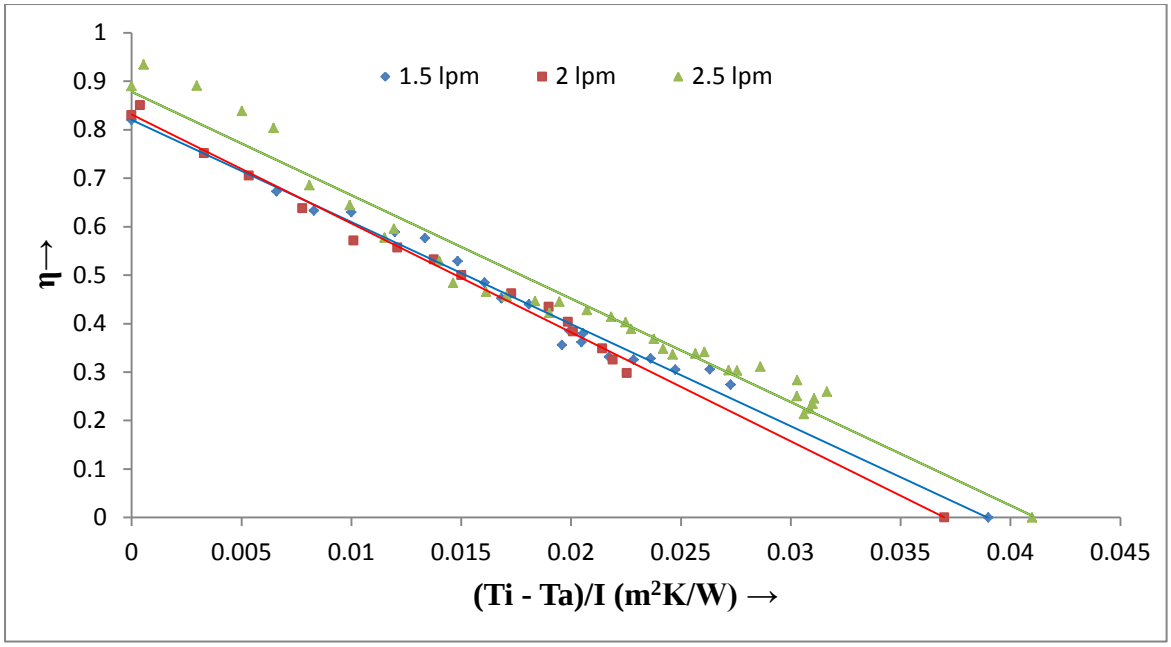

Fig. 5.27(d) Efficiency versus $(T_i - T_a)/I_T$ curve at three flow rates for 0.007% nanofluid

Fig. 5.27 (a) to (d) shows the effect of three flow rates on efficiency for four different concentrations of nanofluid i.e. 0.001%, 0.003%, 0.005% and 0.007% respectively. For 0.001%, 0.003% and 0.005% nanofluid, both efficiency parameters increased up to 2 lpm and then energy absorbed parameter reduced but energy loss parameter became nearly constant. Therefore, maximum efficiency increased up to 2 lpm and decreased for 2.5 lpm flow rate.

Table 5.12 Collector efficiency parameters for TiO_2-water nanofluid

S.No.	Nanofluid volume fraction	F_RU_L			$F_R(\tau\alpha)$			R^2		
		Flow rate (lpm)								
		1.5	2	2.5	1.5	2	2.5	1.5	2	2.5
1	0% (pure water)	14.17	14.09	14.59	45.50	66.67	65.39	0.9185	0.96	0.99
2	0.001%	17.51	18.85	16.83	71.31	82.43	78.14	0.985	0.991	0.992
3	0.003%	22.05	20.74	20.71	77.84	84.43	84.47	0.9504	0.979	0.975
4	0.005%	20.72	22.25	22.47	82.97	94.64	90.76	0.9924	0.994	0.966

5	0.007%	21.06	22.47	21.33	82.03	83.16	87.82	0.9836	0.992	0.982

5.6.2 Effect of volume fraction

Four different concentrations of TiO_2-water nanofluid i.e. 0.001 vol%, 0.003 vol%, 0.005 vol% and 0.007 vol% were prepared and used for the experimental study at three different flow rates of 1.5, 2 and 2.5 lpm and results are presented in the form of efficiency curves in Fig. 5.28 (a) to (c).

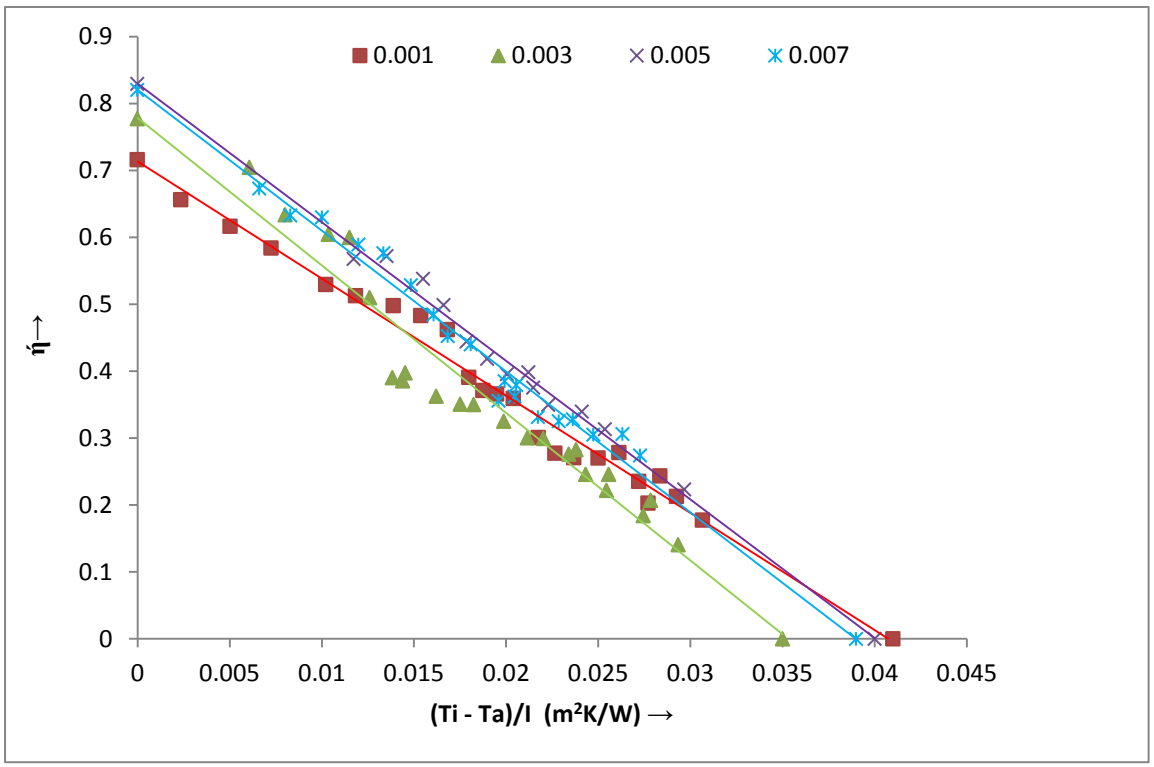

Fig.5.28 (a) Efficiency plots for nanofluid at different nanoparticle concentrations at 1.5 lpm

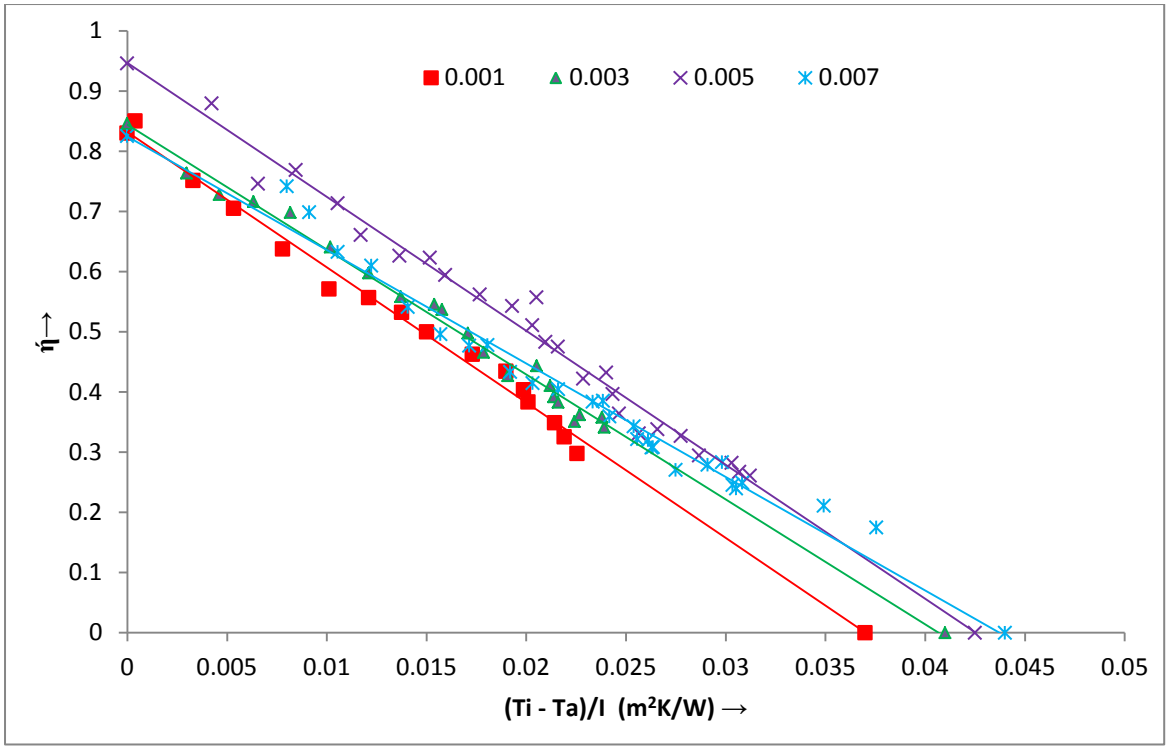

Fig.5.28 (b) Efficiency plots for nanofluid at different nanoparticle concentrations at 2 lpm

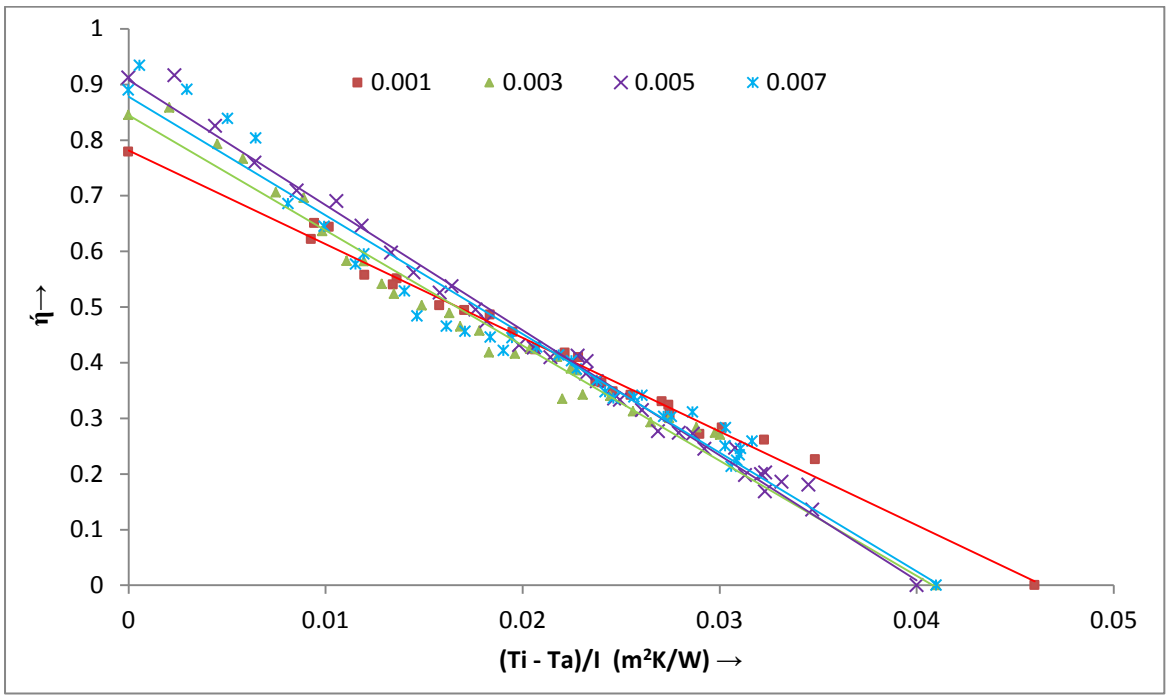

Fig.5.28 (c) Efficiency plots for nanofluid at different nanoparticle concentrations at 2.5 lpm

It is observed from Fig. 5.28 (a) to (c) that, at all three flow rates, maximum collector efficiency increased with nanoparticle concentration from 0.001 to 0.005% (due to

increased absorbed energy parameter $F_R(\tau\alpha)$) and then for 0.007% volume concentration efficiency reduced. The increase in maximum efficiency with nanofluid concentration from 0.001 to 0.005% is 16.4%, 13.8% and 16.15% at 1.5, 2 and 2.5 lpm respectively. The highest increase in absorbed energy parameter and energy loss parameter found to be 32.7 % and 21.7% respectively for 0.005% nanofluid concentration at 2 lpm.

The same experimental results for maximum collector efficiency using TiO_2-water nanofluid were obtained as for using Al_2O_3 –water nanofluid. The reasons for such experimental results may be explained as follows. The maximum efficiency was obtained at 0.005 vol% due to uniform temperature distribution throughout nanofluid volume and an asymptotic value increase in attenuation of sunlight at this concentration. The efficiency decreased for lower and higher nanoparticle concentrations due to uneven distribution of nanofluid film temperature resulting heat losses. The same reasons have been explained in detail in the collector efficiency analysis using Al_2O_3 –water nanofluid.

5.6.3 Effect of volume fraction on single pass temperature rise

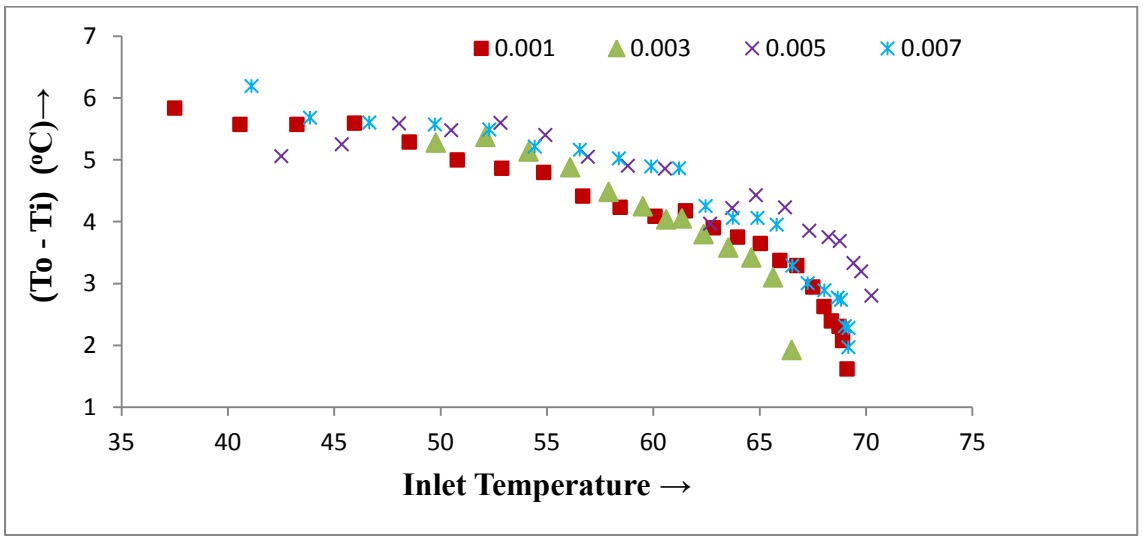

Fig. 5.29 (a) Temperature rise for different nanoparticle concentrations at 1.5 lpm flow rate

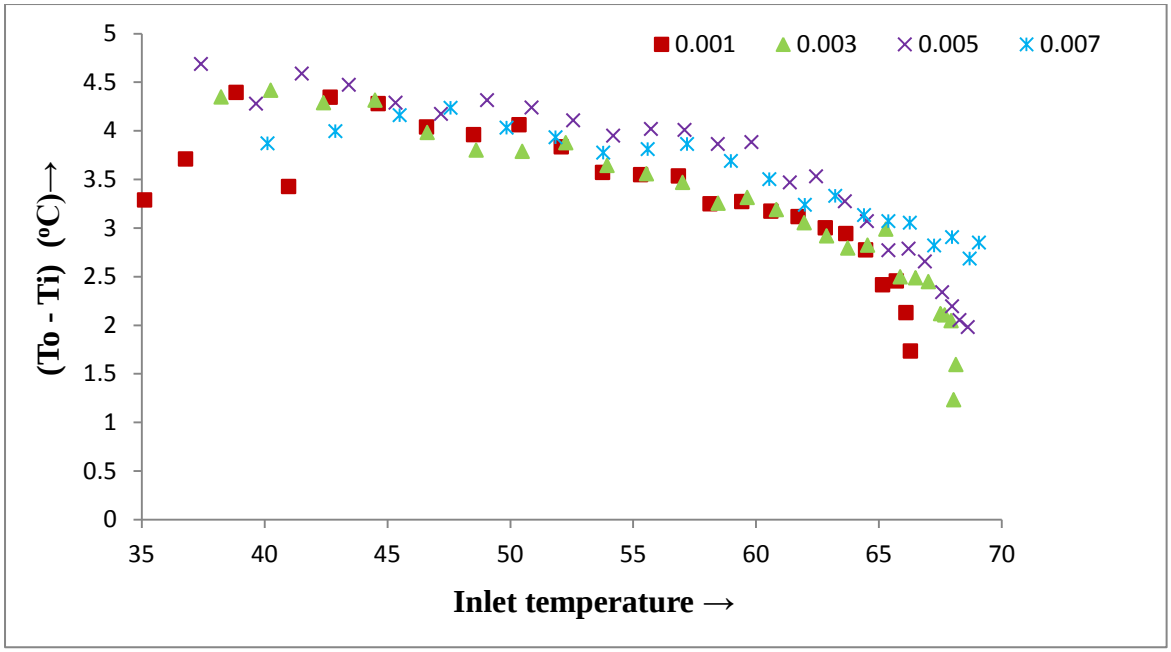

Fig. 5.29 (b) Temperature rise for different nanoparticle concentrations at 2 lpm flow rate

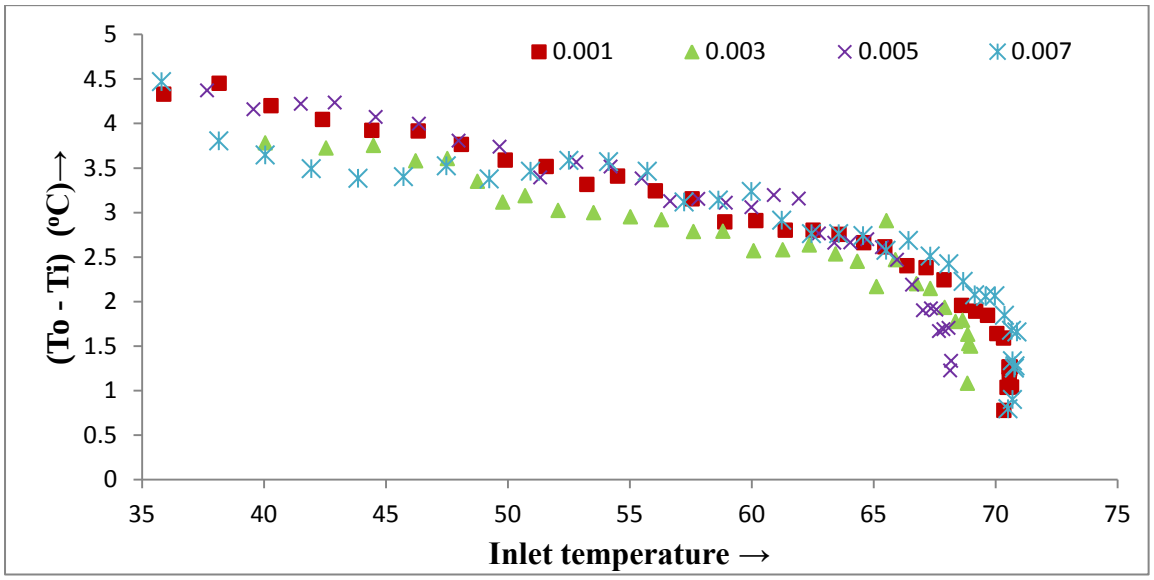

Fig. 5.29 (c) Temperature rise for different nanoparticle concentrations at 2.5 lpm flow rate

Fig. 5.29 (a) - (c) shows the effect of nano particle volume fraction on single pass fluid temperature rise at three flow rates. For all the flow rates it is observed that maximum fluid temperature rise is obtained at 0.005% volume fraction in low temperature range and at 0.007% in higher temperature range at fixed inlet fluid temperature.

5.6.4 Effect of volume fraction on base plate temperature

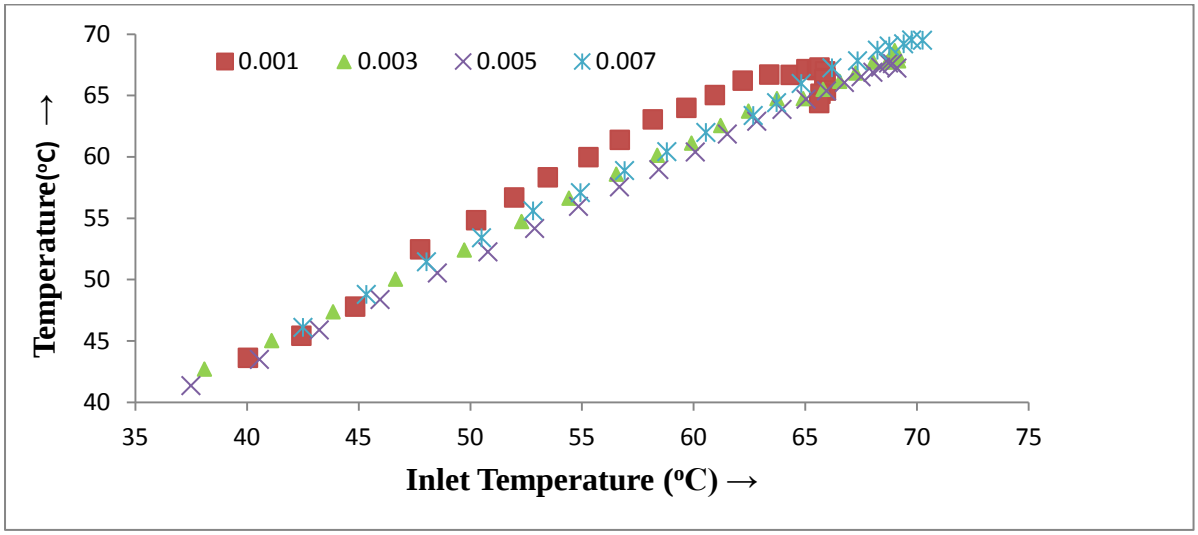

Fig. 5.30 (a) Effect of nanoparticle volume fraction on base plate temperature at 1.5 lpm

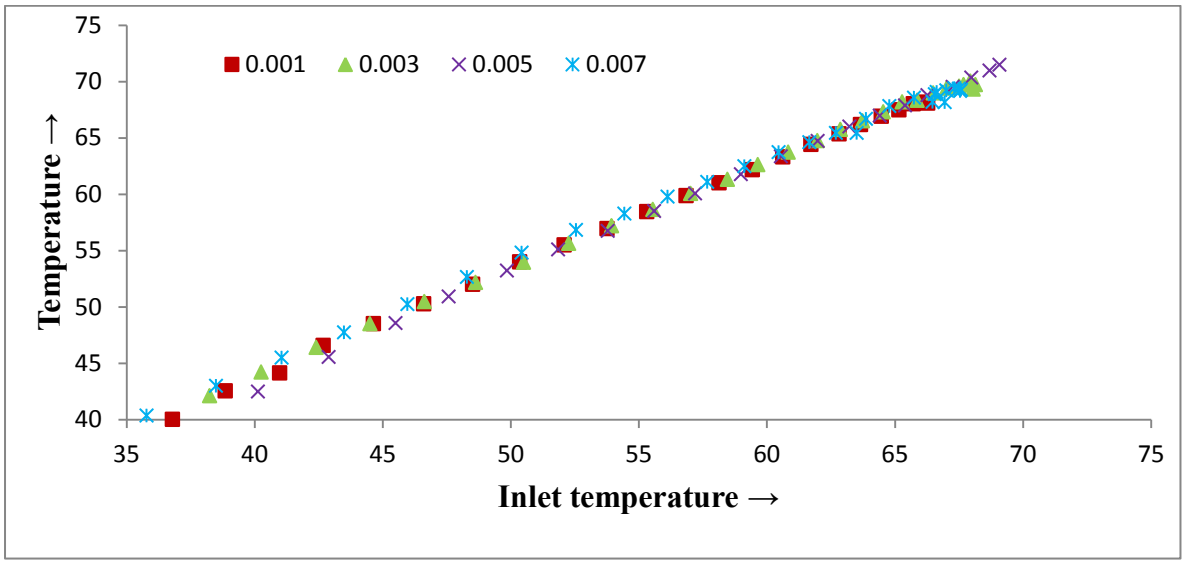

Fig. 5.30 (b) Effect of nanoparticle volume fraction on base plate temperature at 2 lpm

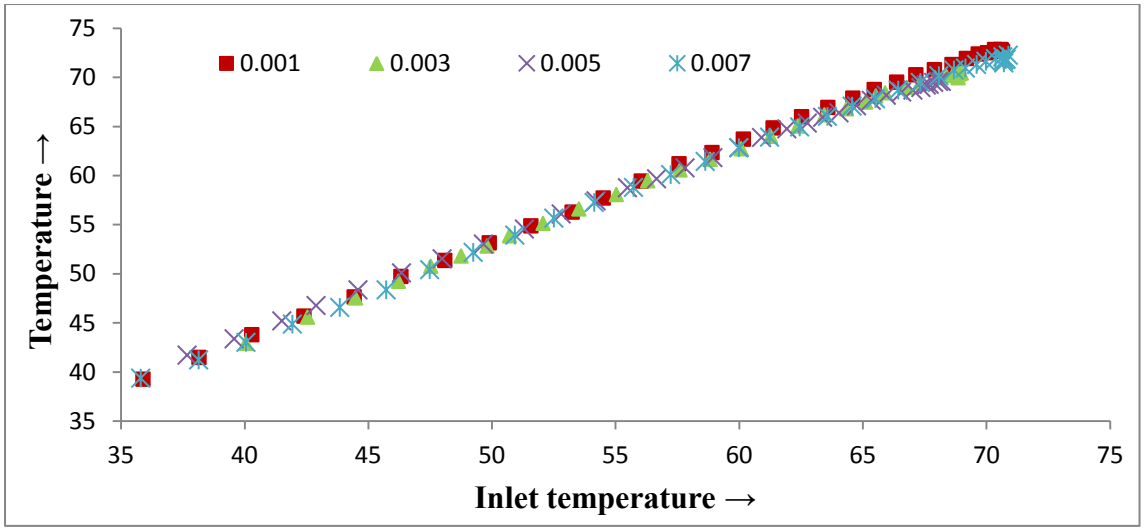

Fig. 5.30 (c) Effect of nanoparticle volume fraction on base plate temperature at 2.5 lpm

Fig. 5.30 (a) to (c) shows the effect of nanoparticle volume fraction on base plate temperature at different flow rates. For three flow rates, it is observed that minimum base plate temperature is obtained at 0.005 vol% nanoparticle concentration indicating uniform temperature distribution within nanofluid film and for lower and higher volume fraction of nanofluid than 0.005%, base plate temperature is slightly higher. These results show optimum nanoparticle volume fraction to be 0.005 vol%. It is also observed that lower base plate temperature is achieved at 2 lpm in comparison to 2.5 lpm (at fixed inlet fluid temperature) indicating better performance at 2 lpm which is optimum flow rate as shown in Fig. 5.23 (b) & (c).

5.6.5 Effect of volume fraction on glass cover temperature

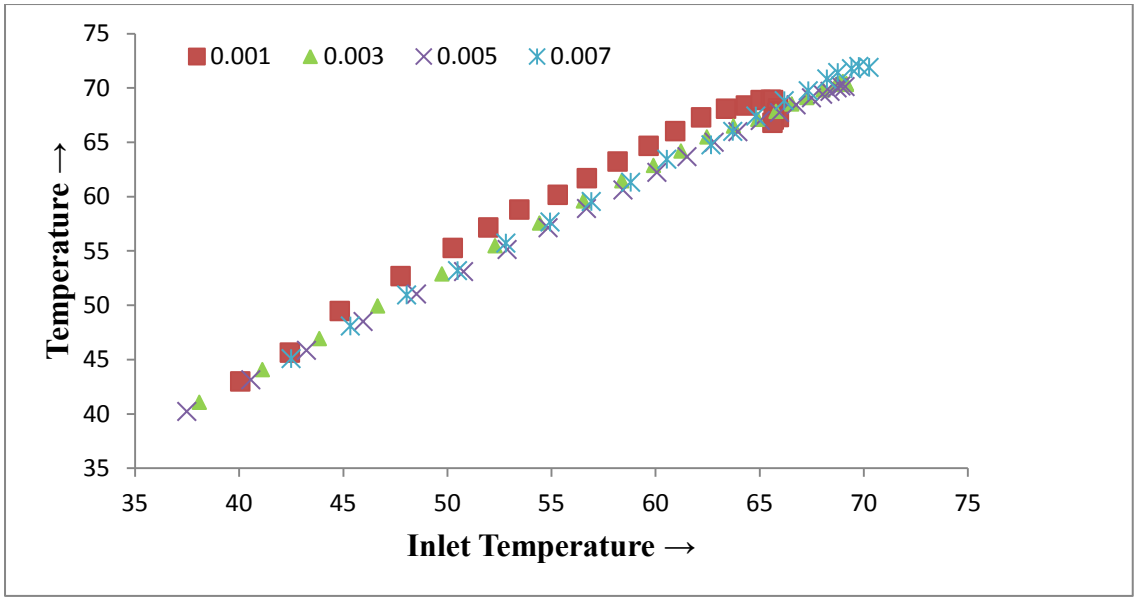

Fig. 5.31(a) Effect of volume fraction on glass plate temperature at 1.5 lpm flow rate

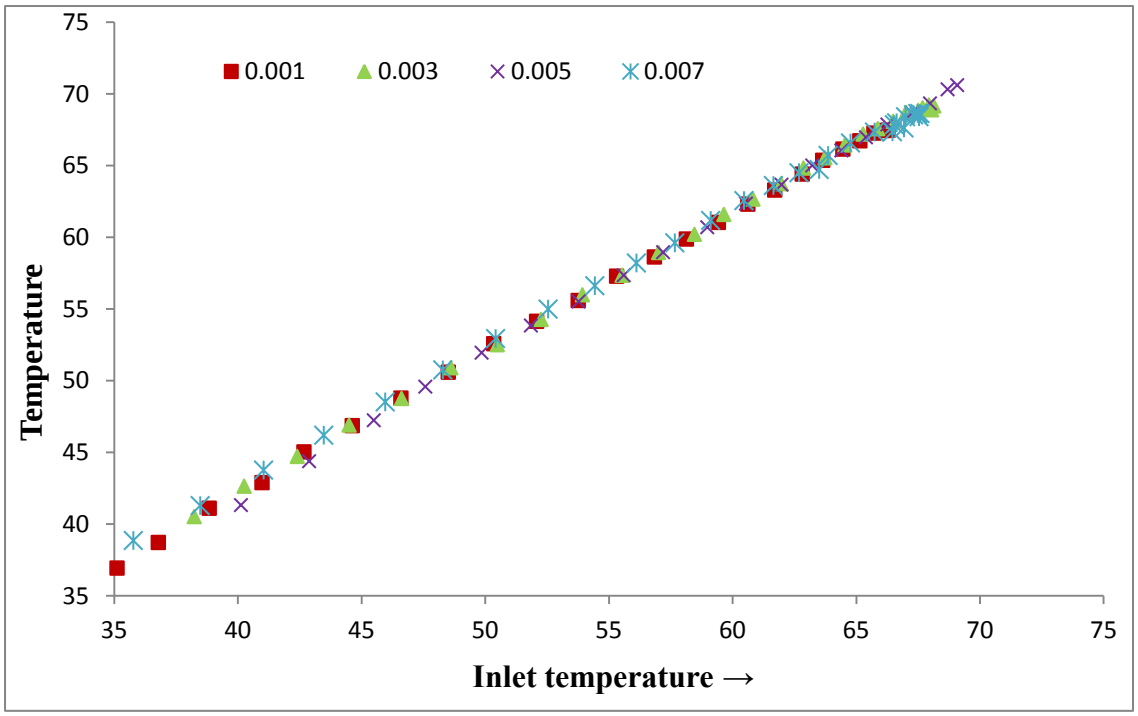

Fig. 5.31(b) Effect of volume fraction on glass plate temperature at 2 lpm flow rate

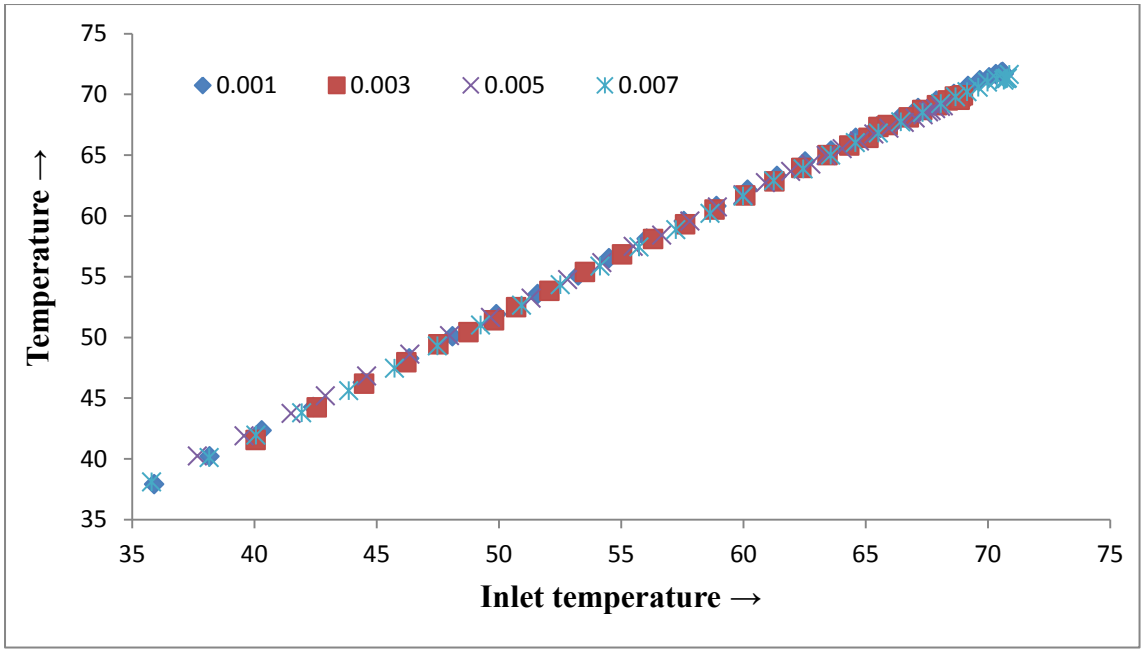

Fig. 5.31(c) Effect of volume fraction on glass plate temperature at 2.5 lpm flow rate

Fig. 5.31 (a) to (c) shows the effect of volume fraction on glass plate temperature at different flow rates with inlet fluid temperature. For all three flow rates, glass plate temperature found to decrease with increase in nanoparticle volume fraction and the minimum glass plate temperature is obtained at 0.005 vol% again indicating uniform temperature distribution within nanofluid film at this volume fraction. For lower and higher volume fraction than 0.005%, glass plate temperature is slightly higher. But, at fixed nanoparticle volume fraction, the increase in inlet fluid temperature increased glass plate temperature due to higher radiation losses at high temperature.

5.6.6 Effect of volume fraction on outlet temperature

(a) At different flow rate

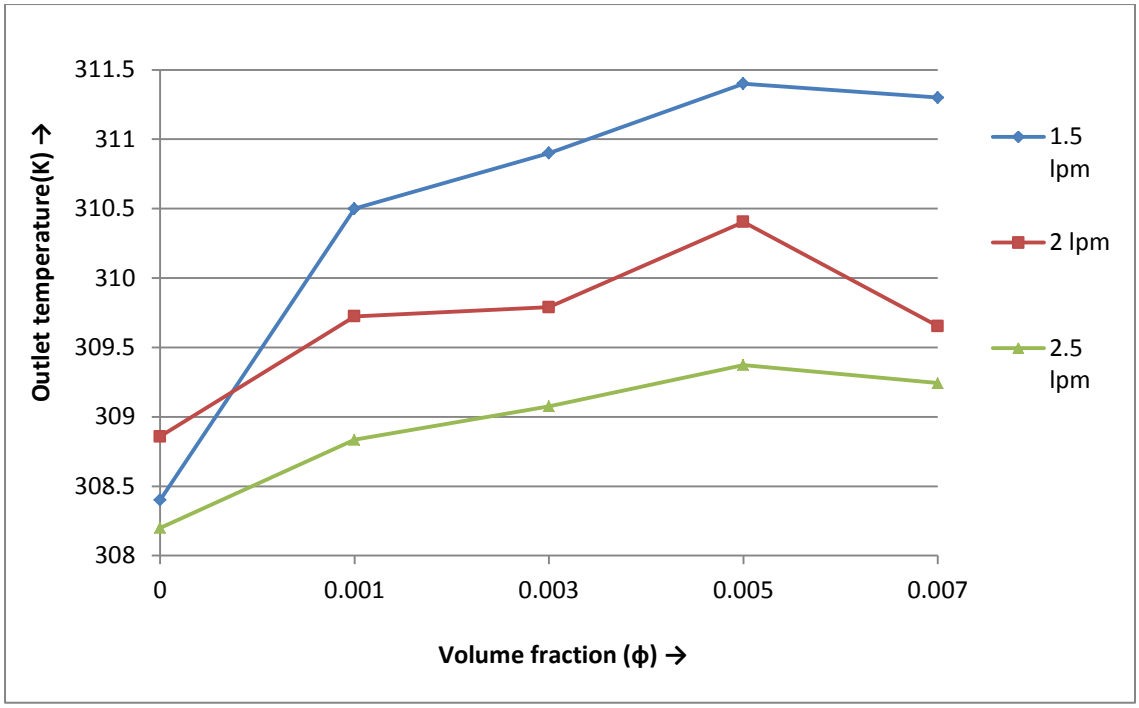

Fig. 5.32 Effect of volume concentration on outlet temperature at three flow rate

(b) At different inlet fluid temperature

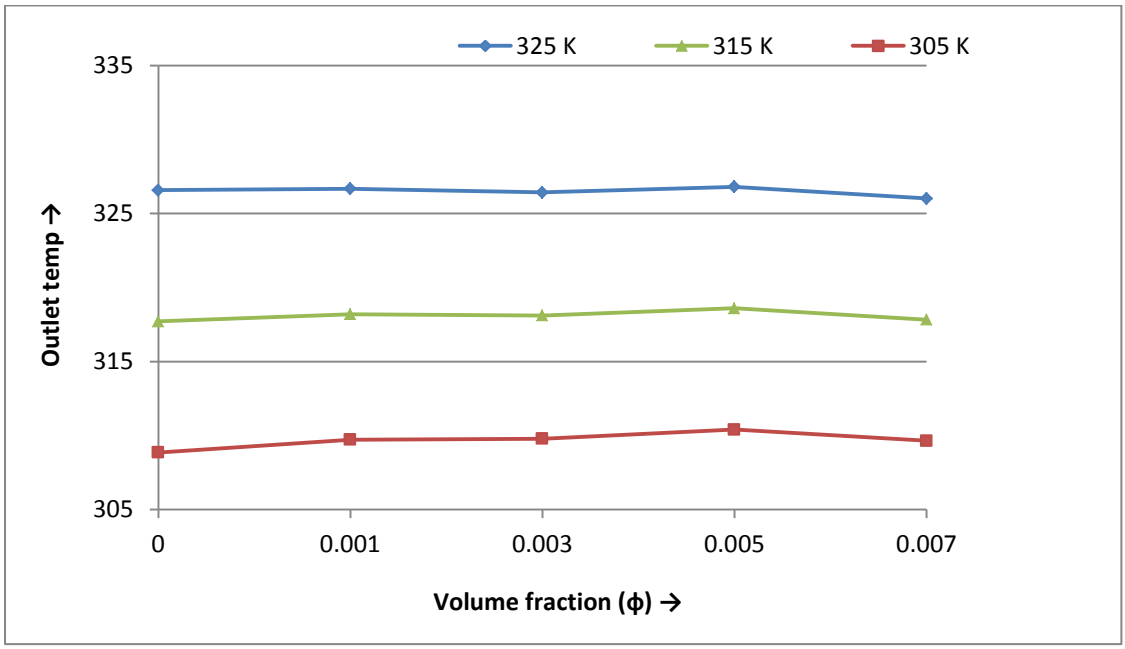

Fig. 5.33 Effect of volume concentration on outlet temperature at different inlet temparature

(c) At different solar radiation

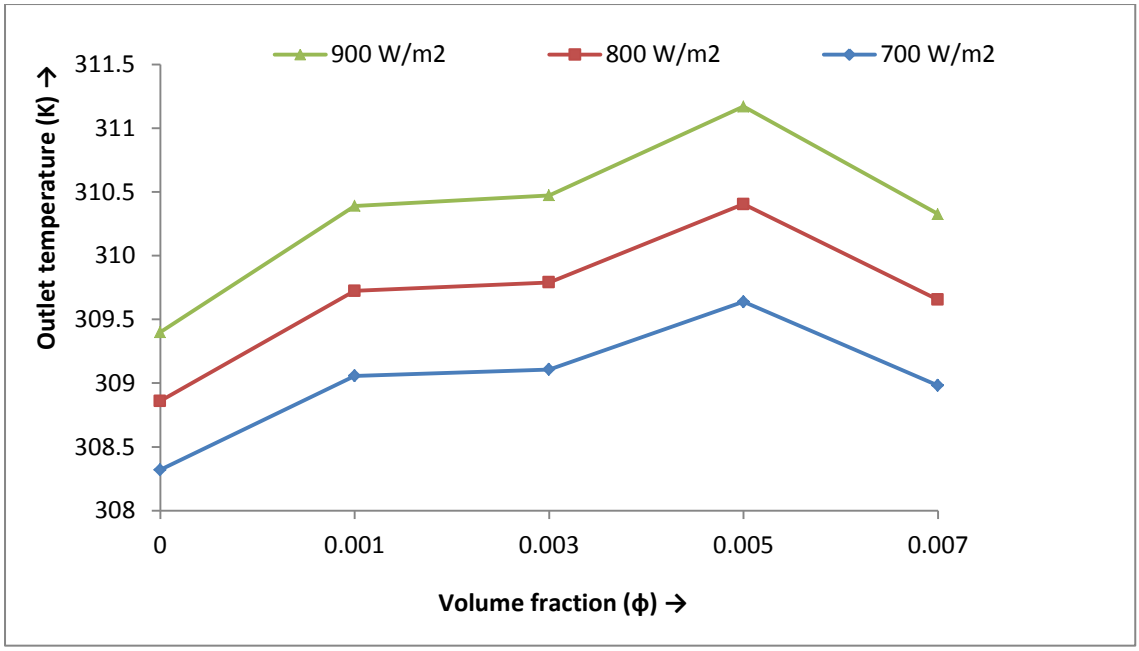

Fig. 5.34 Effect of volume concentration on outlet fluid temperature at different solar radiation

Fig. 5.32 shows the effect of nanoparticle volume concentration on outlet fluid temperature for different flow rates. The maximum outlet fluid temperature is observed at 1.5 lpm flow rate indicating that with the increase in flow rate, the fluid temperature rise decreases due to lower stay time available for fluid in the solar collector for absorption of solar energy. Fig. 5.33 shows the effect of nanoparticle volume concentration on outlet fluid temperature with different inlet fluid temperature. The maximum outlet temperature is obtained at 0.005 volume fraction of nanofluid at all different inlet temperature, indicating the optimum volume fraction at 0.005 vol%.

Fig. 5.34 shows the effect of nanoparticle volume concentration on outlet fluid temperature for different solar radiation. With the increase in radiation intensity, outlet fluid temperature increases with increase in volume fraction up to optimum volume fraction 0.005%.

5.7 Experimental uncertainty analysis

As per ASME guidelines, absolute measurements do not exist and errors arise from many sources. Some of the common sources of error are: calibration errors, data acquisition errors and data reduction errors. Uncertainty in the experimental results in the present work was determined by following ASME guidelines on reporting uncertainties in experimental measurements based on the deviation in experimental parameters [Abernethy et al (1983)]. The major components to uncertainty in collector efficiency are the inaccuracy in flow rate measurement, temperature measurement and solar radiation intensity measurement. The results of uncertainty analysis of the measurements including all the sources of errors are presented in the Table 5.13.

Table 5.13 Results of uncertainty analysis

S.No	PARAMETER	UNCERTAINTY
1	Solar Intensity	±5.6 %
2	Volumetric Flow	±1.4 %
3	Temperature difference	±1.7 %

General form of equation for uncertainty analysis is as given below.

$$U_y^2 = \sum_{i=1}^{n} U_{X_i}^2$$

Where U_y is the total uncertainty of calculated parameter and U_{xi} is the root sum square of scatter and measuring uncertainty of each measured parameter.

The combined uncertainty for evaluating collector efficiency, U_η , was obtained by the following relation

$$(U_\eta)^2 = \left[\left(\frac{\Delta \dot{m}}{\dot{m}}\right)^2 + \left(\frac{\Delta (T_{out} - T_{in})}{T_{out} - T_{in}}\right)^2 + \left(\frac{\Delta I}{I}\right)^2\right]$$

The maximum uncertainty obtained in the present study in determining the collector efficiency, at various tests was around 6%

CHAPTER - 6

CONCLUSIONS

6.1 Summary of work

Three experimental set ups of Direct Absorption Solar Collector (one with glass, and two with aluminum base plates) were designed, fabricated and developed to determine the outlet fluid temperature, single pass fluid temperature rise, base plate temperature, glass temperature and collector efficiency of working fluids (distilled water and two types of nano fluids). Two different types of nanofluids (Al_2O_3–water and TiO_2–water) of four different nanoparticle concentrations (0.001%, 0.003%, 0.005% and 0.007 vol. %) were studied experimentally at three flow rates (i.e. 1.5 lpm, 2 lpm and 2.5 lpm) considering different inlet fluid temperatures (ranging between 35-70^oC). Optical efficiency and capability of raising fluid temperature were considered as the performance evaluation measures. Stable nanofluids were prepared by two step method using procured powder of nano materials and mixing with distilled water for certain period in ultrasonic vibrator and the experiments were performed according to ASHRAE standard 93-86 under actual outdoor conditions. All the instruments used in test set up were properly calibrated and uncertainty analysis was carried out as per ASME guidelines on reporting uncertainties in experimental measurements.

The direct absorption solar collector works on the principle of volumetric absorption as against the surface absorption in conventional tube-in-plate type of collector. The experimental study is carried out from May 2013 to June 2014 between 10 AM to 3.00 PM. During the study inlet and outlet fluid temperatures, base plate and glass temperature, ambient temperature, fluid flow rate, and solar intensity were measured at an

interval of 15 minutes and recorded through data logger. The experimental data were analyzed by plotting collector characteristic curves in terms of efficiency and reduced temperature (Ti-Ta)/I. Two important collector performance parameters namely absorbed energy parameter and energy loss parameters were calculated and used for the collector analysis.

6.2 Findings for DASC using nanofluid

The main findings from the present study are as follows:

I. The use of nanofluid instead of water improved maximum efficiency and outlet fluid temperature due to improved solar energy absorption characteristics of nanofluid.

II. Optical efficiency of the developed direct absorption solar collector found to be 65-95% with the use of nanofluids as against 50-70% in conventional water flat plate collector.

III. Maximum efficiency of direct absorption solar collector improved with the use of nanofluid in place of water for all the three flow rates. Collector (with glass base plate) efficiency enhancement of 8.1% has been observed for 1.5 lpm flow rate at 0.005 vol% Al2O3-water nanofluid as compared to water.

IV. In low temperature range, collector efficiency is higher at 2 lpm due to higher value of absorbed energy parameter and in high temperature range; the collector efficiency is higher at 2.5 lpm due to reduced heat losses. The collector is operated most of the time in the low temperature range hence, 2 lpm is found to be the optimum flow rate for maximum efficiency of the collector.

V. Greater fluid temperature rise is observed at lower flow rates due to higher fluid residence time in collector.

VI. Experimental results with glass base plate collector using Al_2O_3-water nanofluid of 0.001 vol% and 0.005 vol% concentrations at 2 lpm flow rate, showed maximum efficiency improvement by 22.1 % and 32.6% as compared to water. Collector efficiency increased by 14.35% when nanoparticle concentration increased from 0.001 vol% to 0.005 vol% due to enhancement in energy absorbed parameter and then decreased for higher nanoparticle concentration.

VII. Enhancement in optical efficiency with aluminum base plate collector using Al_2O_3-water nanofluid of 0.001% Al_2O_3 concentration was by 12%, 25% and 15% for flow rate of 1.5, 2 and 2.5 lpm respectively compared to pure water. The increase in nanoparticle concentration from 0.001% to 0.005% improved the collector efficiency by 26% (at 1.5 lpm), 10% (at 2.0 lpm) and 8% (at 2.5 lpm) and further increase in nanoparticle concentration from 0.005 % to 0.007% reduced the collector efficiency at all three flow rates.

VIII. Collector optical efficiency increases up to 2 lpm flow rate and then it becomes constant for higher flow rate of 2.5 lpm.

IX. It is observed that the maximum nanofluid temperature rise occurred at 0.005% Al_2O_3 nanoparticle concentration and at 2 lpm flow rate.

X. Results of the study showed that base plate and glass cover temperature decreased with increase in nanofluid concentration resulting in lower convection and radiation losses. Both these temperatures were the lowest at optimum concentration of 0.005% indicating uniform temperature distribution within flowing nanofluid film. The base plate temperature found to be the

highest at 1.5 lpm flow rate and lowest at 2 lpm flow rate. With increase in the inlet fluid temperature, base plate temperature also increased reaching to a maximum temperature of 68^0C. The observed glass plate temperature was higher at 1.5 lpm flow rate and lower at 2 lpm and 2.5 lpm. As the inlet fluid temperature increased, glass plate temperature also increased reaching to a maximum temperature of 62^0C.

XI. During the study for both the nanofluids and considering all four concentrations of nanoparticle the maximum outlet fluid temperature was obtained at 2 lpm and at 0.005% volume fraction at all inlet fluid temperatures.

XII. For aluminum base plate collector the optical efficiency using TiO_2-water nanofluid at 0.005 vol% concentration was 82.97%, 94.64% and 90.76% at 1.5, 2 and 2.5 lpm respectively.

XIII. Present study showed that with Al base plate collector the optical efficiency using TiO_2-water nanofluids was found to be higher than Al_2O_3-water nanofluids for a wide range of temperature at all three flow rates and for all four nanoparticle concentrations considered in the study. Highest increase in optical efficiency was found to be 40% (at 0.001 vol%), 26.8% (at 0.001 vol%) and 17.32% (at 0.003 vol%) in comparison to Al_2O_3-water nanofluid for 1.5 lpm, 2 lpm and 2.5 lpm respectively.

XIV. Results showed that TiO_2 and Al_2O_3 based nanofluid exhibited better and promising solar absorption characteristics than water and can be used as a good solar absorption fluid in solar collectors.

Thus, significant enhancement in solar radiation absorption and collector efficiency make nano-fluids as a suitable heat transfer fluid for solar thermal applications and can also be

used in solar collectors for effectively capturing and transporting thermal energy to ever-growing industrial and domestic needs.

6.3 Scope of future work

Study on direct absorption solar collector is a new concept and results of the study show a promising way of harnessing solar energy. There is a scope for further improvement in performance and in depth study can be performed. The present study has considered collector efficiency analysis using water based Al_2O_3 and TiO_2 nanofluids.

Some recommendations for the future work are as follows:

I. The use of other nanomaterials such as CNT, CuO, ZnO and others should be studied and performance optimization can be done in terms of nanoparticle concentration, flow rate etc.
II. The film thickness should be measured and optimized for different nanofluids.
III. Indoor tests can be performed under controlled conditions and results can be standardized.
IV. The gap between glass cover and base plate can be optimized along with number of glass covers.
V. Concentrated liquid nanofluids instead of nano-powder can be used for better stabilization of nanofluids.
VI. CFD based model can be developed and studied for the system and compared with experimental results.
VII. Evacuated tube collector can also be studied using nanofluids and compared with conventional FPSC and DASC.

REFERENCES

1. Abernethy, R.B., Benedict, R.P., and Dowdell, R.B., 1983. ASME Measurement Uncertainty.

2. Abdelrahman, M., Fumeaux, P., and Suter, P., 1979, "Study of Solid-Gas-Suspensions Used for Direct Absorption of Concentrated Solar Radiation," Sol. Energy, 22(1), pp. 45–48.

3. Akoh, H., Tsukasaki, Y., Yatsuya, S., and Tasaki, A., 1978. Magnetic Properties of Ferromagnetic Uhrafine Particles Prepared by a Vacuum Evaporation on Running Oil Substrate," J Cryst. Growth, Vol. 45, pp. 495-500.

4. Arab, M., Soltanieh, M., and Shafii, M.B., 2012; Experimental investigation of extra- long pulsating heat pipe application in solar water heaters. Experimental thermal and fluid science.

5. Angayarkanni SA., and Philip John., 2015; Review on thermal properties of nanofluids: Recent developments. Advances in Colloid and Interface science, Vol. 225, pp. 146-176.

6. Arai, N., Itaya, Y., Hasatani, M., 1984. Development of a volume heat trap type solar collector using a fine-particle semitransparent liquid suspension (FPSS) as a heat vehicle and heat-storage medium. Sol. Energy 32, 49–56.

7. Arizona Solar Center, 2011. Solar Hot Water: A Primer. <http://www. azsolarcenter.org/tech-science/solar-for-consumers/solar-hot-water/ solar-hot-water-a-primer.html>.

8. ASHRAE Standard 86-93. Methods of testing to determine the thermal performance of solar collectors; 1986. Atlanta, GA, USA.

9. Asnaghi, A., Ladjevardi, S.M., 2012. Solar chimney power plant performance in Iran. Renew. Sustain. Energy Rev. 16 (5), 3383–3390.

10. Bacri, J.C., Perzynski, R., Salin, D., Cabuil, V., Massart, R., 1990. Ionic magnetic fluids: a crossing of chemistry and physics, J. Magn. Magn. Mater. 85, pp. 27.

11. Bertocchi, R., Karni, J., and Kribus, A., 2004, "Experimental Evaluation of a Non-Isothermal High Temperature Solar Particle Receiver," Energy, 29, pp. 687–700.

12. Bjerneld, E.J., Svedberg, F., Kall, M., 2003. Laser-induced growth and deposition of noble metal nanoparticles for surface enhanced Raman scattering, Nano Letters 3 pp. 593-596.

13. Bönnemann, H.; Brijoux, W.;,Brinkmann, R.; Endruschat, U.; Hofstadt, W.; Angermund K., 1999. Rev. Roum. Chim. 44, 1003.

14. Bönnemann, H.; Brijoux, W.; Brinkmann, R.; 1999. WO 99/59713.

15. Bönnemann, H.; Waldöfner, N.; 2002. Chem. Mater., 14, 1115.

16. Bönnemann, H.; Angermund, K.; Bühl, M.;, Endruschat, U.; Mauschick, F.T.; Mörtel, R.; Mynott, R.; Tesche, B.; Waldöfner, N.; 2003. J., Phys. Chem. B. 107, 7507.

17. Bottum EW, 1981. Refrigerant charged phase change solar water heater and space heating systems. ASHRAE Transactions 87(2):397–404.

18. Brust, M. J., 1994. Chem. Soc., Chem. Comm., 7, 801.

19. Budihardjo I, Morrison GL, 2009. Performance of water-in-glass evacuated tube solar water heaters. Solar Energy, 83(1):49–56.

20. Canbazoglu S, Sahinaslan A, Ekmekyapar A, Aksoy YG, Akarsu F, 2005. Enhancement of solar thermal energy storage performance using sodium thiosulfate pentahydrate of a conventional solar water-heating system. Energy Buildings, 37(3):235–42.

21. Carotenuto, G., 2001.Synthesis and characterization of poly (N-vinylpyrrolidone) filled by monodispersed silver clusters with controlled size, Appl. Organometal. Chem. 15, pp. 344.

22. Chaturvedi SK, Chen DT, Kheireddine A,1998. Thermal performance of a variable capacity direct expansion solar-assisted heat pump. Energy Conversion Management ,39(3-4):181–91.

23. Chauhan RS, Kadambi V,1976. Performance of a collector-cum-storage type of solar water heater. Solar Energy, 18(4):327–35.

24. Chen, H., Yang, W., He, Y., Ding, Y., Zhang, L., Tan, C., Lapkin, A.A. and Bavykin, D.V., 2009. Heat transfer and flow behaviour of aqueous suspensions of titanate nanotubes (nanofluids). Powder Technology, 183, pp. 63–72.

25. Chen BR, Chang YW, Lee WS, Chen SL, 2009. Long-term thermal performance of a two-phase thermosyphon solar water heater. Solar Energy 2009; 83(7): 1048–55.

26. Chien CC, Kung CK, Chang CC, Lee WS, Jwo CS, Chen SL,2011. Theoretical and experimental investigations of a two-phase thermosyphon solar water heater. Energy, 36(1):415–23.

27. Chinnappa JCV, Gnanalingam K, 1973. Performance at Colombo, Ceylon, of a pressurized solar water heater of the combined collector and storage type. Solar Energy,15(3):195–204.

28. Choi S.U.S., 1995. Enhancing thermal conductivity of fluids with nanoparticles. Developments and Applications of non-Newtonian Flows, FED-vol. 231/MD-vol. 66. ASME, pp. 99–105.

29. Choi S.U.S, 1999. Nanofluid Technology: Current Status and Future research, Energy Technology Division , Argonne National Laboratory.

30. Choi, S. U. S., and Eastman, J. A. ,1995. Enhancing thermal conductivity of fluids with nanoparticles." International mechanical engineering congress and exhibition, San Francisco, CA.

31. Choi, S. U. S.;Eastman, J. A., 2001. Patent: US 6221275 B1.

32. Choi, S.U.S., Zhang, Z.G., Yu, W., Lockwood, F.E., Grulke, E.A., 2001. Anomalous thermal conductivity enhancement in nano-tube suspensions. Applied Physics Letters 79, 2252-2254.

33. Chyng JP, Lee CP, 2003. Huang BJ. Performance analysis of a solar-assisted heat pump water heater. Solar Energy,74(1):33–44.

34. Close DJ, 1962. The performance of solar water heaters with natural circulation. Solar Energy; 6(1):33–40.

35. Copeland, R. J., Leach, J. and Stein C.,1982. High temperature molten salt solat thermal systems, in Proceedings of 17th International Energy Conversion engineerign Conference, IEEE, New York.

36. Das, S. K., Choi, S. U. S., Yu, W., & Pradeep, T. (2007). Nanofluid Science and Technology. John Wiley & Sons, Inc., Publication.

37. DeSa VG, 1964. Experiments with solar energy utilization at Dacca. Solar Energy, 8(3):83–90 July-September.

38. Duffie, J. A., & Beckman, W. A., 2006. Solar engineering of thermal processes. Wiley publication.

39. Eastman, J. A., Choi, U. S., Li, S., Thompson, L. J., and Lee, S., 1997. Enhanced thermal conductivity through the development of nanofluids. Volume 457 of Materials Research Society Symposium - Proceedings, 3–11. Materials Research Society, Pittsburgh, PA, USA, Boston, MA, USA.

40. Eastman, J. A., Choi, S. U. S., Li, S., Yu, W., and Thompson, L. J., 2001. Anomalously increased effective thermal conductivities of ethylene glycol-based

nanofluids containing copper nanoparticles. Applied Physics Letters, 78, no. 6, 718–720.

41. Ecevit A, Al-Shariah M, Apaydin ED, 1989. Triangular built-in-storage solar water heater. Solar Energy,42(3):253–65.

42. Edlestein, A. S.; Cammarata, R. C.; Eds. 2001, Nanomaterials: Synthesis, Properties and Applications. London: Institute of Physics.

43. Eftekhari, A., Molaei, F., Arami, H., 2006. Flower like bundles of ZnO nanosheets as an intermediate between hollow nanosphere and nanoparticles, Materials Science and Engineering A. 437, pp. 446-450.

44. Esen M, Esen H, 2005. Experimental investigation of a two-phase closed thermo-syphon solar water heater. Solar Energy, 79(5):459–68.

45. Esen, M., Yuksel, T., 2000. Performance of thermosyphon flat plate solar collector with heat pipes. Fırat University, Journal of Science and Engineering ,12 (2), 201–207.

46. Fanny A H, Terlizzi C P, 1985. Testing of refrigerant-charged solar domestic hot water systems. Solar Energy, 35(4):353–66.

47. Farrington, R., Deangelis, M., Morrison L and Dougherty D, 1981. Performance evaluation of a refrigerant-charged thermosyphon solar DHW system. In Proc. AS/ISES annual meeting, Philadelphia, published by the ISES, American Section, 4: 676–680.

48. Fouchet, A., Prellier, W., Mercey, B., Mechin, L., Kulkarni, V. N. and Venkatesan, T. J., 2004. Investigation of laser ablated ZnO thin films grown with Zn metal target: a structural study, Appl. Phys. 96, pp. 3228.

49. Garg HP, Rani U, 1982. Theoretical and experimental studies on collector/storage type solar water heater. Solar Energy, 29(6):467–78.

50. Gleiter, H., 2000. Nanostructure materials: basic concepts and microstructure, Acta Mater. Rev.48, 1-29.

51. Gleiter, H., 1989. Nanocrystalline material, Progress in Material sci. 33, pp. 223-315.

52. Gnanaprakash, G., Philip, J., Kumar, T.J., Raj, B., 2007. Effect of digestion time and alkali addition rate on the physical properties ofmagnetite nanoparticles, J. Phys. Chem. B 111, pp. 7978-7986.

53. Gnanaprakash, G., Philip, J., Raj, B., 2007. Effect of divalent metal hydroxide solubility product on the size of ferrite nanoparticles, Mater. Lett. 61, pp. 4545-4548.

54. Gnanaprakash, G., Mahadevan, S., Jayakumar, T., Kalyanasundaram, P., Philip, J., Raj, B., 2007. Effect of initial pH and temperature of iron salt solutions on formation of magnetite nanoparticles, Mater. Chem. Phys. 103, pp. 168-175.

55. Gnanaprakash, G., Ayyappan, S., Jayakumar, T., Philip, J., Raj, B., 2006. A simple method to produce magnetic nanoparticles with enhanced alpha to gamma-Fe2O3 phase transition temperature, Nanotechnology 17, pp. 5851-5857.

56. Goetzberger A, Rommel M, 1987. Prospects for integrated storage collector systems in central Europe. Solar Energy,39(3):211–9.

57. Gullison, R.E., Frumhoff, P.C., Canadell, J.G., Field, C.B., Nepstad, D.C., Hayhoe, K., et al., 2007. Tropical forests and climate policy.Science 316, 985–986.

58. Guoying X, Xiaosong Z, Shiming D, 2006. A simulation study on the operating performance of a solar-air source heat pump water heater. Applied Thermal Engineering, 26(11-12):1257–65.

59. Gupta CL, Garg HP, 1968. System design in solar water heaters with natural circulation. Solar Energy, 12(12):163–70.

60. Gurin, V.S., Alexeenko, A.A., Zolotovskaya, S.A., Yumashev, K.V., 2006. Copper and copper selenide nanoparticles in the solgel matrices: Structural and optical, Mater. Sci. Eng. C 26, pp. 952-955.

61. Hawlader MNA, Chou SK, Jahangeer KA, Rahman SMA, Lau KWE,2003. Solar-assisted heat-pump dryer and water heater. Applied Energy, 74(1-2):185–93.

62. He Q, Wang S, Zeng S, Zheng Z, 2013. Experimental investigation on photo thermal properties of nanofluids for direct absorption solar thermal energy systems. Energy Conversion Management , 73: 150–7.

63. Hobson PA, Norton B. A, 1989. Design nomogram for direct thermosyphon solar energy water heaters. Solar Energy, 43(2):89–95.

64. Houf W. G., Incropera F. P. and Viskanta R., 1984. Effect of solar radiation on thermal and hyrdodynamic boundary condtions in laminar open channel flow, Journal of Solar Energy Engineering , vol. 106.

65. Huang BJ, Lee JP, Chyng JP. Heat-pipe enhanced solar-assisted heat pump water heater. Solar Energy 2005;78(3):375–81.

66. Huang J, Pu S, Gao W, Que Y, 2010. Experimental investigation on thermal performance of thermosyphon flat-plate solar water heater with a mantle heat exchanger. Energy, 35(9):3563–8.

67. Hunt, A. J., 1978, Small Particle Heat Exchangers, Department of Energy, Lawrence Berkeley Laboratory, Energy and Environment Division, Berkeley, CA.

68. Intergovernmental Panel on Climate Change (IPCC), 2007. Climate Change 2007, Fourth Assessment Report. United Nations, New York.

69. Islam, M., Khan, M., Sarkar, M., 2005. Performance of a two-phase solar collector in water heating. Journal of Energy & Environment 4, 117– 123, technical Note.

70. Jefferson, J. M., 1998. Global Climate Change and the Challenges for Renewable Energy. Florence, Italy, P. 1-7.

71. Javadi, F., Saidur, R., Kamalisarvestani, M., 2013. Investigating performance improvement of solar collectors by using nanofluids, Renew.Sustain .Energy Rev.28, 232–245.

72. Joudi KA, Al-tabbakh AA,1999. Computer simulation of a two phase thermosy-phon solar domestic hot water heating system. Energy Conversion and Management, 40:775–93.

73. Kalogirou, S., 2009. Thermal performance, economic and environmental life cycle analysis of thermosyphon solar water heaters. Solar Energy, 39-48.

74. Kalogirou.S.A, 2004. Solar Thermal Collectors and Applications, Progress in Energy and Combustion Science, 30, 231 – 295.

75. Kamal W, 1984. Performance evaluation of a refrigerant-charged solar collector. In Energex, 84. Regina, Saskatchewan:Pergamon Press,193-197.

76. Kaptan IN, Kilic A, 1996. A theoretical and experimental investigation of a novel built-in-storage solar water heater. Solar Energy, 57(5):393–400.

77. Khanafer, K., Vafai, K., 2011. A critical synthesis of thermophysical characteristics of nanofluids, Int. J. Heat Mass Transf. 54 (2011) 4410–4428.

78. Kameya, Y., Hanamura, K., 2011. Enhancement of solar radiation absorption using nanoparticle suspension." Solar Energy 85, 299-307.

79. Karami, M., Bahabadi, M. A. A., Delfani, S., and Ghozatloo, A., 2014. A new application of carbon nanotubes nanofluid as working fluid of low temperature direct absorption solar collector. Solar Energy Materials & Solar Cells, 121, 114–118 .

80. Kaushika, N.D., Kaushik, S.C., and Bharadwaj, S.C., 1982. Analysis of a flat plate collector with fluid undergoing phase. Applied Energy, 11(3): 233-242.

81. Keblinski, P., S.R. Phillpot, S.U.S. Choi, J.A. Eastman, 2002. Mechanisms of heat flow in suspensions of nano-sized particles (nanofluids), Int. J. Heat Mass Transfer 45 (4), 855–863.

82. Khullar, V., Tyagi, H., Phelan, P. E., Otanicar, T. P., Singh, H., and Taylor, R.A., 2010, "Solar Energy Harvesting Using Nanofluids-Based Concentrating Solar Collector," ASME J. Nanotechnol. Eng. Med., 3(3), p. 031003.

83. Khullar, V., and Tyagi, H., 2013, "A Study on Environmental Impact of Nanofluid-Based Concentrating Solar Water Heating System," Int. J. Environ. Stud., 69(2), pp. 220–232.

84. Kuang YH, Sumathy K, Wang RZ, 2003. Study on a direct-expansion solar-assisted heat pump water heating system. International Journal of Energy Research, 27(5):531–48.

85. Kudish AI, 1985. Santamaura P, Beaufort P. Direct measurement and analysis of thermosyphon flow. Solar Energy, 35(2):167–73.

86. Kumar, R.V., Diamant, Y., Gedanken, A., 2000. Sonochemical synthesis and characterization of nanometer size transition metal oxides from metal acetates, Chem. Mater. 12, pp. 2301.

87. Kumar S. and Tien C. L. (1990), Analysis of combined radiation and convection in a particulate-laden liquid film, Journal of Solar Energy Engineering, vol. 112.

88. Ladjevardi, S.M., Asnaghi, A., Izadkhast, P.S., Kashani, A.H., 2013. Applicability of graphite nanofluids in direct solar energy absorption, Solar Energy 94, 327–334.

89. Lee, D.W., Sharma, A, 2007. Thermal performances of the active and passive water heating systems based on annual operation. Solar Energy, 81, 207–215.

90. Lee, S., Choi, S. U. S., Li, S., and Eastman, J. A., 1999. Measuring thermal conductivity of fluids containing oxide nanoparticles. Journal of Heat Transfer, 121, 280–289.

91. Lenert, A., Zuniga, Y. S. P., and Wang, E. N., 2010, "Nanofluid-Based Absorbers for High Temperature Direct Solar Collectors," 14th International Heat Transfer Conference, Washington, DC, Aug. 8–13, ASME, Paper No. IHTC14-22208, pp. 499–508.

92. Lenert A, Wang EN, 2012. Optimization of nanofluid volumetric receivers for solar thermal energy conversion. Solar Energy, 86: 253–65.

93. Leong, K.Y., Saidur, R., Kazi, S.N., Mamun, A.H., 2010. Performance investigation of an automotive car radiator operated with nanofluid based coolants (nanofluid as a coolant in a radiator). Applied thermal engg 30 , 2685-2692.

94. Lewis, N. S., Crabtree, G. W., 2005. Basic Research Needs for Solar Energy Utilization: Report of the Basic Energy Sciences Workshop on Solar Energy Utilization". US Department of Energy Office of Basic Energy Sciences, April 18–21.

95. Li, S., Hui, Z., Yujie, J., Deren, Y., 2004. CuO nanodendrite synthesized by a novel hydrothermal route, Nanotechnology 15 pp. 1428.

96. Lin, X.Z., Teng, X., Yang, H., 2003. Direct synthesis of narrowly dispersed silver nanoparticles using a single-source precursor, Langmuir 19 pp. 10081.

97. Li XF, Zhu DS, Wang XJ, 2007. Evaluation on dispersion behavior of the aqueous copper nano suspensions. J Colloid Interface Sci, 310:456-63.

98. Li Z, Chen C, Luo H, Zhang Y, Xue Y, 2010. All-glass vacuum tube collector heat transfer model used in forced-circulation solar water heating system. Solar Energy, 84(8):1413–21.

99. Lo, C-H.; Tsung, T-T.; Chen, L-C.; Su, C-H.; Lin, H-M., 2005. J. Nanopart. Res., 7, 313.

100. Long Zhang, Jian Liu, Guodong He, Zhuocheng Ye, Xiaoming Fang, Zhengguo Zhang, 2014. Radiative properties of ionic liquid-based nanofluids for medium-to-high-temperature direct absorption solar collectors.Solar Energy Materials & Solar Cells,130,521-528.

101. Lu, L., Liu, Z.-H., and Xiao, H.-S., 2011, "Thermal Performance of an Open Thermosyphon Using Nanofluids for High-Temperature Evacuated Tubular Solar Collectors," Sol. Energy, 85(2), pp. 379–387.

102. Mahian, O., Kianifar, A., Kalogirou,S.A. Pop I., Wongwises, S., 2013. A review of the applications of nanofluids in solar energy, Int. J. Heat Mass Transf. 57 582–594.

103. Mathioulakis, E., Belessiotis, V., 2002. A new heat-pipe type solar domestic hot water system. Solar Energy, 72 (1), 13–20.

104. Mercatelli, L., Sani, E., Zaccanti, G., Martelli, F., Di Ninni, P., Barison, S., Pagura, C., Agresti, F., and Jafrancesco, D., 2011, "Absorption and Scattering Properties of Carbon Nanohorn-Based Nanofluids for Direct Sunlight Absorbers," Nanoscale Res. Lett., 6(1), p. 282.

105. Mercatelli L, Sani E, Giannini A, Di Ninni P, Martelli F, Zaccanti G., 2012. Carbon nanohorn-based nanofluids: characterization of the spectral scattering albedo. Nanoscale Res Lett, 7:96.

106. Miller, F. J., and Koenigsdorff, R. W., 2000, "Thermal Modeling of a Small-Particle Solar Central Receiver," ASME J. Sol. Energy Eng., 122(1), pp. 23–29.

107. Minardi, J.E., Chuang, H.N., 1975. Performance of a "Black" Liquid Flat- Plate Solar Collector." Solar Energy, 179-183.

108. Moghadam, A.J., M. FarzaneGord, M. Sajadi, M. HoseynZadeh, 2014. Effects of CuO/water nanofluid on the efficiency of a flat plate solar collector, Exp. Therm. Fluid Sci. 58, 914.

109. Mohamad AA, 1997. Integrated solar collector-storage tank system with thermal diode. Solar Energy,61(3):211–8.

110. Morrison GL, Braun JE, 1985. System modelling and operation characteristics of thermosyphon solar water heaters. Solar Energy, 34(4-5):389–405.

111. Mu LJ, Zhu QZ, Si LL, 2010 Radiative properties of nanofluids and performance of a direct solar absorber using nanofluids. 2nd ASME Micro/Nanoscale Heat & Mass Transfer International Conference, 1:549-553.

112. Murshed, S. M. S., Leong, K. C., and Yang, C., 2005. Enhanced thermal conductivity of TiO2 Water based nanofluids. International Journal of Thermal Sciences, 44, no. 4, 367–373.

113. Murshed, S.M.S., Leong, K.C. and Yang, C., 2008. Investigation of thermal conductivity and viscosity of nanofluids. International Journal of Thermal Sciences, 47, 560–568.

114. Nahar, N.M., 2002.Capital cost and economic viability of thermosyphonic solar water heaters manufactured from alternate materials in India." Renewable Energy, 623-635.

115. Nahar, N.M., 2003.Year round performance and potential of a natural circulation type of solar water heater in India." Energy and Buildings , 35: 239-247.

116. Natarajan, E., Sathish, R., 2009. Role of nanofluids in solar water heater. International Journal of advance Manufacturing Systems.

117. Ng KC, Yap C, Khor TH, 2000. Outdoor testing of evacuated-tube heat-pipe solar collectors. Proceedings of the Institution of Mechanical Engineers 2000;214: 23–30 (part E).

118. NIST, 2007. Ref prop version 8.0. Reference Fluid Thermodynamic and Transport Properties. NIST Standard Reference Database 23, Lemon E.W., McLinden M.O., Huber M.L., USA.

119. Okitsu, K., Yue, A., Tanabe, S., Matsumoto, H., 2000. Sonochemical preparation and catalytic behaviour of highly dispersed palladium nanoparticles on alumina, Chem. Mater. 12, pp. 3006.

120. Ong KS, 1974. A finite-difference method to evaluate the thermal performance of a solar water heater. Solar Energy, 16(3-4):137–47.

121. Ong KS, 1976. An improved computer program for the thermal performance of a solar water heater. Solar Energy, 18(3):183–91.

122. Ordaz-Flores, A., Garcı´a-Valladares, O., Go´mez, V.H., 2011. Experimental characterisation and technical feasibility of a closed two-phase vs a conventional solar water heating thermosyphon. Applied Thermal Engineering 31 (6-7), 1313–1322.

123. Otanicar, T.P., Phelan, P.E., Golden J.S., 2009. Optical properties of liquids for direct absorption solar thermal energy systems." Solar Energy, 83 969-977.

124. Otanicar, T.P., Phelan, P.E., Prasher, R.S., Rosengarten, G., Taylor, R.A., 2010. Nanofluid Based Direct Absorption solar collector." Journal of Renewable and sustainable energy, 1-13.

125. Otanicar, T.P., Golden, J.S. , 2009. Comparative Environmental and Economic analysis of conventional and Nanofluid Solar Hot Water Technologies," Environ. Sci. Technol., vol. 43, No.15, pp. 6082–6087.

126. Pantzali, M.N., Mouza, A.A., Paras, S.V., 2009. Investigation the Efficacy of Nanofluids as Coolant in Plate Heat Exchanger(PHE). Chemical Engineering Science 64, 3290-3300.

127. Pastoriza-Santos, I., Liz-Marzan, L.M., 2002. Formation of PVP-protected metal nanoparticles in DMF, Langmuir 18 pp. 2888.

128. Payakaruk T, Terdtoon P, Ritthidech S, 2000. Correlations to predict heat transfer characteristics of an inclined closed two-phase thermosyphon at normal operating conitions. Applied Thermal Engineering, 20(9):781–90.

129. Penner, R.M., 2002. Mesoscopic metal particles and wires by electro deposition, J. Phys. Chem. B 106, pp. 3339.

130. Peyghambarzadeh, S.M., Hashemabadi, S.H., Jamnani, M.S., Hoseini, S.M., 2011: Improving the cooling Performance of Automobile Radiator with Al2O3/Water Nanofluid. Applied Thermal Engineering, 1-6.

131. Pluta Z, Pomierny W, 1995. The theoretical and experimental investigation of the phase-change solar thermosyphon. Renewable Energy, 6(3):317–21.

132. Polvongsri S., and Kiatsiriroat T., "Enhancement of Flat-Plate Solar Collector Thermal Performance with Silver Nano-fluid", The Second TSME International Conference on Mechanical Engineering 19-21 October, 2011.

133. Prasher,R.S., Bhattacharya,P., Phelan,P.E., 2005. Thermal conductivity of nanoscale colloidal solutions (nanofluids), Phys. Rev. Lett. 94, 025901-1–025901-4.

134. Qiu, X.F., Xu, J.Z., Zhu, J.M., Zhu, J.J., Xu, S., Chen H.Y., 2003. Controllable synthesis of palladium nanoparticles via a simple sonoelectrochemical method, J. Mater. Res. 18, pp. 1399.

135. Radhwan A M, Zaki G M, Jamil A, 1990. Refrigerant-charged integrated solar water heater. International Journal of Energy Research,14(4):421–32.

136. Radhwan A M, Zaki G M, 1993. Analysis of refrigerant-charged solar collectors with phase change Heat Recovery Systems and CHP, 13(5):429–39.

137. Raveendran, P. , Fu, J., Wallen, S.L., 2003. Completely green synthesis and stabilization of metal nanoparticles, J. Am. Chem. Soc. 125 pp. 13940.

138. Reddy KS, 2007. Thermal modeling of PCM-based solar integrated collector storage water heating system. Journal of Solar Energy Engineering 2007;129(4): 458–64 November.

139. Reddy KS, Kaushika ND, 1999. Comparative study on transparent insulation materials covers systems for integrated-collector-storage solar water heaters. Solar Energy Materials and Solar Cells, 58(4):431–46.

140. Redpath DAG, Eames PC, Lo SNG, Griffiths PW, 2009. Experimental investigation of natural convection heat exchange within a physical model of the manifold chamber of a thermosyphon heat-pipe evacuated tube solar water heater. Solar Energy,83(7):988–97.

141. Said, Z., Sajid, M.H., Saidur, R., Kamalisarvestani, M., Rahim, N.A., 2013. Radiative properties of nanofluids, Int. Comm. in Heat Mass Transf.59, 46–54.

142. Said, Z., Saidur, R., Rahim, N.A., 2014. Optical properties of metal oxides based nanofluids, Int. Comm. in Heat Mass Transf.59, 46–54.

143. Saidur, R., Leong, K.Y., Mohammad, H.A., 2011. A review on applications and challenges of nanofluids." Renewable and Sustainable Energy Reviews 15: 1646-1668.

144. Saidur, R., T.Meng, Z.Said, M.Hasanuzzaman, A.Kamyar, 2012. Evaluation of the effect of nanofluid-based absorbers on direct solar collector, Int. J. Heat Mass Transf.55, 5899–5907.

145. Sajid, M.H.,Said, Z., Saidur, R., Adikan, F.R.M., Sabri, M.F.M., Rahim, N.A., 2014. A time variant investigation on optical properties of water based Al2O3 nanofluids, Int. Comm. in Heat Mass Transf.50 , 108–116.

146. Sani, E., Barison, S., Pagura, C., Sansoni, P., Fontani, D., 2010. Carbon nanohorns based nanofluids as direct sunlight absorbers . Optics Express, 5179-5187.

147. Sani, E., L.Mercatelli, S.Barison, C.Pagura, F.Agresti, L.Colla, P.Sansoni, 2011. Potential of carbon nanohorn-based suspensions for solar thermal collectors, Solar Energy Material Solar Cells 95, 2994–3000.

148. Schmidt C, Goetzberger A, 1990. Single-tube integrated collector storage systems with transparent insulation and involute reflector. Solar Energy,45(2):93–100.

149. Schreyer, J.M., 1981. Residential application of refrigerant charged solar collectors. Solar Energy 26, 307–312.

150. Seung-Hyun Lee, Seok Pil Jang., 2015. Efficiency of a volumetric receiver using aqueous suspensions of multi-walled carbon nanotubes for absorbing solar thermal energy. Int. J. Heat Mass Transf.80, 58–71.

151. Shariah A, Shalabi B, 1997. Optimal design for thermosyphon solar water heater. Renewable Energy, 11(3):351–61.

152. Smyth M, Eames PC, Norton B, 1999. A comparative performance rating for an integrated solar collector/storage vessel with inner sleeves to increase heat retention. Solar Energy, 66(4):291–303.

153. Sodha MS, Tiwari GN, 1981. Analysis of natural circulation solar water heating systems. Energy Conversion and Management; 21(4):283–8.

154. Soin RS, Raghurman S, Murali V, 1987. Two-phase water heater model and long term performance. Solar Energy; 38(2):105–12.

155. Soin RS, Rao KS, Rao DP, Rao KS, 1979. Performance of flat plate solar collector with fluid undergoing phase change. Solar Energy, 23(1):69–73.

156. Sokolov M, Vaxman M, 1983. Analysis of an integral compact solar water heater. Solar Energy, 30 (3) :237–46.

157. Solar Center Information, 2003. Passive and active solar domestic hot water systems. Tech. Rep., North Carolina Solar Center. <www.ncsc. ncsu.edu>.

158. Suryanarayana, C., 1995. Nanocrystalline materials, Int.Mater.Rev.40 (2), pp. 41.

159. Taylor, R.A., Phelan, P.E., Otanicar, T.P., Adrian, R., Prasher, R., 2011a. Nanofluid optical property characterization: towards efficient direct absorption solar collectors. Nanoscale Research Letters.

160. Taylor, R. A., Phelan, P. E., Otanicar, T. P., Walker, C. A., Nguyen, M., Trimble, S., & Prasher, R., 2011b. Applicability of Nanofluids in High Flux Solar Collectors. Renewable and Sustainable Energy, 3(2),023104

161. Tiwari, A., K. Pradyumna Ghosh, P., Sarkar, J., 2013. Solar Water Heating Using Nanofluids -A Comprehensive Overview And Enveronmental Impact Analysis. International Journal of Emerging Technology and Advanced Engineering, 3(Special Issue 3), 221-224

162. Trisaksri, V., Wongwises, S, 2007. "Critical Review of Heat Transfer Characteristics of Nanofluids." Renewable and Sustainable Energy Reviews 11 512-523.

163. Tyagi, H., Phelen, P., Prasher, P., 2009. Predicted efficiency of a low temperature nanofluid based direct absorption solar collector." journal of solar energy engineering,: 041004 (1-7).

164. Uhlemann R, Bansal NK, 1985. Side-by-side comparison of a pressurized and a nonpressurized solar water heating thermosyphon system. Solar Energy, 34(4-5):317–28.

165. Wagener, M., and Gunther, B., 1997. "Sputtering on liquids - a versatile process for the production of magnetic suspensions." Journal of Magnetism and Magnetic Materials, 201, 41-44.

166. Walker A, Mahjouri F and Stiteler R , 2004. Evacuated-tube heat-pipe solar collec- tors applied to recirculation loop in a federal building: SSA Philadelphia. ASME 2004 International Solar Energy Conference (ISEC2004) Paper no. ISEC2004-65132; 217–222.

167. Wang, X., Xu, X., and Choi, S. U. S., 1999. Thermal conductivity of nanoparticle-fluid mixture. Journal of Thermophysics and Heat Transfer, 13, no. 4, 474–480.

168. Wang, X.Q., Mujumdar, A.S. "A review on nanofluids - Part II: Experiments and Applications." Brazilian Journal of Chemical Engineering 25, no. 4 (2008): 631-648.

169. Wang, X. Q. and A. S. Majumdar, “Heat transfer characteristics of nanofluids, a review,” Int. J. Therm. Sci. 46, 1, 2007.

170. Webb B. W. and Viskanta R., 1985. Analysis of heat transfer and solar radiation absorption in an irradiated thin, falling molten film, Journal of Solar Energy Engineering, vol. 107.

171. Wu, J., and Liu, S., 2002. Low temperature growth of well-alligned ZnO nanorods by chemical vapor deposition, Adv. Mater. 14(3), pp. 215.

172. Xinjian, X., Lei, Y., Xiaosong, Z., Donggen, P., 2007. Review on the development of flat-plate solar collector and its building-integrated designing. In: Proceedings of ISES Solar World Congress 2007: Solar Energy and Human Settlement, pp. 623–626.

173. Xuan, Y., Li, Q., 2000. Heat Transfer enhancement of nanofluids." International Journal of Heat and Fluid Flow 21, 58-64.

174. Yilmaz, T. and Ogulata R.T.. 1990. Influence of the tank height on the efficiency of a two-phase solar water heater. Energy and the Environment 2: 749-755.

175. Yin, B., Ma, H., Wang, S., Chen, S., 2003. Electrochemical synthesis of silver nanoparticles under protection of poly (N-vinylpyrrolidone), J. Phys. Chem. B 107 pp. 8898.

176. Yin, Y., Li, Z., Y., Zhong, Z., Gates, B., Xia, Y., N., Venkateswaran, S., 2002. Synthesis and characterization of stable aqueous dispersions of silver nanoparticles through the tollens process, J. Mater. Chem. 12, pp. 522.

177. Yousefi T., Veysi F., Shojaeizadeh E., Zinadini S.(2012a) " An experimental investigation on the effect of Al2O3- H2O nanofluid on the efficiency of flat - plate solar collectors." Renewable Energy (39): 293-298.

178. Yousefi T., Veysi F., Shojaeizadeh E., Zinadini S.(2012b) " An experimental investigation on the effect of MWCNT- H2O nanofluid on the efficiency of flat - plate solar collectors." Experimental thermal and fluid science (39): 207-212.

179. Yousefi T, Shojaeizadeh E, Veysi F, Zinadini S., 2012c. An experimental investigation on the effect of pH variation of MWCNT–H2O nanofluid on the efficiency of a flatplate solar collector. Sol Energy, 86:771–9.

180. Zamzamian, A., M. KeyanpourRad, M. KianiNeyestani, M. T. Jamal-Abad (2014) “An experimental study on the effect of Cu-synthesized/EG nanofluid on the efficiency of flat - plate solar collectors." Renewable Energy (71): 658-664.

181. Zerrouki, A., A. Boumedien, and K. Bouhadef, 2002. The natural circulation solar water heater model with linear temperature distribution.” Renewable Energy, 26, 549-559.

182. Zhongyang Luo, Cheng Wang, Wei Wei, Gang Xiao, Mingjiang Ni., 2014. Performance improvement of a nanofluid solar collector based on direct absorption collection (DAC) concepts. International Journal of Heat and mass Transfer 75, 262-271.

183. Zhu, H., Lin, Y., and Yin, Y., 2004. A novel one-step chemical method for preparation of copper nanofluids." Journal of Colloid and Interface Science, 277(1), 100-103.

184. Zhu, J., Liu, S., Palchik, O., Koltypin, Y., Gedanken, A., 2000. Shape control synthesis of silver nanoparticles by pulse sonoelectrochemical methods, Langmuir 16 pp. 6396.

Publications from Research

International Journal Papers:

Published

1. H.K Gupta, G.D Agrawal, J. Mathur (2015) ; An experimental investigation of a low temperature Al_2O_3-H_2O nanofluid based direct absorption solar collector. **Solar Energy (Elsevier),** Volume 118, Pages 390-396 **(IF = 3.541)**

2. H.K Gupta, G.D Agrawal, J. Mathur (2015); Experimental study of water based Al_2O_3 nanofluid flow in direct absorption solar collector. **Macromol. Symp.,** 357: 30-37. doi: 10.1002/masy.201400182

3. H.K Gupta, G.D Agrawal, J. Mathur (2015), Investigation for effect of Al_2O_3 –H_2O nanofluid flow rate on the efficiency of direct absorption solar collector, Case Studies in Thermal Engineering **(Elsevier),** Volume 5, Pages:70- 78.

4. Gupta H.K, Agrawal G.D, Mathur J. (2014) Experimental Evaluation on the Effect of Nanofluid Concentration on the Performance of Direct Absorption Solar Collector, International Journal of Advanced Engineering and Nano Technology (IJAENT), ISSN: 2347-6389, Volume 1 Issue 12 Pages:16- 20.

5. H.K Gupta, G.D Agrawal, J. Mathur (2013) Performance comparison of nanofluid based collector & conventional flat plate Collector-A Review, Scientific & Research Journal, ISSN: 2231-0975, Volume X Number 1, 2013.

6. Gupta H.K, Agrawal G.D, Mathur J. (2012) An overview of Nanofluids: A new media towards green environment, INTERNATIONAL JOURNAL OF ENVIRONMENTAL SCIENCES (IJES), ISSN: 0976-4402, Volume 3 Issue 1, July 2012 Pages: 433- 440.

Patent

Submitted patent for "Solar Thermal Energy Collection and conversion through Nanofluid film on Direct Absorption Collector"

Dr. G. D. Agrawal, Hemant Kumar Gupta

Papers Presented in International Seminars/Conferences

1. Gupta H.K., Agrawal G.D., Mathur J.; Nanofluids: "Experimental Evaluation of Using Nanofluid in Direct Absorption Solar Collector", 3rd ETPEES-14, 1-2 November 2014, JNU, New Delhi, India.

(Published in **Energy Technology & Ecological Concerns: A Contemporary Approach, Print ISBN: 978-81-93024-71-3. Page No: 150-154)**

2. H.K Gupta, G.D Agrawal, J. Mathur ; Performance comparison of nanofluid based collector & conventional flat plate Collector-A Review, Nanocon 012: 2nd International conference on Nanotechnology: Innovative Materials, Processes, Products and Applications, 18-19 October 2012, Pune, India.

3. Rajvanshi A.K., Gupta H.K., Agrawal G.D., Mathur J.; Efficiency improvement, Size Reduction and Economic Analysis of Solar Collector with the Use of nanofluids, ICREGA-2012, 4-7 March 2012, AL AIN, UAE.

4. Gupta H.K., Agrawal G.D., Mathur J.; "Advances in nanofluid technology, preparation and stability mechanism", VCAN-2011, 24-25 December 2011, IET, Alwar, Rajasthan, India

5. Gupta H.K., Agrawal G.D., Mathur J.; Nanofluids: "An Emerging Trend in Global Technology, Applications, Limitations and Future Research", IGTT-11, 15-16 October 2011, IET, Alwar, Rajasthan, India.

6. Gupta H.K., Agrawal G.D., Mathur J.; Potential of using nanofluids in solar collectors for energy and environmental benefits, ICEE-15, 17-18 January 2015, KITE, Jaipur, Rajasthan, India.

Papers presented in National seminars/Conferences

1. Gupta H.K.., Agrawal G.D.; Use of Nanofluid as working fluid in direct absorption flat plate solar collector, All India seminar on Nanotechnology applications, MNIT Jaipur, October 6-8, 2012.

2. Gupta H.K.., Agrawal G.D.; Environmental benefits of Flat Plate Solar Collector Using Nanofluids, All India seminar on Air Quality Management, MNIT Jaipur, April 28-29, 2012.

3. Gupta H.K.., Agrawal G.D., Mathur J.; Feasibility of Using Nanofluids in Solar Flat Plate Collectors, National Conference on Sustainable Development in Energy Sector, University of Petroleum & Energy Studies, Dehradun, April 8-9, 2011.

4. Gupta H.K.., Agrawal G.D.; Energy and Environmental Benefits of Using Nanofluids, National conference on Climatic Changes and Sustainable Development, Rajasthan Institute of Engineering & Technology, Jaipur, February 25-26, 2011

APPENDIX-A

Materials and their thermal conductivity

Material	Thermal conductivity [$W \cdot m^{-1} \cdot K^{-1}$]
Aluminum oxide, pure	40
Aluminum, pure	247
Bismuth	7.97
Brass Cu63%	125
Brass Cu70%	121
Brick	1.31
Bronze	42
Carbon nanotube	6,600
Copper, pure	401
Glass	0.8
Gold, pure	314
Iron, cast	55
Iron, pure	34.6
Nickel	90.9
Silver, pure	427
Steel, carbon	36
Steel, stainless	16.3
Water	0.609
Water vapor	0.016
Wood, +>=12% water	0.09091
Wood, oven-dry	0.04
Zinc oxide	21

Source: http://en.wikipedia.org/wiki/List_of_thermal_conductivities

APPENDIX-B

Typical optical properties of some common glazing materials

Material	Thickness *(mm)*	Short-Wave Infrared Solar Transmittance	Long-Wave Infrared Solar Transmittance
Window glass	4	0.83	0.02
Low-iron glass	3	0.89	0.08
Acrylic Glass	3	0.82	0.02
Polyester	0.1	0.87	0.18

Source

http://www.engineeringtoolbox.com/optical-properties-glazing-materials- d_1355.html

APPENDIX-C

BIS 12933(Part 1): 1992 Flat plate solar collector dimensions

Size	Length(L)	Width(W)	Height(H)
A	1860±10	1240±10	100±10
B	2120±10	1030±10	100±10
C	2050±10	930±10	100±10

APPENDIX-D

Thermal Radiation Properties for different Materials

Material	α	ρ	ε	α/ε
White plaster	0.07	0.93	0.91	0.08
Fresh snow	0.13	0.87	0.82	0.16
White paint	0.2	0.8	0.91	0.22
White enamel	0.35	0.65	0.9	0.39
Green paint	0.5	0.5	0.9	0.56
Red brick	0.55	0.45	0.9	0.6
Concrete	0.6	0.4	0.92	0.68
Grey paint	0.75	0.25	0.88	0.79
Black tar paper	0.93	0.07	0.93	1
Flat black paint	0.96	0.04	0.88	1.09
3M Velvet black paint	0.98	0.02	0.9	1.09
Granite	0.55	0.45	0.44	1.25
Graphite	0.78	0.22	0.41	1.9
Aluminum foil	0.15	0.85	0.05	3
Galvanized steel	0.65	0.35	0.13	5

APPENDIX-E

Experimental data for different concentration Al_2O_3-water nanofluid at three flow rates

Table E.1 Experimental and calculated results for distilled water at 1.5 lpm flow rate

TIME	T_i (˚C)	T_o (˚C)	T_{bp1} (˚C)	T_{bp2} (˚C)	T_{gc} (˚C)	T_a (˚C)	RH	v (m/sec)	I_T (W/m^2)	ΔT (℃)	(Ti-Ta)/It	η
10:15	31.7	36	33.1	35	30.7	28.3	33.93	1.37	828	4.3	0.004	0.47
10:30	34	38	35.4	37.2	30.7	28.7	32.55	1.20	852	4	0.006	0.42
10:45	35.1	38.6	36.2	37.9	38.2	29.2	30.81	1.30	912	3.5	0.006	0.34
11:00	39.1	41.8	39.9	41.1	42.3	29.9	28.13	1.24	928	2.7	0.010	0.26
11:15	40.9	43.6	41.7	42.7	43.5	30.1	27.86	1.13	966	2.7	0.011	0.25
11:30	44.4	47	45.2	46.6	45.9	30.5	24.6	1.40	1006	2.6	0.014	0.23
11:45	46.1	48.6	46.9	48.4	47.2	30.9	25.51	1.32	1033	2.5	0.015	0.22
12:00	47.7	50.2	48.7	50.3	47.4	31.1	24.45	1.46	1063	2.5	0.016	0.21
12:15	49.2	51.7	50.2	51.8	49.2	31.4	22.81	1.36	1070	2.5	0.017	0.21
12:30	52	54.1	53.1	54.5	50.9	31.9	22.47	1.11	1084	2.1	0.019	0.17
12:45	53.3	55.2	54.4	55.8	51.9	32.3	22.05	1.13	1050	1.9	0.020	0.16
13:00	54.2	56.1	55.6	57.1	51.6	32.1	21.8	1.41	1046	1.9	0.021	0.16
13:15	55	57	56.4	58.2	52.8	32.3	21.14	2.03	1090	2	0.021	0.16
13:30	57.1	58.6	58.4	59.8	54.2	32.9	20.65	1.22	1080	1.5	0.022	0.12
13:45	57.8	59.2	59.2	60.7	54.6	32.5	20.33	1.38	1072	1.4	0.024	0.11
14:00	58.3	59.8	59.6	61.2	55.3	33.5	19.79	1.64	1102	1.5	0.023	0.12
14:15	59.1	60.3	60.2	61.7	55.5	33.2	19.77	1.79	1022	1.2	0.025	0.10
14:30	59.4	60.5	60.2	61.9	55.4	33.7	19.26	2.88	979	1.1	0.026	0.10
14:45	59.5	60.6	60.6	62.2	55.9	33.6	19.3	1.76	940	1.1	0.028	0.10
15:00	59.8	60.3	60.5	61.4	54.8	33.8	18.97	2.02	892	0.5	0.029	0.05

Table E.2 Experimental and calculated results for 0.001% v.f. Al_2O_3- water nanofluid at 1.5 lpm flow rate

TIME	T_i (˚C)	T_o (˚C)	T_{bp1} (˚C)	T_{bp2} (˚C)	T_{gc} (˚C)	T_a (˚C)	RH	v (m/sec)	I_T (W/m^2)	ΔT	(Ti-Ta)/It	η
10:00	36	40.5	41.7	43.2	39.8	30.3	26.92	1.93	790	4.5	0.007	0.51
10:15	38.2	41.8	44.3	45.9	41.5	30.2	27.42	1.97	828	3.6	0.010	0.39
10:30	40.2	43.2	46.8	48.5	43.4	30.1	26.84	1.56	852	3	0.012	0.32
10:45	42	44.9	49.4	51.3	45.9	30.5	26.64	1.41	912	2.9	0.013	0.28
11:00	43.5	46.5	51.8	53.6	47.7	31	25.95	1.50	928	3	0.013	0.29
11:15	45.4	48.7	53.8	55.8	49.4	30.8	25.57	1.87	966	3.3	0.015	0.31
11:30	47.3	50.4	56.2	57.9	51.6	31.5	24.15	1.55	1006	3.1	0.016	0.28

11:45	49.1	52.1	58.1	60	52.8	31.7	24.31	1.32	1033	3	0.017	0.26
12:00	50.7	53.8	60	61.7	54.1	32.1	23.81	1.42	1063	3.1	0.017	0.26
12:15	52.4	55.2	61.4	63.2	55.1	32.4	23.84	2.01	1070	2.8	0.019	0.23
12:30	53.8	56.7	63.1	64.7	56.5	32.7	23.71	2.05	1084	2.9	0.019	0.24
12:45	56.3	59.2	64.5	65.7	57.7	32.9	23.79	2.02	1050	2.9	0.022	0.25
13:00	57	59.2	66.2	67.3	58.5	33.3	22.33	2.03	1046	2.2	0.022	0.24
13:15	57.7	59.9	66.3	67.1	57.5	33.4	23.16	2.00	1090	2.2	0.023	0.25
13:30	58.3	60.1	66.4	66.9	60	33.3	23.49	2.07	1080	1.8	0.022	0.24
13:45	58.2	59.6	66.7	68.1	61	34	21.93	1.51	1072	1.4	0.023	0.24
14:00	57.8	60.6	67.8	69.3	60.7	34.8	19.18	2.06	1102	2.8	0.021	0.231
14:15	58.7	61.4	67.8	68.6	60.1	34.9	18.57	3.01	1022	2.7	0.023	0.24
14:30	59.5	61.6	67.6	68.3	60	34.6	18.67	2.92	979	2.1	0.025	0.195
14:45	60	61.6	67.9	68.6	60.6	34.8	18.18	2.53	940	1.6	0.027	0.155

Table E.3 Experimental and calculated results for 0.003% v.f. Al_2O_3- water nanofluid at 1.5 lpm flow rate

TIME	T_i (℃)	T_o (℃)	T_{bp1} (℃)	T_{bp2} (℃)	T_{gc} (℃)	T_a (℃)	RH	v (m/sec)	I_T (W/m^2)	ΔT	(Ti-Ta)/It	η
10:00	32.5	36.6	34.1	36	39.6	27	39.88	1.62	790	4.2	0.007	0.48
10:15	35.4	39.4	36.9	39.1	37.5	27	38.53	1.58	799	4	0.011	0.45
10:30	38.4	42.4	40	42.1	39.3	27.3	36.83	1.63	868	4	0.013	0.41
10:45	40.9	44.9	42.6	44.9	41.1	27.7	37.73	1.24	912	4	0.014	0.39
11:00	43.4	47.4	45.1	47.6	42.8	27.7	34.36	1.50	968	4	0.016	0.37
11:15	45.1	48.8	46.6	49	44.7	28.4	34.22	1.41	996	3.7	0.017	0.33
11:30	46.1	50	47.7	50.5	45.2	28.5	32.82	1.45	1032	3.9	0.017	0.34
11:45	48.1	51.9	49.6	52.3	46.9	29.4	31.9	1.51	1056	3.8	0.018	0.32
12:00	50.8	54.5	52.3	55.1	49.7	29.3	30.78	0.90	1058	3.7	0.020	0.31
12:15	52.1	55.7	53.4	56.1	49.8	29.6	30.2	1.67	1065	3.6	0.021	0.30
12:30	54.4	57.7	55.6	58	51.1	30.7	28.19	1.04	1060	3.3	0.022	0.28
12:45	56.3	59.6	57.3	59.6	53.2	30.3	28.81	1.36	1065	3.3	0.024	0.28
13:00	57.2	60.3	58.4	60.7	54.5	30.9	28.35	1.08	1063	3.1	0.025	0.26
13:15	57.9	60.5	58.9	61	53.2	31.1	27.57	1.51	1071	2.6	0.025	0.22
13:30	59.1	61.4	60	61.8	54.8	31	26.1	1.58	1043	2.3	0.027	0.2
13:45	59.9	61.9	60.7	62.3	55	31.8	24.54	1.22	1032	2	0.027	0.17
14:00	60.3	62.2	61.1	62.4	55	32.1	23.81	1.16	1021	1.9	0.028	0.16
14:15	60.7	62.4	61.4	62.6	54.8	32.5	23.66	1.20	1000	1.7	0.028	0.15
14:30	61.3	62.8	61.9	62.7	55.7	32.1	23.74	1.57	955	1.5	0.031	0.14
14:45	61.5	62.6	61.9	62.7	55	32.4	22.72	1.60	904	1.1	0.032	0.11
15:00	61.3	62.2	61.7	62.2	54.2	32.3	22.12	1.76	849	0.9	0.034	0.09

Table E.4 Experimental and calculated results for 0.005% v.f. Al_2O_3- water nanofluid at 1.5 lpm flow rate

TIME	T_i (˚C)	T_o (˚C)	T_{bp1} (˚C)	T_{bp2} (˚C)	T_{gc} (˚C)	T_a (˚C)	RH	v (m/sec)	I_T (W/m^2)	ΔT	(Ti-Ta)/It	η
10:00	36.4	39.8	37.8	39.8	37.4	26.5	32.92	1.76	826	3.4	0.012	0.37
10:15	38.6	41.8	40	41.8	37.5	27	27.77	1.41	834	3.2	0.014	0.34
10:30	40.6	43.8	41.9	43.7	39.6	27.1	32.2	1.41	880	3.2	0.015	0.32
10:45	44.3	47.7	45.8	47.7	42.1	27.6	27.52	1.38	925	3.4	0.018	0.33
11:00	46.2	49.6	47.7	49.4	43.7	28.1	25.82	1.89	984	3.4	0.018	0.31
11:15	48	51.6	49.5	51.3	45.4	28.3	25.62	1.25	1054	3.6	0.019	0.30
11:30	49.9	53.3	51.4	53.1	47	28.7	25.43	1.63	1101	3.4	0.019	0.28
11:45	51.4	54	52.9	54.6	48	28.9	24.56	1.60	1027	2.6	0.022	0.22
12:00	52.8	56.2	54.4	56	49.7	29.2	24.28	1.53	1114	3.4	0.021	0.27
12:15	55.2	58.3	56.6	58.1	51.5	29.6	24.72	1.41	1125	3.1	0.023	0.24
12:30	56.2	59.2	57.8	59.2	51.8	29.7	23.73	1.49	1126	3	0.024	0.24
12:45	57.3	60	58.8	60.3	51.7	29.8	24.8	1.56	1126	2.7	0.024	0.21
13:00	58.2	60.8	59.9	61.3	54.1	30.4	23.85	1.86	1128	2.6	0.025	0.20
13:15	59.3	61.8	60.9	62.2	55	30.8	23.58	1.96	1135	2.5	0.025	0.19
13:30	60.2	62.7	61.6	62.9	55.8	30.4	22.11	1.58	1122	2.5	0.027	0.20
13:45	61.5	63.2	62.6	63.9	56.1	31.1	21.1	1.67	1106	1.7	0.027	0.13
14:00	62.1	63.8	63	64	57.1	31	22.04	1.75	1042	1.7	0.030	0.14
14:15	62.6	64.1	63.4	64.3	56	31.3	22.02	1.69	999	1.5	0.031	0.13
14:30	63	64.5	63.8	64.8	57	31.6	20.01	1.54	972	1.5	0.032	0.14
14:45	63.2	64.5	63.8	64.6	56.3	31.7	18.93	2.71	894	1.3	0.035	0.13

Table E.5 Experimental and calculated results for 0.007% v.f. Al_2O_3- water nanofluid at 1.5 lpm flow rate

TIME	T_i (˚C)	T_o (˚C)	T_{bp1} (˚C)	T_{bp2} (˚C)	T_{gc} (˚C)	T_a (˚C)	RH	v (m/sec)	I_T (W/m^2)	ΔT	(Ti-Ta)/It	η
10:00	35.8	40	37.3	39.7	38.3	28.2	30.72	0.89	782	4.2	0.010	0.48
10:15	38.7	42.7	40.1	42.1	39.1	28.1	29.4	1.08	838	4	0.013	0.43
10:30	41	45	42.6	44.8	40.3	29	29.11	1.10	898	4	0.013	0.40
10:45	43.4	47.4	45.1	47.3	42.6	29.5	27.27	1.06	948	4	0.015	0.38
11:00	45.6	49.7	47.4	49.4	44.8	29.3	26.64	1.27	977	4.1	0.017	0.37
11:15	47.9	51.8	49.5	51.4	46.1	30	24.34	1.58	989	3.9	0.018	0.35
11:30	49.9	53.6	51.3	53.1	47.6	30.1	21.49	1.54	1046	3.7	0.019	0.32
11:45	51.9	55.7	53.2	55.3	49.2	30.7	20	1.64	1087	3.8	0.020	0.31

12:00	53.9	57.6	55.5	57.3	50.5	30.7	19.7	1.53	1112	3.7	0.021	0.30
12:15	57.5	60.7	58.7	60.2	52.9	31.2	18.67	1.65	1124	3.2	0.023	0.25
12:30	58.7	61.7	60	61.5	52.6	31.4	14.53	2.18	1152	3	0.024	0.23
12:45	59.7	62.7	61	62.5	53.7	31.6	15.34	2.06	1134	3	0.025	0.23
13:00	60.8	63.4	61.9	63.2	56.5	32.1	15.75	2.02	1129	2.6	0.025	0.20
13:15	61.7	64.1	62.7	64.2	56.2	31.9	15.36	2.09	1123	2.4	0.027	0.19
13:30	62.3	64.6	63.3	64.6	57.5	32	15.13	2.14	1128	2.3	0.027	0.18
13:45	63	65.1	63.9	65.1	57.4	32.5	14.16	1.75	1108	2.1	0.028	0.17
14:00	63.9	65.6	64.5	65.7	58.5	32.5	14.08	2.13	1061	1.7	0.030	0.14
14:15	64.2	65.7	64.6	65.8	57.9	32.7	13.24	2.13	1025	1.5	0.031	0.13
14:30	64.5	66.1	64.9	66.1	58.7	33	12.55	1.79	974	1.6	0.032	0.14
14:45	64.7	65.9	65.2	66	58.4	33.3	12.8	1.53	923	1.2	0.034	0.11
15:00	64.6	65.4	64.8	65.4	57.1	33.2	12.72	2.13	903	0.8	0.035	0.08

Table E.6 Experimental and calculated results for distilled water at 2 lpm flow rate

TIME	T_i (˚C)	T_o (˚C)	T_{bp1} (˚C)	T_{bp2} (˚C)	T_{gc} (˚C)	T_a (˚C)	RH	v (m/sec)	I_T (W/m^2)	ΔT	(Ti-Ta)/It	η
10:15	36	40.8	36.7	40.8	37.9	35.9	15.57	1.59	844	4.8	0.00	0.70
10:30	38.4	42.7	39.5	43.6	40	36.3	14.02	1.88	888	4.3	0.00	0.59
10:45	40.9	45.4	44.6	48.1	43.7	36.6	13.53	1.51	971	4.5	0.00	0.57
11:00	45.7	50.1	46.6	50.3	45.4	36.4	15.11	2.08	982	4.4	0.01	0.55
11:15	47.9	52.1	48.4	51.9	46.4	37	12.57	2.00	1029	4.2	0.01	0.50
11:30	51	55.2	50.5	54.2	48.5	36.5	11.84	2.26	1075	4.2	0.01	0.48
11:45	52.9	57.1	52.4	56	49.8	36.9	10.6	2.31	1086	4.2	0.01	0.47
12:00	56.2	60	56	59.5	53.3	36.9	9.97	1.99	1105	3.8	0.02	0.42
12:15	57.7	61.6	57.7	61	54.9	37.3	10.7	2.21	1094	3.9	0.02	0.44
12:30	59.2	62.7	59.1	62.2	55.3	37.8	9.76	1.86	1112	3.5	0.02	0.38
12:45	61.5	64.6	60.9	63.9	56.5	37.4	9.67	2.24	1129	3.1	0.02	0.33
13:00	63.6	66.5	62	64.7	56.6	37.9	10.32	1.85	1099	2.9	0.02	0.32
13:15	64.4	67.2	63.1	65.9	58.5	38	10.17	2.06	1097	2.8	0.02	0.31
13:30	65	67.7	63.5	66.2	58	38	10.25	2.23	1073	2.7	0.03	0.31
13:45	66.1	68.4	64.3	66.9	58.6	38	10.8	2.06	1053	2.3	0.03	0.27
14:00	66.4	68.6	64.9	66.9	58.7	38	11.04	2.80	998	2.2	0.03	0.27
14:15	66.7	68.9	65.3	67.3	59.8	38.2	10.65	1.97	973	2.2	0.03	0.28
14:30	67.4	68.9	65.5	67.4	60	34.9	10.73	2.04	943	1.5	0.03	0.19
14:45	67.4	68.4	65.5	67.3	59.5	34.6	10.58	2.21	903	1	0.04	0.13
15:00	67	68.6	65.6	66.7	59.1	34.2	11.74	2.36	860	1.6	0.04	0.23

Table E.7 Experimental and calculated results for 0.001% v.f. Al_2O_3- water nanofluid at 2 lpm flow rate

TIME	T_i (℃)	T_o (℃)	T_{bp1} (℃)	T_{bp2} (℃)	T_{gc} (℃)	T_a (℃)	RH	v (m/sec)	I_T (W/m^2)	ΔT	(Ti-Ta)/It	η
10:15	38.2	42.8	40.2	44.2	39.8	30.3	19.56	1.31	844	4.6	0.009	0.67
10:30	40.6	44.9	42.1	46.2	41.6	30.6	20.11	1.44	871	4.3	0.011	0.61
10:45	42.6	46.9	44.3	48.3	43.9	30.9	19.48	1.44	966	4.3	0.012	0.55
11:00	46.6	50.9	48.2	51.9	47	31.2	18.45	1.65	999	4.3	0.015	0.53
11:15	48.7	52.7	50.1	53.5	48.7	31.5	18.23	1.56	1023	4	0.017	0.48
11:30	50.5	54.6	52.2	56	50.7	31.8	17.72	1.48	1054	4.1	0.018	0.48
11:45	52.1	56.3	54.3	58	51.9	32.5	18.06	1.40	1062	4.2	0.018	0.48
12:00	55.4	59.2	57.5	60.7	53.7	32.6	16.62	1.51	1098	3.8	0.021	0.42
12:15	56.8	60.6	59.3	62.7	55.5	33.2	16.19	1.60	1077	3.8	0.022	0.43
12:30	58.8	62.1	61.5	64.2	56.5	33.7	15.29	1.86	1097	3.3	0.023	0.37
12:45	60.2	63.6	62.5	64.7	57.2	33.8	14.84	1.55	1100	3.4	0.024	0.38
13:00	61.3	64.3	63.8	66.2	59	33.9	14.07	2.09	1104	3	0.025	0.33
13:15	62.2	64.8	64.5	66.5	58.5	34.7	12.78	2.29	1105	2.6	0.025	0.29
13:30	62.9	65.3	65.2	67	60.4	34.9	12.09	2.08	1077	2.4	0.026	0.27
13:45	64.3	66.5	65.8	67.6	59.8	35.7	9.65	1.53	1055	2.2	0.027	0.25
14:00	64.8	67	66.3	67.9	60.8	35.7	10.4	1.36	1043	2.2	0.028	0.26
14:15	65.1	67.1	66.5	68.1	60.2	35.7	10.24	1.96	1025	2	0.029	0.24
14:30	65.7	67.4	66.4	68.1	60.6	35.6	9.05	1.46	948	1.7	0.032	0.22
14:45	65.8	67.3	66.5	68	60.1	36	9.46	1.78	908	1.5	0.033	0.20
15:00	66	67.2	66.4	67.8	60.8	36.2	8.75	1.41	885	1.2	0.034	0.16

Table E.8 Experimental and calculated results for 0.003% v.f. Al_2O_3- water nanofluid at 2 lpm flow rate

TIME	T_i (℃)	T_o (℃)	T_{bp1} (℃)	T_{bp2} (℃)	T_{gc} (℃)	T_a (℃)	RH	v (m/sec)	I_T (W/m^2)	ΔT	(Ti-Ta)/It	η
10:00	32	36.6	33.5	36.6	37.4	29.3	33.73	1.65	715	4.6	0.004	0.79
10:15	34.6	39	36.1	39.1	37.5	29.5	33.26	1.97	780	4.4	0.007	0.69
10:30	39	43.4	40.4	43.5	40.6	30.3	30.4	1.70	831	4.4	0.010	0.65
10:45	41.3	45.5	42.6	45.6	41.8	30.5	29.92	1.79	867	4.2	0.012	0.59
11:00	45.4	49.6	46.8	49.7	44.9	30.8	29.51	1.66	912	4.2	0.016	0.56
11:15	47.4	51.5	48.8	51.8	45.8	31.9	26.9	2.16	950	4.1	0.016	0.53
11:30	50.3	54.3	51.6	54.4	48.7	31.9	26.02	1.63	980	4	0.019	0.53
11:45	52.2	56.1	53.5	56.3	49.7	32.5	24.66	1.48	1003	3.9	0.020	0.48

12:00	53	57	54.4	57.4	51.6	33.4	24.8	1.52	1002	4	0.020	0.49
12:15	55.4	59.1	56.8	59.5	52.7	32.6	24.41	1.89	1012	3.7	0.023	0.45
12:30	56.5	60	57.8	60.4	54.1	33.1	24.73	1.46	1010	3.5	0.023	0.42
12:45	58.4	61.6	59.6	62	55.2	33	24.84	1.78	1020	3.2	0.025	0.38
13:00	59.2	62.2	60.3	62.6	56.1	33.7	24.15	2.01	1004	3	0.025	0.36
13:15	60.6	63.4	61.6	63.8	55.2	33.3	24.68	1.95	1039	2.8	0.026	0.33
13:30	61.3	64.3	62.5	64.8	57.3	34.2	23.14	1.54	1022	3	0.027	0.36
13:45	62.7	65	63.5	65.3	57.9	34.2	22.84	1.33	991	2.3	0.029	0.28
14:00	63	65.1	63.7	65.4	58	34.3	23.14	1.59	942	2.1	0.030	0.27
14:15	63.5	65.7	64.2	65.9	59.3	34.4	21.42	1.63	918	2.2	0.032	0.29
14:30	63.8	65.7	64.4	66.1	58.4	34.8	21.45	1.49	872	1.9	0.033	0.26
14:45	64.3	65.7	64.7	65.8	57.2	35	20.7	1.40	856	1.4	0.034	0.20
15:00	64.4	65.5	64.5	65.6	58	34.5	21.81	1.43	813	1.1	0.037	0.16

Table E.9 Experimental and calculated results for 0.005% v.f. Al_2O_3- water nanofluid at 2 lpm flow rate

TIME	T_i (˚C)	T_o (˚C)	T_{bp1} (˚C)	T_{bp2} (˚C)	T_{gc} (˚C)	T_a (˚C)	RH	v (m/sec)	I_T (W/m^2)	ΔT	(Ti-Ta)/It	η
10:00	34.7	40.1	36.4	39.6	45.1	33.5	24.14	1.21	708	5.4	0.002	0.93
10:15	37	41.8	38.7	41	43.2	33.6	24.14	1.47	834	4.8	0.004	0.70
10:30	41.2	45.6	42.8	45.4	42	33.6	23.47	1.34	855	4.4	0.009	0.63
10:45	43.2	47.7	44.9	48.2	42.7	33.8	23.48	1.43	888	4.5	0.011	0.62
11:00	47.1	51.6	48.7	51.9	46.4	33.9	23.19	1.30	949	4.5	0.014	0.58
11:15	48.9	53.3	50.6	53.8	48.5	34	23.05	1.50	976	4.4	0.015	0.55
11:30	52.1	56.2	53.6	56.8	50.7	34.8	23.25	1.39	1018	4.1	0.017	0.49
11:45	53.5	57.5	55.1	58.2	49.7	34.7	22.64	1.61	1032	4	0.018	0.47
12:00	55.9	59.7	57.4	60.2	52	34.8	21.3	1.77	1032	3.8	0.020	0.45
12:15	57.2	61.1	58.7	61.6	53.6	34.5	21.96	1.78	1039	3.9	0.022	0.46
12:30	59.3	62.7	60.5	63.4	53	34.8	21.68	1.98	1041	3.4	0.024	0.40
12:45	60	63.4	61.2	63.7	48	35.4	20.66	1.74	1050	3.4	0.023	0.39
13:00	61.8	65	62.9	65.4	53.1	35.2	20.49	1.80	1053	3.2	0.025	0.37
13:15	62.4	65.4	63.6	66	51.3	35.1	20.83	2.07	1057	3	0.026	0.34
13:30	63.7	66.4	64.7	66.8	54.1	35.8	20.07	1.82	1029	2.7	0.027	0.32
13:45	64.1	66.7	65	67.2	53.4	35.9	19.96	1.52	1020	2.6	0.028	0.31
14:00	64.9	67	65.6	67.4	54.4	35.9	20.23	1.88	965	2.1	0.030	0.26
14:15	65.1	67	65.7	67.4	48.6	36	18.33	2.12	936	1.9	0.031	0.25
14:30	65.3	66.6	65.5	67	50.7	36.1	19.48	1.97	900	1.3	0.032	0.17
14:45	65.2	66.6	65.7	67	52.8	36.3	18.65	1.31	870	1.4	0.033	0.19

Table E.10 Experimental and calculated results for 0.007% v.f. Al_2O_3- water nanofluid at 2 lpm flow rate

TIME	T_i (˚C)	T_o (˚C)	T_{bp1} (˚C)	T_{bp2} (˚C)	T_{gc} (˚C)	T_a (˚C)	RH	v (m/sec)	I_T (W/m^2)	ΔT	(Ti-Ta)/It	η
10:00	35.2	40.6	36.9	40.5	41.3	33.9	21.77	1.19	772	5.4	0.002	0.86
10:15	37.9	42.9	39.5	42.8	41.5	34.4	21.42	1.65	815	5	0.004	0.75
10:30	40.4	45.3	41.9	45.2	43.4	34.5	21.13	1.34	857	4.9	0.007	0.70
10:45	42.7	47.4	44.2	47.5	44.1	35	20.48	1.43	896	4.7	0.009	0.64
11:00	47.6	52.1	48.9	51.7	48.1	35.3	20.23	1.37	950	4.5	0.013	0.58
11:15	49.7	53.9	51.2	53.8	48.5	35.7	19.84	1.24	965	4.2	0.015	0.53
11:30	51.6	55.9	52.9	55.4	50.8	36	19.36	1.71	988	4.3	0.016	0.53
11:45	55.1	59	56.3	58.4	52.6	36.3	19.56	1.81	1017	3.9	0.018	0.47
12:00	56.6	60.2	57.8	59.7	54.4	36.8	18.29	1.82	1011	3.6	0.020	0.43
12:15	58	61.5	59.2	61	55.6	36.9	17.3	1.73	1014	3.5	0.021	0.42
12:30	60.1	63.1	61.2	62.8	55.9	37.2	17.24	1.51	1048	3	0.022	0.35
12:45	61.1	64	62.1	63.7	58.4	37.1	17.16	1.60	1050	2.9	0.023	0.34
13:00	63	65.6	63.8	65.2	59.9	37.6	16.49	1.64	1056	2.6	0.024	0.30
13:15	63.6	65.9	64.4	65.7	59.2	37.8	16.27	1.80	1051	2.3	0.025	0.26
13:30	64.1	66.4	64.9	66.2	60.1	37.7	16.03	2.28	1040	2.3	0.025	0.27
13:45	64.6	66.7	65.3	66.6	60.2	38.1	15.5	2.31	1031	2.1	0.026	0.25
14:00	65	66.8	65.7	66.9	59.4	38.2	15.2	2.22	980	1.8	0.027	0.22
14:15	65.3	67.2	66.1	67.5	61.3	38.2	14.73	1.84	946	1.9	0.029	0.24
14:30	65.7	67.2	66.2	67.1	61	38.1	14.96	2.08	902	1.5	0.031	0.20
14:45	66	67.3	66.3	67.2	61.2	38.4	14.59	1.77	846	1.3	0.033	0.18
15:00	66	67.3	66.5	67.4	60.2	38.9	13.75	2.38	885	1.3	0.031	0.18

Table E.11 Experimental and calculated results for distilled water at 2.5 lpm flow rate

TIME	T_i (˚C)	T_o (˚C)	T_{bp1} (˚C)	T_{bp2} (˚C)	T_{gc} (˚C)	T_a (˚C)	RH	v (m/sec)	I_T (W/m^2)	ΔT	(Ti-Ta)/It	η
10:00	36.5	40.1	37.7	39.7	42.2	36.4	15.11	1.39	792	3.6	0.000	0.66
10:15	40.9	44.2	41.8	43.8	43	36.8	13.5	1.66	850	3.3	0.005	0.56
10:30	42.8	46.2	43.8	45.8	43.5	37.3	11.83	1.58	879	3.4	0.006	0.56
10:45	46.4	49.7	47.6	49.4	45.7	37.1	12.81	2.08	927	3.3	0.010	0.51
11:00	49.8	53.1	50.8	52.6	48.9	37.5	10.31	2.05	986	3.3	0.012	0.48
11:15	52.9	55.9	53.7	55.5	50.7	37.7	10.27	1.86	1015	3	0.015	0.43
11:30	54.2	57.2	55.1	56.7	51.6	37.9	10.64	1.93	1029	3	0.016	0.42
11:45	56.9	59.9	57.8	59.4	54.9	37.6	10.23	2.02	1066	3	0.018	0.40
12:00	59.1	61.8	59.8	61.4	54.9	38.2	9.7	1.84	1058	2.7	0.020	0.37
12:15	60.2	62.6	60.7	62.4	55.3	38.3	10.02	2.27	1065	2.4	0.021	0.32
12:30	62	64.4	62.7	64.1	57	38.6	9.87	1.90	1080	2.4	0.022	0.32

12:45	63.7	66	64.3	65.8	58.3	38.3	9.7	2.31	1097	2.3	0.023	0.30
13:00	65.1	67.4	65.8	67.2	59.6	39	8.85	2.13	1101	2.3	0.024	0.30
13:15	66.4	68.6	67.1	68.4	60.6	38.7	8.6	1.95	1100	2.2	0.025	0.29
13:30	67	69.1	67.6	68.8	61.1	38.5	7.84	2.07	1089	2.1	0.026	0.28
13:45	68.1	69.8	68.5	69.8	61.7	39	8.22	1.50	1059	1.7	0.027	0.23
14:00	68.5	70	68.9	69.9	61.3	38.9	8.61	2.15	1001	1.5	0.030	0.21
14:15	68.9	70.3	69.4	70.4	62.5	39	8.01	2.03	968	1.4	0.031	0.21
14:30	69	70.4	69.3	70.2	61.6	39.1	8.78	1.68	944	1.4	0.032	0.21
14:45	69.1	70.2	69.3	69.9	61.8	39.6	8.55	1.86	901	1.1	0.033	0.17
15:00	68.8	69.6	68.9	69.5	59.9	39.1	9.17	1.99	845	0.8	0.035	0.13

Table E.12 Experimental and calculated results for 0.001% v.f. Al_2O_3- water nanofluid at 2.5 lpm flow rate

TIME	T_i (˚C)	T_o (˚C)	T_{bp1} (˚C)	T_{bp2} (˚C)	T_{gc} (˚C)	T_a (˚C)	RH	v (m/sec)	I_T (W/m^2)	ΔT	(Ti-Ta)/It	η
10:00	40.3	43.6	41.4	43.8	41.5	36.5	19.73	1.32	739	3.3	0.005	0.64
10:15	42.3	45.5	43.4	45.7	42.8	37	19.15	1.89	774	3.2	0.007	0.60
10:30	46	49.1	47	49.2	45.2	37.4	19.09	2.31	823	3.1	0.010	0.54
10:45	49.3	52.3	50.2	52.4	47.6	37.5	19.02	1.69	870	3	0.014	0.50
11:00	52.4	55.2	53.2	55.2	50	38	17.13	1.93	915	2.8	0.016	0.44
11:15	53.5	56.4	54.3	56.3	51.2	37.9	18.43	1.28	918	2.9	0.017	0.45
11:30	56.3	59.1	57.2	59.2	53.7	38.1	16.47	2.11	961	2.8	0.019	0.43
11:45	58.6	61.2	59.4	61.3	54.7	38.7	14.47	2.32	986	2.6	0.020	0.38
12:00	59.7	62.2	60.3	62.3	55.9	39.3	14.93	2.32	990	2.5	0.021	0.36
12:15	61.5	63.9	62.1	63.8	57	39	15.16	1.96	988	2.4	0.023	0.35
12:30	63.1	65.5	63.7	65.4	58.6	39.1	15.31	2.43	1032	2.4	0.023	0.33
12:45	63.8	65.9	64.3	65.8	59.4	39	13.69	2.24	1035	2.1	0.024	0.29
13:00	65.1	67.1	65.6	66.9	60.4	39.3	15.01	2.80	1032	2	0.025	0.28
13:15	65.7	67.6	66.1	67.3	60.5	39.2	14.95	2.56	1017	1.9	0.026	0.27
13:30	66.6	68.2	66.9	68	60.9	39.5	14.73	2.56	979	1.6	0.028	0.23
13:45	66.8	68.4	67.1	68.2	61	39.9	13.48	2.86	968	1.6	0.028	0.24
14:00	67.2	68.5	67.4	68.3	60.6	40	13.87	2.45	931	1.3	0.029	0.20
14:15	67.1	68.3	67.3	68.4	61	39.9	13.61	2.38	906	1.2	0.030	0.19
14:30	67.1	68.2	67.2	68.1	60.6	40.2	13.45	2.78	895	1.1	0.030	0.17
14:45	66.8	67.9	66.9	67.7	60.8	40.1	13.01	1.94	834	1.1	0.032	0.19

Table E.13 Experimental and calculated results for 0.005% v.f. Al_2O_3- water nanofluid at 2.5 lpm flow rate

TIME	T_i (˚C)	T_o (˚C)	T_{bp1} (˚C)	T_{bp2} (˚C)	T_{gc} (˚C)	T_a (˚C)	RH	v (m/sec)	I_T (W/m^2)	ΔT	(Ti-Ta)/It	η
10:00	41.1	44.4	42	44	41.6	34.2	38.6	1.90	684	3.3	0.010	0.69
10:15	44.5	47.8	45.4	47.4	43.7	35	38.13	2.06	747	3.3	0.013	0.64
10:30	46.2	49.4	47.2	49	45.1	35.1	35.54	1.43	770	3.2	0.014	0.60
10:45	49.5	52.6	50.4	52.2	47.6	35.7	34.3	1.44	814	3.1	0.017	0.55
11:00	52.7	55.5	53.5	55.1	49.8	35.6	32.14	1.59	849	2.8	0.020	0.47
11:15	54	56.9	54.9	56.5	50.8	36.3	28.99	1.33	877	2.9	0.020	0.47
11:30	56.6	59.3	57.4	59	52.9	36	30.42	1.64	930	2.7	0.022	0.42
11:45	57.7	60.4	58.5	59.9	53.8	36.3	28.55	1.74	918	2.7	0.023	0.42
12:00	59.8	62.4	60.6	62	55.8	37.3	26.4	1.49	900	2.6	0.025	0.41
12:15	61.6	64.2	62.5	63.9	57.4	37.7	24.94	1.58	957	2.6	0.025	0.39
12:30	62.6	65.2	63.4	64.8	58.4	38.2	24.82	1.57	973	2.6	0.025	0.38
12:45	64	66	64.7	65.8	59	37.7	24.79	1.86	971	2	0.027	0.29
13:00	65.1	67.3	65.8	67.1	60.8	38.7	22.82	1.34	955	2.2	0.028	0.33
13:15	65.8	67.8	66.5	67.7	61	38.9	22.19	0.80	967	2	0.028	0.3
13:30	66.9	68.6	67.5	68.9	62.2	38.8	21.84	1.12	936	1.7	0.030	0.26
13:45	67.1	68.6	67.5	68.9	62.3	38.5	21.75	1.41	920	1.5	0.031	0.23
14:00	67.5	68.9	67.9	69	62.7	39.1	21.1	1.14	866	1.4	0.033	0.23
14:15	67.8	68.9	68	69	63	39.3	20.96	1.05	846	1.1	0.034	0.18
14:30	67.9	69	68.2	69	62.5	39.7	19.83	1.80	835	1.1	0.034	0.19
14:45	67.9	68.6	68	68.8	61.9	39.4	20.66	1.72	783	0.7	0.036	0.13

APPENDIX-F

Experimental data for different concentration TiO_2-water nanofluid at three flow rates

Table F.1 Experimental and calculated results for 1.5 lpm and 0.001% v.f. TiO_2 nanofluid

TIME	T_i (˚C)	T_o (˚C)	T_{bp1} (˚C)	T_{bp2} (˚C)	T_{gc} (˚C)	T_a (˚C)	I (W/m^2)	ΔT (˚C)	(Ti-Ta)/It	η
10:00	41.12	46.72	44.06	45.76	44.27	39.3	773.7	5.605	0.00235	0.65
10:15	43.87	49.44	46.94	48.6	46.14	39.75	818.7	5.572	0.00503	0.61
10:30	46.66	52.15	49.94	51.62	48.44	40.48	851.5	5.491	0.00726	0.58
10:45	49.74	54.96	52.89	54.54	50.24	40.61	892.6	5.217	0.01023	0.53
11:00	52.3	57.47	55.48	57.07	52.37	41.51	911.3	5.161	0.01185	0.51
11:15	54.43	59.46	57.55	59.14	54.1	41.74	914	5.026	0.01389	0.49
11:30	58.39	63.25	61.46	62.92	57.32	42.36	952.8	4.861	0.01682	0.46
11:45	59.91	64.16	62.86	64.22	57.99	42.2	985.2	4.25	0.01798	0.39
12:00	61.23	65.29	64.19	65.47	59.61	42.63	991.8	4.062	0.01875	0.37
12:15	62.47	66.53	65.47	66.71	60.74	42.88	1004	4.059	0.0195	0.36
12:30	63.74	67.7	66.48	67.69	61.75	43.42	996.5	3.951	0.0204	0.36
12:45	64.91	68.2	67.11	67.99	61.47	43.33	991.8	3.291	0.02176	0.30
13:00	66.55	69.44	68.52	69.41	62.89	43.65	967.2	2.891	0.02368	0.27
13:15	67.27	70.04	69.12	69.97	63.69	44.04	929.1	2.772	0.025	0.27
13:30	68.05	70.79	69.82	70.61	64.81	44.76	891.3	2.738	0.02613	0.27
13:45	68.68	71	70.3	70.9	64.53	44.44	890.9	2.313	0.02721	0.23
14:00	68.84	70.81	70.44	71.47	64.96	44.39	882.3	1.973	0.02771	0.20
14:15	69.01	71.3	70.57	71.63	65.67	44.96	848.5	2.282	0.02835	0.24
14:30	69.17	71.1	70.42	71.32	65.15	45.11	822.6	1.932	0.02925	0.21
14:45	69.18	70.72	70.33	71.02	64.58	45.07	786.4	1.538	0.03066	0.17

Table F.2 Experimental and calculated results for 1.5 lpm and 0.003% v.f. TiO_2 nanofluid

TIME	T_i (˚C)	T_o (˚C)	T_{bp1} (˚C)	T_{bp2} (˚C)	T_{gc} (˚C)	T_a (˚C)	I (W/m^2)	ΔT (˚C)	(Ti-Ta)/It	η
10:00	44.85	51.33	49.47	51.62	43.95	39.82	827.8	6.481	0.00608	0.71
10:15	47.76	53.87	52.66	54.6	50.3	40.81	866.9	6.105	0.00801	0.64
10:30	50.28	56.31	55.26	57.05	52.58	40.97	897.7	6.028	0.01037	0.61
10:45	51.97	58.07	57.14	58.85	54.48	41.44	915.7	6.103	0.0115	0.60
11:00	53.48	58.71	58.8	60.63	56	41.83	924.4	5.238	0.0126	0.51

11:15	55.31	59.5	60.14	62.52	57.38	41.91	968.3	4.196	0.01383	0.39
11:30	56.71	60.91	61.69	63.98	58.75	42.59	981.2	4.204	0.01439	0.38
11:45	58.18	62.53	63.23	65.48	60.59	43.87	984.9	4.347	0.01453	0.40
12:00	59.68	63.73	64.67	66.71	61.27	43.38	1005	4.049	0.01621	0.36
12:15	62.2	66.05	67.3	69.01	63.36	44.15	989.5	3.85	0.01824	0.35
12:30	63.39	66.92	68.06	69.79	63.58	43.97	976.5	3.526	0.01989	0.32
12:45	64.36	67.54	68.37	69.91	63.42	44.19	953	3.18	0.02117	0.30
13:00	65.07	68.15	68.89	70.33	63.95	44.63	927	3.081	0.02204	0.30
13:15	65.55	68.34	68.89	70.34	63.78	44.21	911.7	2.796	0.0234	0.27
13:30	65.65	68.44	68.88	70.35	64.17	44.49	888.8	2.792	0.02381	0.28
13:45	65.9	68.33	68.1	69.69	64.18	44.28	888.4	2.424	0.02433	0.24
14:00	65.86	68.13	67.66	68.88	63.7	44.53	833.9	2.276	0.02557	0.24
14:15	65.93	67.59	67.32	68.14	62.61	43.66	811.1	1.658	0.02745	0.18
14:30	65.69	67.47	67.09	67.81	62.45	44.06	776.6	1.788	0.02785	0.20
14:45	65.63	66.81	66.78	67.31	61.42	43.42	756.9	1.183	0.02935	0.14

Table F.3 Experimental and calculated results for 1.5 lpm and 0.005% v.f. TiO_2 nanofluid

TIME	T_i (˚C)	T_o (˚C)	T_{bp1} (˚C)	T_{bp2} (˚C)	T_{gc} (˚C)	T_a (˚C)	I (W/m^2)	ΔT (˚C)	(Ti-Ta)/It	η
11:00	49.79	55.07	52.71	54.33	51.79	40.01	833.7	5.279	0.01173	0.55
11:15	52.12	57.49	55.04	56.56	53.82	40.73	842.1	5.372	0.01353	0.55
11:30	54.15	59.28	57.08	58.44	55.36	40.9	854.8	5.13	0.01551	0.52
11:45	56.1	60.98	58.88	60.23	56.96	41.52	877.8	4.881	0.01661	0.48
12:00	57.91	62.4	60.53	61.76	57.96	41.74	905.1	4.481	0.01787	0.43
12:15	59.52	63.76	61.95	63.09	59.23	42.24	910.6	4.247	0.01897	0.40
12:30	61.36	65.41	63.67	64.77	60.83	42.02	912	4.05	0.02121	0.38
12:45	62.38	66.18	64.49	65.58	61.37	42.89	907.5	3.799	0.02148	0.36
13:00	63.54	67.12	65.59	66.55	62.38	43.07	918.2	3.578	0.02229	0.34
13:15	64.62	68.04	66.52	67.47	63.33	42.84	903.1	3.42	0.02412	0.33
13:30	65.65	68.75	67.26	68.14	63.89	43.12	888.1	3.101	0.02537	0.30

Table F.4 Experimental and calculated results for 1.5 lpm and 0.007% v.f. TiO_2 nanofluid

TIME	T_i (˚C)	T_o (˚C)	T_{bp1} (˚C)	T_{bp2} (˚C)	T_{gc} (˚C)	T_a (˚C)	I (W/m^2)	ΔT (˚C)	(Ti-Ta)/It	η
9:45	42.52	47.58	45.08	46.64	45.52	38.1	668	5.06	0.00661	0.68
10:00	45.36	50.61	48.07	49.52	48.04	39.24	737	5.251	0.0083	0.64
10:15	48.05	53.64	50.92	52.62	50.22	40.16	788.1	5.586	0.01001	0.64
10:29	50.51	55.99	53.18	54.87	51.89	40.59	826.6	5.481	0.012	0.60
10:44	52.83	58.43	55.72	57.31	53.84	41.3	863.1	5.6	0.01335	0.58
10:59	54.94	60.34	57.64	59.06	55.05	41.46	907.7	5.401	0.01485	0.54
11:13	56.93	61.98	59.54	60.8	56.94	42.04	926.2	5.051	0.01607	0.49
11:28	58.82	63.72	61.3	62.67	58.12	42.58	963.9	4.906	0.01684	0.46
11:44	60.56	65.42	63.42	64.45	59.5	42.81	980.8	4.857	0.01809	0.45
11:58	62.67	66.64	64.74	65.82	60.88	43.26	990.5	3.967	0.0196	0.36
12:13	63.72	67.95	65.98	67.09	61.71	43.39	989.1	4.223	0.02056	0.38
12:28	64.83	69.26	67.41	68.43	63.49	44.46	1022	4.427	0.01994	0.39
12:42	66.2	70.43	68.8	69.68	64.79	44.93	1038	4.231	0.02048	0.37
12:55	67.35	71.2	69.72	70.65	64.99	44.9	1033	3.852	0.02173	0.33
13:09	68.24	71.99	70.81	71.58	65.78	44.83	1024	3.749	0.02286	0.33
13:23	68.77	72.46	71.42	71.92	66.1	45.15	999.9	3.689	0.02362	0.33
13:39	69.42	72.76	71.76	72.25	66.11	45.38	971.4	3.333	0.02475	0.31
13:54	69.78	72.97	71.97	72.45	66.53	45.35	927.9	3.195	0.02633	0.31
14:09	70.27	73.07	71.87	72.37	66.58	45.47	909.1	2.805	0.02727	0.28

Table F.5 Experimental and calculated results for 2 lpm and 0.001% v.f. TiO_2 nanofluid

TIME	T_i (˚C)	T_o (˚C)	T_{bp1} (˚C)	T_{bp2}(˚C)	T_{gc}(˚C)	T_a (˚C)	I(W/m^2)	ΔT(˚C)	(Ti-Ta)/It	η
10:00	40.25	44.67	42.63	44.21	42.59	34.03	682.5	4.416	0.009	0.77
10:15	42.4	46.69	44.72	46.4	44.19	34.68	732.2	4.29	0.011	0.70
10:30	46.63	50.61	48.75	50.47	46.22	35.45	794.6	3.982	0.014	0.60
10:45	48.62	52.42	50.9	52.16	47.43	35.63	827.3	3.801	0.015	0.55
11:00	52.27	56.14	54.26	55.63	50.44	36.46	875.4	3.877	0.018	0.53
11:15	53.94	57.58	55.99	57.19	51.41	36.51	908.3	3.643	0.019	0.48
11:30	55.55	59.1	57.36	58.63	52.7	36.71	926.5	3.557	0.020	0.46
11:45	58.46	61.71	60.21	61.32	54.81	37.1	915.5	3.254	0.023	0.43
12:00	59.65	62.97	61.59	62.63	55.94	37.5	928.6	3.315	0.023	0.42
12:15	60.83	64.02	62.66	63.72	56.63	37.67	958.3	3.189	0.024	0.39
12:30	62.88	65.8	64.82	65.75	58.37	37.84	979.1	2.919	0.025	0.35
12:45	63.74	66.53	65.55	66.51	59.1	37.98	979.5	2.792	0.026	0.34

13:00	64.55	67.37	66.45	67.3	60.07	38.47	989.3	2.823	0.026	0.34
13:15	65.88	68.37	67.58	68.33	60.15	38.48	996.4	2.496	0.027	0.30
13:30	66.5	68.99	68.1	68.97	61.31	38.5	962.4	2.488	0.029	0.31
13:45	67.52	69.64	68.84	69.56	61.54	39.22	917.9	2.12	0.030	0.28
14:00	67.69	69.8	69.03	69.72	61.59	39.56	926.6	2.106	0.030	0.27
14:15	67.95	70	69.22	70.03	62.32	39.8	922.1	2.047	0.031	0.26
14:30	68.14	69.74	69.15	69.73	61.86	39.6	817.5	1.596	0.034	0.23

Table F.6 Experimental and calculated results for 2 lpm and 0.003% v.f. TiO_2 nanofluid

TIME	T_i (˚C)	T_o (˚C)	T_{bp1} (˚C)	T_{bp2} (˚C)	T_{gc} (˚C)	T_a (˚C)	I (W/m^2)	ΔT (˚C)	(Ti-Ta)/It	η
10:00	42.89	46.88	44.39	45.56	44.37	39.8	669.3	3.996	0.00462	0.71
10:15	45.51	49.67	47.24	48.55	46.67	41.02	708.4	4.161	0.00633	0.70
10:30	47.58	51.81	49.59	50.92	48.74	41.53	740	4.235	0.00818	0.68
10:45	51.85	55.78	53.85	55.1	51.62	42.13	802.4	3.934	0.01211	0.58
11:00	53.79	57.56	55.53	56.74	53.3	42.48	824.6	3.776	0.01371	0.54
11:15	55.6	59.41	57.36	58.48	54.83	42.47	852.4	3.811	0.0154	0.53
11:30	58.98	62.67	60.69	61.75	57.85	43.55	903.9	3.69	0.01707	0.48
11:45	60.55	64.05	62.36	63.35	59.39	44.16	916.9	3.501	0.01787	0.45
12:00	61.99	65.23	63.66	64.73	60.31	44.34	924.8	3.237	0.01909	0.42
12:15	63.23	66.56	65	65.99	61.5	44.44	915.5	3.329	0.02053	0.43
12:30	65.4	68.47	66.96	67.88	63.48	44.97	955.7	3.07	0.02138	0.38
12:45	66.27	69.33	67.87	68.78	64.04	45.25	972.9	3.055	0.02161	0.37
13:00	67.26	70.08	68.68	69.52	64.54	45.27	980.5	2.821	0.02242	0.34
13:15	68.7	71.39	70.33	70.97	65.92	45.76	959.6	2.686	0.02391	0.33
13:30	69.08	71.93	70.62	71.47	66.35	45.95	971.7	2.85	0.0238	0.35

Table F.7 Experimental and calculated results for 2 lpm and 0.005% v.f. TiO_2 nanofluid

TIME	T_i (˚C)	T_o (˚C)	T_{bp1} (˚C)	T_{bp2} (˚C)	T_{gc} (˚C)	T_a (˚C)	I (W/m^2)	ΔT (˚C)	(Ti-Ta)/It	η
10:00	37.41	42.1	39.1	40.26	40.71	34.67	648	4.689	0.00423	0.86
10:15	41.52	46.11	43.28	44.61	42.6	35.39	725.3	4.588	0.00846	0.75
10:30	43.43	47.9	45.37	46.71	44.03	35.39	762.5	4.474	0.01055	0.70
10:45	47.18	51.36	49.12	50.47	46.65	36.13	810.1	4.175	0.01364	0.62
11:00	49.06	53.37	51.04	52.43	48.12	36.28	842	4.315	0.01518	0.61
11:15	50.87	55.11	52.91	54.29	49.82	37.05	866.8	4.239	0.01595	0.58

11:30	54.19	58.14	56.19	57.49	51.92	37.13	884.3	3.95	0.01929	0.53
11:45	55.72	59.74	57.7	59	53.68	37.73	877	4.018	0.02052	0.54
12:00	58.46	62.32	60.6	61.77	55.35	38.08	972.1	3.863	0.02096	0.47
12:15	59.82	63.71	61.95	63.24	56.92	38.38	993	3.884	0.02159	0.46
12:30	62.45	65.99	64.46	65.77	59.12	38.59	993.3	3.533	0.02402	0.42
12:45	63.62	66.89	65.65	67.03	60.21	39.2	1003	3.274	0.02433	0.39
13:00	65.4	68.17	67.32	68.66	61.01	39.3	1017	2.77	0.02565	0.32
13:15	66.21	69	68.16	69.47	62.11	39.57	1002	2.788	0.02658	0.33
13:30	67.58	69.92	69.32	70.57	62.95	39.91	965.3	2.339	0.02867	0.29
13:45	67.99	70.18	69.69	70.89	63.39	39.35	944.9	2.194	0.0303	0.27
14:00	68.29	70.34	70.02	71.2	63.34	39.66	933.1	2.054	0.03069	0.26
14:15	68.63	70.6	70.22	71.38	63.59	39.87	921.1	1.979	0.03122	0.25

Table F.8 Experimental and calculated results for 2 lpm and 0.007% v.f. TiO_2 nanofluid

TIME	T_i (˚C)	T_o (˚C)	T_{bp1} (˚C)	T_{bp2} (˚C)	T_{gc} (˚C)	T_a (˚C)	I (W/m^2)	ΔT (˚C)	(Ti-Ta)/It	η
10:00	35.78	40.75	38.84	40.34	44.21	35.5	702	4.973	0.0004	0.85
10:15	38.49	43.2	41.28	42.98	43.56	36	752.4	4.712	0.00331	0.75
10:30	43.49	47.93	46.19	47.74	45.27	36.97	836.6	4.445	0.00779	0.63
10:45	45.97	50.05	48.51	50.22	46.94	37.3	857.2	4.078	0.01012	0.57
11:00	48.29	52.41	50.75	52.65	48.86	37.54	887.7	4.117	0.01211	0.55
11:15	52.55	56.52	54.99	56.81	51.86	38.22	954.1	3.972	0.01502	0.49
11:30	54.44	58.1	56.61	58.27	52.97	38	950.3	3.662	0.0173	0.46
11:45	57.68	60.88	59.61	61.09	55.34	38.72	953.9	3.206	0.01987	0.40
12:00	59.13	62.32	61.17	62.49	56.08	39.03	999.8	3.192	0.0201	0.38
12:15	60.47	63.42	62.55	63.74	56.94	38.69	1016	2.952	0.02143	0.34
12:30	62.7	65.26	64.49	65.43	58.18	39.41	1033	2.564	0.02255	0.29

Table F.9 Experimental and calculated results for 2.5 lpm and 0.001% v.f. TiO_2 nanofluid

TIME	T_i (˚C)	T_o (˚C)	T_{bp1} (˚C)	T_{bp2}(˚C)	T_{gc}(˚C)	T_a (˚C)	I(W/m^2)	ΔT(˚C)	(Ti-Ta)/It	η
10:00	35.1	38.4	36.9	37.9	36.5	29.9	549.4	3.3	0.009	0.65
10:15	38.8	43.2	41.1	42.5	40.8	31.7	768.2	4.4	0.009	0.62
10:30	41.0	44.4	42.9	44.1	40.9	31.8	675.5	3.4	0.013	0.55
10:45	44.6	48.9	46.9	48.5	45.1	33.1	860.4	4.3	0.014	0.54
11:00	46.6	50.6	48.8	50.3	46.1	32.8	872.7	4.0	0.016	0.50
11:15	50.4	54.4	52.6	54.0	48.8	33.7	908.3	4.1	0.018	0.48
11:30	52.1	55.9	54.1	55.5	50.1	34.2	916.0	3.8	0.019	0.45
11:45	55.3	58.9	57.3	58.4	52.7	34.9	922.6	3.5	0.022	0.42
12:00	56.8	60.4	58.6	59.9	53.9	35.4	937.7	3.5	0.023	0.41
12:15	59.4	62.7	61.0	62.2	56.0	36.0	976.4	3.3	0.024	0.36
12:30	60.6	63.8	62.3	63.3	57.0	36.2	991.4	3.2	0.025	0.34
12:45	62.8	65.8	64.4	65.4	58.8	36.1	988.0	3.0	0.027	0.33
13:00	63.7	66.6	65.4	66.2	59.5	36.6	986.3	2.9	0.028	0.32
13:15	65.2	67.6	66.7	67.5	60.6	37.2	966.1	2.4	0.029	0.27
13:30	65.7	68.2	67.3	68.0	61.4	37.4	941.5	2.5	0.030	0.28
13:45	66.1	68.2	67.4	68.2	61.2	37.5	886.3	2.1	0.032	0.26
14:00	66.3	68.0	67.5	68.1	60.7	37.3	832.2	1.7	0.035	0.22

Table F.10 Experimental and calculated results for 2.5 lpm and 0.003% v.f. TiO_2 nanofluid

TIME	T_i (˚C)	T_o (˚C)	T_{bp1} (˚C)	T_{bp2} (˚C)	T_{gc} (˚C)	T_a (˚C)	I (W/m^2)	ΔT (˚C)	(Ti-Ta)/It	η
10:00	42.55	46.27	44.24	45.57	44.55	39.38	703.1	3.723	0.00451	0.79
10:15	46.22	49.8	47.94	49.24	47.53	40.54	759.4	3.58	0.00749	0.70
10:30	49.8	52.92	51.4	52.81	49.94	40.94	800.9	3.117	0.01107	0.58
10:45	50.72	53.9	52.48	53.86	50.93	40.92	819.3	3.186	0.01195	0.58
11:00	53.53	56.52	55.37	56.6	53.14	41.98	856.9	2.997	0.01348	0.52
11:15	55.04	57.99	56.82	58.05	54.45	41.96	879.1	2.951	0.01489	0.506
11:30	57.62	60.4	59.31	60.57	56.47	42.51	897.3	2.785	0.01684	0.46
11:45	60.09	62.66	61.67	62.73	58.69	43.26	919.7	2.57	0.0183	0.41
12:00	61.28	63.86	62.84	63.99	59.62	43.07	928	2.579	0.01962	0.42
12:15	63.45	65.98	64.99	66.18	61.33	43.32	924.9	2.532	0.02176	0.4

12:30	65.12	67.29	66.41	67.49	62.5	43.8	968	2.166	0.022	0.3
12:45	65.53	68.44	67.31	68.1	62.87	43.58	963.4	2.908	0.02279	0.45
13:00	66.78	68.98	68.1	68.98	64.15	44.59	961.8	2.2	0.02307	0.3
13:15	67.33	69.47	68.71	69.45	64.57	44.22	944.9	2.147	0.02446	0.34
13:30	68.37	70.14	69.51	70.21	64.94	44.31	907.4	1.774	0.02651	0.29
13:45	68.88	70.51	69.85	70.4	64.87	44.03	861.9	1.631	0.02883	0.28
14:00	68.91	70.44	69.85	70.36	64.57	44.03	835.7	1.529	0.02976	0.27

Table F.11 Experimental and calculated results for 2.5 lpm and 0.005% v.f. TiO_2 nanofluid

TIME	T_i (℃)	T_o (℃)	T_{bo1} (℃)	T_{bo2} (℃)	T_{gc} (℃)	T_a (℃)	I (W/m^2)	ΔT (℃)	(Ti-Ta)/It	η
10:00	40.3	44.5	42.34	43.77	42.86	37.06	737.1	4.198	0.0044	0.74
10:15	44.44	48.36	46.3	47.61	45.14	37.59	801.2	3.922	0.00854	0.64
10:30	48.1	51.87	50.09	51.35	47.75	38.11	844.1	3.764	0.01183	0.58
10:45	49.9	53.49	51.9	53.13	48.9	38.32	869	3.585	0.01333	0.54
11:00	53.26	56.57	55.1	56.28	51.22	38.84	912.9	3.313	0.01579	0.47
11:15	56.05	59.3	58.13	59.44	53.86	39.34	948.8	3.242	0.01761	0.44
11:30	58.91	61.81	60.81	62.35	56.12	39.65	971.3	2.893	0.01983	0.39
11:45	60.18	63.08	62.14	63.69	57.18	39.87	987.2	2.907	0.02058	0.38
12:00	62.53	65.33	64.48	65.98	59.12	40.11	983.3	2.801	0.02281	0.37
12:15	64.6	67.26	66.41	67.86	61.02	41.08	1013	2.659	0.02323	0.34
12:30	65.48	68.09	67.35	68.75	61.66	40.9	1034	2.613	0.02378	0.33
12:45	67.16	69.54	68.86	70.24	63	41.35	1035	2.378	0.02495	0.30
13:00	67.9	70.14	69.47	70.79	63.42	40.98	1032	2.244	0.02607	0.28
13:15	69.2	71.1	70.67	71.9	64.16	41.25	1001	1.892	0.02794	0.25
13:30	69.68	71.52	71.15	72.39	64.91	41.55	981.7	1.843	0.02865	0.24
13:45	70.34	71.93	71.65	72.82	65.11	41.64	932.1	1.589	0.0308	0.22
14:00	70.56	71.83	71.79	72.77	64.6	41.54	927.1	1.264	0.0313	0.19
14:15	70.61	71.88	71.85	72.81	64.85	41.4	903.9	1.263	0.03232	0.18
14:30	70.57	71.68	71.54	72.44	64.95	41.85	866.7	1.112	0.03315	0.17
14:45	70.49	71.52	71.44	72.33	65	41.85	829.5	1.034	0.03452	0.16
15:00	70.35	71.12	71.22	71.98	64.08	41.51	830.7	0.777	0.03471	0.12

Table F.12 Experimental and calculated results for 2.5 lpm and 0.007% v.f. TiO_2 nanofluid

TIME	T_i (˚C)	T_o (˚C)	T_{bp1} (˚C)	T_{bp2} (˚C)	T_{gc} (˚C)	T_a (˚C)	I (W/m^2)	ΔT (˚C)	(Ti-Ta)/It	η
10:00	42.93	47.43	45.2	46.64	45.54	40.78	724.4	4.498	0.00297	0.93
10:15	44.95	49.33	47.12	48.67	46.89	41.17	750.7	4.388	0.00502	0.88
10:30	48.58	52.36	50.61	52.05	49.59	42.17	790.9	3.778	0.0081	0.72
10:45	52.02	55.36	54.05	55.51	52.01	42.44	831.3	3.342	0.01152	0.61
11:00	55.35	58.55	57.39	58.89	54.96	43.16	869.7	3.203	0.01401	0.55
11:15	56.87	59.87	58.92	60.43	56.32	43.87	888.4	2.995	0.01464	0.51
11:30	59.32	62.18	61.25	62.62	58.39	43.96	899.3	2.859	0.01708	0.48
11:45	61.59	64.31	63.54	64.9	59.97	44.04	922.3	2.711	0.01903	0.44
12:00	62.73	65.61	64.6	65.96	61.36	44.67	927.6	2.876	0.01947	0.46
12:15	65.09	67.76	66.86	68.2	63.26	44.89	925.1	2.668	0.02184	0.43
12:30	66.93	69.55	68.74	69.9	64.7	44.93	967.5	2.62	0.02274	0.41
12:45	67.8	70.27	69.55	70.73	65.37	44.91	962.9	2.47	0.02378	0.39
13:00	69.13	71.38	70.86	71.88	66.26	45.48	960.6	2.25	0.02463	0.35
13:15	70.1	72.31	71.7	72.72	67.27	45.9	928.3	2.208	0.02607	0.36
13:30	70.45	72.38	71.94	72.94	66.95	45.65	912.5	1.929	0.02718	0.32
13:45	70.79	72.69	72.16	73.15	67.44	46	899.4	1.9	0.02756	0.32
14:00	71	72.89	72.33	73.2	67.4	46.05	871.6	1.89	0.02863	0.32

Bio-data of the Author

Hemant Kumar Gupta was born on 26th Sep., 1978 to sh. Banbari Lal Gupta and smt. Geeta Gupta. He passed his bachelor of engineering in Mechanical Engineering in 2001 from M.B.M. Engineering College, Jodhpur. He completed his M. E. (Mechanical Engineering) with specialization in Thermal Engineering from M.B.M. Engineering College, Jodhpur in 2003.

After completing his master degree, he joined teaching profession as lecturer in Mechanical Engineering in Marwar Engineering College and Research Center (MECRC) Jodhpur in August 2003 and served for three years. After that, he served as an associate professor & head for Alwar Institute of Engineering and Technology, Alwar (2 years) and Siddhi vinayak college, Alwar (2 years) near to his home town. In July 2010, he got selected in MNIT, Jaipur as PhD research scholar.

He has been pursuing doctoral studies at Malaviya National Institute of Technology, Jaipur since 2010. He has worked under the research project entitled "Experimental Study on Flat Plate Solar Collector (Direct Absorption type) Using Nano-Fluids" sponsored by Department of Science & Technology (DST) during his Ph.D. work. He is a life member of Institute of Engineers and Indian Society of Technical Education. He has published 20 research papers in various international journals and conferences.